Analysis of Dynamics near Heteroclinic Networks using Projected Maps

David Cornelis Groothuizen Dijkema

A thesis submitted in fulfilment of the requirements for the degree of
Doctor of Philosophy in Mathematics,
the University of Auckland,
2025.

Abstract

Heteroclinic cycles and networks are flow-invariant structures in a dynamical system composed of saddle-type objects and connecting heteroclinic orbits. Near an attracting heteroclinic cycle or network, trajectories spend increasingly long periods of time near each equilibrium without converging to any one of them. A trajectory near a heteroclinic cycle always follows the same sequence of equilibria, whereas near a heteroclinic network trajectories can switch between subcycles, and so their analysis is more complicated.

In this thesis, we present a new methodology to analyse heteroclinic networks: the *projected map*, a piecewise-smooth discrete map that reduces the complexity of analysing a network. We use this projected map to study the Kirk–Silber, Δ-clique, and tournament networks in $\mathbb{R}^4$. Our analysis resolves a claim from 1994 that there is no regular or irregular cycling near these three networks. We prove that previously identified conditions for stability of a heteroclinic cycle can be determined at the network's switching equilibrium, and that stability loss of the cycle can correspond to a *border-collision bifurcation* in the projected map. We extend this result to arbitrary heteroclinic networks in higher dimensions and prove a general result about stability loss of component cycles in a network.

We also consider the continuity of the projected map at its switching manifold. We prove that, for the Kirk–Silber network, the projected map is discontinuous due to the presence of a separatrix near the network. For the Δ-clique and tournament networks, no such separatrix exists, and the projected map is therefore continuous.

Lastly, we consider larger networks that exhibit regular and irregular cycling between subcycles. We construct the projected map of these networks. To do so, we describe how to resolve complications that arise if the switching equilibrium has multiple incoming heteroclinic orbits. We relate regular cycling near these networks to periodic orbits in the projected map, and changes in stability to border-collision bifurcations. We find that irregular cycling corresponds to an apparent strange attractor. We expect this analysis will allow us to prove the structure of regular and irregular cycling near these and other networks.

Acknowledgements

Throughout this PhD, my supervisors Claire Postlethwaite and Vivien Kirk have been the best supervisors any student has ever had. I thank them both for everything that they have done for me—for their guidance and contributions—for giving me space to explore this topic, and for supporting me when I got stuck—for always encouraging me to do everything as well as I possibly could—for sharing with me their knowledge of dynamical systems theory—for all the time they gave to me—for reading my work so thoroughly and giving me feedback on my talks—for their patience and understanding—for correcting all the "which"s which were wrong—for putting up with me. I am especially grateful for the support of Claire's Marsden grant for funding this research and my stipend, and also funding attendance at conferences and my research visits. Most of all, I thank Claire for taking a chance on a disenchanted engineering student who emailed her during a COVID lockdown, and the enthusiasm she has shown that convinced me I could do this when I felt I couldn't.

I thank David Simpson at Massey University for discussions that led to the idea of the projected map, and I thank him for the interest he has shown in my work and the help he has provided me throughout my PhD.

In June 2023, I had the pleasure to visit Alastair Rucklidge at the University of Leeds. The work presented in Chapter V was begun in Leeds, and I thank him for the ideas he suggested there and the time he gave to me. I thank him for the advice, guidance, and support he has provided me on so many occasions, his encouragement in my academic pursuits, for the hospitality he and Beverly showed me, and also for convincing me that I needed a TLR.

I also had the pleasure to visit Sofia Castro at the University of Porto in June 2023. I thank Sofia for inviting me to come to Porto and for the work we did together during that week, for giving me the opportunity to present my first seminar, and also for suggesting I attend during the week of *São João*. I thank Sofia and Peter for the incredible kindness, hospitality, and generosity they showed me during my week in Porto.

I thank the Department of Mathematics for supporting my attendance at numerous

conferences in New Zealand, Australia, and further away. I also thank the University of Auckland for providing me with an extension to my scholarship in these last six months of my PhD.

To everybody within the Department of Mathematics, and all my friends without, to those I have known since before I started this PhD, and those I had the pleasure to meet along the way, I thank you all for making these three years and counting the most enjoyable and unforgettable experience, and all the fun we could have together: the cryptic crosswords, OGH, the drinks and dinners, morning coffee, going to the footy and ice hockey, Hobbiton, shuffleboard, bowling, billiards, and darts, watching *Julie and Julia* in A&E, the road trips and camping trips, tramping and bird watching, hiking in the snow or on a glacier, unexpected fords,[1] looking for kiwi, drinking *Kingfisher Strong* in a Nelson holiday park carpark, surviving the Pacific, Hobbiton, not crossing Tongariro, Hobbiton, and everything else. I am grateful that there are simply too many of you to name, and I thank you all.

Lastly, I thank my family, for the unstinting support they have shown me in this, as in all my endeavours.

To the memory of my Omas and Opas,

Marie Theodorus Groothuizen
Ceridwen Beinol Hughes
Cornelis Dijkema
Helena Johanna Wilhelmina Bakker

[1] Sorry again.

There is nothing like looking, if you want to find something. You certainly usually find something, if you look, but it is not always quite the something you were after.

— J R R Tolkien

The Hobbit, or

There and Back Again

Y así, del poco dormir y del mucho leer, se le secó el cerebro de manera, que vino a perder el juicio.

— Miguel de Cervantes

The Ingenious Gentleman

Don Quixote of La Mancha

Contents

List of Figures

1 Introduction

Heteroclinic cycles and networks are structures in dynamical systems composed of flow-invariant sets and connecting heteroclinic orbits. These flow-invariant sets may include hyperbolic saddle-type equilibria, periodic orbits, chaotic sets, or other cycles and networks. Although heteroclinic orbits can be of high codimension, heteroclinic cycles and networks can be robust in certain dynamical systems. In particular, when the system contains flow-invariant subspaces, the heteroclinic orbits may be saddle–sink connections when restricted to these subspaces. Therefore, heteroclinic cycles and networks can be robust to sufficiently small perturbations that preserve the invariance of these subspaces, which may be forced, for example, by symmetries of the dynamical system, or properties of some underlying physical model.

Near an attracting heteroclinic cycle or network composed of equilibria and connecting heteroclinic orbits, a trajectory typically spends a long period of time in a small neighbourhood of one equilibrium. The trajectory then rapidly transitions to the next equilibrium, and, after a time, then transitions to the next equilibrium in the cycle or network, and this process continues indefinitely, with the trajectory asymptotic to no single equilibrium. This behaviour of nearby trajectories allows heteroclinic cycles and networks to be employed in models of intermittent phenomena and intransitive relations, and so applied to a variety of disciplines.

The study of heteroclinic cycles and networks has continually provided new developments and unexpected results. These structures can be strongly attracting but not asymptotically stable, and bifurcations of cycles and networks can also be quite complicated. Changes in the stability of a heteroclinic cycle have been identified that do not seem to align with com-

mon definitions of a bifurcation. The asymptotic dynamics of trajectories near networks can qualitatively change without a change in the stability of the network or its component cycles. For heteroclinic networks in particular, many papers have focussed on particular examples, producing many interesting and unique results. Recently, these results have often concerned the long-term behaviour of trajectories, but a complete understanding of the possible dynamics is lacking. Even for heteroclinic cycles, novel results and examples have recently been considered, and many unanswered questions remain.

§1 An historical overview of heteroclinic cycles and networks

The earliest known example of a heteroclinic cycle in the literature appears in a paper by May and Leonard [ML75]. They considered a generalised Lotka–Volterra model of cyclic competition between three species, and observed that, for some parameter values, trajectories are typically not asymptotic to an equilibrium or limit cycle. In their words,

> …[A] nonlinear study of this domain of parameter space reveals …a wider class of asymptotic solutions in which the system cycles from being composed almost wholly of population 1, to almost wholly 2, to almost wholly 3, back to 1, but with the time to complete the cycle becoming longer and longer (being proportional to the length of time the system has been running), and with the system coming in turn ever closer to the points with 1 alone, 2 alone and 3 alone, yet never actually converging on any one point… [ML75, p. 244]

May and Leonard describe here the behaviour associated with a trajectory asymptotic to an attracting heteroclinic cycle. We show an example of such a trajectory in Figure 1.1.

After May and Leonard's initial study, heteroclinic cycles were encountered in various models of population dynamics, such as in the works of Gilpin [Gil75], Grossberg [Gro78], Coste, Peyraud, and Coullet [CPC79], Schuster, Sigmund, and Wolff [SSW79], Kirlinger [Kir89], or Sikder and Roy [SR94], amongst others. The dynamical properties of the cycle itself were not investigated in these papers, and their terminology reflects a different way of thinking about these structures. For example, the behaviour that we now understand to be a trajectory asymptotic to an attracting heteroclinic cycle was described as "*unstable oscillation[s] of ever-lengthening period*" [Gil75], and the cycle itself was sometimes referred to as an "*orbit of infinite period*" [CPC79]. The earliest definition we can find in the literature of a heteroclinic cycle is in a 1976 paper on the 3-body problem by Easton [Eas76], though, again,

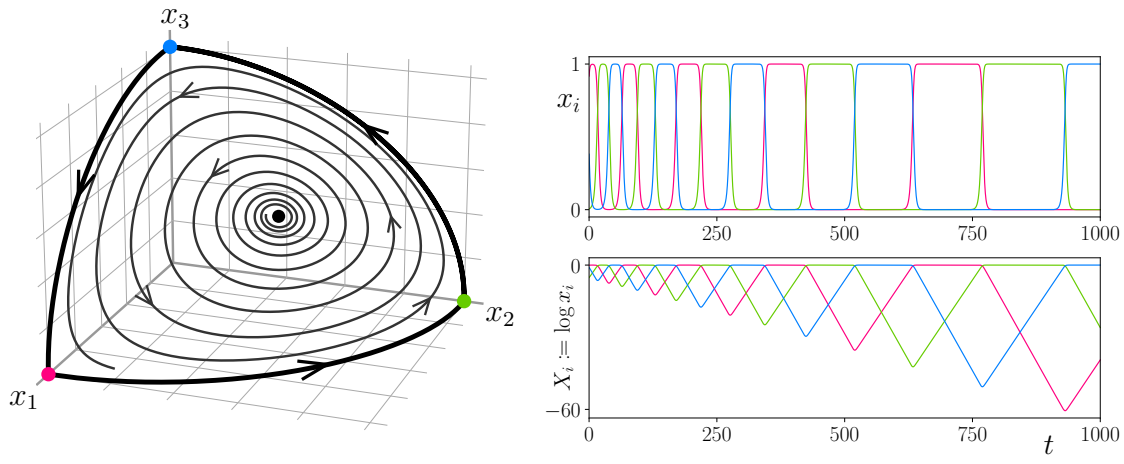

(a) (b)

Figure 1.1: An example of a trajectory near a heteroclinic cycle of three equilibria, which was studied in [ML75] and [GH88]. A part of the trajectory is shown in phase space in (a), and two timeseries are shown in (b), in normal (top) and logarithmic (bottom) coordinates. In (a), the three coloured dots are hyperbolic saddles, and are the equilibria of the cycle, and the black dot is an unstable focus. Only a portion of the trajectory is shown for visual clarity. In (b), the values of x_1, x_2, and x_3 (and the corresponding logarithmic coordinates), are shown in red, green, and blue, respectively. Parameter values and initial conditions used to produce this figure are given in §B.4. See [Gro25a] for an animation of this timeseries.

the cycle itself was not studied in this paper.

Other early examples of heteroclinic cycles are found in studies of fluid dynamics. Building on the work of Küppers and Lortz [KL69] concerning convection in a fluid layer heated from below and rotating about a normal axis, Busse and Clever [BC79] and Busse and Heikes [BH80, HB80] found that, beyond the critical Taylor number, convection rolls are unstable to rolls orientated at approximately 60°. In [HB80], they derived equations for the amplitude of these convection rolls that were the same as the equations considered by May and Leonard [ML75]. Since then, analysis of the Küppers–Lortz instability with models that contain heteroclinic cycles has continued [Swi84, Sow85, HPA98, TMG00, Lau01, Daw01, BSC06]. Knobloch and Silber [KS93] considered a generalisation of this problem with oscillatory rotating convection, and identified the existence of a heteroclinic cycle between four states. This cycle provided an explanation of the observed instability of travelling and standing rolls, analogous to the Küppers–Lortz instability of steady rolls. Aubry, Holmes, Lumley, and Stone [AHL88, AHL89] and Berkooz, Holmes, and Lumley [BHL91] studied fluid flow in a channel and the associated turbulent boundary layer. The truncated ODEs of the dynamics in the wall region were found to contain a heteroclinic cycle associated with turbulent bursting [AHL88, AHL89, BHL91]. Stone and Holmes [SH89, SH91] similarly observed heteroclinic

cycles in truncated ODE models of turbulence. Other examples of heteroclinic cycles in applications are seen in models of geodynamos and geomagnetic reversal [ACO01, MPR01] and in experimental investigations of von Kármán swirling flows [NMQ05].

In dynamical systems theory, early studies of heteroclinic cycles considered equivariant dynamical systems—that is, systems that have certain symmetries. The presence of symmetries can result in heteroclinic orbits that are robust to sufficiently small symmetric perturbations [Fie80, Rei84, GH88]. Dos Reis [Rei84] proved the structural stability of heteroclinic cycles—though they termed cycles "*hyperbolic graphs of a vector field*"—to sufficiently small equivariant perturbations for a class of vector fields on two-manifolds. The first explicit proof of the structural stability of a specific heteroclinic cycle was given by Guckenheimer and Holmes [GH88], who considered a cycle equivalent to that studied by May and Leonard [ML75]. Other early examples of robust heteroclinic cycles include those that exist in systems that are equivariant with respect to the group $\mathrm{O}(2)$ [AGH88, MCG89, Arm89b, CH91, KM95b, SMH05] and $\mathrm{O}(3)$ [AC91, CA91, PK01, CG96].

A study of heteroclinic cycles in $\mathbb{R}^4$ in [CKM97] initiated a means to classify heteroclinic cycles in systems with symmetry. For dynamical systems equivariant with respect to groups of symmetries, the representation-theoretic properties of these groups can be used to classify the heteroclinic cycles that occur in these systems. Chossat, Krupa, Melbourne, and Scheel [CKM97] were able to classify into three different types all cycles in $\mathbb{R}^4$ in which all equilibria lie in the same group orbit. These are known as type A, B, and C cycles. The characterisation of a cycle as being of type A, B, or C depends on where the cycle lies relative to certain fixed-point subspaces. Krupa and Melbourne [KM04] later completed the classification of all cycles of type B and C in $\mathbb{R}^4$. The complete classification of cycles of type A required considerable additional effort [Sot02a, Sot02b]. Chossat, Lohse, and Podvigina, in a series of papers [PC15, PC17, CLP18] extended this classification still further (into cycles said to be *pseudo-simple*) after realising that certain assumptions had previously been implicitly made, and Sottocornola [Sot05] and Podvigina [Pod13] have begun extending this work to $\mathbb{R}^5$.

Podvigina [Pod12] introduced a definition of a broad class of heteroclinic cycles, which they called type Z cycles. Garrido da Silva and Castro [GC19] introduced the notion of *quasi-simple* cycles, which generalises the notion of type Z cycles by replacing the fixed-point subspaces of the system with subspaces whose flow-invariance is forced by any means, not necessarily symmetry.

In [GH88], Guckenheimer and Holmes also consider the stability of the heteroclinic cycle they study, not just its robustness. The vector field linearised at any one of the three equilibria of the Guckenheimer–Holmes cycle has three eigenvalues, which are the same for all three equilibria due to the symmetry of the system: one negative eigenvalue corresponding to

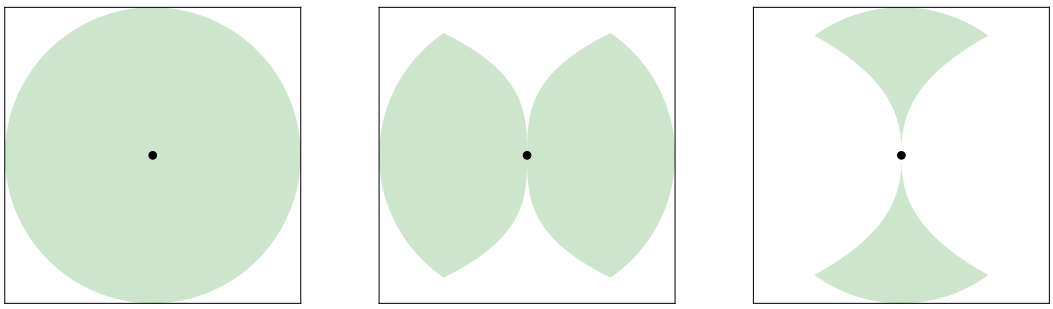

(a) (b) (c)

Figure 1.2: Schematic representations of the basin of attraction of an invariant set that is (a) asymptotically stable, (b) essentially asymptotically stable, or (c) essentially completely unstable. In each figure, the invariant set X is represented by the black dot at the centre, and the basin of attraction of X is shaded green.

the radial direction in phase space, and one single negative eigenvalue (known as *contracting*) and one single positive eigenvalue (known as *expanding*) that correspond to directions tangent to the heteroclinic cycle. Guckenheimer and Holmes prove that if the contracting eigenvalue is greater in absolute value than the expanding eigenvalue, the cycle is asymptotically stable. In [Mel91], Melbourne considered a heteroclinic cycle composed of two equilibria that is attracting but not asymptotically stable: all initial conditions in a cusp-shaped region of phase space abutting the heteroclinic cycle give rise to trajectories that are not asymptotic to the cycle. To address this difference, Melbourne introduced the concept of *essential asymptotic stability*. The primary idea of this definition is that the proportion of initial conditions in a neighbourhood of the cycle that are asymptotic to the cycle increases to 1 as the neighbourhood shrinks. Therefore, although the cycle is not asymptotically stable, it is strongly attracting in some sense. Heteroclinic cycles can also be only weakly attracting without being completely unstable if the proportion of initial conditions in a neighbourhood of the cycle that are asymptotic to the cycle decreases to 0 as the neighbourhood shrinks. Such a cycle is said to be *essentially completely unstable*. Diagrammatic representations of these concepts are shown in Figure 1.2.

However, the stability of a cycle can be yet more subtle. The geometry of the basin of attraction of the cycle may change from one component heteroclinic orbit to another, and, as a result, the cycle may not be essentially asymptotically stable or essentially completely unstable. In [Pod12], Podvigina introduced a new concept, *fragmentary asymptotic stability*, which incorporates all possible stability arrangements. This definition is formulated by considering the Lebesgue measure of the set of all trajectories that both start, and remain in forward time in, a small neighbourhood of the cycle.

The stability of a heteroclinic cycle is typically analysed using return maps defined on

cross-sections that lie close to each equilibrium. If the return maps of a cycle have a certain form—which holds if the cycle falls into classes known as being of type Z [Pod12] or quasi-simple [GC19]—these return maps can be transformed into logarithmic coordinates where the resulting map is linear. This linear action is defined by a *transition matrix*, a process that was first introduced by Hofbauer [Hof87] and Field and Swift [FS91]. Podvigina [Pod12] has given three necessary and sufficient conditions on the eigenvalues and eigenvectors of the transition matrices of a cycle of type Z that guarantee the cycle is fragmentarily asymptotically stable. Garrido da Silva and Castro [GC19] extended these results to quasi-simple cycles. From the transition matrices of a cycle, *stability indices* can be calculated. These indices were introduced by Podvigina and Ashwin [PA11], and quantify the relative size of the basin of attraction of a cycle along each heteroclinic orbit.

Many authors have also studied bifurcations of heteroclinic cycles, which are often considered to be *resonant* or *transverse*. A resonance bifurcation is a global bifurcation, and occurs when an algebraic condition on the eigenvalues of the linearised vector field at the equilibria of the cycle is satisfied [SC92]. Generically, a resonance bifurcation is associated with the birth or death of a long-period periodic orbit, and the heteroclinic cycle changes stability after the bifurcation. On the other hand, a transverse bifurcation is a local bifurcation, and occurs when an eigenvalue of the linearised vector field at an equilibrium changes sign, and can result in most subtle changes in the type of stability of the cycle.

In their original paper, May and Leonard [ML75] observed a degenerate resonance bifurcation of a heteroclinic cycle—though they did not use this terminology—and they described the infinite family of stable periodic orbits that exists at the bifurcation. Guckenheimer and Holmes [GH88] also noted the existence of this family of periodic orbits. The first detailed study of a resonance bifurcation of a heteroclinic cycle appears to be that of Hofbauer [Hof87]. They proved that the loss of stability of the cycle was associated with the creation of a long-period periodic orbit. This study was followed by studies in equivariant bifurcation theory [AGH88, Arm89a, FS91, SC92]. The algebraic condition for a resonance bifurcation of all type B and C cycles in $\mathbb{R}^4$ was completed by Krupa and Melbourne [KM04]. A general condition for a resonant bifurcation of a robust homoclinic cycle—one where all equilibria lie in the same group orbit—of type C with any number of equilibria was determined by Postlethwaite and Dawes [PD10], who had earlier studied a codimension-two resonant bifurcation of a cycle that was not of type Z [PD06].

The earliest study of a transverse bifurcation we can identify is that of Campbell and Holmes [CH91]. Chossat, Krupa, Melbourne, and Scheel [CKM97] give a comprehensive study of transverse bifurcations of homoclinic cycles in $\mathbb{R}^4$, and identify the conditions under which a long-period periodic orbit bifurcates from the cycle. Lohse [Loh15] gives a complete

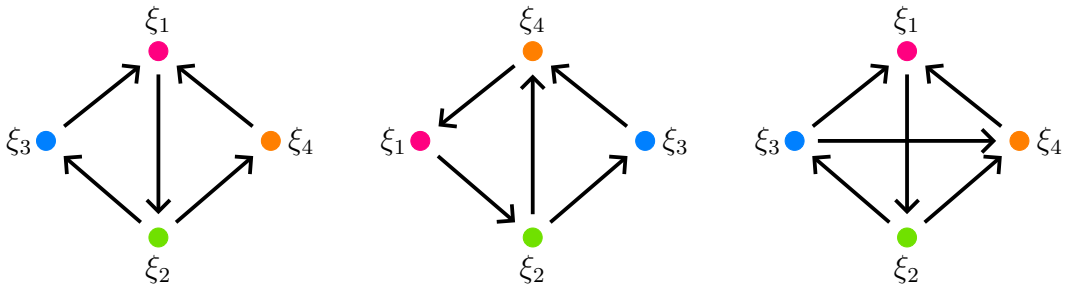

Figure 1.3: Diagrammatic representations of three heteroclinic networks between four equilibria in $\mathbb{R}^4$: (a) the Kirk–Silber network [KS94], (b) the Δ-clique network, and (c) the tournament network. All three networks were also studied in [Bra94] as networks on the tetrahedron. Coloured vertices represent hyperbolic saddle equilibria, and directed edges represent robust heteroclinic orbits.

study of transverse bifurcations of cycles of type B and type C in $\mathbb{R}^4$. Podvigina [Pod12] generalised many of these results by considering resonant and transverse bifurcations of heteroclinic cycles of type Z.

The study of bifurcations and stability of heteroclinic cycles has produced many novel and unexpected developments. In 2010, Postlethwaite [Pos10] identified a new bifurcation of a type C cycle in $\mathbb{R}^4$ that is associated with a pair of eigenvalues of the linearised vector field at one equilibrium becoming complex conjugate. This bifurcation changes the stability of the cycle, from essentially asymptotically stable to completely unstable, but is qualitatively different from those that had been studied before. Most notably, it is not associated with the birth or death of another dynamical object, such as a long-period periodic orbit.

An early example of an unexpected bifurcation of a heteroclinic cycle was studied by Kirk and Silber [KS94], where a cycle loses stability in the full system to perturbations in an orthogonal direction, though through neither a resonant nor transverse bifurcation, while still remaining asymptotically stable in a proper subspace that contains the cycle. This change in the dynamics of trajectories near the cycle does not necessarily seem to meet strict definitions of a bifurcation: for example, Guckenheimer and Holmes define a bifurcation as "*[a parameter] value…for which the flow…is not structurally stable…*" [GH83, Definition 3.1.1, p. 119]. Nevertheless, new types of asymptotic behaviour of trajectories arise that are qualitatively different, and there are changes to the stability properties of the flow-invariant structures in the system. As such, this example illustrates the complications that arise when studying heteroclinic cycles and the structures they can form. In particular, this bifurcation occurred because the cycle was part of a larger structure, known as a *heteroclinic network*.

Informally, a heteroclinic network is a connected union of heteroclinic cycles. A het-

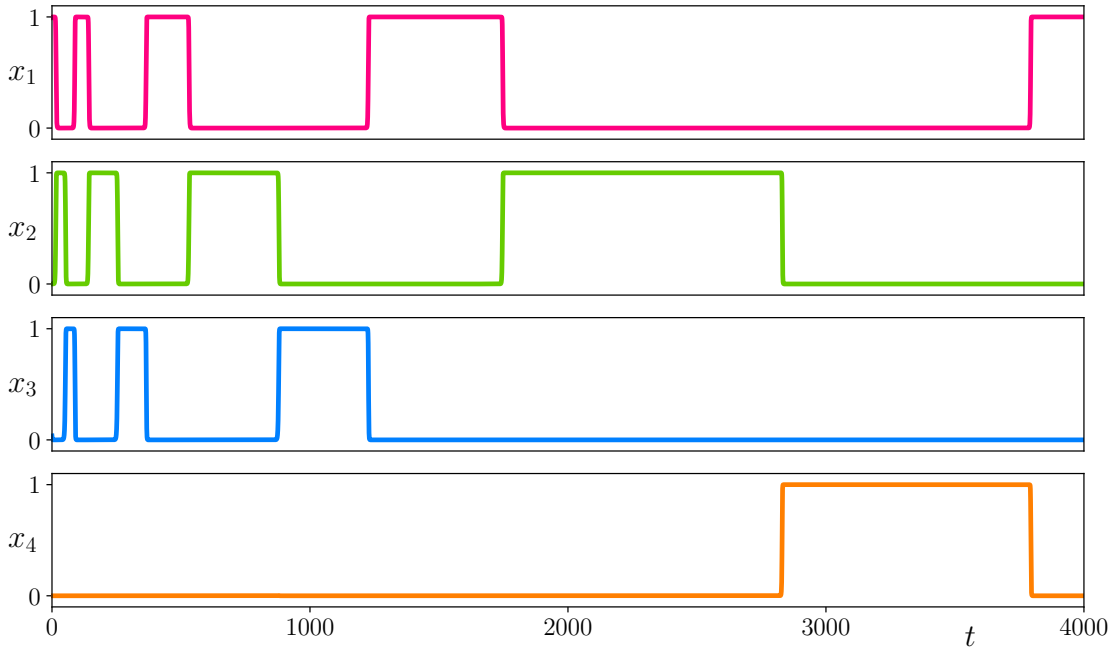

Figure 1.4: An example of a trajectory near the Kirk–Silber network that switches from one component cycle to the other. Parameter values and initial conditions used to produce this figure are given in §B.4.

eroclinic network exists in many of the equivariant systems discussed above, because of the symmetries of the system. However, the behaviour of trajectories near each component cycle is related by symmetry, and flow-invariant hyperplanes lie between all component cycles. Therefore, it is natural to eliminate this redundancy by identifying all cycles in the same group orbit [KS94, KM04, Pod12]. The earliest example in the literature of a heteroclinic network without this redundancy appears to be a 1992 study of equivariant bifurcation theory by Field and Richardson [FR92]. The network in [FR92] is composed of five equilibria and ten heteroclinic orbits, and has a structure equivalent to a complete graph on five vertices. However, Field and Richardson do not consider the network structure, only the network's component cycles in isolation. They note that the cycles co-exist, but do not consider the larger, connected structure. Early comprehensive studies of heteroclinic networks were completed by Kirk and Silber [KS94] and Brannath [Bra94], both in 1994. The networks studied in these papers are shown in Figure 1.3.

Kirk and Silber [KS94] studied the union of two cycles, each containing three equilibria, that share one heteroclinic orbit. These cycles are equivalent to that studied by [ML75] and [GH88]. Trajectories near the Kirk–Silber network are asymptotic to only one component cycle. However, they may make finitely many excursions around one cycle before switching to the other cycle. This switch can only occur once, and only in a particular direction, which

depends on the parameter values of the system. An example of a trajectory that switches between the cycles of the Kirk–Silber network is shown in Figure 1.4. Brannath also studied the Kirk–Silber network, as well as the two other networks that may be defined on the edges of the 3-simplex in $\mathbb{R}^4$. For certain parameter values, Brannath showed that trajectories may switch from one component cycle to the other, but that the ω-limit of a trajectory is one cycle, and not a larger subset of the network or the whole network. Brannath only considered these networks assuming certain relations between parameter values, but claimed "*…that there should be a quite general (but non-trivial) argument which excludes such a 'switching' for networks on* S_3*…*" [Bra94, p. 1381].

Since these early studies by Brannath and Kirk and Silber, several authors have studied heteroclinic networks, including their classification, stability properties, the dynamics of nearby trajectories, and also various methods to realise a given strongly-connected graph as a heteroclinic network in a dynamical system. For example, similar to the work to classify heteroclinic cycles, Castro and Lohse [CL16a] and Podvigina and Lohse [PL19] have classified all heteroclinic networks in $\mathbb{R}^4$ composed of simple heteroclinic cycles. Ashwin and Postlethwaite [AP13] give an algorithm to construct an equivariant vector field that realises a given strongly-oriented graph with n vertices as a heteroclinic network in $\mathbb{R}^n$. Stability of heteroclinic networks has been studied in [DH09, KPR12, AMY16, CL14, PCL20]. Moreover, several studies have considered heteroclinic networks in coupled cell systems [AF99, Fie15, AD17], various examples of interesting dynamics near networks [RL14, VVM20, HOP21, LR23, PR23], and their emergence in spatially-extended models of cyclic competition [GP23]. Several studies have been motivated by Boussineq convection [PA07, CLP10, PCL19]. Heteroclinic networks have also found applications in various fields, including neuroscience [AGR15, ACN16, YZS24] and cosmology [HU06, LRT13, SN23, LU24].

Kirk and Silber [KS94] and Brannath [Bra94] both considered switching of trajectories between cycles of the network, and many authors have considered such switching near heteroclinic networks in higher dimensions. Postlethwaite and Dawes [PD05] considered a heteroclinic network in $\mathbb{R}^6$ composed of six equilibria, shown in Figure 1.6(b). They showed that trajectories exist that are asymptotic to a larger subset of the network than one component cycle. In particular, they showed that there is sustained switching between subcycles of the network, and that this switching may happen in a periodic or aperiodic sequence. Similar behaviour is observed in trajectories near networks in $\mathbb{R}^5$ [CL16b]—see Figures 1.5(a) and 1.5(b)—and near a network in $\mathbb{R}^6$ [Pod23]—see Figure 1.6(a).

Some authors have introduced a notion of "switching" in heteroclinic networks that is unrelated to the ideas of the switching of a trajectory between subcycles of a network defined in [KS94]. These authors say that there is switching near a network if, for any infinite

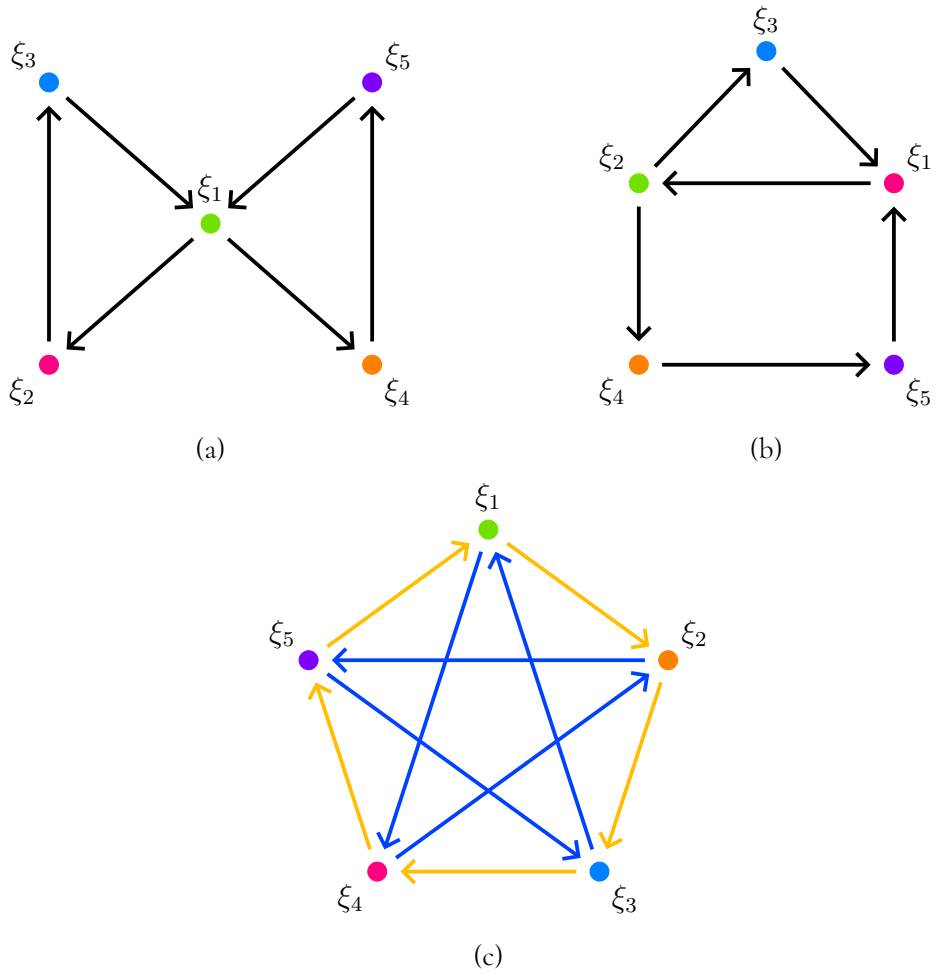

Figure 1.5: Diagrammatic representations of three heteroclinic networks between five equilibria in $\mathbb{R}^5$: (a) the bowtie network, (b) the house network, and (c) the Rock–Paper–Scissors–Lizard–Spock network. In (c), the heteroclinic orbits are coloured amber and blue for class A and B orbits, respectively.

sequence of heteroclinic orbits in the network, a trajectory exists that follows this sequence. Aguiar, Castro, and Labouriau [ACL04] study a network composed of two equilibria with complex eigenvalues, and prove that there is infinite switching near this network, due to the presence of a horseshoe of suspended horseshoes. They also prove that there is no infinite switching in a network that contains the Kirk–Silber network as a subnetwork. The same authors also prove infinite switching occurs in a class of networks in $\mathbb{R}^4$ [ACL06]. Other papers that have studied this type of infinite switching include [AC10, HK10, RLA11, Agu11, IR15, Rod16, RC23]. Recent work by Castro and Garrido da Silva [CG23] has considered this alternate notion of switching in more detail. In particular, they considered heteroclinic networks composed of a certain type of cycle (so-called *quasi-simple* cycles), where the linearised vector field at every equilibrium has only real eigenvalues. They proved that there exist some

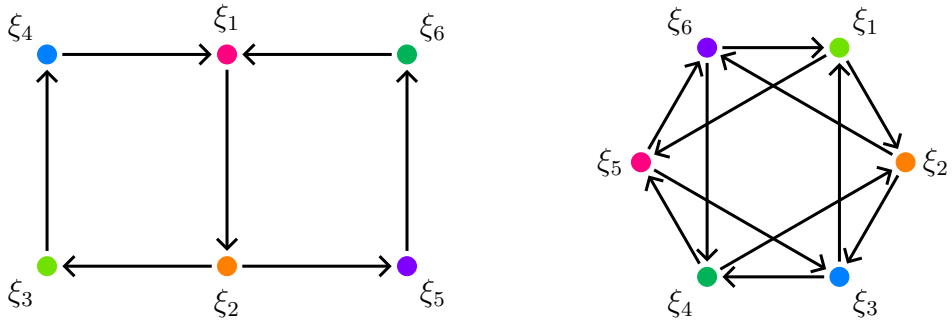

(a) (b)

Figure 1.6: Diagrammatic representations of two heteroclinic networks between six equilibria in $\mathbb{R}^6$: (a) Podvigina's two-cycle network [Pod23] and (b) the Postlethwaite–Dawes network [PD05].

sequences of heteroclinic orbits, which may be finite or infinite, that are not followed by any trajectory.

The dynamics near heteroclinic networks can be extremely intricate. Postlethwaite and Rucklidge [PR22] studied the dynamics of trajectories near the Rock–Paper–Scissors–Lizard–Spock network, a network in $\mathbb{R}^5$ composed of five equilibria. See Figure 1.5(c). This network also appeared in [FR92], and was also studied in [CFG22]. The heteroclinic orbits of this network can be classified as being either class A or B, and each equilibrium has an incoming and outgoing heteroclinic orbit of each class. Postlethwaite and Rucklidge studied trajectories that are asymptotic to this network and that follow certain periodic sequences of A and B orbits. In particular, they calculated regions of parameter space where certain periodic sequences are fragmentarily asymptotically stable, and showed that these regions create complicated patterns in parameter space, with two notable features. First, there is a Farey-like concatenation of certain stable periodic sequences. Second, these regions form chains in parameter space, where successive regions that belong to the same chain meet at a codimension-two point. Moreover, the corresponding root sequences of regions in the same chain are related by the exchange of an A with a BB. Postlethwaite and Rucklidge found that many of these stability regions lie outside the region of parameter space where the sufficient conditions of [PCL20] and [AMY16] for asymptotic stability hold, implying that these conditions are not necessary for the network to be at least fragmentarily asymptotically stable.

Evidently, the study of heteroclinic cycles and networks over the last five decades has provided many fruitful developments. For heteroclinic cycles, many general results have been derived about their classification and stability. There are several similar results for heteroclinic networks, though they are more sparse. In addition to considerations about classification and stability, for heteroclinic networks there is the additional complication of determin-

ing and understanding the possible routes that a trajectory can take around the network. In this regard, the study of heteroclinic networks is much more complicated, and only recently has it become fully evident how nuanced these properties can be. Most studies until now have focussed on specific examples of heteroclinic networks, and even then have not necessarily been able to completely classify all possible dynamics of trajectories near these networks. It would be desirable to have an understanding of how the structure of the network affects the dynamics of nearby trajectories. In other words, given a representation of a network as a directed graph, what topological features of this graph affect the dynamics of trajectories and how. Such an understanding would allow us to determine the properties of large classes of networks without studying them individually.

This thesis is concerned with the dynamics of trajectories near heteroclinic networks. In particular, we are interested in developing tools that help us analyse this dynamics and the long-term behaviour of trajectories. We develop a new methodology, the *projected map*, which is an extension of the transition matrix method, and we use this projected map to analyse the dynamics near certain heteroclinic networks. Although we cannot yet determine how features of a network affect the dynamics of nearby trajectories, we are able to understand the relationship between certain properties of dynamical systems containing heteroclinic networks and how they manifest in the projected map, and identify how the more complicated properties of heteroclinic networks that have so far been numerically computed but not analytically proven may be explained by employing the network's projected map.

§2 Outline of thesis

The remainder of this thesis is organised as follows.

In Chapter II, we overview the relevant background of this thesis. We give the technical definition of a heteroclinic cycle and network in §3, where we also consider some of the basic properties of these structures. We define in §4 the various notions of stability that apply to cycles and networks. The itinerary of a trajectory near a heteroclinic network is defined in §5. We also define the switching of trajectories between subcycles of a network, and give the definition of the regular or irregular cycling of a trajectory near a network. Analysis of heteroclinic cycles and networks, and necessary and sufficient conditions for the fragmentary asymptotic stability of a cycle, are presented in §6. In §7, we provide some basic notions from the theory of piecewise-smooth dynamical systems used in the following chapters.

Chapter III is concerned with deriving the *projected map* of a heteroclinic network, a piecewise-smooth map, and the analysis of the dynamics of trajectories near heteroclinic

networks in $\mathbb{R}^4$. We derive the return map of the Kirk–Silber network in §9 and then use it to define the projected map of the network. Then, in §10, we classify the dynamics of trajectories near the Kirk–Silber network with the projected map, through an analysis of the fixed points of this map and their stability and admissibility. In §11, we classify dynamics of trajectories near the Δ-clique network using its projected map. The projected map of the Δ-clique network is qualitatively different from that of the Kirk–Silber network, and more care is needed in using the projected map to deduce the dynamics of the network. In §12, we consider the tournament network. We provide its projected map, but, due to its complexity, do not provide an analysis to the same extent as the other two networks. Instead, we give a qualitative overview of the important aspects of its analysis and the resulting dynamics of trajectories near the tournament network. These results resolve the claim of Brannath [Bra94] that there is no regular or irregular cycling near these networks.

In the analysis in Chapter III, a certain relationship is identified between admissibility of fixed points of the projected map and Podvigina's third condition for stability. We generalise this relationship in Chapter IV for the projected map of an arbitrary heteroclinic network. We construct this projected map and derive some of its properties in §13. We prove in §14 that a border-collision bifurcation of the projected map, and thus a corresponding condition of certain transition matrices, corresponds to stability loss of a heteroclinic cycle in a network. In §15, we briefly consider Podvigina's two other conditions for stability of a heteroclinic cycle, and how the breaking of these conditions can manifest in the projected map.

In Chapter III, one of the observed properties of the projected map of the Kirk–Silber network is that it is discontinuous on the point that divides the two pieces of the projected map, while the projected maps of the Δ-clique network and tournament network are continuous on these points. Chapter V is concerned with studying this (dis)continuity, and we focus on the Kirk–Silber network and Δ-clique network for simplicity. We construct a *completed* return map in §17 that captures all trajectories near the two networks. To construct this map, we must linearise along the entire two-dimensional unstable manifold of the equilibrium near which the projected map is defined, which presents many difficulties. Although we cannot explicitly write down most of this map, we can derive sufficient properties about components of this map to resolve the continuity or discontinuity of the projected map. An analysis of this map in §18 allows us to prove that the discontinuity in the case of the Kirk–Silber network is due to the presence of a separatrix that causes the completed return map to be discontinuous in the limit as a trajectory approaches the network. No such separatrix exists in the case of the Δ-network, and so its projected map is continuous.

The dynamics of trajectories near networks in higher dimensions is considered in Chapter VI. We begin in §19 with the two-cycle network considered by Podvigina [Pod23]. We give

numerical examples of trajectories near this network that regularly switch between the subcycles of the network, and construct a bifurcation set of regular cycling near the network. We construct the network's projected map, and then relate periodic orbits in this map to regular cycling of trajectories near the network. The Rock–Paper–Scissors–Lizard–Spock network, studied by Postlethwaite and Rucklidge [PR22], is considered in §20. We overview their results, and then construct the network's projected map. The structure of the network presents additional complications to deriving the projected map. We again relate regular cycling to periodic orbits in this projected map, and also consider how irregular cycling near the network appears to emerge as a chaotic attractor in the projected map.

Lastly, in Chapter VII, we summarise our findings and discuss avenues for future research.

II | Background

In this chapter, we give the necessary background to understand the results presented in this thesis. We begin in §3 with the definitions of a heteroclinic cycle and a heteroclinic network, and some useful related concepts. We then proceed in §4 to give various definitions of stability relevant to the nuanced properties of heteroclinic cycles and networks, the most important of which are an invariant structure's δ-local basin of attraction and fragmentary asymptotic stability. In §5, we give the definition of an itinerary, which allows us to determine the route a trajectory takes around a network. We use this definition to define the property of a trajectory switching between subcycles of a network. We also introduce the notion of an eventually periodic itinerary with a particular root sequence, which allows us to define regular and irregular cycling between subcycles. Analysis of the stability of a heteroclinic cycle or network is introduced in §6. We construct a return map near the Guckenheimer–Holmes cycle in §6.1 as a simple example. General results for an arbitrary heteroclinic cycle are given in §6.2, and in §6.3 we extend these ideas to root sequences. Lastly, §7 briefly presents relevant ideas from the theory of piecewise-smooth dynamical systems, including the admissibility of fixed points and periodic orbits.

§3 Heteroclinic cycles and networks

We consider continuous-time dynamical systems of the form

$$\dot{x} = f(x), \tag{3.1}$$

where $x \in \mathbb{R}^n$ and $f\colon \mathbb{R}^n \to \mathbb{R}^n$ is an (at least) C^1-smooth vector field.

For a point $x_0 \in \mathbb{R}^n$, let $\phi(x_0, t)$ be the flow generated by (3.1) through x_0. Let ξ_j and ξ_k be two equilibria of (3.1). A ***heteroclinic orbit*** $\phi_{jk}(t)$ is a solution to (3.1) such that $\phi_{jk}(t) \to \xi_j$ as $t \to -\infty$ and $\phi_{jk}(t) \to \xi_k$ as $t \to \infty$. We also write $\xi_j \to \xi_k$ for a heteroclinic orbit $\phi_{jk}(t)$. We note that, by this definition as a specific solution to the ODEs (3.1), a heteroclinic orbit is a specific trajectory in phase-space. A heteroclinic orbit is thus also a one-dimensional submanifold of $W^u(\xi_j) \cap W^s(\xi_k) \neq \emptyset$. For convenience, we say that $\xi_j \to \xi_k$ is an *outgoing* orbit of ξ_j and *incoming* orbit of ξ_k.

Definition 3.1. A ***heteroclinic cycle*** is a set $\mathcal{C} \subseteq \mathbb{R}^n$ that is the union of a set of m distinct hyperbolic saddles $\{\xi_1, \ldots, \xi_m\}$ and a set of heteroclinic orbits $\{\phi_{12}(t), \ldots, \phi_{m1}(t)\}$, where $\phi_{jk}(t)$ is a heteroclinic orbit from ξ_j to ξ_k.

When discussing the equilibria of heteroclinic cycles with m equilibria, we implicitly take all operations involving indices modulo m, and therefore that $\xi_{m+1} \equiv \xi_1$.

Definition 3.2. Let $\mathcal{C}_1, \ldots, \mathcal{C}_s$, for $s \geq 2$, be a finite collection of heteroclinic cycles, such that there is at least one equilibrium not contained in every cycle. Then the union $\mathcal{N} = \bigcup_{j=1}^{s} \mathcal{C}_j$ is a ***heteroclinic network*** if, for every pair of equilibria, there exists a sequence of heteroclinic orbits connecting them; that is, if $\xi_a, \xi_b \in \mathcal{N}$, then there exists a set of p equilibria $\{\xi_{\ell_1}, \ldots, \xi_{\ell_p}\} \subseteq \mathcal{N}$ and p heteroclinic orbits $\{\phi_{\ell_1\ell_2}(t), \ldots, \phi_{\ell_p\ell_1}(t)\} \subseteq \mathcal{N}$, such that $\xi_{\ell_1} \equiv \xi_a$, $\xi_{\ell_p} \equiv \xi_b$, and $\phi_{\ell_i\ell_j}(t)$ is a heteroclinic orbit from ξ_{ℓ_i} to ξ_{ℓ_j}, where p is a positive integer.

Using this definition, there exists at least one equilibrium in the network with two outgoing heteroclinic orbits that are asymptotic to two distinct equilibria; that is, there exists three distinct equilibria ξ_k, ξ_x and ξ_y such that $\xi_k \to \xi_x$ and $\xi_k \to \xi_y$ are orbits of the heteroclinic network. We refer to all equilibria with two outgoing heteroclinic orbits that are asymptotic to two distinct equilibria as ***switching equilibria***.

As shown by Ashwin and Postlethwaite [AP13], any given strongly-oriented graph composed of n vertices can be realised as a heteroclinic cycle or network in an n-dimensional dynamical system, where the system of ODEs (3.1) takes the form

$$\dot{x}_j = x_j\left(1 - \|x\|_2^2 + \sum_{k\neq j} \alpha_{kj} x_k^2\right). \tag{3.2}$$

Other systems of ODEs also exist that contain robust heteroclinic cycles. These include, for example, the ODEs (3.2) with the addition of higher-order terms, and these equations are topologically conjugate, in the positive orthant, to generalised Lotka–Volterra equations (also said to be of May–Leonard type) following the coordinate transform $x_j^2 \mapsto x_j$.

It is straightforward to verify that the equations (3.2) have a hyperbolic saddle equilibrium ξ_j on each of the n coordinate axes at unit distance from the origin in the positive orthant. Moreover, they are $\mathbb{Z}_2^n$-equivariant, where the symmetries are reflections in each of the n coordinate hyperplanes. These symmetries ensure that the coordinate axes

$$L_j = \{(x_1, \ldots, x_j, \ldots, x_n) \in \mathbb{R}^n \mid x_i = 0 \text{ for all } i \neq j\}$$

and coordinate planes

$$P_{jk} = \{(x_1, \ldots, x_j, \ldots, x_k, \ldots, x_n) \in \mathbb{R}^n \mid x_i = 0 \text{ for all } i \neq j, k\}$$

are flow-invariant. For a given strongly-oriented graph, specific choices of the signs of the parameters α_{kj} ensure that certain equilibria are hyperbolic saddles or sinks in certain flow-invariant coordinate planes, and thus that the desired heteroclinic orbits exist between them. The given graph is thus realised as a heteroclinic network in the flow of the dynamical system.

A heteroclinic connection between a hyperbolic saddle and a hyperbolic sink in an invariant subspace is robust to sufficiently small perturbations that preserve the invariance of the subspace. As a result, the heteroclinic cycles and networks we consider are robust, and occur as codimension-zero phenomena; that is, they exist for an open set of parameter values.

When considering heteroclinic cycles and networks, the dimension of the stable or unstable manifold of an equilibrium may be greater than 1. Therefore, for two equilibria ξ_j and ξ_k, the intersection $W^u(\xi_j) \cap W^s(\xi_k) \neq \emptyset$ may be a submanifold of dimension two or more. An infinite number of heteroclinic orbits $\xi_j \to \xi_k$ therefore exist. As such, we emphasise that Definition 3.1 only allows for one heteroclinic orbit between two equilibria, and therefore a heteroclinic cycle is a one-dimensional flow-invariant structure. In the remainder of this thesis, we consider only heteroclinic networks that have one heteroclinic orbit between two equilibria, and therefore all heteroclinic networks we study are one-dimensional flow-invariant structures. Many of the networks we consider have $\dim(W^u(\xi_j) \cap W^s(\xi_k)) \geq 2$ for certain equilibria. In these cases, we highlight the single heteroclinic orbit we consider to be a component of the network, and this orbit is always contained in the flow-invariant coordinate plane P_{jk}.

Let ξ_j, ξ_k, and ξ_ℓ be three distinct equilibria of a heteroclinic cycle such that $\xi_j \to \xi_k$ and $\xi_k \to \xi_\ell$ are heteroclinic orbits of the cycle. Therefore, the orbit $\xi_j \to \xi_k$ lies in the coordinate plane P_{jk}, and the orbit $\xi_k \to \xi_\ell$ in $P_{k\ell}$. In [KM04], Krupa and Melbourne classify the eigenvalues of $\mathrm{D}f(\xi_k)$ as radial, contracting, expanding, or transverse depending on the subspace in which their corresponding eigenspace lies; this classification is given in Table 3.1.

Table 3.1: Classification of eigenvalues of $\mathrm{D}f(\xi_k)$ [KM04].

Eigenvalue class	Eigenvector subspace
Radial (r)	$V_k(r) = L_k \equiv P_{jk} \cap P_{k\ell}$
Contracting (c)	$V_k(c) = P_{jk} \cap L_k^{\perp}$
Expanding (e)	$V_k(e) = P_{k\ell} \cap L_k^{\perp}$
Transverse (t)	$V_k(t) = (P_{jk} + P_{k\ell})^{\perp}$

This definition, however, leads to some ambiguity in the case of heteroclinic networks. Suppose that ξ_a, ξ_k, ξ_x, and ξ_y are four distinct equilibria of a heteroclinic network such that $\xi_a \to \xi_k \to \xi_x$ and $\xi_a \to \xi_k \to \xi_y$ are heteroclinic orbits of the network. Therefore, ξ_a and ξ_k belong to more than one component cycle of the network—which we label $\mathcal{C}_{[x]}$ and $\mathcal{C}_{[y]}$—and ξ_k is a switching equilibrium of the network. Then, according to the definitions in Table 3.1, we can consider the eigenvalues of $\mathrm{D}f(\xi_k)$ with respect to the $\mathcal{C}_{[x]}$ cycle or the $\mathcal{C}_{[y]}$ cycle. For example, the expanding eigenspace could either be defined by $P_{kx} \cap L_k^{\perp}$ or $P_{ky} \cap L_k^{\perp}$. In the former case, the eigenvector of $\mathrm{D}f(\xi_k)$ in the direction of ξ_y belongs to the transverse eigenspace. In the latter case, the eigenvector of $\mathrm{D}f(\xi_k)$ in the direction of ξ_x belongs to the transverse eigenspace. Similarly, if there are two incoming heteroclinic orbits that are asymptotic to ξ_k, $\mathrm{D}f(\xi_k)$ has eigenvalues that can be classified as contracting or transverse, depending on which cycle is being considered.

We adopt the convention of [PCL20] and say that an eigenvalue of $\mathrm{D}f(\xi_k)$ is (globally) contracting if the corresponding eigenvector lies in the contracting eigenspace with respect to at least one cycle, that an eigenvalue of $\mathrm{D}f(\xi_k)$ is (globally) expanding if the corresponding eigenvector lies in the expanding eigenspace with respect to at least one cycle, and that an eigenvalue of $\mathrm{D}f(\xi_k)$ is (globally) transverse if the corresponding eigenvector lies in the transverse eigenspace with respect to *all* cycles of which ξ_k is a component equilibrium. Usually, we omit the word *globally*. However, we include it when it is useful to highlight this property. In the few specific instances that we need to emphasise that we are considering eigenvalues with respect to a particular cycle, we shall precede the name of the eigenvalue with *locally*; that is, locally contracting, locally expanding, or locally transverse. Note that all globally transverse eigenvalues are locally transverse, but that the converse does not necessarily hold.

With respect to the above example, the eigenvalues of $\mathrm{D}f(\xi_k)$ whose eigenvectors lie in the direction of ξ_x or ξ_y are both expanding. However, if we specifically consider the $\mathcal{C}_{[x]}$ cycle, then the eigenvalue whose eigenvector lies in the direction of ξ_y is *locally transverse*.

We write $-c_{kl} < 0$, $e_{kl} > 0$, and $-t_{kl}$ for the contracting, expanding, and transverse eigenvalues of $\mathrm{D}f(\xi_k)$. The constants c_{kl} and e_{kl} are necessarily positive. The constants t_{kl}

can be positive or negative. In this thesis, we consider only networks such that all transverse eigenvalues are negative; that is, that $-t_{kl} < 0$ and so the constants t_{kl} are positive.

§4 Stability of invariant sets

Stability properties of heteroclinic cycles and networks can be subtle, because positive locally transverse eigenvalues affect the geometry of the basin of attraction of the cycle or network. We assume throughout this section that X is a heteroclinic cycle or network, though these definitions readily apply to any compact flow-invariant set.

First, we write $d(\cdot,\cdot)$ for the usual Euclidean distance on $\mathbb{R}^n$, and define $d(y,X) = \inf_{x\in X} d(y,x)$. We write $\mu(\cdot)$ for the Lebesgue measure, and for a set $S \subseteq \mathbb{R}^n$, we write $\overline{S}$ for its topological closure. For any $r > 0$, we define the ***generalised ball of radius*** r of X, $N_r(X)$, as the set of all points $y \in \mathbb{R}^n$ within distance r from X:

$$N_r(X) = \{y \in \mathbb{R}^n \mid d(y,X) < r\}.$$

We define the ***ω-limit set*** of a point $x_0 \in \mathbb{R}^n$ as

$$\omega(x_0) = \bigcap_{T>0} \overline{\{\phi(x_0,t) \mid t > T\}}.$$

We say that a trajectory $\phi(x_0,t)$ is asymptotic to X if $\omega(x_0) \subseteq X$. The ***basin of attraction*** of X, $\mathcal{B}(X)$, is

$$\mathcal{B}(X) = \{x \in \mathbb{R}^n \mid \omega(x) \subseteq X\}.$$

The basin of attraction of X may include points that are quasi-asymptotic, but not asymptotic, to X; that is, trajectories starting near X that are asymptotic to X may first move away from X. Therefore, we also define, for all $\delta > 0$, the ***δ-local basin of attraction*** of X, $\mathcal{B}_\delta(X)$, as

$$\mathcal{B}_\delta(X) = \{x \in \mathbb{R}^n \mid \omega(x) \subseteq X \text{ and } \phi(x,t) \in N_\delta(X) \text{ for all } t \geq 0\}.$$

In [Pod12, Definition 2], Podvigina introduced the definition of fragmentary asymptotic stability: X is ***fragmentarily asymptotically stable*** if $\mu(\mathcal{B}_\delta(X)) > 0$ for all $\delta > 0$.

For a set $B \subseteq \mathbb{R}^n$ such that $X \subseteq \overline{B}$, X is ***asymptotically stable relative to*** B if, for every neighbourhood U of X, there exists a neighbourhood V of X, such that, for all $x \in V \cap B$, $\phi(x,t) \in U$ for all $t \geq 0$, and $\omega(x) \subseteq X$ [Ura64]. The set X is ***asymptotically stable*** if it is asymptotically stable relative to a neighbourhood of X, and X is ***essentially asymptotically***

stable if it is asymptotically stable relative to a set B such that

$$\lim_{r\to 0} \frac{\mu(B \cap N_r(X))}{\mu(N_r(X))} = 1.$$

It is generally agreed in the literature [Bra94, PA11, Loh15] that this definition of essential asymptotic stability is the corrected version of the definition given by Melbourne [Mel91] and Krupa and Melbourne [KM95b], and that the definition of essential asymptotic stability in [Mel91, Definition 1.1] is in fact equivalent to fragmentary asymptotic stability.

The set X is ***essentially completely unstable*** if it is asymptotically stable relative to a set B such that

$$\lim_{r\to 0} \frac{\mu(B \cap N_r(X))}{\mu(N_r(X))} = 0.$$

We schematically represent examples of invariant sets that satisfy different notions of stability in Figure 1.2.

If $\mu(\mathcal{B}(X)) = 0$ and there exists a set $D \subseteq \mathbb{R}^n$ of Lebesgue measure 0 such that $\mathcal{B}(X) \setminus (X \cup D)$ is non-empty, then X is ***almost completely unstable***. If there exists a neighbourhood U of X, and a set $D \subseteq \mathbb{R}^n$ of Lebesgue measure 0, such that, for all $x \in U \setminus D$, $\phi(x,t) \notin U$ for some $t > 0$, then X is ***completely unstable***. Note that these three definitions of essentially completely unstable, almost completely unstable, and completely unstable differ slightly from those used in some parts of the literature [Loh15, KM95b].

§5 Itineraries and cycling

Let $\mathcal{N}$ be a heteroclinic network containing the equilibria $\xi_1, \dots, \xi_m$.

For a trajectory sufficiently close to $\mathcal{N}$, we define its *itinerary* as the indices of the sequence of equilibria the trajectory visits; that is, $\mathcal{W} = (a_n)$, where $a_n \in \{1, \dots, m\}$. If the trajectory leaves a small neighbourhood of the network, the itinerary is a finite sequence, whereas a trajectory that is asymptotic to the network has an itinerary indexed by $\mathbb{N}$. We focus on this latter case. For convenience, let $I = \{1, \dots, m\}$.

We fix some $0 < H \ll \frac{1}{2} \min_{j,k\in I} d(\xi_j, \xi_k)$. As in [AP13, PR22], we define the function $\chi\colon \mathbb{R}^n \to I \cup \{0\} = \{0, \dots, m\}$ by

$$\chi(x_0) = \begin{cases} k, & \text{if there exists a } k \in I \text{ such that } d(x_0, \xi_k) < H, \\ 0, & \text{otherwise.} \end{cases}$$

The choice of H ensures that this function is well-defined.

Definition 5.1. For a point $x_0 \in \mathbb{R}^n$, the trajectory $\phi(x_0, t)$ has ***itinerary*** $\mathcal{W} = (a_n)_{n\in\mathbb{N}}$, where $a_n \in I$, if there exists some neighbourhood U of $\mathcal{N}$ such that $\phi(x_0, t) \in U$ for all $t \geq 0$, and there exists strictly increasing sequences of positive real numbers $(t_n)_{n\in\mathbb{N}}$ and $(s_n)_{n\in\mathbb{N}}$, where $t_n < s_n < t_{n+1}$ for all n, such that

1. $\chi(\phi(x_0, t)) = a_n$ for all $t_n < t < s_n$; and
2. $\chi(\phi(x_0, t)) = 0$ for all $s_n < t < t_{n+1}$.

The times t_n and s_n are the times that the trajectory enters and leaves a small neighbourhood of the equilibrium ξ_{a_n} and, between s_n and t_{n+1} the trajectory is close to the heteroclinic orbit $\xi_{a_n} \to \xi_{a_{n+1}}$. For example, the trajectory in Figure 1.1 has itinerary $(123)^\infty$, and the trajectory in Figure 1.4 has itinerary $(123)^3(124)^\infty$.

Definition 5.2. An itinerary $\mathcal{W}$ is ***eventually periodic with minimal period*** p ***and with root sequence*** $\mathcal{X} \in I^p$ if there exists a positive integer N such that $\mathcal{W}_{N+j} = \mathcal{X}_j$ for $1 \leq j \leq p$ and, for all $n > N$, $\mathcal{W}_{n+p} = \mathcal{W}_n$ and there does not exist a $p' < p$ such that $\mathcal{W}_{n+p'} = \mathcal{W}_n$.

If $\mathcal{C} = \xi_1 \to \xi_2 \to \cdots \to \xi_\ell \to \xi_1$ is a cycle of $\mathcal{N}$, let $\mathcal{X} = (12\ldots\ell)$. If a trajectory is asymptotic to $\mathcal{C}$, then its itinerary is eventually periodic with minimal period ℓ and root sequence some circular shift of $\mathcal{X}$. We say that $\mathcal{X}$, and every circular shift thereof, are the root sequences of $\mathcal{C}$.

Definition 5.3. If $\mathcal{C}_1$ and $\mathcal{C}_2$ are cycles of $\mathcal{N}$ with an equilibrium in common, then a trajectory $\phi(x_0, t)$ ***switches*** from $\mathcal{C}_1$ to $\mathcal{C}_2$ if there exists a root sequence $\mathcal{X}_1$ of $\mathcal{C}_1$ and $\mathcal{X}_2$ of $\mathcal{C}_2$ such that the itinerary of $\phi(x_0, t)$ has $(\mathcal{X}_1\mathcal{X}_2)$ as a subsequence.

Therefore, for a trajectory to have switched between cycles, it must, starting in a small neighbourhood of an equilibrium they have in common, make at least one full excursion around one cycle before returning to that equilibrium and then make at least one full excursion around the other cycle before returning to that equilibrium. We emphasise that our definition of *switching* is a property of a particular *trajectory*, and not a property of the heteroclinic network. This definition of switching is unrelated to the various notions of *switching at a node*, *switching along a connection*, or *finite switching* and *infinite switching near a network* used in papers such as [ACL04, CL16b, CG23]. Here, *switching* is used as it was by Kirk and Silber in [KS94].

If there is sustained switching between cycles of a network, we say that there is regular or irregular cycling, which has been studied in papers such as [PD05, PR22, Pod23].

Definition 5.4. If $\mathcal{C}_1, \ldots, \mathcal{C}_\mathrm{s}$ are cycles of a heteroclinic network, then a trajectory ***regularly cycles between*** $\mathcal{C}_1, \ldots, \mathcal{C}_\mathrm{s}$ if there exists a root sequence $\mathcal{X}_\ell$ of each cycle $\mathcal{C}_\ell$ such that the itinerary of $\phi(x_0, t)$ is eventually periodic with root sequence $(\mathcal{X}_1 \ldots \mathcal{X}_\mathrm{s})$.

Definition 5.5. A trajectory ***irregularly cycles*** if its itinerary is not eventually periodic.

We can extend the notions of stability in §4 to root sequences. We adapt the following from [PR22].

Definition 5.6. Given a root sequence $\mathcal{X} \in I^p$, for some positive integer p, the ***δ-local basin of attraction of $\mathcal{X}$***, $\mathcal{B}_\delta(\mathcal{X})$, is the set of all points $x \in \mathbb{R}^n$ such that $\omega(x) \subseteq \mathcal{N}$, $\phi(x,t) \in N_\delta(\mathcal{N})$ for all $t \geq 0$, and the itinerary of $\phi(x,t)$ is eventually periodic with minimal period p and with root sequence $\mathcal{X}$.

Definition 5.7. A root sequence $\mathcal{X} \in I^p$, for some positive integer p, is ***fragmentarily asymptotically stable*** if, for all $\delta > 0$, $\mu(\mathcal{B}_\delta(\mathcal{X})) > 0$.

§6 Return maps and transition matrices

The typical method to analyse the stability of heteroclinic cycles and networks, and the dynamics of nearby trajectories, is with return maps. In this section, we first construct a return map for the cycle studied by Guckenheimer and Holmes [GH88] (equivalent to that studied by May and Leonard [ML75]), as a simple example of the process to follow. This example follows the process outlined, for example, in [Mel91, Hof94, KS94, KM95a], or [Gle94, §12.3] in the case of a homoclinic bifurcation. We then discuss the general theory of return maps.

A return map is composed from two different types of maps: *local maps* and *global maps*, sometimes referred to, respectively, as *first-hit maps* and *connecting diffeomorphisms*. Local maps describe the behaviour of trajectories in a small neighbourhood of an equilibrium, and are constructed with the linearised flow near the equilibrium. Global maps describe the behaviour of trajectories close to the cycle's heteroclinic orbits, as the trajectory transitions from a small neighbourhood of one equilibrium to the next.

6.1 Return map for the Guckenheimer–Holmes cycle

The Guckenheimer–Holmes cycle is composed of three equilibria and three heteroclinic orbits: $\xi_1 \to \xi_2 \to \xi_3 \to \xi_1$. We show a representation of this cycle in Figure 6.1.

In the case of the Guckenheimer–Holmes cycle, the ODEs (3.2) take the form

$$\begin{aligned} \dot{x}_1 &= x_1\big(1 - \|x\|_2^2 - c_1 x_2^2 + e_1 x_3^2\big), \\ \dot{x}_2 &= x_2\big(1 - \|x\|_2^2 - c_1 x_3^2 + e_1 x_1^2\big), \\ \dot{x}_3 &= x_3\big(1 - \|x\|_2^2 - c_1 x_1^2 + e_1 x_2^2\big). \end{aligned} \tag{6.1}$$

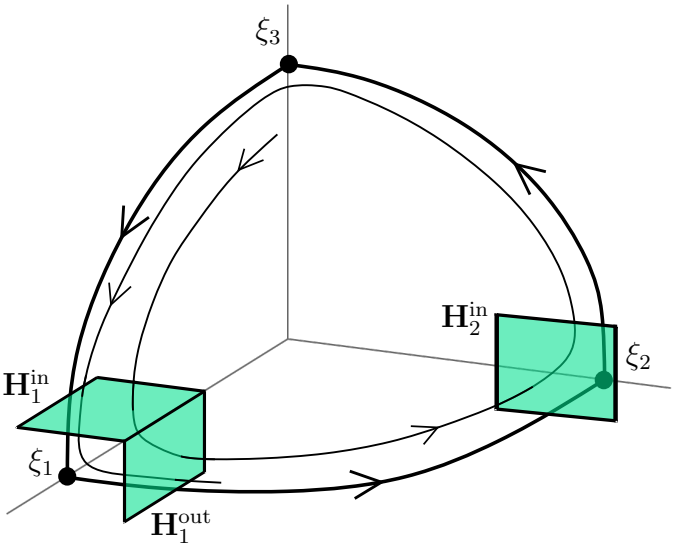

Figure 6.1: A visualisation of the Guckenheimer–Holmes cycle and the cross-sections used in its analysis. The local map ψ_1 approximates the dynamics of the orbits near ξ_1, contained between $\mathbf{H}_1^{\text{in}}$ and $\mathbf{H}_1^{\text{out}}$. The global map Ψ_{12} approximates the dynamics near the heteroclinic orbit from ξ_1 and ξ_2, between $\mathbf{H}_1^{\text{out}}$ and $\mathbf{H}_2^{\text{in}}$. Heteroclinic orbits are shown as bold lines, whereas the thinner line shows an example trajectory near the cycle.

These equations are $\mathbb{Z}_3 \ltimes \mathbb{Z}_2^3$-equivariant, generated by a cyclic permutation of the coordinate axes

$$\rho\colon (x_1, x_2, x_3) \mapsto (x_2, x_3, x_1)$$

and a reflection across the (x_2, x_3)-plane

$$\kappa_1\colon (x_1, x_2, x_3) \mapsto (-x_1, x_2, x_3).$$

A reflection across the (x_1, x_3)-plane is given by $\kappa_2 = \rho^2\kappa_1\rho$ and across the (x_1, x_2)-plane by $\kappa_3 = \rho\kappa_1\rho^2$. These reflections ensure that each coordinate axis and plane are flow-invariant fixed-point subspaces of some isotropy subgroup, and therefore that the cycle is robust.

We begin by constructing a local map near ξ_1, and to do so we define two cross-sections:

$$\mathbf{H}_1^{\text{in}} = \big\{(x_1, x_2, x_3) \in \mathbb{R}^3 \mid |x_1 - 1| < h, 0 \leq x_2 < h, x_3 = h\big\}$$

and

$$\mathbf{H}_1^{\text{out}} = \big\{(x_1, x_2, x_3) \in \mathbb{R}^3 \mid |x_1 - 1| < h, x_2 = h, 0 \leq x_3 < h\big\},$$

for some $h \ll 1$, sufficiently small to ensure the cross-sections are defined in a neighbourhood of approximate linear flow. The local map is then $\psi_1\colon \mathbf{H}_1^{\text{in}} \to \mathbf{H}_1^{\text{out}}$. The dynamical system defined by (3.2) has two important properties that help us construct this map. First, the

existence of n invariant planes near a hyperbolic equilibrium ensures that the linearised flow is at least C^1-diffeomorphic to the flow of the system, regardless of any resonances between the n eigenvalues of $\mathrm{D}f(\xi_1)$ [Hof94].

Second, the invariant-sphere theorem [Fie96] allows us to disregard the radial coordinate x_1, as it is not relevant in determining the stability of the cycle [Kru97]. As a result, since x_3 is fixed on $\mathbf{H}_1^{\text{in}}$, the only relevant coordinate on $\mathbf{H}_1^{\text{in}}$ is x_2, and since x_2 is fixed on $\mathbf{H}_1^{\text{out}}$, the only relevant coordinate on $\mathbf{H}_1^{\text{out}}$ is x_3.

The local map is properly defined with three variables: one is fixed by the definition of the cross-section, one is the radial coordinate, and a third coordinate. The first two variables have no effect on the stability of a heteroclinic cycle, nor the behaviour of nearby trajectories. The third coordinate only is relevant in the analysis of the local map. Therefore, in all that follows, we choose to abuse notation in the interests of simplicity when presenting this map—as well as the global map and compositions involving these maps—by providing only the expression of the map for relevant coordinates.

The relevant linearised flow near ξ_1 is

$$\begin{aligned}\dot{x}_2 &= e_1 x_2,\\ \dot{x}_3 &= -c_1 x_3.\end{aligned}$$

Since $\mathbf{H}_1^{\text{out}}$ is defined by $x_2 = h$, an initial condition $(x_1(0), x_2(0), x_3(0)) \in \mathbf{H}_1^{\text{in}}$ first strikes $\mathbf{H}_1^{\text{out}}$ at time

$$T = -\frac{1}{e_1}\log\left(\frac{x_2(0)}{h}\right),$$

known as the *residence time*. Since $x_3(0) = h$, we have $x_3(T) = h\left(\frac{x_2(0)}{h}\right)^{\frac{c_1}{e_1}}$. The local map is therefore given, to lowest order, by

$$\psi_1(x_2) = \left(h\left(\frac{x_2}{h}\right)^{\frac{c_1}{e_1}}\right).$$

We now construct the global map, which requires us to define

$$\mathbf{H}_2^{\text{in}} = \left\{(x_1, x_2, x_3) \in \mathbb{R}^3 \mid |x_2 - 1| < h, 0 \le x_3 < h, x_1 = h\right\}.$$

The global map is then $\Psi_{12}\colon \mathbf{H}_1^{\text{out}} \to \mathbf{H}_2^{\text{in}}$. The radial coordinate near ξ_2 is now x_2, and so, since x_1 is fixed, the relevant coordinate is x_3, the same as $\mathbf{H}_1^{\text{out}}$. Moreover, the (x_1, x_2)-plane is flow invariant, and therefore $\Psi_{12}(0) = 0$. We Taylor expand Ψ_{12} and find the leading order

expansion of the global map is

$$\Psi_{12}(x_3) = Ax_3,$$

for some $\mathcal{O}(1)$ positive constant A. We again have abused notation and present only the coordinate relevant to the analysis of the heteroclinic cycle.

Composing the local and global maps gives a map $\varphi_{312} = \Psi_{12}\psi_1 \colon \mathbf{H}_1^{\text{in}} \to \mathbf{H}_2^{\text{in}}$ defined by

$$\varphi_{312}(x_2) = Ah\Big(\frac{x_2}{h}\Big)^{\frac{c_1}{e_1}}.$$

We refer to this map as a *basic map*. In general, we need to construct two additional basic maps, $\varphi_{123} = \Psi_{23}\psi_2 \colon \mathbf{H}_2^{\text{in}} \to \mathbf{H}_3^{\text{in}}$ and $\varphi_{231} = \Psi_{31}\psi_3 \colon \mathbf{H}_3^{\text{in}} \to \mathbf{H}_1^{\text{in}}$. We can then compose these three maps together to construct three *full return maps*, which are to leading order:

$$\begin{aligned}
\Phi_1 &= \varphi_{231}\varphi_{123}\varphi_{312} \colon \mathbf{H}_1^{\text{in}} \to \mathbf{H}_1^{\text{in}},\\
\Phi_2 &= \varphi_{312}\varphi_{231}\varphi_{123} \colon \mathbf{H}_2^{\text{in}} \to \mathbf{H}_2^{\text{in}},\\
\Phi_3 &= \varphi_{123}\varphi_{312}\varphi_{231} \colon \mathbf{H}_3^{\text{in}} \to \mathbf{H}_3^{\text{in}}.
\end{aligned}$$

However, by the symmetry ρ, we have $\Phi_1 = (\rho\varphi_{312})^3$, and $\Phi_2 = \rho\Phi_1$ and $\Phi_3 = \rho^2\Phi_3$. Therefore, any fixed point of φ_{312} is also a fixed point of Φ_1, and thus also of the other two full return maps, with the same stability properties. As a result, we need only analyse the map φ_{312}.

We thus consider the following map, which is a leading order approximation of the flow of the dynamical system for all trajectories sufficiently close to the heteroclinic network:

$$y \mapsto ky^{\delta},$$

where $0 \leq y < h \ll 1$, $\delta = \frac{c_1}{e_1}$, and k is a positive constant. Again, we have abused notation here to present only the relevant coordinate.

The stability of the cycle can be determined from this map alone. The fixed point $y^\star = 0$ represents the heteroclinic cycle, and the fixed point $y^\star = k^{1/(1-\delta)}$, when it exists, represents a periodic orbit that lies in a small neighbourhood of the cycle. The cycle is stable when $\delta > 1$ and unstable when $\delta < 1$. A resonance bifurcation occurs at $\delta = 1$, which is supercritical if $k < 1$ and subcritical if $k > 1$. (The degenerate resonance bifurcation observed in [ML75, GH88] occurs if $k = 1$.)

6.2 Conditions for fragmentary asymptotic stability of a heteroclinic cycle

The analysis of a heteroclinic cycle with a return map defined on a cross-section is somewhat different from similar analysis of other types of invariant objects. For example, when considering a periodic orbit, only one cross-section needs to be defined, and thus only one return map needs to be considered. Where this cross-section is defined does not affect our conclusions derived from the analysis of the dynamics of trajectories near the periodic orbit; that is, analysis of a return map to any cross-section defined transverse to the periodic orbit provides qualitatively the same results. However, analysing a heteroclinic cycle presents additional complications. First, points on one cross-section may give rise to trajectories that do not return to that cross-section. However, for a different cross-section, all trajectories that arise from points on that cross-section may return to that cross-section. Second, trajectories may be asymptotic to the intersection of the heteroclinic cycle and a cross-section at one equilibrium, but not at other equilibria.

Therefore, the local maps ψ_{ijk} and global maps Ψ_{jk}, and therefore also the resulting basic maps φ_{ijk}, are generically different. Moreover, the full return maps Φ_j, although all defined in terms of the same basic maps, also differ, because the basic maps are composed in a different order for each full return map. As a result, the full return maps can have qualitatively different dynamics.

Therefore, when studying a heteroclinic cycle, we can only determine the asymptotic stability of the cycle by analysing full return maps for each equilibrium and verifying that trajectories are asymptotic to the cycle at each cross-section. In particular, under the flow of the dynamical system, an open set of initial conditions on a cross-section may not return to that cross-section, but that may only be the case for one particular cross-section. There is no way, however, to understand what may happen at each cross-section *a priori*. Therefore, it is necessary to consider a full return map for each equilibrium of the cycle.

For a heteroclinic cycle $\mathcal{C}$ composed of m equilibria $\xi_1, \dots, \xi_m$, there are m local maps $\psi_{ijk} \colon \mathbf{H}_j^{\mathrm{in},i} \to \mathbf{H}_j^{\mathrm{out},k}$ and m global maps $\Psi_{jk} \colon \mathbf{H}_j^{\mathrm{out},k} \to \mathbf{H}_k^{\mathrm{in},j}$. These maps can be composed into basic maps $\varphi_{ijk} = \Psi_{jk}\psi_{ijk} \colon \mathbf{H}_j^{\mathrm{in},i} \to \mathbf{H}_k^{\mathrm{in},j}$, which are then composed into full return maps $\Phi_j \colon \mathbf{H}_j^{\mathrm{in},i} \to \mathbf{H}_j^{\mathrm{in},i}$. As was the case for the specific examples given above for the Guckenheimer–Holmes cycle, these maps are a leading order approximation of the flow generated by the dynamical system for trajectories sufficiently close to the heteroclinic cycle. Moreover, when presenting these maps in the remainder of this thesis, we abuse notation as we did for the Guckenheimer–Holmes cycle and only present the coordinates of the map that are relevant to the analysis of the heteroclinic cycle.

For any cycle constructed with the simplex realisation [AP13], the dimension of the return map is $m-2$, as this realisation gives only one radial coordinate at each equilibrium. In the case that an equilibrium belongs to more than one cycle in a heteroclinic network, the full return map must be defined in a piecewise manner, to account for the trajectories that cycle around the different component cycles. For an equilibrium of a network $\mathcal{N}$ that is a component of the $\mathcal{C}_k$ cycle, we write $\Phi_j^{(k)}$ for the component of the return map to ξ_j that describes the behaviour of trajectories that make an excursion around the $\mathcal{C}_k$ cycle.

The basic maps and full return maps can be expressed in logarithmic coordinates with *transition matrices*. For any map $F\colon \mathbb{R}^p \to \mathbb{R}^p$ that has the form

$$F(x_1,\dots,x_p) = \left(C_1 x_1^{\alpha_{11}}\dots x_p^{\alpha_{1p}},\dots,C_p x_1^{\alpha_{p1}}\dots x_p^{\alpha_{pp}}\right), \tag{6.2}$$

where the C_j and α_{jk} are real numbers, we define its transition matrix $M(F)$ as

$$M(F) = \begin{pmatrix} \alpha_{11} & \cdots & \alpha_{1p} \\ \vdots & \ddots & \vdots \\ \alpha_{p1} & \cdots & \alpha_{pp} \end{pmatrix}.$$

It is straightforward to verify that, if F_1 and F_2 are functions of the form in (6.2), then $M(F_1\circ F_2) = M(F_1)M(F_2)$.

For type Z [Pod12] and quasi-simple [GC19] heteroclinic cycles, basic maps and full return maps have the form in (6.2). For basic maps φ_{ijk}, we write $m_{ijk} \equiv M(\varphi_{ijk})$, and refer to these matrices as *basic transition matrices*. For full return maps Φ_j, we write $M_j \equiv M(\Phi_j)$, and refer to these matrices as *full transition matrices*. Since each Φ_j is the composition of basic maps, the full transition matrices are products of basic transition matrices.

For a return map Φ_j defined on $\mathbf{H}_j^{\text{in}}$, the origin of $\mathbf{H}_j^{\text{in}}$ is the intersection of the heteroclinic cycle with $\mathbf{H}_j^{\text{in}}$. (Specifically, the origin is the intersection with the heteroclinic orbit $\xi_j \to \xi_k$.) A trajectory beginning at some point $x_0 \in \mathbf{H}_j^{\text{in}}$ is asymptotic to the heteroclinic cycle if $\lim_{n\to\infty}\Phi_j^n(x_0) = 0$. Since $0 < x < h \ll 1$, $X_0 \coloneqq \log x_0 < 0$, where we take a component-wise logarithm; that is, for $x = (x_1,\dots,x_n)\in\mathbb{R}^n$, $\log x = (\log x_1,\dots,\log x_n)$. Therefore, when we move to logarithmic coordinates, a trajectory is asymptotic to the heteroclinic cycle when $\lim_{n\to\infty} M_j^n X_0 \to -\infty$. We note that, when moving to logarithmic coordinates, the Lebesgue measure of a set may become unbounded [Pod12]. Therefore, the measure of a set is always considered in terms of the original coordinates $x\in\mathbb{R}^n$, even if we define the set in logarithmic coordinates. Podvigina [Pod12] gives sufficient conditions for fragmentary asymptotic stability of a heteroclinic cycle using properties of the eigenvalues and eigenvectors of the full transition matrices.

Theorem 6.1 ([Pod12, Theorem 5]). *For $1 \leq j \leq m$, let M_j be the full transition matrices associated with a heteroclinic cycle $\mathcal{C}$. Let $\lambda_{\max}$ denote the eigenvalue of M_j with largest absolute value, and $w_{\max}$ an associated eigenvector. The heteroclinic cycle $\mathcal{C}$ is fragmentarily asymptotically stable if, for all full transition matrices M_j, the following three conditions hold:*

(I) *$\lambda_{\max}$ is real;*

(II) *$\lambda_{\max} > 1$; and*

(III) *all entries of $w_{\max}$ are nonzero and have the same sign.*

As noted in [GC19], these conditions are in fact also necessary.

We do not reproduce here the proof of this theorem, as it is quite technical. However, it is reasonably straightforward to understand the fundamental idea behind the proof, which we now outline.

Let M be an $n \times n$ diagonalisable matrix with eigenvalues $\lambda_1, \ldots, \lambda_n$ and corresponding eigenvectors $w_1, \ldots, w_n$. Without loss of generality, we assume that $|\lambda_1| > |\lambda_j|$ for all $j > 1$. For any vector $v \in \mathbb{R}^n$, there exist constants $a_1, \ldots, a_n \in \mathbb{R}$ such that $v = \sum_j a_j w_j$. Then repeated mapping under M can be expressed as

$$M^k w = \sum_j \lambda_j^k a_j w_j. \tag{6.3}$$

Therefore, under iteration, as $k \to \infty$, the vector $M^k w$ is aligned with the eigenvector w_1, since the corresponding eigenvalue λ_1 has greatest absolute value. If the trajectory corresponding to v is asymptotic to the network, then as we noted previously $\lim_{k\to\infty} M^k v \to -\infty$. Therefore, we need to understand the conditions under which the expression in (6.3) diverges in all components to $-\infty$.

First, if $|\lambda_{\max}| \leq 1$, then, if $\lim_{k\to\infty} M^k v$ exists, the individual components of the iterates of $M^k v$ vanish or converge to a finite value. If $\lambda_{\max} \in \mathbb{C}$ and $|\lambda_{\max}| > 1$, then $\lim_{k\to\infty} M^k v$ does not exist, because the iterates of $M^k v$ are attracted to the plane spanned by the two eigenvectors of the complex-conjugate pair of eigenvalues $\lambda_{\max}$. If $\lambda_{\max} \in \mathbb{R}$ but $\lambda_{\max} < -1$, then $\lim_{k\to\infty} M^k v$ also does not exist as the signs of the individual components of $M^k v$ eventually alternate with odd and even k.

Therefore, only if $\lambda_{\max} \in \mathbb{R}$ and $\lambda_{\max} > 1$ do all individual components of $M^k v$ diverge in absolute value to ∞. For all components to diverge to $-\infty$, every component of $w_{\max}$ needs to be strictly positive or every component needs to be strictly negative—since if $w \in \mathbb{R}^n_+$ is an eigenvector of M, then so is $-w \in \mathbb{R}^n_-$, and vice-versa. Thus, we see that if any of these conditions are not satisfied, the measure of the δ-local basin of attraction must

vanish, as at most a set of Lebesgue measure 0 may diverge to $-\infty$ in every component under iteration of M.

The most complicated step in the proof is, assuming all three conditions in Theorem 6.1, constructing a set of points in the negative orthant that diverge in every coordinate to $-\infty$ under iteration of M, and then showing that this set has strictly positive Lebesgue measure.

For the full proof of this theorem, see [Pod12, Theorem 5].

As discussed at the start of this subsection, without any additional information, we need to confirm that the three properties in Theorem 6.1 are satisfied for every full transition matrix. This process is equivalent to determining, when studying the full return maps Φ_j, that all trajectories that begin on $\mathbf{H}_j^{\text{in}}$ return to $\mathbf{H}_j^{\text{in}}$ and are asymptotic to the cycle. However, Podvigina [Pod12] also proves that these conditions do not need to be verified for all full transition matrices. To understand why, suppose that for a cycle $\mathcal{C}$ of n equilibria $\xi_1, \dots, \xi_n$, we define n basic maps φ_{ijk}. Then the full transition matrix M_1 is defined by

$$M_1 = m_{(n-1)n1} \dots m_{234} m_{123} m_{n12}.$$

Moreover, the remaining transition matrices M_j for $1 < j \leq n$ are defined by some cyclic permutation of the product that defines M_1, and so take the form

$$M_j = m_{(j-2)(j-1)j} \dots m_{123} m_{n12} m_{(n-1)n1} \dots m_{j(j+1)(j+2)} m_{(j-1)j(j+1)}.$$

Next, assume λ is an eigenvalue of M_1 with eigenvector w. Then

$$\begin{aligned}
&M_j\big(m_{(j-2)(j-1)j} \dots m_{123} m_{n12}\big) w \\
&\quad = \big(m_{(j-2)(j-1)j} \dots m_{123} m_{n12} m_{(n-1)n1} \dots m_{(j-1)j(j+1)}\big)\big(m_{(j-2)(j-1)j} \dots m_{123} m_{n12}\big) w \\
&\quad = \big(m_{(j-2)(j-1)j} \dots m_{123} m_{n12}\big)\big(m_{(n-1)n1} \dots m_{(j-1)j(j+1)} m_{(j-2)(j-1)j} \dots m_{123} m_{n12}\big) w \\
&\quad = \big(m_{(j-2)(j-1)j} \dots m_{123} m_{n12}\big) M_1 w \\
&\quad = \lambda\big(m_{(j-2)(j-1)j} \dots m_{123} m_{n12}\big) w.
\end{aligned}$$

Therefore, we find that λ is also an eigenvalue of M_j, with eigenvector

$$\big(m_{(j-2)(j-1)j} \dots m_{123} m_{n12}\big) w;$$

that is, an eigenvector of M_j with eigenvalue λ is a multiple of an eigenvector w of M_1 with eigenvalue λ, pushed forward to the cross-section $\mathbf{H}_j^{\text{in},j-1}$, using the product of the basic transition matrices that map from $\mathbf{H}_1^{\text{in}}$ to $\mathbf{H}_j^{\text{in}}$.

Therefore, we need only check $\lambda_{\max} \in \mathbb{R}$ and $\lambda_{\max} > 1$ for one full transition matrix; if

this condition is satisfied for one full transition matrix, it is guaranteed to be satisfied for all full transition matrices, because all full transition matrices have the same spectrum. Next, if the eigenvector $w_{\max}$ of M_j satisfies the third condition of Theorem 6.1, and if $m_{(j-1)j(j+1)}$ has no negative entries, then the eigenvector $w_{\max}$ of M_{j+1} is guaranteed to also satisfy this condition. If $m_{(j-1)j(j+1)}$ has negative entries, it is no longer guaranteed that the eigenvector $w_{\max}$ of M_{j+1} satisfies this condition.

Therefore, let L be the set of indices $1 \leq \ell \leq n$ such that $m_{(\ell-1)\ell(\ell+1)}$ has negative entries. Then Theorem 6.1 holds if $\lambda_{\max} \in \mathbb{R}$ and $\lambda_{\max} > 1$ for M_1, and if, for all $\ell \in L$, all components of the eigenvector $w_{\max}$ of $M_{\ell+1}$ are non-zero and have the same sign. We emphasise that it is not that only these full transition matrices need to satisfy Podvigina's three conditions while other transition matrices can break the three conditions, but that verifying the conditions hold for these full transition matrices guarantees they hold for all full transition matrices.

This result can greatly reduce the number of computations required when determining if a heteroclinic cycle is fragmentarily asymptotically stable.

6.3 Conditions for fragmentary asymptotic stability of a root sequence

We can extend the result in Theorem 6.1 to a root sequence $\mathcal{X} \in I^p$ with minimal period some positive integer p, where $I = \{1, \ldots, m\}$ is again the set of indices of the equilibria of the network. Let $\mathcal{X}^{(k)}$ be the k-th left shift of $\mathcal{X}$; that is, $\mathcal{X}^{(k)}_j = \mathcal{X}_{j+k}$, where the subscript is taken modulo p. For example, if $\mathcal{X} = (1234)$, then $\mathcal{X}^{(1)} = (2341)$, $\mathcal{X}^{(2)} = (3412)$, and so on. Clearly, $\mathcal{X}^{(0)} = \mathcal{X}^{(p)} = \mathcal{X}$.

Next, let $\mathcal{X} = (a_1 a_2 \ldots a_p) \in I^p$ be a root sequence. We define the full transition matrix $M_{\mathcal{X}^{(0)}}$ as

$$M_{\mathcal{X}^{(0)}} = m_{a_{p-1}a_p a_1} m_{a_{p-2}a_{p-1}a_p} \ldots m_{a_2 a_3 a_4} m_{a_1 a_2 a_3} m_{a_p a_1 a_2};$$

that is, it is the full transition matrix found by multiplying the basic transition matrices that, beginning at the first equilibrium ξ_{a_1}, follow the given root sequence. For each $1 \leq k < p$, we define the matrix $M_{\mathcal{X}^{(k)}}$ similarly, by multiplying the basic transition matrices that follow the given root sequence $\mathcal{X}^{(k)}$, beginning at ξ_{a_k}. This matrix has the general form

$$M_{\mathcal{X}^{(k)}} = m_{a_{k-2}a_{k-1}a_k} m_{a_{k-3}a_{k-2}a_{k-1}} \ldots m_{a_{k+1}a_{k+2}a_{k+3}} m_{a_k a_{k+1}a_{k+2}} m_{a_{k-1}a_k a_{k+1}}.$$

We refer to the set of p transition matrices $\{M_{\mathcal{X}^{(k)}}\}$ for $0 \leq k < p$ as the ***collection of full transition matrices associated with*** $\mathcal{X}$. With this information, we give the following result,

which follows from [Pod12, Theorem 5], and which was also given as [PR22, Lemma 1].

Theorem 6.2. *Suppose $\mathcal{X} \in I^p$ is a root sequence, where p is a positive integer, and consider the collection of full transition matrices associated with this root sequence, $\{M_{\mathcal{X}^{(k)}} \mid 0 \leq k < p\}$. For each matrix, let $\lambda_{\max}$ and $w_{\max}$ be as in Theorem 6.1. Then, the root sequence $\mathcal{X}$ is fragmentarily asymptotically stable if and only if, for all full transition matrices $M_{\mathcal{X}^{(k)}}$:*

(I) *$\lambda_{\max}$ is real;*

(II) *$\lambda_{\max} > 1$; and*

(III) *all entries of $w_{\max}$ are nonzero and have the same sign.*

Again, to verify these results hold true for all full transition matrices, it suffices to check only a subset of the transition matrices. All matrices again have the same spectrum. Consider the set L of indices of all basic transition matrices $m_{(\ell-1)\ell(\ell+1)}$ that have a negative entry. Then only for the non-negative integers $k < p$ such that $\mathcal{X}_1^{(k)} = \ell + 1$ do we need to verify that $M_{\mathcal{X}^{(k)}}$ satisfies the third condition in Theorem 6.2.

§7 Piecewise-smooth dynamical systems

We conclude this chapter with a very brief overview of some of the theory of piecewise-smooth dynamical systems.

Consider a set $\mathcal{D} \subseteq \mathbb{R}^n$, finitely many subsets $S_i \subseteq \mathcal{D}$ with non-empty interior such that $\cup_i \overline{S_i} = \mathcal{D}$, and a collection of smooth functions $F_i \colon S_i \to \mathcal{D}$. A ***piecewise-smooth dynamical system*** is a map $F \colon \cup_i S_i \to \mathcal{D}$ defined by

$$F(x) = F_i(x), \text{ if } x \in S_i. \tag{7.1}$$

We assume the boundaries of the sets S_i are piecewise-smooth codimension-one manifolds. As such, the set $\Sigma_{ij} \coloneqq \overline{S_i} \cap \overline{S_j}$ is either a smooth codimension-one manifold or empty. The sets Σ_{ij} that are non-empty are called ***switching manifolds***. Formal solutions to the equation $F_i(x^\star) = x^\star$ may satisfy $x^\star \in S_i$, in which case we say that the fixed point is ***admissible***. However, if $x^\star \in S_j$ for some $j \neq i$, then we say that the fixed point is ***virtual***. If $x^\star \in \Sigma_{ij}$ for some $j \neq i$ such that Σ_{ij} is non-empty, we say there is a ***border-collision bifurcation***. If $x^\star \notin \mathcal{D}$, we also say that the fixed point is virtual.

It is possible for piecewise-smooth dynamical systems to have periodic orbits, and it is important to consider their admissibility. Let I be the index set of the partitions S_i of

the domain of the dynamical system (7.1). We can associate to an orbit $(x_j)_{n\in\mathbb{N}}$ of (7.1) the symbol sequence $\mathcal{X}\colon \mathbb{N} \to I$ by setting $\mathcal{X}_j = i \in I$ if $x_j \in S_i$. Then, if $\mathcal{X} \in I^p$ for some positive integer p, a set of p points $\{x_j\}_{j=1}^p$ forms an ***admissible $\mathcal{X}$-orbit of period*** p if

$$x_{i+1} = F_{\mathcal{X}_i}(x_i),$$

and each $x_i \in S_{\mathcal{X}_i}$; that is, each point of the periodic orbit lies in the correct domain of F.

These definitions are all that we need. However, for more on the general theory of piecewise-smooth dynamical systems, see [Sim16] for a review article, and [BBC08] for a comprehensive exposition.

III The projected map of heteroclinic networks in $\mathbb{R}^4$

The contents of this chapter are adapted from [GKP24, §2–4].

In this chapter, we analyse the dynamics of trajectories near three heteroclinic networks in $\mathbb{R}^4$: the Kirk–Silber network, the Δ-clique network, and the tournament network. We classify the behaviour of trajectories near these networks by introducing a new methodology in the study of heteroclinic cycles and networks: the *projected map*. This map is a piecewise-smooth one-dimensional map, derived from the network's transition matrices, which allows us to more easily determine the itineraries of trajectories near a network. We can also more easily determine the stability conditions of a component heteroclinic cycle. The results of this chapter confirm the claim by Brannath [Bra94] that there is no regular or irregular cycling of trajectories near these three networks. For any two given cycles, trajectories may switch at most once between them, and only in a particular direction, which depends on parameter values.

We begin in §8 by defining the three networks we consider.

In §9, we construct the projected map of the Kirk–Silber network. We first summarise the results of Kirk and Silber [KS94] and relate them to the work of Podvigina [Pod12]. We then consider the return map at the switching equilibrium of the Kirk–Silber network, and use properties of this return map to motivate the construction of a projected map. We then construct the projected map of the Kirk–Silber network and prove it is well-defined.

We classify the dynamics of trajectories near the Kirk–Silber network in §10 by studying the dynamics of the projected map. We calculate its fixed points and their stability and admissibility. We also show that a border-collision bifurcation of a fixed point of the projected map corresponds to stability loss of a component cycle of the network, as Podvigina's third condition for stability is no longer satisfied. This result allows us to study only the

projected map, and thus simplifies the analysis of the network. We also consider the continuity of the projected map on its switching manifold, and present some numerical examples of trajectories near the network.

We study in §11 the Δ-clique network. We present its projected map, and then use this map to classify the dynamics of trajectories near the network, which shows a qualitative difference from the results concerning the Kirk–Silber network. The analysis of the projected map is complicated by the fact that Podvigina's second stability condition is not necessarily realised as a property of the projected map, and so some care must be taken. Importantly, however, the correspondence between a border-collision bifurcation and Podvigina's third stability condition is maintained.

Lastly, we consider the tournament network in §12. We give the projected map of this network, but do not study it to the same detail as for the Kirk–Silber and Δ-clique networks, due to its complexity. We instead give an overview of how the projected map can be used to study the dynamics of the network, and present some examples of interesting dynamics near this network.

§8 Three heteroclinic networks in $\mathbb{R}^4$

We begin by defining the three heteroclinic networks in $\mathbb{R}^4$ that we study in this chapter. These three networks are all composed of four equilibria, $\xi_1, \dots, \xi_4$, which lie at unit distance from the origin in the positive orthant on each of the four coordinate axes. These networks are built from three different heteroclinic cycles. We assume that these cycles and networks are defined with the simplex realisation of Ashwin and Postlethwaite [AP13], and thus dynamical systems defined by the ODEs (3.2). The three different networks we consider are formed by specific choices of the signs of the constants α_{jk} in (3.2). We give explicit examples of the ODEs that admit the three networks we consider in (10.2), (11.2), and (12.2).

We consider two cycles with three equilibria:[1] $\mathcal{C}_{[3]} = \xi_1 \to \xi_2 \to \xi_3 \to \xi_1$ and $\mathcal{C}_{[4]} = \xi_1 \to \xi_2 \to \xi_4 \to \xi_1$. We consider one cycle with four equilibria:[2] $\mathcal{C}_{[34]} = \xi_1 \to \xi_2 \to \xi_3 \to \xi_4 \to \xi_1$.

The three heteroclinic networks we study are:

1. The *Kirk–Silber network* [KS94], the union of two cycles: $\mathcal{N}_{\mathrm{KS}} = \mathcal{C}_{[3]} \cup \mathcal{C}_{[4]}$.

2. The Δ*-clique network*, the union of two cycles: $\mathcal{N}_{\Delta} = \mathcal{C}_{[34]} \cup \mathcal{C}_{[4]}$.

[1] In the terminology of Krupa and Melbourne [KM04], these cycles are of type B_3^-.
[2] Of type C_4^- [KM04].

3. The *tournament network*, the union of all three cycles: $\mathcal{N}_{\mathrm{T}} = \mathcal{C}_{[3]} \cup \mathcal{C}_{[34]} \cup \mathcal{C}_{[4]}$.

Figure 1.3 gives diagrammatic representations of these three networks. The Kirk–Silber network was first studied in [KS94]. The directed triangle of heteroclinic orbits $\xi_2 \to \xi_4$ and $\xi_2 \to \xi_3 \to \xi_4$ in the second network was termed a Δ-clique in [ACL20, PCL20], and so we name it the Δ-*clique network*. The graph of the third network is the only one of the three networks that forms a tournament in the graph-theoretic sense, and so we name it the *tournament network*. The tournament network is also studied in [CFL24], where it is known as the *Jungle Game*. As shown by Castro and Lohse [CL16a] and Lohse and Podvigina [PL19], these are the only three heteroclinic networks in $\mathbb{R}^4$ that contain four equilibria and are constructed from type Z cycles.

As mentioned in §3, we consider only a single one-dimensional heteroclinic orbit to be part of each cycle and thus each network. For all three networks, all heteroclinic orbits $\xi_j \to \xi_k$ are contained in the two-dimensional flow-invariant (x_j, x_k)-coordinate plane. In the case of the Kirk–Silber network, there is a two-dimensional continuum of orbits $W^u(\xi_2) \cap W^s(\xi_3)$ and $W^u(\xi_2) \cap W^s(\xi_4)$, as well as $W^u(\xi_3) \cap W^s(\xi_1)$ and $W^u(\xi_4) \cap W^s(\xi_1)$. For the Δ-clique and tournament networks, the intersection $W^u(\xi_2) \cap W^s(\xi_4)$ is also two-dimensional, as is $W^u(\xi_3) \cap W^s(\xi_1)$ for the tournament network. All of these intersections are properly contained in some three-dimensional subspace, but only a single one-dimensional heteroclinic orbit is properly contained in a two-dimensional plane. For all three networks, only this heteroclinic orbit is considered to be part of the network.

§9 Construction of the projected map

To construct the projected map of the Kirk–Silber network, we begin by constructing its return maps and transition matrices, following the methodology we outlined in §6.

9.1 Return maps near the Kirk–Silber network

Consider, for example, $\xi_3 = (0, 0, 1, 0)$. We define local coordinates by translating ξ_3 to the origin, writing $u_3 = x_3 - 1$. Rescaling the coordinates as necessary to ensure we are in a neighbourhood of approximate linear flow, we define two cross-sections in a small neighbourhood of ξ_3:

$$\mathbf{H}_3^{\mathrm{in},2} = \big\{(x_1, x_2, u_3, x_4) \;\big|\; |u_3| < 1, x_2 = 1, 0 < x_1, x_4 < 1\big\}$$

and

$$\mathbf{H}_3^{\text{out},1} = \big\{(x_1, x_2, u_3, x_4) \;\big|\; |u_3| < 1, x_1 = 1, 0 < x_2, x_4 < 1\big\}.$$

The cross-section $\mathbf{H}_3^{\text{in},2}$ is transverse to the orbit $\xi_2 \to \xi_3$, and $\mathbf{H}_3^{\text{out},1}$ is transverse to $\xi_3 \to \xi_1$.

In the system (3.2), there is an attracting invariant sphere [Fie96], and so the radial coordinate u_3 does not affect the stability of the cycle [KS94, Kru97, Pod12]. Thus, we can consider two-dimensional subsets of the cross-sections, and the relevant coordinates are x_1, and x_4 in $\mathbf{H}_3^{\text{in},2}$ and x_2 and x_4 $\mathbf{H}_3^{\text{out},1}$. The local map $\psi_{231}\colon \mathbf{H}_3^{\text{in},2} \to \mathbf{H}_3^{\text{out},1}$ approximates the dynamics of trajectories between these two cross-sections using the linear flow near ξ_3 and the residence time of a trajectory between the two sections, and is given, to leading order, by

$$\psi_{231}(x_1, x_4) = \left(x_1^{\frac{c_{32}}{e_{31}}}, x_4\, x_1^{\frac{t_{34}}{e_{31}}}\right).$$

Again, we have abused notation in presenting this local map, and only give the expressions for coordinates that affect the analysis of the $\mathcal{C}_{[3]}$ cycle. We continue to do this for all maps in this chapter, though we do not explicitly highlight it each time.

To approximate the dynamics near the orbit $\xi_3 \to \xi_1$, we define a cross-section in a small neighbourhood of ξ_1, transverse to the heteroclinic orbit $\xi_3 \to \xi_1$:

$$\mathbf{H}_1^{\text{in},3} = \big\{(u_1, x_2, x_3, x_4) \;\big|\; |u_1| < 1, x_3 = 1, 0 < x_2, x_4 < 1\big\}.$$

Again, the radial coordinate, now u_1, can be neglected. The relevant coordinates are $(x_2, x_4) \in \mathbf{H}_1^{\text{in},3}$, the same as those on $\mathbf{H}_3^{\text{out},1}$. By the flow-invariance of the coordinate hyperplanes, the global map $\Psi_{31}\colon \mathbf{H}_3^{\text{out},1} \to \mathbf{H}_1^{\text{in},3}$ can be written, to lowest order, as

$$\Psi_{31}(x_2, x_4) = (\alpha_{31} x_2, \beta_{31} x_4),$$

where α_{31} and β_{31} are $\mathcal{O}(1)$ positive constants.

We define the basic map $\varphi_{231} = \Psi_{31} \circ \psi_{231}\colon \mathbf{H}_3^{\text{in},2} \to \mathbf{H}_1^{\text{in},3}$. After repeating this process for all equilibria and appropriate cycles, we compose these basic maps into the six full return maps of the network, $\Phi_j\colon \mathbf{H}_j^{\text{in},i} \to \mathbf{H}_j^{\text{in},i}$. We write $\Phi_j^{(3)}$ or $\Phi_j^{(4)}$ for a return map to an incoming cross-section defined near ξ_j that describes trajectories that make an excursion around the $\mathcal{C}_{[3]}$ or $\mathcal{C}_{[4]}$ cycle, respectively.

For the Kirk–Silber network, only m_{123} and m_{124} have negative entries (see §B.1), and so we only have to check the stability conditions of Theorem 6.1 at ξ_3 and ξ_4. Applying the conditions of Theorem 6.1 to the full transition matrices $M_3^{(3)}$ and $M_4^{(4)}$ allows us to conclude that the $\mathcal{C}_{[3]}$ cycle is fragmentarily asymptotically stable if and only if $\delta_3 > 1$ and $\nu_3 > 0$,

and that the $\mathcal{C}_{[4]}$ cycle is fragmentarily asymptotically stable if and only if $\delta_4 > 1$ and $\nu_4 > 0$, where

$$\begin{aligned} \delta_3 =& \frac{c_{13}c_{21}c_{32}}{e_{12}e_{23}e_{31}} > 0, \\ \delta_4 =& \frac{c_{14}c_{21}c_{42}}{e_{12}e_{24}e_{41}} > 0, \\ \nu_3 =& \frac{t_{34}}{e_{31}} + \frac{c_{14}c_{32}}{e_{12}e_{31}} - \frac{c_{13}c_{32}e_{24}}{e_{12}e_{23}e_{31}}, \end{aligned} \tag{9.1}$$

and

$$\nu_4 = \frac{t_{43}}{e_{41}} + \frac{c_{13}c_{42}}{e_{12}e_{41}} - \frac{c_{14}c_{42}e_{23}}{e_{12}e_{24}e_{41}}.$$

These conditions for stability were derived by Kirk and Silber in [KS94]. Moreover, Kirk and Silber [KS94] prove that, if $\nu_3 < 0$, then trajectories switch from the $\mathcal{C}_{[3]}$ cycle to the $\mathcal{C}_{[4]}$ cycle, and vice-versa if $\nu_4 < 0$. They also show that ν_3 and ν_4 cannot both be simultaneously negative.

The equilibrium ξ_2 has more than one outgoing heteroclinic orbit, and so it is a switching equilibrium of the Kirk–Silber network. Moreover, for the Kirk–Silber network, ξ_2 is the only switching equilibrium. As such, where a trajectory strikes $\mathbf{H}_2^{\text{in},1}$ determines which cycle the trajectory next cycles around. Therefore, to study the itinerary of trajectories near the Kirk–Silber network, we focus our analysis on $\mathbf{H}_2^{\text{in},1}$. We define the incoming cross-section at ξ_2 as

$$\mathbf{H}_2^{\text{in},1} = \big\{(x_1, u_2, x_3, x_4) \;\big|\; |u_2| < 1, x_1 = 1, 0 < x_3, x_4 < 1\big\}.$$

The relevant coordinates on this section are x_3 and x_4. The curve $x_3^{e_{24}} = x_4^{e_{23}}$ divides $\mathbf{H}_2^{\text{in},1}$ into trajectories that leave a small neighbourhood of ξ_2 in the direction of ξ_3 or ξ_4.

We consider the subsets of $\mathbf{H}_2^{\text{in},1}$ defined by

$$\Gamma_3 = \left\{ x \in \mathbf{H}_2^{\text{in},1} \mid (1-\epsilon) x_3^{\frac{e_{24}}{e_{23}}} > x_4 \right\} \tag{9.2}$$

and

$$\Gamma_4 = \left\{ x \in \mathbf{H}_2^{\text{in},1} \mid (1-\epsilon) x_4^{\frac{e_{23}}{e_{24}}} > x_3 \right\}, \tag{9.3}$$

where $0 < \epsilon < 1$. The term $(1-\epsilon)$ excludes from Γ_3 and Γ_4 all points that lie too close to the separatrix dividing the basins of attraction of the $\mathcal{C}_{[3]}$ and $\mathcal{C}_{[4]}$ cycles, and so trajectories that do not strike $\mathbf{H}_3^{\text{in},2}$ or $\mathbf{H}_4^{\text{in},2}$. In defining these subsets, and other subsets of cross-sections, we

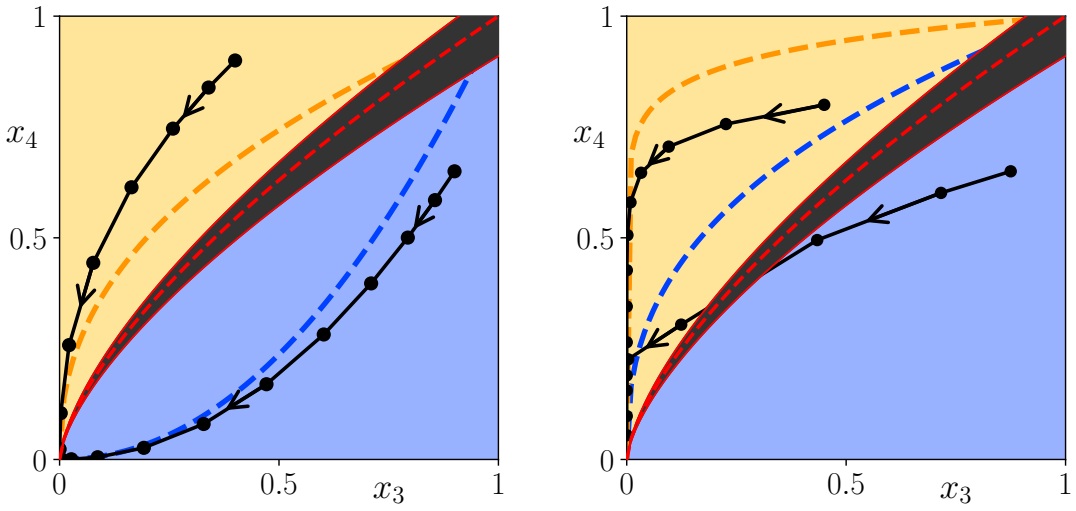

Figure 9.1: Examples of the action of the return map $\Phi\colon \mathbf{H}_2^{\text{in},1} \to \mathbf{H}_2^{\text{in},1}$ for (a) $\nu_3 > 0$ and (b) $\nu_3 < 0$. Points in the same orbit have been joined for clarity only. The domain Γ_3 is shaded blue, Γ_4 orange, and the excluded cusp Γ_c black. The dashed blue and orange lines are the curves Σ_3^* and Σ_4^* (defined in §9.2). The switching curve Σ_s is a dashed red line, and Σ_c^- and Σ_c^+ are solid red lines. Parameter values and initial conditions for these figures are given in §B.5.1.

again abuse notation and do not explicitly include the coordinate that is fixed to define the cross-section, nor the radial coordinate.

We refer to the subset of $\mathbf{H}_2^{\text{in},1}$ between Γ_3 and Γ_4 as the *excluded cusp*, defined as $\Gamma_c := \mathbf{H}_2^{\text{in},1} \setminus (\Gamma_3 \cup \Gamma_4)$. We refer to the curve defined by $x_3^{e_{24}} = x_4^{e_{23}}$ as the *switching curve*, and denote it Σ_s. Furthermore, the boundary between Γ_c and Γ_3 is denoted Σ_c^+, and the boundary between Γ_c and Γ_4 is denoted Σ_c^-. Unlike Kirk and Silber, we do not need to assume that $e_{23} > e_{24}$, as we are not concerned with the conditions for essential asymptotic stability of the component cycles, only that they are fragmentarily asymptotically stable. We do however assume the genericity condition that $e_{23} \neq e_{24}$. Therefore, either Γ_3 or Γ_4 can be cusp-shaped, and the other is shaped like the complement of a cusp.

The sets Γ_3 and Γ_4 are the domains of definition of the local maps $\psi_{123}\colon \Gamma_3 \to \mathbf{H}_2^{\text{out},3}$ and $\psi_{124}\colon \Gamma_4 \to \mathbf{H}_2^{\text{out},4}$, respectively, and so also of the full return maps $\Phi_2^{(3)}\colon \Gamma_3 \to \mathbf{H}_2^{\text{in},1}$ and $\Phi_2^{(4)}\colon \Gamma_4 \to \mathbf{H}_2^{\text{in},1}$. The full return map $\Phi_2\colon \Gamma_3 \cup \Gamma_4 \to \mathbf{H}_2^{\text{in},1}$ is, to lowest order, and presenting only the relevant coordinates,

$$\Phi_2(x_3, x_4) = \begin{cases} \Phi_2^{(3)}(x_3, x_4) = (A_{32} x_3^{\delta_3}, B_{32} x_3^{\rho_3} x_4), & \text{if } (x_3, x_4) \in \Gamma_3, \\ \Phi_2^{(4)}(x_3, x_4) = (A_{42} x_3 x_4^{\rho_4}, B_{42} x_4^{\delta_4}), & \text{if } (x_3, x_4) \in \Gamma_4, \end{cases} \tag{9.4}$$

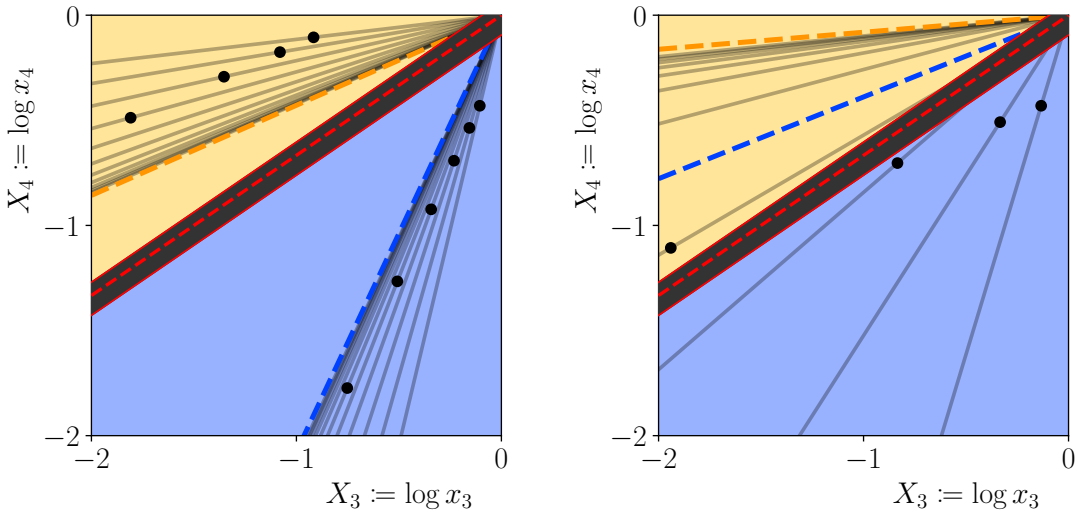

Figure 9.2: Examples of the action of the map $M\colon \mathbb{R}^2_- \to \mathbb{R}^2_-$ for (a) $\nu_3 > 0$ and (b) $\nu_3 < 0$. In this figure, vectors extend from the origin to the black dots, and the linear subspace containing each vector is a solid grey line. The domain of $\mathcal{D}_3$ is shaded blue, $\mathcal{D}_4$ orange, and $\mathcal{D}_c$ black. The dashed blue and orange lines are the eigenspaces W_3^* and W_4^*. The vectors can be seen to converge to these eigenspaces under iteration of M. The switching subspace W_s is a dashed red line, and the two affine subspaces W_c^- and W_c^+ are solid red lines. For clarity, (b) shows the logarithm of only one of the trajectories in Figure 9.1(b), that trajectory that switches from the $\mathcal{C}_{[3]}$ cycle to the $\mathcal{C}_{[4]}$ cycle. Parameter values and initial conditions for these figures are given in §B.5.1.

where A_{32}, B_{32}, A_{42}, and B_{42} are $\mathcal{O}(1)$ constants, and

$$\rho_3 = -\frac{e_{24}}{e_{23}} + \frac{c_{21}t_{34}}{e_{23}e_{31}} + \frac{c_{14}c_{21}c_{32}}{e_{12}e_{23}e_{31}}$$

and

$$\rho_4 = -\frac{e_{23}}{e_{24}} + \frac{c_{21}t_{43}}{e_{24}e_{41}} + \frac{c_{13}c_{21}c_{42}}{e_{12}e_{24}e_{41}}.$$

As shown by Kirk and Silber [KS94], if $\delta_3 > 1$, then $\nu_3 > 0$ implies $\rho_3 > 0$, and if $\delta_4 > 1$, then $\nu_4 > 0$ implies $\rho_4 > 0$. From here, our primary focus is this return map, and so we write simply $\Phi \equiv \Phi_2$, $\Phi_3 \equiv \Phi_2^{(3)}$, and $\Phi_4 \equiv \Phi_2^{(4)}$. Examples of the action of the map Φ are shown in Figure 9.1 for both $\nu_3 > 0$ (panel (a))—where there is no switching between cycles—and $\nu_3 < 0$ (panel (b))—where there is switching from the $\mathcal{C}_{[3]}$ to $\mathcal{C}_{[4]}$ cycle.

The return maps Φ_3 and Φ_4 have corresponding transition matrices

$$M_3 = \begin{pmatrix} \delta_3 & 0 \\ \rho_3 & 1 \end{pmatrix}$$

and

$$M_4 = \begin{pmatrix} 1 & \rho_4 \\ 0 & \delta_4 \end{pmatrix}.$$

Let $X_3 := \log x_3 < 0$ and $X_4 := \log x_4 < 0$. These matrices act on subsets of $\mathbb{R}^2_-$—the negative orthant of $\mathbb{R}^2$—that correspond to the sets Γ_3 and Γ_4 in logarithmic coordinates. We label these subsets as $\mathcal{D}_3$ and $\mathcal{D}_4$, respectively. We define $\mathcal{D}_c$ to be Γ_c in logarithmic coordinates. Setting $w_s = (1, \frac{e_{24}}{e_{23}})$, which we call the *switching vector*, we define the *switching subspace* W_s as the span of w_s, which is Σ_s in logarithmic coordinates. We also write W_s^+ and W_s^- for the one-dimensional affine subspaces that correspond to the curves Σ_c^+ and Σ_c^-. The lines W_s^+ and W_s^- are parallel to W_s and do not pass through the origin.

We can then define a map $M : \mathcal{D}_3 \cup \mathcal{D}_4 \to \mathbb{R}^2_-$ by

$$M(X_3, X_4) = \begin{cases} M_3(X_3, X_4) = \begin{pmatrix} \delta_3 & 0 \\ \rho_3 & 1 \end{pmatrix} \begin{pmatrix} X_3 \\ X_4 \end{pmatrix}, & \text{if } (X_3, X_4) \in \mathcal{D}_3, \\ \\ M_4(X_3, X_4) = \begin{pmatrix} 1 & \rho_4 \\ 0 & \delta_4 \end{pmatrix} \begin{pmatrix} X_3 \\ X_4 \end{pmatrix}, & \text{if } (X_3, X_4) \in \mathcal{D}_4. \end{cases}$$

We write w_3^* for the eigenvector $(\delta_3 - 1, \rho_3)$ of M_3 with eigenvalue δ_3, and w_4^* for the eigenvector $(\rho_4, \delta_4 - 1)$ of M_4 with eigenvalue δ_4. We write W_3^* for the eigenspace of M_3 that is the span of w_3^*, and similarly for W_4^*. We also write $w_3^- = (0, 1)$ and W_3^- for its span, and $w_4^- = (1, 0)$ and W_4^- for its span. These are, respectively, eigenvectors of M_3 and M_4, both with eigenvalue 1.

9.2 Motivating the projected map

Write V_a for the one-dimensional linear subspace of $\mathbb{R}^2$ defined by $X_4 = aX_3$, where $a > 0$. Then, all vectors $X \in V_a$ in the domain of M are mapped by M into the same one-dimensional subspace, $V_{h(a)}$, where

$$h(a) = \begin{cases} h_3(a) = \frac{a+\rho_3}{\delta_3}, & \text{if } a > \frac{e_{24}}{e_{23}}, \\ \\ h_4(a) = \frac{a\delta_4}{1+a\rho_4}, & \text{if } a < \frac{e_{24}}{e_{23}}. \end{cases}$$

The map $h_3(a)$ has a fixed point $a_3^* = \frac{\rho_3}{\delta_3 - 1}$, and $V_{a_3^*}$ is the eigenspace W_3^*. The map $h_4(a)$ has a fixed point $a_4^* = \frac{\delta_4 - 1}{\rho_4}$, and $V_{a_4^*}$ is the eigenspace W_4^*.

These properties of M_3 and M_4 as linear maps have analogues in the return maps Φ_3 and

Φ_4, which was previously considered in [Pos10]. For $a > 0$, consider the one-dimensional subspace defined by $X_4 = aX_3$, restricted to the negative orthant. Taking exponentials gives a curve $x_4 = x_3^a$ in $\mathbf{H}_2^{\text{in},1}$. We note that any point $(q_3, q_4) \in \mathbf{H}_1^{\text{in},2}$ lies on the curve $x_4 = x_3^a$, where $a = \log q_4 / \log q_3$. All points on the curve $x_4 = x_3^a$ that are in the domain of Φ are mapped into the curve $x_4 = x_3^{h(a)}$. Write Σ_3^* and Σ_4^* for the curves defined by $x_4 = x_3^{a_3^*}$ and $x_4 = x_3^{a_4^*}$, respectively. The curves Σ_3^* and Σ_4^* are invariant under the action of Φ_3 and Φ_4, respectively. The eigenspaces W_3^* and W_4^* correspond to these invariant curves in logarithmic coordinates.

Since we are interested in not just the stability properties of the Kirk–Silber network and its component cycles, but also in classifying the behaviour of nearby trajectories, we can determine the itinerary of trajectories by which part of the domain of the return map Φ they pass through. For a given $a > 0$, all points x_0 in the curve $x_4 = x_3^a$ give rise to disjoint trajectories in phase space, $\phi(x_0, t)$. However, the sequence of points $\Phi^n(x_0)$ at which these trajectories strike the cross-section $\mathbf{H}_2^{\text{in},1}$ all lie in the same sequence of curves $x_4 = x_3^{h^n(a)}$. Therefore, these trajectories have the same itinerary. With this information, we highlight the primary advantage of the methodology we introduce here: we can simplify the analysis of trajectories near the network by identifying all trajectories that lie on the same curve $x_4 = x_3^a$, thereby reducing the complexity of the problem by one dimension.

9.3 The projected map of the Kirk–Silber network

We define the set

$$S = \big\{(X_3, X_4) \in \mathbb{R}^2_- \mid X_3 + X_4 = -1\big\}. \tag{9.5}$$

By identifying any point in S with its first coordinate, we can, without ambiguity, identify the set S with the open interval $(-1, 0) \subseteq \mathbb{R}_-$. We cannot, however, use the closed interval $[-1, 0]$, which includes the limit points -1 and 0. These points correspond, respectively, to the X_3- and X_4-axes, and so correspond to the original coordinates, x_4 and x_3, respectively, being $\mathcal{O}(1)$. These points are not in the domain of the original return map Φ. We also choose to identify S with a subset of the negative real line as a reminder that these points represent vectors in the negative orthant.

We define the projection $\Pi\colon \mathbb{R}^2_- \to S$ of any vector $X \in \mathbb{R}^2_-$ onto S by taking the first coordinate of the intersection of the line segment S with the subspace containing X:

$$\Pi\colon X = (X_3, X_4) \mapsto \frac{-1}{(1,1)\cdot X} e_1 \cdot X = \frac{-X_3}{X_3 + X_4}, \tag{9.6}$$

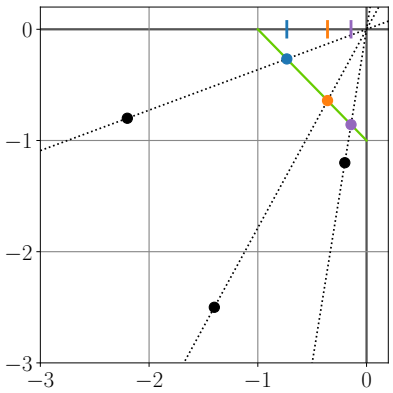

Figure 9.3: Three examples of determining a vector's projection onto the line segment S, which is shown as a green line. The three vectors extend from the origin to the black points, and the linear subspaces containing them are the dotted lines. The intersection of each linear subspace and S as a line segment is given by a coloured point, and the horizontal components are the three correspondingly coloured ticks on the X_3-axis.

where $e_1 = (1, 0)$ is the first standard basis vector. Figure 9.3 depicts this projection. For all $X \in \mathbb{R}^2_-$ and $\alpha > 0$,

$$\Pi(\alpha X) = \Pi(X).$$

Therefore, all vectors in the same linear subspace are represented by the same point in S.

We define the projected map as the induced action of the map M on S. Let

$$\vartheta_s \coloneqq \Pi(w_s) = \frac{-1}{1 + \dfrac{e_{24}}{e_{23}}}.$$

We define the intervals $\Theta_3 = (\vartheta_s, 0)$ and $\Theta_4 = (-1, \vartheta_s)$, and so $S = \Theta_4 \cup \{\vartheta_s\} \cup \Theta_3$. For a point $\vartheta \in S$, if $\vartheta_s < \vartheta$, with corresponding vectors in $\mathcal{D}_3$,

$$\begin{aligned} M(\vartheta, -1-\vartheta) &= M_3(\vartheta, -1-\vartheta) \\ &= \begin{pmatrix} \delta_3 & 0 \\ \rho_3 & 1 \end{pmatrix} \begin{pmatrix} \vartheta \\ -1-\vartheta \end{pmatrix} \\ &= \begin{pmatrix} \delta_3 \vartheta \\ (\rho_3 - 1)\vartheta - 1 \end{pmatrix} \end{aligned} \tag{9.7}$$

and, if $\vartheta < \vartheta_{\mathrm{s}}$, with corresponding vectors in $\mathcal{D}_4$,

$$\begin{aligned} M(\vartheta, -1-\vartheta) &= M_4(\vartheta, -1-\vartheta) \\ &= \begin{pmatrix} 1 & \rho_4 \\ 0 & \delta_4 \end{pmatrix} \begin{pmatrix} \vartheta \\ -1-\vartheta \end{pmatrix} \\ &= \begin{pmatrix} (1-\rho_4)\vartheta - \rho_4 \\ \delta_4(-1-\vartheta) \end{pmatrix}. \end{aligned} \tag{9.8}$$

With the action of M_3 in (9.7) and M_4 in (9.8), we apply the projection in (9.6), deriving maps

$$f_3 = \Pi(M_3(\vartheta, -1-\vartheta))\colon \Theta_3 \to S$$

and

$$f_4 = \Pi(M_4(\vartheta, -1-\vartheta))\colon \Theta_4 \to S.$$

We combine these maps into the projected map $f_{\mathrm{KS}}\colon \Theta_3 \cup \Theta_4 \to S$:

$$f_{\mathrm{KS}}(\vartheta) = \begin{cases} f_3(\vartheta) = \dfrac{-\delta_3\vartheta}{(\delta_3+\rho_3-1)\vartheta - 1}, & \text{if } \vartheta \in \Theta_3, \\ \\ f_4(\vartheta) = \dfrac{(1-\rho_4)\vartheta - \rho_4}{(\delta_4+\rho_4-1)\vartheta + \delta_4 + \rho_4}, & \text{if } \vartheta \in \Theta_4. \end{cases} \tag{9.9}$$

The projected map f_{KS} is a piecewise-smooth dynamical system, and the point ϑ_{s} is its switching manifold. Figure 9.4 gives schematic representations of this projected map for a variety of relations between parameters.

We now show that this map is well-defined and describes the dynamics of trajectories in all sufficiently small neighbourhoods of the Kirk–Silber network.

9.4 Well-definedness of the projected map

We first discuss why the projected map might not be well-defined. The full return map $\Phi\colon \Gamma_3 \cup \Gamma_4 \to \mathbf{H}_2^{\mathrm{in},1}$ is the map from which the projected map is ultimately derived. As discussed in §9.1, this map is not defined on the entirety of the cross-section $\mathbf{H}_2^{\mathrm{in},1}$, due to the excluded cusp Γ_{c}, defined around the switching curve Σ_{s}. When moving to logarithmic coordinates, the set Γ_{c} becomes the subset $\mathcal{D}_c \subseteq \mathbb{R}^2_-$—defined around the switching subspace W_{s}—whose boundaries are the affine subspaces W_{s}^- and W_{s}^+. These subspaces project onto the set S, and so we might think that all $\vartheta \in S$ such that $\Pi(W_{\mathrm{s}}^-) < \vartheta < \Pi(W_{\mathrm{s}}^+)$ must be excluded from the domain of the projected map. We show here that, in fact, only ϑ_{s}, which

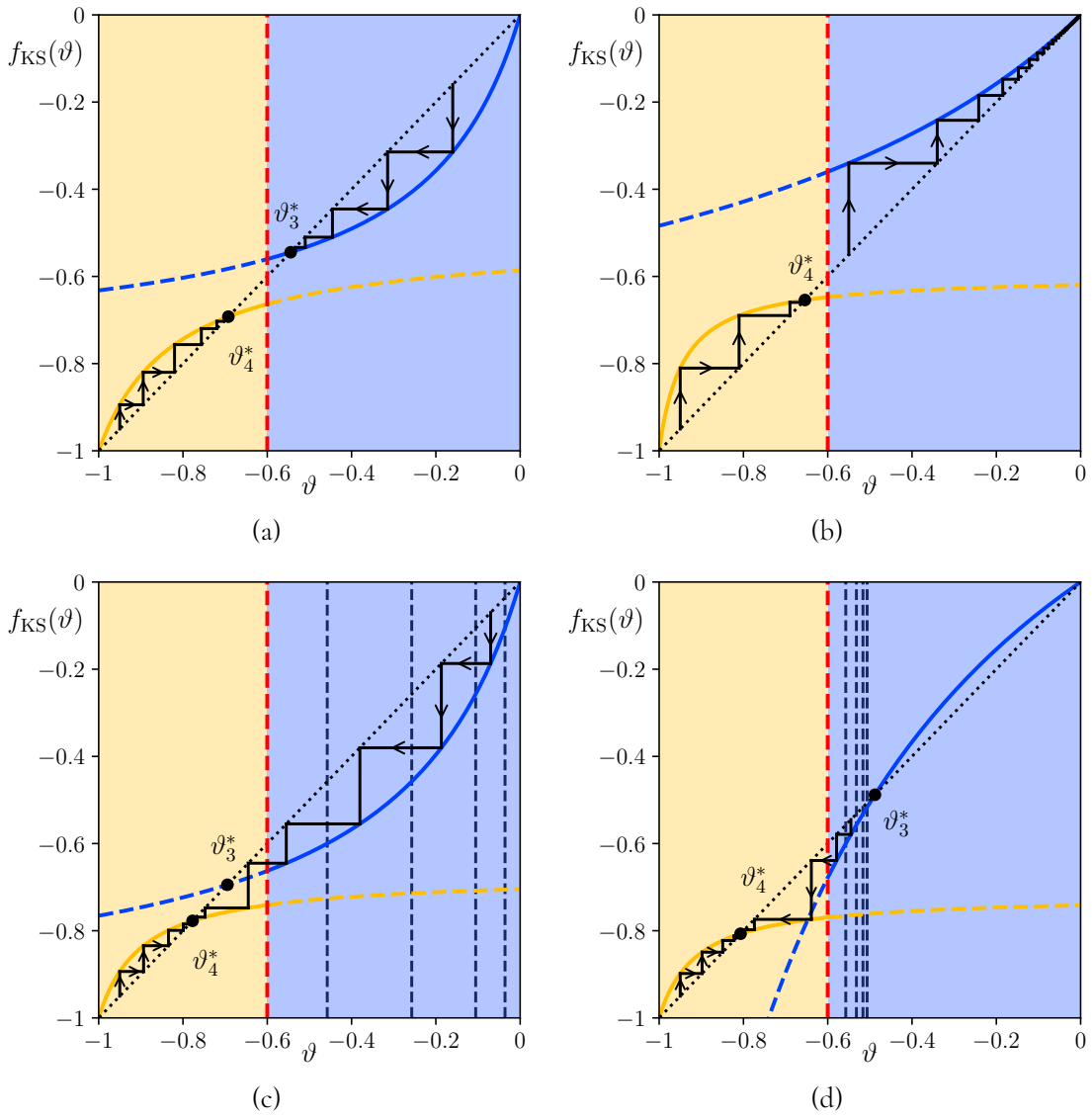

Figure 9.4: Schematic representations of the projected map of the Kirk–Silber network as cobweb plots, for different relations between parameters: (a) $\delta_3 > 1$ and $\nu_3 > 0$, (b) $\delta_3 < 1$ and $\nu_3 > 0$, (c) $\delta_3 > 1$ and $\nu_3 < 0$, and (d) $\delta_3 < 1$ and $\nu_3 < 0$. In all examples, the domain Θ_3 is shaded blue and the domain Θ_4 orange. The dashed red line indicates ϑ_s. The dotted black line is $f_{\mathrm{KS}}(\vartheta) = \vartheta$. Each function f_3 and f_4 is shown as solid in its domain of definition and dashed otherwise. In all four figures, $\delta_4 > 1$ and $\nu_4 > 0$. In (c) and (d), the values $\mathcal{E}_n$ (see (10.1)) are indicated by dashed black lines for $n = 1, 2, 3, 4$. Parameter values and initial conditions for these figures are given in §B.5.2.

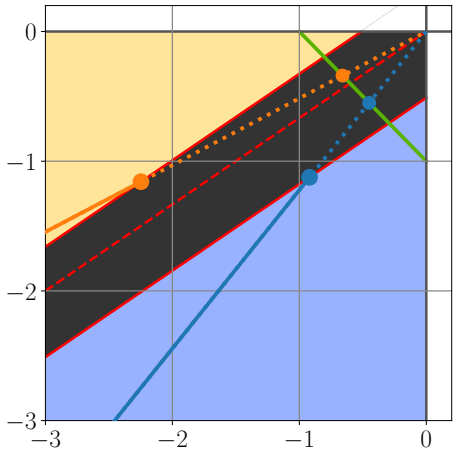

Figure 9.5: Two examples of points in S that are not ϑ_{s}, given by the coloured dots on S, the solid green line. The linear subspace through each point is shown as solid for vectors in the domain of M, and dotted for vectors in $\mathcal{D}_c$. The solid lines are examples of the half-lines $L(\vartheta)$. The point $p(\vartheta)$ in each case is shown as a correspondingly coloured point on the solid red lines. In this figure, we use $e_{23} = 1.2$, $e_{24} = 0.8$, and $\epsilon = 0.4$, for visual clarity.

corresponds to the switching curve Σ_{s}, must be excluded.

Let ϑ be a point of S that is not ϑ_{s}. This point is the projection of any vector in the linear subspace $W(\vartheta)$ defined by $X_4 = -\frac{1+\vartheta}{\vartheta}X_3$, and this subspace is not W_{s}. As W_{s}^+ and W_{s}^- are parallel to W_{s}, $W(\vartheta)$ intersects W_{s}^+ or W_{s}^- at some point $p(\vartheta) \in \mathbb{R}^2_-$, given by

$$p(\vartheta) = \begin{cases} p_3(\vartheta) = W(\vartheta) \cap W_{\mathrm{s}}^+ = \left(\frac{-\vartheta \log(1-\epsilon)}{\frac{e_{24}}{e_{23}}\vartheta + 1 + \vartheta}, \frac{(1+\vartheta)\log(1-\epsilon)}{\frac{e_{24}}{e_{23}}\vartheta + 1 + \vartheta} \right) & \text{if } \vartheta_{\mathrm{s}} < \vartheta, \\ p_4(\vartheta) = W(\vartheta) \cap W_{\mathrm{s}}^- = \left(\frac{\vartheta \log(1-\epsilon)}{\vartheta + \frac{e_{23}}{e_{24}}(1+\vartheta)}, \frac{-(1+\vartheta)\log(1-\epsilon)}{\vartheta + \frac{e_{23}}{e_{24}}(1+\vartheta)} \right) & \text{if } \vartheta < \vartheta_{\mathrm{s}}. \end{cases} \tag{9.10}$$

If we set

$$\alpha^*(\vartheta) = \begin{cases} \alpha_3^*(\vartheta) = \frac{-\log(1-\epsilon)}{\frac{e_{24}}{e_{23}}\vartheta + 1 + \vartheta} & \text{if } \vartheta_{\mathrm{s}} < \vartheta, \\ \alpha_4^*(\vartheta) = \frac{\log(1-\epsilon)}{\vartheta + \frac{e_{23}}{e_{24}}(1+\vartheta)} & \text{if } \vartheta < \vartheta_{\mathrm{s}}, \end{cases}$$

then all vectors in the half-line $L(\vartheta) = \{\alpha(\vartheta, -(1+\vartheta)) \mid \alpha > \alpha^*(\vartheta)\} \subseteq \mathbb{R}^2_-$ extending from, but not including, the point $p(\vartheta)$ are in the domain of M and project onto ϑ. Figure 9.5 shows examples of the process of finding the point $p(\vartheta)$ and the half-line $L(\vartheta)$.

Next, since M is defined by the linear action of the matrices M_3 and M_4, we know that, for all $v, w \in L(\vartheta)$, $M(v) = tM(w)$ for some t. Thus, the projection of $M(v)$ onto S is the same as that of $M(w)$; that is, $\Pi(M(v)) = \Pi(M(w))$.

Hence, for any point $\vartheta \in S$ such that $\vartheta \neq \vartheta_{\mathrm{s}}$, we define the projected map f as the

projection onto S of the image under M of $\alpha(\vartheta, -1-\vartheta)$ for any $\alpha > \alpha^*(\vartheta)$:

$$f_{\mathrm{KS}}\colon \vartheta \mapsto \frac{-1}{(1,1)\cdot M(\alpha(\vartheta,-(1+\vartheta)))} e_1 \cdot M(\alpha(\vartheta,-(1+\vartheta))), \tag{9.11}$$

and this mapping is well-defined. In (9.11), we have not cancelled the constant α to emphasise that this scaling is needed so that the vector $\alpha(\vartheta, -1-\vartheta)$ is in the domain of M.

In summary, we do not have to exclude from the domain of definition of the projected map those ϑ such that $\Pi(W_{\mathrm{s}}^-) < \vartheta < \Pi(W_{\mathrm{s}}^+)$. We instead take the projected map f_{KS} as being defined only for the projection of those vectors in the linear subspace $W(\vartheta)$ that lie on the half-line $L(\vartheta)$, and so we are in the domain of M.

The following proposition allows us to use the dynamics of f_{KS} to understand the dynamics of trajectories near heteroclinic networks. For this proposition, we define $\Sigma(\vartheta)$ as the curve in $\mathbf{H}_2^{\mathrm{in},1}$ that, in logarithmic coordinates, projects onto $\vartheta \in S$:

$$\Sigma(\vartheta) = \left\{(x_3, x_4) \in \mathbf{H}_2^{\mathrm{in},1} \mid x_4 = x_3^{-\frac{1+\vartheta}{\vartheta}}\right\}.$$

Proposition 9.1. Let $T \subseteq S$ be a subset of S for which ϑ_{s} is not a (topological) limit point. Then for all sufficiently small neighbourhoods of the origin in $\mathbf{H}_2^{\mathrm{in},1}$, the curve $\Sigma(\vartheta)$ is disjoint from the excluded cusp Γ_{c} for all $\vartheta \in T$.

Proof. We begin by defining $d^* := \inf\{d(t, \vartheta_{\mathrm{s}}) \mid t \in T\}$. Since ϑ_{s} is not a limit point of T, $d^* > 0$. We set $\alpha^* = \max\{\alpha^*(\vartheta_{\mathrm{s}} - d^*), \alpha^*(\vartheta_{\mathrm{s}} + d^*)\}$. Then, for all $\vartheta \in T$, all vectors in the half-lines

$$L(\vartheta) = \left\{(\alpha\vartheta, -\alpha(1+\vartheta)) \in \mathbb{R}^2_- \mid \alpha > \alpha^*\right\} \subseteq W(\vartheta)$$

are disjoint from $\mathcal{D}_c$ and so are in the domain of M. Therefore, all points on the curve

$$\Lambda(\vartheta) = \left\{\left(e^{\alpha\vartheta}, e^{-\alpha(1+\vartheta)}\right) \in \mathbf{H}_2^{\mathrm{in},1} \mid \alpha > \alpha^*\right\} \subseteq \Sigma(\vartheta)$$

are disjoint from the excluded cusp Γ_{c} and so are in the domain of Φ. If

$$r^* = \inf_{\vartheta \in T} \sup_{x \in \Lambda(\vartheta)} d(0, x),$$

then, for all $r < r^*$, the restriction of $\Sigma(\vartheta)$ to the open neighbourhood of radius r of the origin lies outside the excluded cusp Γ_{c} for all $\vartheta \in T$. ■

Therefore, if $\vartheta \in \Theta_3 \cup \Theta_4$ and $\left(f_{\mathrm{KS}}^n(\vartheta)\right)_{n\in\mathbb{N}}$ is the forward orbit from ϑ, then, if this orbit is not asymptotic to ϑ_{s}, the orbit describes the dynamics of trajectories in all sufficiently small neighbourhoods of the given network.

§10 The Kirk–Silber network

To help us classify the dynamics of trajectories near the Kirk–Silber network, we first define the following two subsets of $\mathbf{H}_2^{\text{in},1}$:

$$\Gamma_3^- = \left\{ x \in \Gamma_3 \mid (1-\epsilon) x_3^{\frac{e_{24}}{e_{23}}} > x_4 > x_3^{\frac{\rho_3}{\delta_3 - 1}} \right\} \subseteq \Gamma_3,$$

which is nonempty only if $\delta_3 < 1$ and $\nu_3 < 0$, and

$$\Gamma_4^- = \left\{ x \in \Gamma_4 \mid (1-\epsilon) x_4^{\frac{e_{23}}{e_{24}}} > x_3 > x_4^{\frac{\rho_4}{\delta_4 - 1}} \right\} \subseteq \Gamma_4,$$

which is nonempty only if $\delta_4 < 1$ and $\nu_4 < 0$.

We now use the projected map to classify the dynamics of trajectories near the Kirk–Silber network. In particular, we prove the following theorem.

Theorem 10.1. (a) *If $\delta_3 > 1$ and $\nu_3 > 0$, then the $\mathcal{C}_{[3]}$ cycle is fragmentarily asymptotically stable. All trajectories starting in Γ_3 are asymptotic to the $\mathcal{C}_{[3]}$ cycle, with itinerary $(231)^\infty$.*

(b) *If $\delta_3 > 1$ and $\nu_3 < 0$, then the $\mathcal{C}_{[3]}$ cycle is almost completely unstable. All trajectories starting in Γ_3 are eventually mapped into Γ_4. If, in addition, $\delta_4 > 1$, these trajectories switch from the $\mathcal{C}_{[3]}$ cycle to the $\mathcal{C}_{[4]}$ cycle, to which they are then asymptotic. For all positive integers n, there exists an open set of trajectories starting in Γ_3 with the itinerary $(231)^n(241)^\infty$.*

(c) *If $\delta_3 < 1$, then the $\mathcal{C}_{[3]}$ cycle is completely unstable. If $\nu_3 < 0$, then all trajectories starting in Γ_3^- sufficiently close to the network are eventually mapped into Γ_4. If, in addition, $\delta_4 > 1$, these trajectories switch from the $\mathcal{C}_{[3]}$ cycle to the $\mathcal{C}_{[4]}$ cycle, to which they are then asymptotic. For all positive integers n, there exists an open set of trajectories in Γ_3 with the itinerary $(231)^n(241)^\infty$. All other trajectories starting near the cycle leave a neighbourhood of the cycle.*

(d) *If $\delta_4 > 1$ and $\nu_4 > 0$, then the $\mathcal{C}_{[4]}$ cycle is fragmentarily asymptotically stable. All trajectories starting in Γ_4 are asymptotic to the $\mathcal{C}_{[4]}$ cycle, with itinerary $(241)^\infty$.*

(e) *If $\delta_4 > 1$ and $\nu_4 < 0$, then the $\mathcal{C}_{[4]}$ cycle is almost completely unstable. All trajectories starting in Γ_4 are eventually mapped into Γ_3. If, in addition, $\delta_3 > 1$, these trajectories switch from the $\mathcal{C}_{[4]}$ cycle to the $\mathcal{C}_{[3]}$ cycle, to which they are then asymptotic. For all positive integers n, there exists an open set of trajectories starting in Γ_4 with the itinerary $(241)^n(231)^\infty$.*

(f) *If $\delta_4 < 1$, then the $\mathcal{C}_{[4]}$ cycle is completely unstable. If $\nu_4 < 0$, then all trajectories starting in Γ_4^- sufficiently close to the network are eventually mapped into Γ_3. If, in addition, $\delta_3 > 1$,*

these trajectories switch from the $\mathcal{C}_{[4]}$ cycle to the $\mathcal{C}_{[3]}$ cycle, to which they are then asymptotic. For all positive integers n, there exists an open set of trajectories in Γ_4 with the itinerary $(241)^n(231)^\infty$. All other trajectories starting near the cycle leave a neighbourhood of the cycle.

The results in (a), (b), (d), and (e) were proven in [KS94], though not using the terminology we have used here. We rederive these results to demonstrate how trajectories near a heteroclinic network can be analysed with its projected map. We also derive new results in (c) and (f) concerning switching from a completely unstable cycle.

The proof of Theorem 10.1 proceeds as follows:

- In sections 10.1 to 10.3, we prove results about the fixed points of f_{KS} which are used in the remainder of the proof.
- In §10.4, we prove (a) and (d) of Theorem 10.1, and the parts of (c) and (f) where $\nu_3 > 0$ and $\nu_4 > 0$, respectively. These parts of Theorem 10.1 correspond to parameter values for which all fixed points of the map f_{KS} are admissible.
- In §10.5, we prove (b) and (e) of Theorem 10.1, and the parts of (c) and (f) where $\nu_3 < 0$ or $\nu_4 < 0$, respectively. These parts of Theorem 10.1 correspond to parameter values for which one fixed point of the map f_{KS} is virtual.

We prove these results for only the $\mathcal{C}_{[3]}$ cycle, as the proof for the $\mathcal{C}_{[4]}$ cycle is equivalent. However, we highlight where properties of the maps f_3 and f_4 are different.

10.1 Fixed points, admissibility, and stability

Both f_3 and f_4 (see (9.9)) have only one fixed point that can lie in S,

$$\vartheta_3^* = \frac{1-\delta_3}{\delta_3+\rho_3-1}$$

and

$$\vartheta_4^* = \frac{-\rho_4}{\delta_4+\rho_4-1}.$$

These fixed points correspond to the eigenspaces W_3^* and W_4^*. We now determine when these fixed points are admissible or virtual, and when border-collision bifurcations occur.

Consider the case that $\delta_3+\rho_3>1$ and $\delta_4+\rho_4>1$. Rearranging $\vartheta_3^* > \vartheta_{\mathrm{s}}$ gives

$$\rho_3 - \frac{e_{24}}{e_{23}}(\delta_3-1) \equiv \frac{c_{21}}{e_{23}}\nu_3 > 0.$$

Since c_{21} and e_{23} are both positive, ϑ_3^* is admissible if and only if $\nu_3 > 0$ and it is virtual if and only if $\nu_3 < 0$. A border-collision bifurcation occurs at $\nu_3 = 0$. Equivalent results hold for ϑ_4^* and ν_4.

Now, in the case that $\delta_3 + \rho_3 < 1$, ϑ_3^* is virtual if and only if $\nu_3 > 0$, and admissible if and only if $\nu_3 < 0$. The same holds for ϑ_4^* when $\delta_4 + \rho_4 < 1$.

The maps f_3 and f_4 each have one additional fixed point: $\vartheta_3^- = 0$ and $\vartheta_4^- = -1$, respectively. These correspond to the eigenspaces W_3^- and W_4^-, respectively. These points are not in the domains of the maps f_3 and f_4, but it is useful to consider them in our analysis.

To determine the stability of ϑ_3^* and ϑ_4^*, we calculate that

$$\mathrm{D}f_3(\vartheta) = \frac{\delta_3}{\left((\delta_3 + \rho_3 - 1)\vartheta - 1\right)^2}$$

and

$$\mathrm{D}f_4(\vartheta) = \frac{\delta_4}{\left((\delta_4 + \rho_4 - 1)\vartheta + \delta_4 + \rho_4\right)^2}.$$

Since δ_3 and δ_4 are both positive, $\mathrm{D}f_3(\vartheta) > 0$ and $\mathrm{D}f_4(\vartheta) > 0$ for all $\vartheta \in S$, and so both functions are strictly increasing.

Evaluating $\mathrm{D}f_3(\vartheta)$ and $\mathrm{D}f_4(\vartheta)$ at ϑ_3^* and ϑ_4^* gives

$$\mathrm{D}f_3(\vartheta_3^*) = \frac{1}{\delta_3}$$

and

$$\mathrm{D}f_4(\vartheta_4^*) = \frac{1}{\delta_4}.$$

Therefore, ϑ_3^* is asymptotically stable when $\delta_3 > 1$, and ϑ_4^* is asymptotically stable when $\delta_4 > 1$. Additionally, $\mathrm{D}f_3(\vartheta_3^-) = \delta_3$ and $\mathrm{D}f_4(\vartheta_4^-) = \delta_4$. At the point of stability loss, $\vartheta_3^* = \vartheta_3^-$ and $\vartheta_4^* = \vartheta_4^-$. Thus, if f_3 and f_4 were studied as functions of the real line, these bifurcations would be transcritical bifurcations.

10.2 Equivalence of the border-collision bifurcation and Podvigina's third stability condition

As discussed at the beginning of §6.2, when studying a heteroclinic cycle, it may be that there is only one equilibrium at which an open set of initial conditions exists that does not return to that equilibrium under the flow of the system. As such, since the projected map f_{KS} is derived from the transition matrices M_3 and M_4 only, we do not know *a priori* that stability of the cycles can necessarily be determined by studying this map alone. Podvigina's results

tell us that stability can be determined by studying the full transition matrices at ξ_3 and ξ_4, since the only basic transition matrices with negative entries are m_{123} and m_{124}. However, it is in fact possible to establish an equivalence between the border-collision bifurcations of ϑ_3^* and ϑ_4^* and the stability conditions at ξ_3 and ξ_4, respectively; this equivalence allows us to deduce whether a trajectory is asymptotic to the $\mathcal{C}_{[3]}$ or $\mathcal{C}_{[4]}$ cycle from examination of the projected map only.

Recall that we use the shorthand $M_3 \equiv M_2^{(3)}$ and $M_4 \equiv M_2^{(4)}$. The full transition matrix M_3 is defined by the following product of basic transition matrices:

$$M_3 \equiv M_2^{(3)} = m_{312}m_{231}m_{123}.$$

The transition matrix $M_3^{(3)}$ is defined by

$$M_3^{(3)} = m_{123}m_{312}m_{231}.$$

As such, $M_3^{(3)} = m_{123}M_3m_{123}^{-1}$, and similarly for $M_4 \equiv M_2^{(4)}$ and $M_4^{(4)} = m_{124}M_4m_{124}^{-1}$. We write $w_{\max}^{(2)}$ for the eigenvector of M_3 whose eigenvalue has greatest absolute value, and similarly write $w_{\max}^{(3)}$ for that eigenvector of $M_3^{(3)}$.

Therefore, if w is an eigenvector of M_3, then $m_{123}w$ is an eigenvector of $M_3^{(3)}$, and, if w is an eigenvector of $M_3^{(3)}$, then $m_{123}^{-1}w$ is an eigenvector of M_3. The key observation is that the image of the switching vector $w_s = \left(1, \frac{e_{24}}{e_{23}}\right)$ under m_{123} is

$$m_{123}w_s = \begin{pmatrix} \frac{c_{21}}{e_{23}} & 0 \\ -\frac{e_{24}}{e_{23}} & 1 \end{pmatrix} \begin{pmatrix} 1 \\ \frac{e_{24}}{e_{23}} \end{pmatrix} = \begin{pmatrix} \frac{c_{21}}{e_{23}} \\ 0 \end{pmatrix}.$$

Therefore, if the eigenvector $w_{\max}^{(2)}$ of M_3 lies in W_s, the eigenvector $w_{\max}^{(3)}$ of $M_3^{(3)}$ does not satisfy condition (III) of Theorem 6.1 because it has a 0 entry. Similarly, at the bifurcation $\nu_3 = 0$, the eigenvector $w_{\max}^{(3)}$ of $M_3^{(3)}$ is $(\delta_3 - 1, 0)$, and we find that

$$m_{123}^{-1}w_{\max} = \begin{pmatrix} \frac{e_{23}}{c_{21}} & 0 \\ \frac{e_{24}}{c_{21}} & 1 \end{pmatrix} \begin{pmatrix} \delta_3 - 1 \\ 0 \end{pmatrix} = \frac{e_{23}}{c_{21}}(\delta_3 - 1) \begin{pmatrix} 1 \\ \frac{e_{24}}{e_{23}} \end{pmatrix} \in W_s.$$

Therefore, Podvigina's third stability condition in Theorem 6.1 at ξ_3 is equivalent to the admissibility of the eigenvector $w_{\max}^{(2)}$ of M_3, and a border-collision bifurcation of the eigenvector $w_{\max}^{(2)}$ of M_3 corresponds to a 0 in the eigenvector $w_{\max}^{(3)}$ of $M_3^{(3)}$.

With a similar argument for the matrix m_{124}, we have proved the following proposition.

Proposition 10.2. Suppose $\delta_3 > 1$. The fixed point ϑ_3^* of f_3 is admissible if and only if $w_{\max}$ of $M_3^{(3)}$ satisfies Podvigina's third condition for stability. Suppose $\delta_4 > 1$. The fixed point ϑ_4^* is admissible if and only if the eigenvector $w_{\max}$ of $M_4^{(4)}$ satisfies Podvigina's third condition for stability.

As mentioned after Theorem 6.1, Podvigina's third stability condition only needs to be verified for $M_3^{(3)}$. We can then conclude that, if $(f_{\mathrm{KS}}^n(\vartheta))$ is an orbit of f_{KS} that is asymptotic to an admissible ϑ_3^*, then all corresponding trajectories near the Kirk–Silber network are asymptotic to the origin in *all* cross-sections of the $\mathcal{C}_{[3]}$ cycle. A similar argument applies to the $\mathcal{C}_{[4]}$ cycle. Hence, we can analyse the dynamics of trajectories near the Kirk–Silber network by only studying the projected map.

10.3 Discontinuity of the projected map of the Kirk–Silber network at ϑ_{s}

We now consider the limiting behaviour of f_3 and f_4 as $\vartheta \to \vartheta_{\mathrm{s}}$. The projected map is not defined at ϑ_{s} because of the method used to construct the return map Φ. The functions f_3 and f_4 can nevertheless be formally evaluated at ϑ_{s}.

We consider the projected map f_{KS} to be continuous if

$$\lim_{\vartheta \searrow \vartheta_{\mathrm{s}}} f_3(\vartheta) = \lim_{\vartheta \nearrow \vartheta_{\mathrm{s}}} f_4(\vartheta).$$

In the case of the Kirk–Silber network, we find that

$$\lim_{\vartheta \searrow \vartheta_{\mathrm{s}}} f_3(\vartheta) = \frac{-c_{32}c_{13}}{c_{32}(c_{13}+c_{14}) + e_{12}t_{34}},$$

and

$$\lim_{\vartheta \nearrow \vartheta_{\mathrm{s}}} f_4(\vartheta) = \frac{-(c_{42}c_{13} + e_{12}t_{43})}{c_{42}(c_{13}+c_{14}) + e_{12}t_{43}},$$

which, generically, are not equal. Therefore, the projected map of the Kirk–Silber network is discontinuous. This discontinuity can be seen in all four examples in Figure 9.4.

10.4 Dynamics when $\nu_3 > 0$ and $\nu_4 > 0$

We first prove (a) and (d) of Theorem 10.1, and the parts of (c) and (f) where $\nu_3 > 0$ and $\nu_4 > 0$, respectively, and so consider the dynamics of f_{KS} when both ϑ_3^* and ϑ_4^* are admissible.

We first assume $\delta_3 > 1$. It is straightforward to show that, for all $\vartheta \in \Theta_3$, $f_{\mathrm{KS}}(\vartheta) \in \Theta_3$. It is also straightforward to show that, if $\vartheta > \vartheta_3^*$, then $f_{\mathrm{KS}}(\vartheta) < \vartheta$, and if $\vartheta < \vartheta_3^*$, then $f_{\mathrm{KS}}(\vartheta) > \vartheta$. Hence, ϑ_3^* is globally attracting in Θ_3 if $\delta_3 > 1$. A similar analysis shows that ϑ_4^* is globally attracting in Θ_4 if $\delta_4 > 1$. Hence, we have proven (a) of Theorem 10.1. Examples

of orbits under iteration of the projected map for $\delta_3, \delta_4 > 1$ and $\nu_3, \nu_4 > 0$ are shown in Figure 9.4(a).

When $\delta_3 < 1$, $\vartheta_3^* > \vartheta_3^- = 0$, and f_3 has no fixed points in Θ_3. However, for all $\vartheta \in \Theta_3$, $f_{\mathrm{KS}}(\vartheta) \in \Theta_3$ and $f_{\mathrm{KS}}(\vartheta) > \vartheta$. Therefore, $\lim_{n\to\infty} f_{\mathrm{KS}}^n(\vartheta) = \vartheta_3^- = 0$, and so there is no $\vartheta \in \Theta_3$ asymptotic to a point in S. The $\mathcal{C}_{[3]}$ cycle is thus completely unstable. Hence, we have proven the first part of (c) of Theorem 10.1. Examples of orbits under iteration of the projected map when $\delta_3 < 1$ are shown in Figure 9.4(b).

10.5 Dynamics when either $\nu_3 < 0$ or $\nu_4 < 0$

We now prove (b) and (e) of Theorem 10.1, and the parts of (c) and (f) where $\nu_3 < 0$ or $\nu_4 < 0$, respectively. Thus we assume that either $\nu_3 < 0$ or $\nu_4 < 0$. As noted in section 9.1, Kirk and Silber show that these values cannot simultaneously be negative. We give the analysis of the dynamics of f_{KS} when $\nu_3 < 0$, and the analysis in the case of $\nu_4 < 0$ is similar.

We first assume that $\delta_3 > 1$. Since $\nu_3 < 0$, ϑ_3^* is virtual, and $\vartheta_3^* < \vartheta_{\mathrm{s}}$. For all $\vartheta \in \Theta_3$, $f_{\mathrm{KS}}(\vartheta) < \vartheta$. However, there now exist $\vartheta \in \Theta_3$ such that $f_{\mathrm{KS}}(\vartheta) \notin \Theta_3$. For all non-negative integers n, define $\mathcal{E}_n$ as the n-th pre-image of ϑ_{s} under f_3; in particular, $f_{\mathrm{KS}}(\mathcal{E}_{n+1}) = \mathcal{E}_n$ and $f_{\mathrm{KS}}^n(\mathcal{E}_n) = \vartheta_{\mathrm{s}}$. The exact value of $\mathcal{E}_n$ is

$$\mathcal{E}_n = \frac{\vartheta_{\mathrm{s}}}{\delta_3^n + \vartheta_{\mathrm{s}}\left(\delta_3^n - 1 + \rho_3 \sum_{k=0}^{n-1} \delta_3^k\right)}. \tag{10.1}$$

Note that $\mathcal{E}_0 = \vartheta_{\mathrm{s}}$, and, for all n, $\mathcal{E}_n < \mathcal{E}_{n+1} < 0$, and $\lim_{n\to\infty} \mathcal{E}_n = \vartheta_3^- = 0$. (We note that, strictly speaking, by Proposition 9.1, the points $\mathcal{E}_n$ must also be excluded from the domain of definition of the map f_3, but we do not make that explicit here.)

For all $\vartheta \in (\mathcal{E}_0, \mathcal{E}_1)$, $f_{\mathrm{KS}}(\vartheta) \in \Theta_4$. Moreover, for all $\vartheta \in (\mathcal{E}_n, \mathcal{E}_{n+1})$, $f_{\mathrm{KS}}(\vartheta) \in (\mathcal{E}_{n-1}, \mathcal{E}_n)$ and so $f_{\mathrm{KS}}^{n+1}(\vartheta) \in \Theta_4$. Therefore, all points in Θ_3 that are not a pre-image of ϑ_{s} are eventually mapped into Θ_4 after a finite number of iterations.

If $\delta_4 > 1$, ϑ_4^* is globally attracting in Θ_4, and so all $\vartheta \in \Theta_3$, except the points $\mathcal{E}_n$, are asymptotic to ϑ_4^*. However, by [KM04, Theorem 2.4], the $\mathcal{C}_{[3]}$ cycle remains asymptotically stable in the subspace S_{123} defined by $x_4 = 0$, and so $\mathcal{C}_{[3]}$ is almost completely unstable. Hence, we have completed the proof of (b) of Theorem 10.1. Examples of orbits under iteration of the projected map that switch from Θ_3 to Θ_4 are shown in Figure 9.4(c).

The same analysis can be done in the case of $\nu_4 < 0$, showing that all points in Θ_4, except those that are a pre-image of ϑ_{s}, are eventually mapped into Θ_3.

If $\delta_3 < 1$, then since $\nu_3 < 0$, ϑ_3^* is admissible but repelling in Θ_3. As such, all $\vartheta > \vartheta_3^*$ are asymptotic to ϑ_3^-, as was the case when $\nu_3 > 0$. However, $\lim_{n\to\infty} \mathcal{E}_n = \vartheta_3^*$, for the

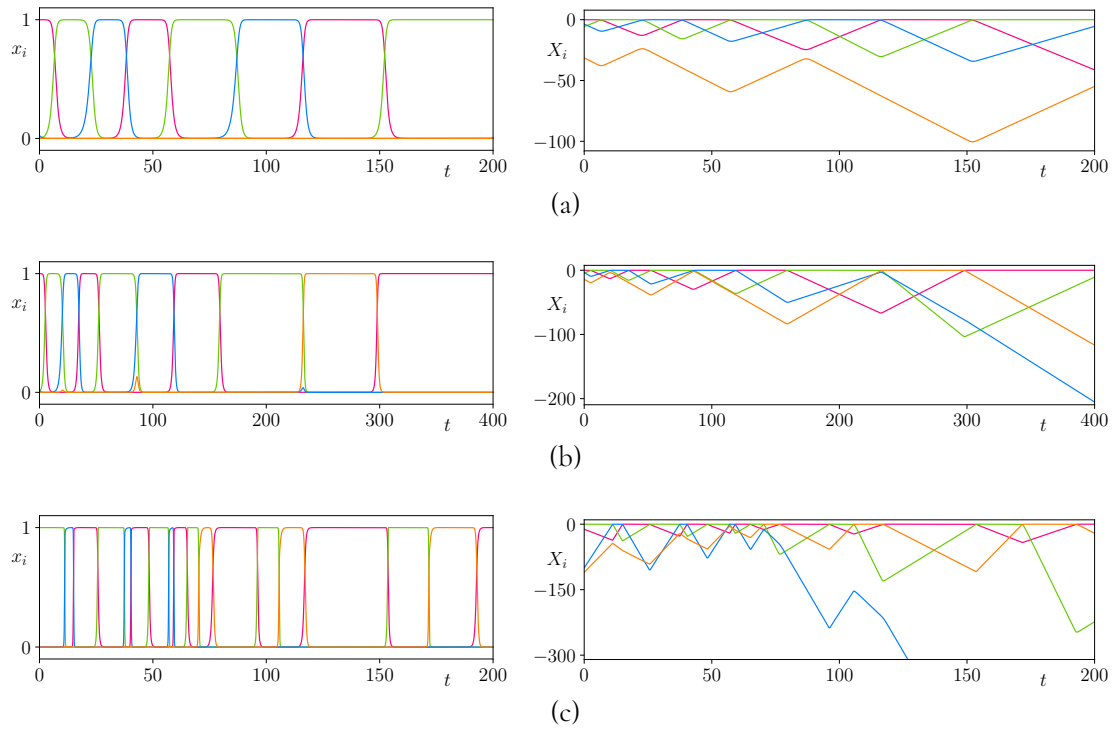

Figure 10.1: Example timeseries of trajectories near the Kirk–Silber network, where (a) $\delta_3 > 1$ and $\nu_3 > 0$, (b) $\delta_3 > 1$ and $\nu_3 < 0$, and (c) $\delta_3 < 1$ and $\nu_3 < 0$. The colours red, green, blue, and orange correspond to x_1, x_2, x_3, and x_4, respectively, and similarly for the X_i. In all three examples, $\delta_4 > 1$ and $\nu_4 > 0$, and the values of δ_3 and ν_3 are as indicated. Parameter values and initial conditions for these figures are given in §B.5.2.

$\mathcal{E}_n$ defined in (10.1). Thus, all $\vartheta \in (\vartheta_{\mathrm{s}}, \vartheta_3^*)$ are mapped into Θ_4 after a finite number of iterations. The subset $\vartheta \in (\vartheta_{\mathrm{s}}, \vartheta_3^*) \subseteq \Theta_3$ is the projection of the subset $\Gamma_3^- \subseteq \mathbf{H}_2^{\mathrm{in},1}$. We have therefore completed the proof of (c) of Theorem 10.1. An example of the projected map with $\delta_3 < 1$ and $\nu_3 < 0$ is shown in Figure 9.4(d).

Hence, we have completed the proof of Theorem 10.1.

10.6 Numerical examples

We conclude our study of the Kirk–Silber network by presenting some numerical examples of the phenomena we have described in this section. We consider the system of ODEs

$$\begin{aligned}
\dot{x}_1 &= x_1\big(1 - \|x\|_2^2 - c_{21}x_2^2 + e_{31}x_3^2 + e_{41}x_4^2\big),\\
\dot{x}_2 &= x_2\big(1 - \|x\|_2^2 + e_{12}x_1^2 - c_{32}x_3^2 - c_{42}x_4^2\big),\\
\dot{x}_3 &= x_3\big(1 - \|x\|_2^2 - c_{13}x_1^2 + e_{23}x_2^2 - t_{43}x_4^2\big),\\
\dot{x}_4 &= x_4\big(1 - \|x\|_2^2 - c_{14}x_1^2 + e_{24}x_2^2 - t_{34}x_3^2\big),
\end{aligned} \tag{10.2}$$

where c_{jk}, e_{jk}, and t_{jk} are positive real numbers. System (10.2) is $\mathbb{Z}_2^4$-equivariant, and contains a Kirk–Silber network. The four equilibria of the network lie at unit distance from the origin on the four coordinate axes in the positive orthant. A sufficient condition for the flow generated by the vector field (10.2) to contain an attracting invariant sphere is for all constants e_{jk} to be strictly less than unity [Fie96, CFL24]. However, this condition is not necessary, and so we do not explicitly make this assumption here, though we assume that the parameters satisfy the contracting condition of the invariant sphere theorem [Fie96].

To minimise roundoff error when computing f for trajectories close to the network, we follow [PD05] and use the change of coordinates $X_j := \log x_j$, and numerically integrate the resulting ODEs $\dot{X}_j$ with a variety of parameter values. Figure 10.1 shows three different trajectories near the Kirk–Silber network. The timeseries in Figure 10.1(a) is an example of a trajectory asymptotic to the $\mathcal{C}_{[3]}$ cycle. The example in Figure 10.1(b) has the same initial conditions as Figure 10.1(a), but the parameters are now such that $\nu_3 < 0$, and the trajectory switches from the almost completely unstable $\mathcal{C}_{[3]}$ cycle to the $\mathcal{C}_{[4]}$ cycle. This trajectory has itinerary $(123)^2(124)^\infty$. Figure 10.1(c) shows an example of switching from a completely unstable $\mathcal{C}_{[3]}$ cycle to a stable $\mathcal{C}_{[4]}$ cycle, with itinerary $(231)^3(241)^\infty$.

§11 The Δ-clique network

We now study the Δ-clique network using its projected map. Following the process outlined in §9.3, we derive the projected map of the Δ-clique network, $f_\Delta\colon \Theta_{34} \cup \Theta_4 \to S$:

$$f_\Delta(\vartheta) = \begin{cases} f_{34}(\vartheta) = \dfrac{(\alpha_2 - \alpha_1)\vartheta + \alpha_2}{(\alpha_1 - \alpha_2 + \alpha_3 - \alpha_4)\vartheta - \alpha_2 - \alpha_4}, & \text{if } \vartheta \in \Theta_{34}, \\ f_4(\vartheta) = \dfrac{(1-\rho_4)\vartheta - \rho_4}{(\delta_4 + \rho_4 - 1)\vartheta + \delta_4 + \rho_4}, & \text{if } \vartheta \in \Theta_4, \end{cases} \tag{11.1}$$

where

$$\begin{aligned} \alpha_1 &= \frac{c_{21}c_{43}}{e_{23}e_{41}} + \frac{c_{21}c_{42}t_{13}}{e_{23}e_{41}e_{12}} - \frac{c_{32}e_{24}t_{13}}{e_{34}e_{23}e_{12}} - \frac{c_{43}e_{24}t_{31}}{e_{41}e_{23}e_{34}} - \frac{c_{42}e_{24}t_{13}t_{31}}{e_{41}e_{23}e_{12}e_{34}}, \\ \alpha_2 &= \frac{c_{32}t_{13}}{e_{34}e_{12}} + \frac{c_{43}t_{31}}{e_{41}e_{34}} + \frac{c_{42}t_{13}t_{31}}{e_{41}e_{12}e_{34}} > 0, \\ \alpha_3 &= \frac{c_{14}c_{21}c_{42}}{e_{12}e_{23}e_{41}} - \frac{c_{14}c_{32}e_{24}}{e_{12}e_{34}e_{23}} - \frac{c_{14}c_{42}e_{24}t_{31}}{e_{12}e_{41}e_{23}e_{34}}, \\ \alpha_4 &= \frac{c_{14}c_{32}}{e_{12}e_{34}} + \frac{c_{14}c_{42}t_{31}}{e_{12}e_{41}e_{34}} > 0, \end{aligned}$$

and

$$\rho_4 = -\frac{e_{23}}{e_{24}} + \frac{c_{21}c_{43}}{e_{24}e_{41}} + \frac{c_{21}c_{42}t_{13}}{e_{24}e_{41}e_{12}}.$$

The definition of δ_4 is the same as for the Kirk–Silber network in (9.1). The derivation of these expressions can be found in the §B.1.

The maps $f_{34}\colon \Theta_{34} \to S$ and $f_4\colon \Theta_4 \to S$ describe the dynamics of trajectories near the $\mathcal{C}_{[34]}$ cycle and the $\mathcal{C}_{[4]}$ cycle, respectively. The map f_4 is analogous to that for the Kirk–Silber network, with the exception that ρ_4 has a slightly different definition as a result of the differing topologies of the Kirk–Silber and Δ-clique networks.

The domain Θ_{34} of f_{34} corresponds to the set $\Gamma_{34} \subseteq \mathbf{H}_2^{\mathrm{in},1}$ of trajectories that leave a neighbourhood of ξ_2 in the direction of ξ_3, and therefore cycle around the $\mathcal{C}_{[34]}$ cycle. The domain Θ_4 corresponds to those trajectories that cycle around the $\mathcal{C}_{[4]}$ cycle. These domains are $\Theta_{34} = (\vartheta_{\mathrm{s}}, 0)$ and $\Theta_4 = (-1, \vartheta_{\mathrm{s}})$.

For the purposes of describing the dynamics that can be observed near the Δ-clique network, we introduce the following expression for the $\mathcal{C}_{[4]}$ cycle:

$$\nu_4 = \frac{c_{43}}{e_{41}} + \frac{c_{42}t_{13}}{e_{41}e_{12}} - \frac{c_{14}c_{42}e_{23}}{e_{12}e_{24}e_{41}},$$

and the following expressions for the $\mathcal{C}_{[34]}$ cycle:

$$\begin{aligned}
\tau_{34} &= \alpha_1 + \alpha_4 = \operatorname{tr} M_{34},\\
\delta_{34} &= \alpha_1\alpha_4 - \alpha_2\alpha_3 = \det M_{34} = \frac{c_{14}c_{21}c_{32}c_{43}}{e_{12}e_{23}e_{34}e_{41}} > 0,\\
\omega_{34} &= \tau_{34}^2 - 4\delta_{34},\\
\lambda_{34}^{\pm} &= \frac{1}{2}(\tau_{34} \pm \sqrt{\omega_{34}}),\\
\zeta_{34} &= \alpha_1 - \alpha_2 + \alpha_3 - \alpha_4,
\end{aligned}$$

and

$$\beta_{34} = \alpha_3 + \frac{1}{2}(\alpha_1 - \alpha_4) + \frac{e_{24}}{e_{23}}\left(\alpha_2 + \frac{1}{2}(\alpha_4 - \alpha_1)\right).$$

The expression for ν_4 here is slightly different to that in §9.1, again due to the differing topologies of the two networks, but bifurcations when $\nu_4 = 0$ correspond to the same dynamical phenomena.

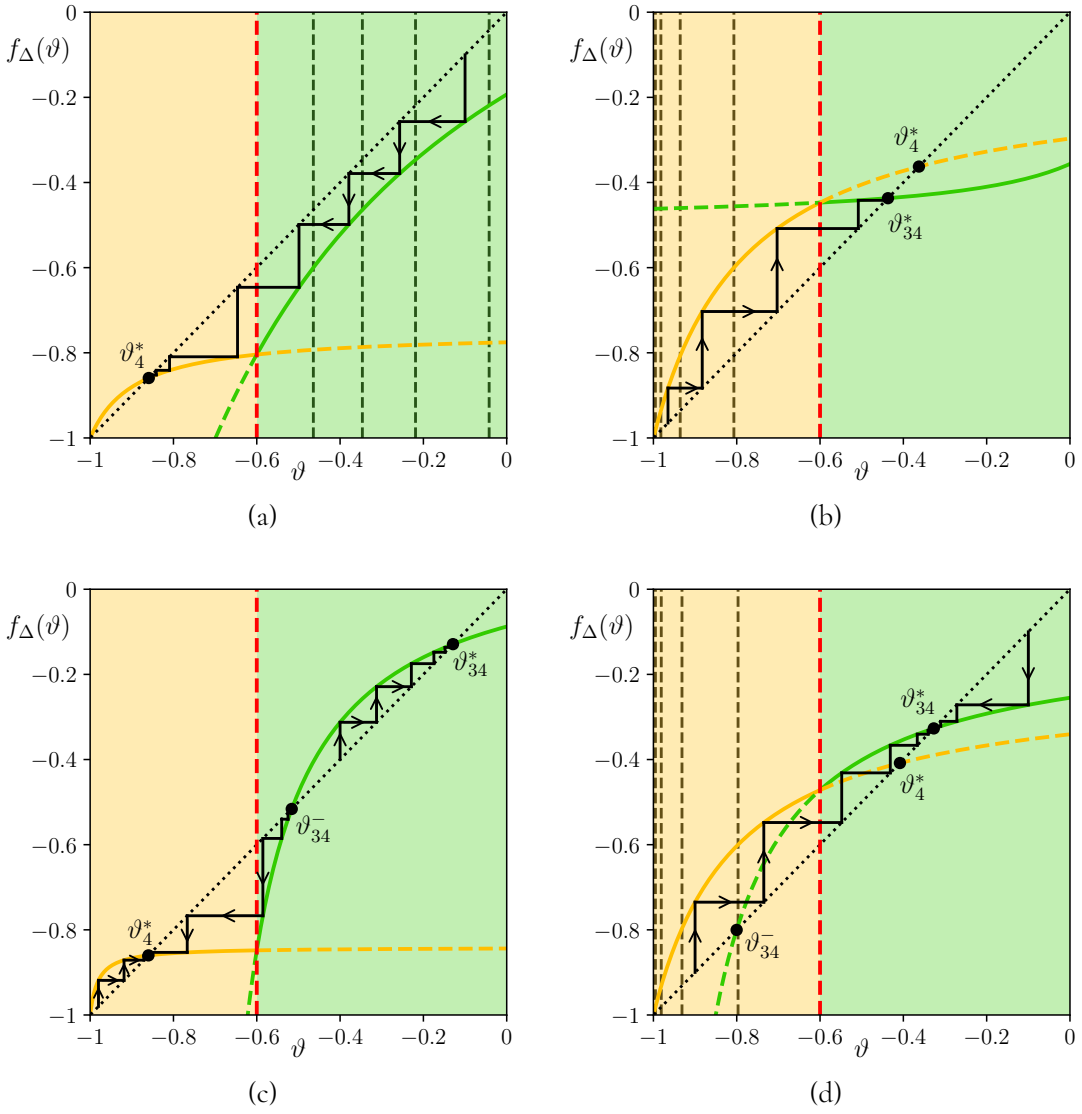

Figure 11.1: Schematic representations of the projected map of the Δ-clique network as cobweb plots, for different relations between parameters: (a) $\omega_{34} < 0$, (b) ϑ_{34}^c created in a virtual fold with $\nu_4 < 0$, (c) ϑ_{34}^c created in an admissible fold with $\nu_4 > 0$, and (d) ϑ_{34}^c created in an admissible fold with $\nu_4 < 0$. In all examples, the domain Θ_{34} is shaded green and the domain Θ_4 orange. The dashed red line indicates ϑ_s. The dotted black line is $f(\vartheta) = \vartheta$. Each function f_{34} and f_4 is shown as solid in its domain of definition and dashed otherwise. In all three figures, $\delta_4 > 1$ and $\tau_{34} > 0$. In (a), (b), and (d), the values $\mathcal{E}_n$ are indicated by dashed black lines for $n = 1, 2, 3, 4$. In (c), the interval $(\vartheta_s, \vartheta_{34}^-)$ is also partitioned by $\mathcal{E}_n$, but we do not plot these lines for visual clarity. Parameter values and initial conditions for these figures are given in §B.5.3.

We introduce the following two subsets of Γ_{34}:

$$\Gamma_{34}^{-} = \left\{ x \in \Gamma_{34} \mid (1-\epsilon)x_3^{\frac{e_{24}}{e_{23}}} > x_4 > x_3^{\frac{\lambda_{34}^{+}-\alpha_1-\alpha_3}{-\lambda_{34}^{+}+\alpha_2+\alpha_4}} \right\},$$

$$\Gamma_{34}^{+} = \left\{ x \in \Gamma_{34} \mid x_4 \leq x_3^{\frac{\lambda_{34}^{+}-\alpha_1-\alpha_3}{-\lambda_{34}^{+}+\alpha_2+\alpha_4}} \right\} = \Gamma_{34} \setminus \Gamma_{34}^{-},$$

which are non-empty only if $\omega_{34}, \tau_{34}, \nu_4 > 0$ and $\zeta_{34}, \beta_{34} < 0$. We define Γ_4^{-} as in §10. In the remainder of this section, we use the projected map to prove the following theorem about dynamics near the Δ-clique network.

Theorem 11.1. (a) *If $\omega_{34} > 0$ and $\tau_{34} > \min\{2, 1+\delta_{34}\}$, and either*

(i) *$\zeta_{34} < 0$ and $\beta_{34} < 0$; or*

(ii) *$\zeta_{34} < 0$, $\beta_{34} > 0$, and $\nu_4 < 0$; or*

(iii) *$\zeta_{34} > 0$ and $\nu_4 < 0$*

then the $\mathcal{C}_{[34]}$ cycle is fragmentarily asymptotically stable. In cases (ii) *and* (iii)*, and in case* (i) *if $\nu_4 < 0$, all trajectories starting in Γ_{34} are asymptotic to the $\mathcal{C}_{[34]}$ cycle, with itinerary $(2341)^\infty$. In case* (i) *if $\nu_4 > 0$, all trajectories starting in Γ_{34}^{+} are asymptotic to the $\mathcal{C}_{[34]}$ cycle, with itinerary $(2341)^\infty$, and all trajectories starting in Γ_{34}^{-} are mapped into Γ_4. If, in addition, $\delta_4 > 1$, these trajectories switch from the $\mathcal{C}_{[34]}$ cycle to the $\mathcal{C}_{[4]}$ cycle, to which they are then asymptotic, and, for all positive integers n, there exists an open set of trajectories in Γ_{34}^{-} with the itinerary $(2341)^n(241)^\infty$.*

(b) *If $\omega_{34} > 0$ and $\tau_{34} > \min\{2, 1+\delta_{34}\}$, and either*

(i) *$\zeta_{34} < 0$, $\beta_{34} > 0$, and $\nu_4 > 0$; or*

(ii) *$\zeta_{34} > 0$ and $\nu_4 > 0$*

then the $\mathcal{C}_{[34]}$ cycle is completely unstable, and all trajectories starting in Γ_{34} are mapped into Γ_4. If, in addition, $\delta_4 > 1$, these trajectories switch from the $\mathcal{C}_{[34]}$ cycle to the $\mathcal{C}_{[4]}$ cycle, to which they are then asymptotic, and there exists an open set of trajectories in Γ_{34} with the itinerary $(2341)^n(241)^\infty$ for all positive integers n less than some N^*.

(c) *If $\omega_{34} > 0$ and $0 < \tau_{34} < \min\{2, 1+\delta_{34}\}$, then the $\mathcal{C}_{[34]}$ cycle is completely unstable.*

(i) *If any of the cases in* (b) *hold, then all trajectories starting in Γ_{34} sufficiently close to the network are mapped into Γ_4. If, in addition, $\delta_4 > 1$, these trajectories switch from the*

$\mathcal{C}_{[34]}$ cycle to the $\mathcal{C}_{[4]}$ cycle, to which they are then asymptotic, and there exists an open set of trajectories in Γ_{34} with the itinerary $(2341)^n(241)^\infty$ for all positive integers n less than some N^*.

(ii) *If* (a)(i) *holds with $\nu_4 > 0$, all trajectories starting in Γ_{34}^- sufficiently close to the network are mapped into Γ_4. If, in addition, $\delta_4 > 1$, these trajectories switch from the $\mathcal{C}_{[34]}$ cycle to the $\mathcal{C}_{[4]}$ cycle, to which they are then asymptotic, and, for all positive integers n, there exists an open set of trajectories in Γ_{34}^- with the itinerary $(2341)^n(241)^\infty$. All other trajectories starting near $\mathcal{C}_{[34]}$ leave a neighbourhood of $\mathcal{C}_{[34]}$.*

(iii) *If* (a)(i) *holds with $\nu_4 < 0$, or if* (a)(ii) *or* (a)(iii) *holds, all trajectories starting near $\mathcal{C}_{[34]}$ leave a neighbourhood of $\mathcal{C}_{[34]}$.*

(d) *If $\omega_{34} < 0$ or $\tau_{34} < 0$, then the $\mathcal{C}_{[34]}$ cycle is completely unstable. All trajectories starting in Γ_{34} sufficiently close to the network are mapped into Γ_4. If, in addition, $\delta_4 > 1$, these trajectories switch from the $\mathcal{C}_{[34]}$ cycle to the $\mathcal{C}_{[4]}$ cycle, to which they are then asymptotic, and there exists an open set of trajectories in Γ_{34} with the itinerary $(2341)^n(241)^\infty$ for all positive integers n less than some N^*. All other trajectories starting near $\mathcal{C}_{[34]}$ leave a neighbourhood of $\mathcal{C}_{[34]}$.*

(e) *If $\delta_4 > 1$ and $\nu_4 > 0$, then the $\mathcal{C}_{[4]}$ cycle is fragmentarily asymptotically stable. All trajectories starting in Γ_4 are asymptotic to the $\mathcal{C}_{[4]}$ cycle, with itinerary $(241)^\infty$.*

(f) *If $\delta_4 > 1$ and $\nu_4 < 0$, then the $\mathcal{C}_{[4]}$ cycle is almost completely unstable and all trajectories starting in Γ_4 are mapped into Γ_{34}. If, in addition, any of the conditions in* (a) *hold, these trajectories switch from the $\mathcal{C}_{[4]}$ cycle to the $\mathcal{C}_{[34]}$ cycle, to which they are then asymptotic, and, for all positive integers n, there exists an open set of trajectories in Γ_4 with the itinerary $(241)^n(2341)^\infty$.*

(g) *If $\delta_4 < 1$, then the $\mathcal{C}_{[4]}$ cycle is completely unstable. If $\nu_4 < 0$, then all trajectories starting in Γ_4^- sufficiently close to the network are mapped into Γ_{34}. If, in addition, any of the conditions in* (a) *hold, these trajectories switch from the $\mathcal{C}_{[4]}$ cycle to the $\mathcal{C}_{[34]}$ cycle, to which they are then asymptotic, and, for all positive integers n, there exists an open set of trajectories in Γ_4 with the itinerary $(241)^n(2341)^\infty$. All other trajectories starting near $\mathcal{C}_{[4]}$ leave a neighbourhood of $\mathcal{C}_{[4]}$.*

Note that (a)(i) and (e) indicate a qualitative difference between the dynamics near the Kirk–Silber and the Δ-clique networks: if there is bistability of the two cycles of the Δ-clique network, then there must be switching from the $\mathcal{C}_{[34]}$ cycle to the $\mathcal{C}_{[4]}$ cycle, whereas there is no switching near the Kirk–Silber network if there is bistability of the two cycles.

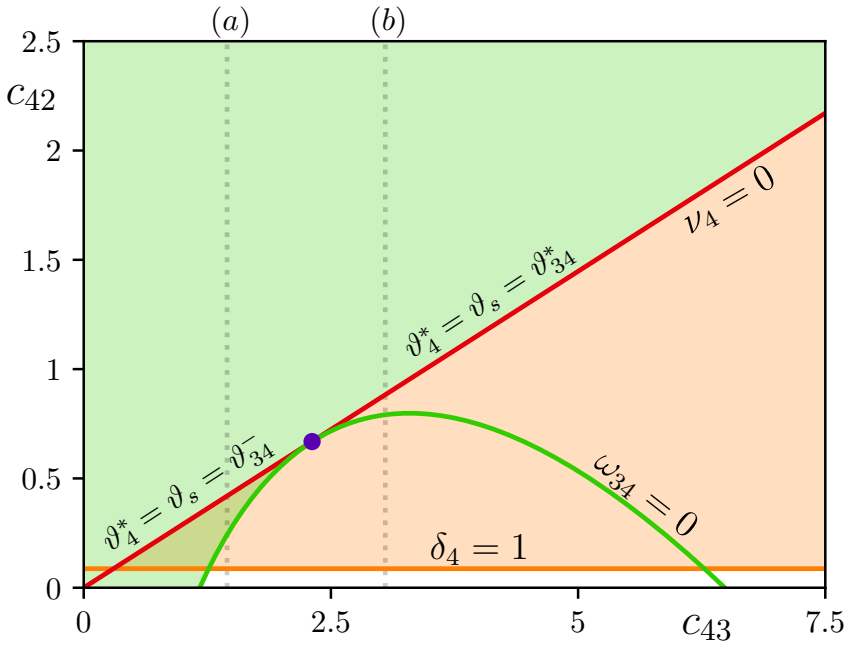

Figure 11.2: A bifurcation set of the Δ-clique network. The set is shaded orange where the $\mathcal{C}_{[4]}$ cycle is fragmentarily asymptotically stable, and shaded green where the $\mathcal{C}_{[34]}$ cycle is fragmentarily asymptotically stable. Solid lines correspond to relations between parameter values as indicated. The green line is the locus of the fold bifurcation of ϑ_{34}^* and ϑ_{34}^-. The red line is the locus of the border-collision bifurcation of ϑ_4^* and also one of ϑ_{34}^* and ϑ_{34}^-, and the orange line is the locus of the transcritical bifurcation of ϑ_4^* and ϑ_4^-. Faint dotted lines correspond as labelled to parameter values of the bifurcation diagrams in Figure 11.3. For all parameter values in the bifurcation set, $\tau_{34} > \min\{2, 1 + \delta_{34}\}$. The purple dot is the location of the codimension-two point where $\vartheta_{34}^c = \vartheta_s$ if $\omega_{34} = 0$. Parameter values for this figure are given in §B.5.3.

The proofs of (e), (f), and (g) are the same as for the Kirk–Silber network, and so we omit them. The other parts of the theorem are proved in the following sections, as follows:

- In sections 11.1 and 11.2, we prove results about the fixed points of f_Δ which are used in the remainder of the proof.
- In §11.3, we prove (d) of Theorem 11.1. This part of Theorem 11.1 corresponds to parameter values for which fixed points of f_{34} either do not exist, or cannot be admissible.
- In §11.4, we prove (a)(ii), (a)(iii), (b), and (c)(i) of Theorem 11.1. These parts of Theorem 11.1 correspond to parameter values for which fixed points of f_{34} are created in a virtual fold bifurcation.
- In §11.5, we prove (a)(i), and (c)(ii) and (iii) of Theorem 11.1. These parts of Theo-

rem 11.1 correspond to parameter values for which fixed points of f_{34} are created in an admissible fold bifurcation.

For clarity, we provide the following summary of Theorem 11.1, highlighting its most important features:

- The results of Theorem 11.1(a) define when the $\mathcal{C}_{[34]}$ cycle is fragmentarily asymptotically stable and when trajectories switch from the stable $\mathcal{C}_{[34]}$ cycle to the $\mathcal{C}_{[4]}$ cycle.
- The results of Theorem 11.1(b) define when the $\mathcal{C}_{[34]}$ cycle has lost stability through a breaking of condition (III) of Theorem 6.1, and which corresponds to a border-collision bifurcation in the projected map. For these parameter values, all trajectories that start near the $\mathcal{C}_{[34]}$ cycle switch to the $\mathcal{C}_{[4]}$ cycle.
- The results of Theorem 11.1(c) define when the $\mathcal{C}_{[34]}$ cycle has lost stability in a resonance bifurcation, which corresponds to a breaking of condition (II) of Theorem 6.1, but for which $\lambda_{\max} > 0$. For these parameter values, only some trajectories switch from the $\mathcal{C}_{[34]}$ cycle to the $\mathcal{C}_{[4]}$ cycle.
- The results of Theorem 11.1(d) define when the $\mathcal{C}_{[34]}$ cycle has lost stability in a manner that corresponds to a breaking of condition (I) of Theorem 6.1, or a breaking of condition (II) of Theorem 6.1 and $\lambda_{\max} < 0$. For these parameter values, only some trajectories switch from the $\mathcal{C}_{[34]}$ cycle to the $\mathcal{C}_{[4]}$ cycle.

Figure 11.2 gives a bifurcation set that summarises some of the results of Theorem 11.1.

11.1 Fixed points, existence, admissibility, and stability

The fixed points of the map f_4, and their admissibility, are the same as for the Kirk–Silber network in §10.1.

The fixed points of the map f_{34} are

$$\vartheta_{34}^{*} = \frac{-\lambda_{34}^{+} + \alpha_2 + \alpha_4}{\zeta_{34}}$$

and

$$\vartheta_{34}^{-} = \frac{-\lambda_{34}^{-} + \alpha_2 + \alpha_4}{\zeta_{34}}.$$

These fixed points exist if and only if $\omega_{34} \geq 0$, and, if $\omega_{34} = 0$,

$$\vartheta_{34}^{*} = \vartheta_{34}^{-} = \vartheta_{34}^{\mathrm{c}} := \frac{2\alpha_2 + \alpha_4 - \alpha_1}{2\zeta_{34}}.$$

Table 11.1: Admissibility of ϑ_{34}^* and ϑ_{34}^- when $\tau_{34} > 0$.

		$\nu_4 > 0$	$\nu_4 < 0$
$\zeta_{34} < 0$	$\beta_{34} > 0$	ϑ_{34}^*: virtual ϑ_{34}^-: virtual	ϑ_{34}^*: admissible ϑ_{34}^-: virtual
	$\beta_{34} < 0$	ϑ_{34}^*: admissible ϑ_{34}^-: admissible	ϑ_{34}^*: admissible ϑ_{34}^-: virtual
$\zeta_{34} > 0$	—	ϑ_{34}^*: virtual ϑ_{34}^-: virtual	ϑ_{34}^*: admissible ϑ_{34}^-: virtual

In the next subsection, we confirm that the bifurcation at $\omega_{34} = 0$ is a fold bifurcation. Assuming $\omega_{34} = 0$, we say that the fold bifurcation is virtual if $\vartheta_{34}^{\mathrm{c}}$ is virtual, and we say the fold bifurcation is admissible if $\vartheta_{34}^{\mathrm{c}}$ is admissible. If $\tau_{34} < 0$ or $\zeta_{34} > 0$, then, if $\omega_{34} = 0$, the fold is virtual. However, if $\tau_{34} > 0$ and $\zeta_{34} < 0$, then, if $\omega_{34} = 0$, the fold is virtual if and only if $\beta_{34} > 0$, and the fold is admissible if and only if $\beta_{34} < 0$.

If $\tau_{34} < 0$, then both ϑ_{34}^* and ϑ_{34}^- are virtual. If $\tau_{34} > 0$, the admissibility of ϑ_{34}^* and ϑ_4^- depends on ζ_{34}, β_{34} and ν_4. We present these results in Table 11.1. Since the admissibility of these fixed points depends on ν_4, at the point of the border-collision bifurcation, where $\nu_4 = 0$, ϑ_4^* also undergoes a border-collision bifurcation. This relationship can be seen from the continuity of the projected map of Δ-clique network (see §11.2): if $f_4(\vartheta_{\mathrm{s}}) = \vartheta_{\mathrm{s}}$, then $f_{34}(\vartheta_{\mathrm{s}}) = \vartheta_{\mathrm{s}}$ also and there is a border-collision bifurcation of a fixed point of f_{34}.

With the same reasoning as in §10.2 we derive the following proposition, which allows us to study the stability of the heteroclinic cycles $\mathcal{C}_{[34]}$ and $\mathcal{C}_{[4]}$ at the switching equilibrium ξ_2:

Proposition 11.2. Suppose $\omega_{34} > 0$ and $\tau_{34} > \min\{2, 1 + \delta_{34}\}$. The fixed point ϑ_{34}^* is admissible if and only if the eigenvector $w_{\max}$ of $M_3^{(34)}$ satisfies Podvigina's third condition for stability. Suppose $\delta_4 > 1$. The fixed point ϑ_4^* is admissible if and only if the eigenvector $w_{\max}$ of $M_4^{(4)}$ satisfies Podvigina's third condition for stability.

The stability of fixed points of the map f_4 is the same as for the Kirk–Silber network in §10.1. Calculating $\mathrm{D}f_{34}(\vartheta)$ gives

$$\mathrm{D}f_{34}(\vartheta) = \frac{\delta_{34}}{(\zeta_{34}\vartheta - \alpha_2 - \alpha_4)^2},$$

Since $\delta_{34} > 0$, $\mathrm{D}f_{34}$ is strictly positive. Evaluating at ϑ_{34}^* and ϑ_{34}^- gives

$$\mathrm{D}f_{34}(\vartheta_{34}^*) = \frac{\delta_{34}}{\tau_{34}\lambda_{34}^+ - \delta_{34}}$$

and

$$\mathrm{D}f_{34}(\vartheta_{34}^-) = \frac{\delta_{34}}{\tau_{34}\lambda_{34}^- - \delta_{34}}.$$

At the bifurcation point $\omega_4 = 0$, where $\vartheta_{34}^* = \vartheta_{34}^- = \vartheta_{34}^c$, $\mathrm{D}f_{34}(\vartheta_{34}^c) = 1$, and therefore this bifurcation is generically a fold bifurcation.

Assume $\omega_{34} > 0$. If $\tau_{34} > 0$, $0 < \mathrm{D}f_{34}(\vartheta_{34}^*) < 1$, and ϑ_{34}^* is asymptotically stable, while $1 < \mathrm{D}f_{34}(\vartheta_{34}^-)$, and ϑ_{34}^- is unstable. If $\tau_{34} < 0$, $1 < \mathrm{D}f_{34}(\vartheta_{34}^*)$, and ϑ_{34}^* is unstable, while $0 < \mathrm{D}f_{34}(\vartheta_{34}^-) < 1$, and ϑ_{34}^- is asymptotically stable. We give bifurcation diagrams of the fixed points, and their admissibility, in Figure 11.3(a) when the fold is admissible, and in Figure 11.3(b) when the fold is virtual.

In Figure 11.3(a), we see that, when the fold bifurcation is admissible, the fixed points of f_{34} and f_4 are both admissible for values of c_{42} less than the critical value of the border-collision bifurcation. After the bifurcation, both are virtual. As such, this border-collision bifurcation is known as a *nonsmooth fold*. Indeed, near where the thick solid orange line and the thick dotted green line meet, the bifurcation diagram resembles a fold bifurcation, but the curve is not differentiable at the bifurcation point. A nonsmooth fold border-collision occurs when the two fixed points cross the switching manifold in the opposite direction at the point of the bifurcation. In contrast, the border-collision bifurcation seen in Figure 11.3(b) is described as being *persistent*. An admissible fixed point exists for values of c_{42} less than and greater than the critical value, and the two fixed points cross the switching manifold in the same direction.

Stability of a fixed point ϑ^* of the projected map is equivalent to, under iteration of the transition matrix, a vector converging to the eigenspace that projects onto ϑ^*. Such convergence requires the corresponding eigenvalue of that eigenspace having the greatest absolute value of the spectrum of the transition matrix. In the case of $\mathcal{C}_{[3]}$ and $\mathcal{C}_{[4]}$ cycles, this condition also corresponds to Podvigina's second stability condition $\lambda_{\max} > 1$. However, in the case of the $\mathcal{C}_{[34]}$ cycle, if $\tau_{34} > 0$ and so ϑ_{34}^* is stable, $\lambda_{\max} = \lambda_{34}^+$, whereas Podvigina's second condition is satisfied only if $\tau_{34} > \min\{2, 1 + \delta_{34}\}$; that is, $\lambda_{34}^+ > 1$.

All full transition matrices of the $\mathcal{C}_{[4]}$ cycle have an eigenvector with eigenvalue 1. Thus, when the loss of stability of this cycle is associated with Podvigina's second stability condition, there is also a change in the stability of fixed points of the projected map, as the eigenvalue with greatest absolute value also changes. In the case of the $\mathcal{C}_{[34]}$ cycle, the eigenvalue λ_{34}^+ can become smaller than 1 but remain $\lambda_{\max}$, and so there is no change in the stability of the fixed points of the projected map. For this reason, we also need to impose the condition $\tau_{34} > \min\{2, 1 + \delta_{34}\}$, as this condition is not captured in the dynamics of the projected map.

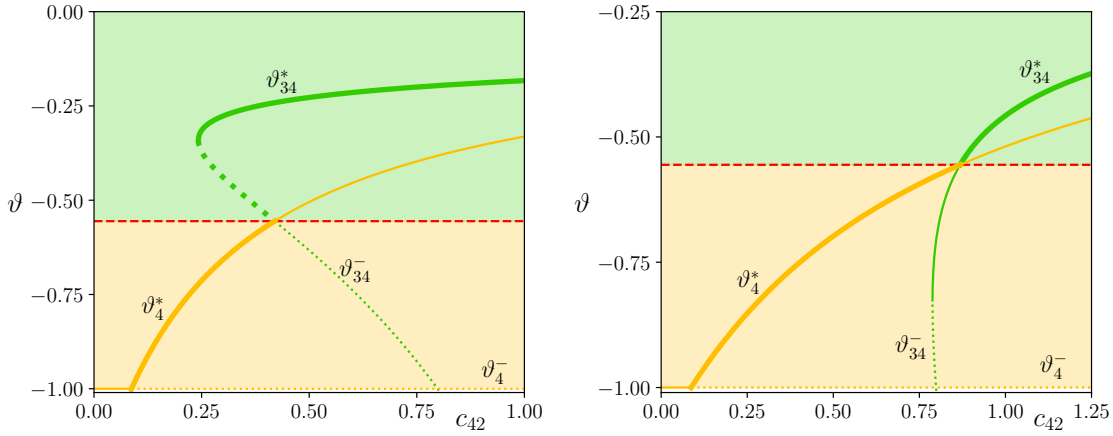

(a) (b)

Figure 11.3: Bifurcation diagrams of the fixed points of f_4 and f_{34} for (a) $c_{43} = 1.45$, and so the fold is admissible and (b) $c_{43} = 3.05$, and so the fold is virtual. The domain of f_4 is shaded orange, and of f_{34} is shaded green. Stable fixed points are solid, and unstable dotted. Admissible fixed points are thick lines and virtual fixed points are thin lines. The switching manifold ϑ_s is the dashed red line. All other parameter values are the same as those in Figure 11.2.

11.2 Continuity of the projected map of the Δ-clique network at ϑ_s

In the case of the Δ-clique network, we find that

$$\lim_{\vartheta \searrow \vartheta_s} f_{34}(\vartheta) = \frac{-(c_{42}t_{13} + e_{12}c_{43})}{c_{42}(t_{13} + c_{14}) + e_{12}c_{43}},$$

and

$$\lim_{\vartheta \nearrow \vartheta_s} f_4(\vartheta) = \frac{-(c_{42}t_{13} + e_{12}c_{43})}{c_{42}(t_{13} + c_{14}) + e_{12}c_{43}}.$$

Therefore, the projected map of the Δ-clique network is continuous, which can be seen in all four examples in Figure 11.1, where the two functions have the same value at ϑ_s, given by the dashed red line.

11.3 Dynamics with $\omega_{34} < 0$ or $\tau_{34} < 0$

We begin by proving (d) of Theorem 11.1.

Note that $f_\Delta(0), f_\Delta(\vartheta_s) \in S$, regardless of parameter values, and so $f_\Delta(0) < 0$ and $f_\Delta(\vartheta_s) > -1$. When $\omega_{34} < 0$ or $\tau_{34} < 0$, f_{34} either has no fixed points, or has no fixed points in Θ_{34}, respectively. Therefore, $f_{34}(\vartheta) < \vartheta$ for all $\vartheta \in \Theta_{34}$ and so, for all ϑ, there

exists a positive integer n such that $f_{34}^n(\vartheta) \in \Theta_4$. As in §10.5, we define, for all non-negative integers n, $\mathcal{E}_n$ as the n^{th} pre-image of ϑ_{s} in Θ_{34}; that is, $f_4^n(\mathcal{E}_n) = \vartheta_{\text{s}}$. In §10.5, there are simple expressions for $\mathcal{E}_n$ due to the simplified form of the matrices M_3 and M_4 of the Kirk–Silber network. The nature of the matrix M_{34} of the Δ-clique network means there is no simple expression for $\mathcal{E}_n$, beyond expressions involving matrix multiplication. Since there are no f_{34}-invariant sets in Θ_{34} when $\omega_{34} < 0$ or $\tau_{34} < 0$, there is some N^* such that $\mathcal{E}_n > 0$ for all $n \geq N^*$. We have therefore proven (d) of Theorem 11.1.

An example of the dynamics of the projected map under these parameter values is shown in Figure 11.1(a).

11.4 Dynamics with a virtual fold

We now consider dynamics when $\omega_{34} > 0$, $\tau_{34} > 0$ (when the fold bifurcation is virtual) and so prove (a)(ii), (a)(iii), (b), and (c)(i) of Theorem 11.1.

Under these parameter values, if $\nu_4 > 0$, then both ϑ_{34}^* and ϑ_{34}^- are virtual, but ϑ_4^* is admissible. For all $\vartheta \in \Theta_{34}$, $f_{34}(\vartheta) < \vartheta$. Therefore, for every $\vartheta \in \Theta_{34}$, there is some n such that $f_\Delta^n(\vartheta) \in \Theta_4$. With the same reasoning as in §11.3, the number of iterations n is bounded above by some N^*, proving (b).

At $\nu_4 = 0$, both ϑ_{34}^* and ϑ_4^* undergo a border-collision bifurcation and coincide with ϑ_{s}. For $\nu_4 < 0$, ϑ_{34}^* is admissible and ϑ_4^* virtual. Under these parameter values, $f_{34}(\vartheta) > \vartheta$ for all $\vartheta \in (\vartheta_{\text{s}}, \vartheta_{34}^*)$, and $f_{34}(\vartheta) < \vartheta$ for all $\vartheta \in (\vartheta_{34}^*, 0)$. Therefore, ϑ_{34}^* is globally attracting in Θ_{34}. If $\lambda_{34}^+ > 1$—or, equivalently, $\tau_{34} > \min\{2, 1 + \delta_{34}\}$—the $\mathcal{C}_{[34]}$ cycle is fragmentarily asymptotically stable. We have therefore proven (a)(ii) and (a)(iii) of Theorem 11.1.

In the case that $0 < \tau_{34} < \min\{2, 1 + \delta_{34}\}$, $0 < \lambda_{\max} < 1$, the $\mathcal{C}_{[34]}$ cycle is completely unstable [Pod12]. Trajectories beginning near the cycle leave a neighbourhood of the cycle if $\nu_4 < 0$. If $\nu_4 > 0$, trajectories beginning sufficiently close to the network switch from the $\mathcal{C}_{[34]}$ to $\mathcal{C}_{[4]}$ cycle before they leave a neighbourhood of the network, completing the proof of (c)(i).

An example of the dynamics of the projected map under these parameter values is shown in Figure 11.1(b). Note that the projected map looks qualitatively the same under these parameter values if the $\mathcal{C}_{[34]}$ cycle is unstable and $0 < \tau_{34} < \min\{2, 1 + \delta_{34}\}$. Therefore, in this case, an additional check must be completed to derive dynamics of trajectories near the network from the projected map.

11.5 Dynamics with an admissible fold

We last consider dynamics when $\omega_{34} > 0$, $\tau_{34} > 0$ (when the fold bifurcation is admissible) and so prove (a)(i), and (c)(ii) and (iii) of Theorem 11.1.

If $\nu_4 > 0$, then ϑ_{34}^- and ϑ_{34}^* are both admissible, and $\vartheta_{34}^- < \vartheta_{34}^*$. For all $\vartheta \in \big(\vartheta_{\rm s}, \vartheta_{34}^-\big) \cup (\vartheta_{34}^*, 0)$, $f_\Delta(\vartheta) < \vartheta$, and for all $\vartheta \in \big(\vartheta_{34}^-, \vartheta_{34}^*\big)$, $f_\Delta(\vartheta) > \vartheta$. Therefore, ϑ_{34}^* is attracting in $\big(\vartheta_{34}^-, 0\big)$, which corresponds to Γ_{34}^+. Again, we require $\tau_{34} > \min\{2, 1+\delta_{34}\}$ for the $\mathcal{C}_{[34]}$ cycle to be fragmentarily asymptotically stable. For all $\vartheta \in \big(\vartheta_{\rm s}, \vartheta_{34}^-\big)$, there is an n such that $f_\Delta^n(\vartheta) \in \Theta_4$. We again write $\mathcal{E}_n$ for the n-th preimage of $\vartheta_{\rm s}$. For these parameter values, $\mathcal{E}_n < \mathcal{E}_{n+1}$, and $\lim_{n\to\infty} \mathcal{E}_n = \vartheta_{34}^-$, and again there is no simple expression for each $\mathcal{E}_n$. However, since this limit is a fixed point, n is not bounded above. The interval $\big(\vartheta_{\rm s}, \vartheta_{34}^-\big)$ corresponds to the set Γ_{34}^-.

At $\nu_4 = 0$, both ϑ_{34}^- and ϑ_4^* undergo a border-collision bifurcation and coincide with $\vartheta_{\rm s}$. For $\nu_4 < 0$, both ϑ_{34}^- and ϑ_4^* are virtual, but ϑ_{34}^* remains admissible and is now globally attracting in Θ_{34}. Again, if $\tau_{34} > \min\{2, 1+\delta_{34}\}$, the $\mathcal{C}_{[34]}$ cycle is f.a.s, completing the proof of (a) of Theorem 11.1. The case where $0 < \tau_{34} < \{2, 1+\delta_{34}\}$ is the same as in §11.4, except now, if $\nu_4 > 0$, trajectories beginning in Γ_{34}^- sufficiently close to the network switch between cycles, completing the proof of (c) of Theorem 11.1, which also completes the proof of Theorem 11.1.

An example of the dynamics of the projected map under these parameter values is shown in Figure 11.1(c). Again, note that the projected map looks qualitatively the same under these parameter values if the $\mathcal{C}_{[34]}$ cycle is unstable and $0 < \tau_{34} < \min\{2, 1+\delta_{34}\}$.

11.6 Numerical examples

We consider the ODEs

$$\begin{aligned}
\dot{x}_1 &= x_1\big(1 - \|x\|_2^2 - c_{21}x_2^2 - t_{31}x_3^2 + e_{41}x_4^2\big),\\
\dot{x}_2 &= x_2\big(1 - \|x\|_2^2 + e_{12}x_1^2 - c_{32}x_3^2 - c_{42}x_4^2\big),\\
\dot{x}_3 &= x_3\big(1 - \|x\|_2^2 - t_{13}x_1^2 + e_{23}x_2^2 - c_{43}x_4^2\big),\\
\dot{x}_4 &= x_4\big(1 - \|x\|_2^2 - c_{14}x_1^2 + e_{24}x_2^2 + e_{34}x_3^2\big),
\end{aligned} \tag{11.2}$$

where c_{jk}, e_{jk}, and t_{jk} are positive real numbers. System (11.2) is $\mathbb{Z}_2^4$-equivariant, and contains a Δ-clique network. All four equilibria of the network lie at unit distance from the origin on the four coordinate axes in the positive orthant. Again, we assume that the parameters satisfy the contracting condition of the invariant sphere theorem [Fie96].

We again use the change of coordinates $X_i := \log x_j$, and numerically integrate the

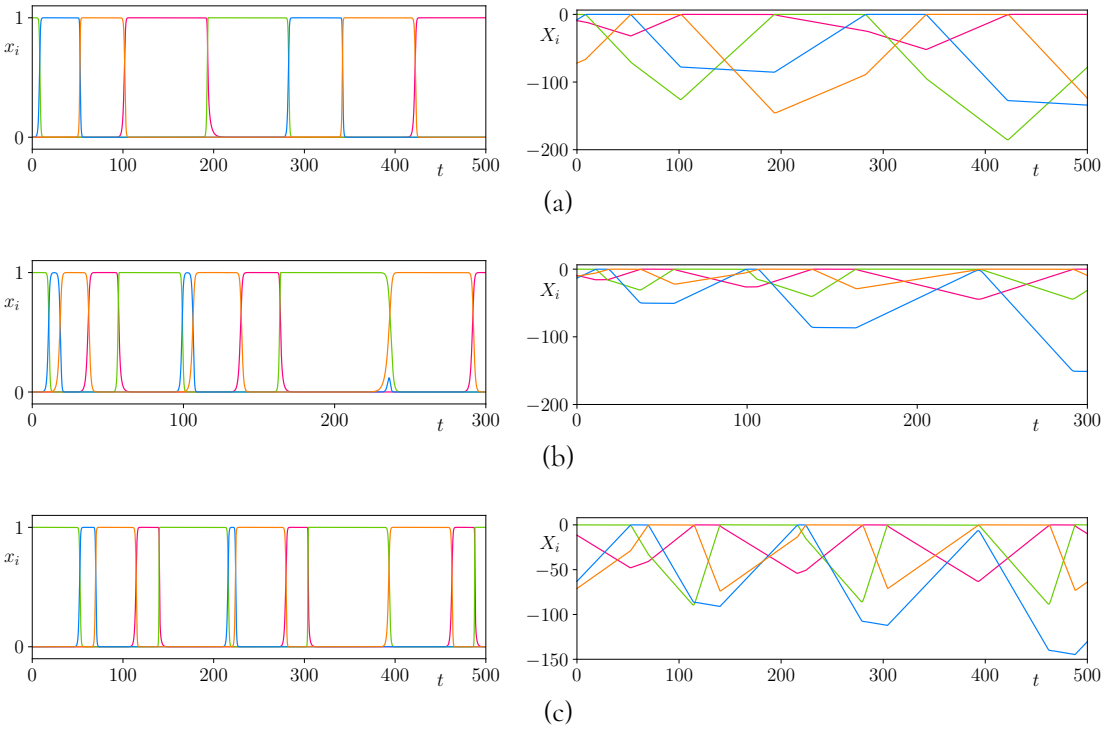

Figure 11.4: Example timeseries of trajectories near the Δ-clique network: (a) an admissible fold with $x(0) \in \Gamma_{34}^{+}$, (b) an admissible fold with $x(0) \in \Gamma_{34}^{-}$, and (c) $\omega_{34} < 0$. The colours red, green, blue, and orange correspond to x_1, x_2, x_3, and x_4, respectively, and similarly for the X_i. In all three examples, $\delta_4 > 1$ and $\nu_4 > 0$. Parameter values and initial conditions for these figures are given in §B.5.3.

resulting ODEs $\dot{X}_j$ with a variety of parameter values. Three different examples are found in Figure 11.4. Parameter values in Figures 11.4(a) and 11.4(b) are identical, and the projected map in these examples looks like Figure 11.1(c). Both cycles are fragmentarily asymptotically stable, with a subset of Γ_{34} switching to the $\mathcal{C}_{[4]}$ cycle. These trajectories have itinerary $(2341)^\infty$ and $(2341)^2(241)^\infty$, respectively. The trajectory in Figure 11.4(c) switches between cycles with itinerary $(2341)^2(241)^\infty$. Under these parameter values, the projected map looks like Figure 11.1(a).

§12 The tournament network

The tournament network is defined as the union of the cycles $\mathcal{C}_{[3]}$, $\mathcal{C}_{[4]}$, and $\mathcal{C}_{[34]}$. Therefore, the tournament network—unlike the Kirk–Silber and Δ-clique networks—contains subnetworks:

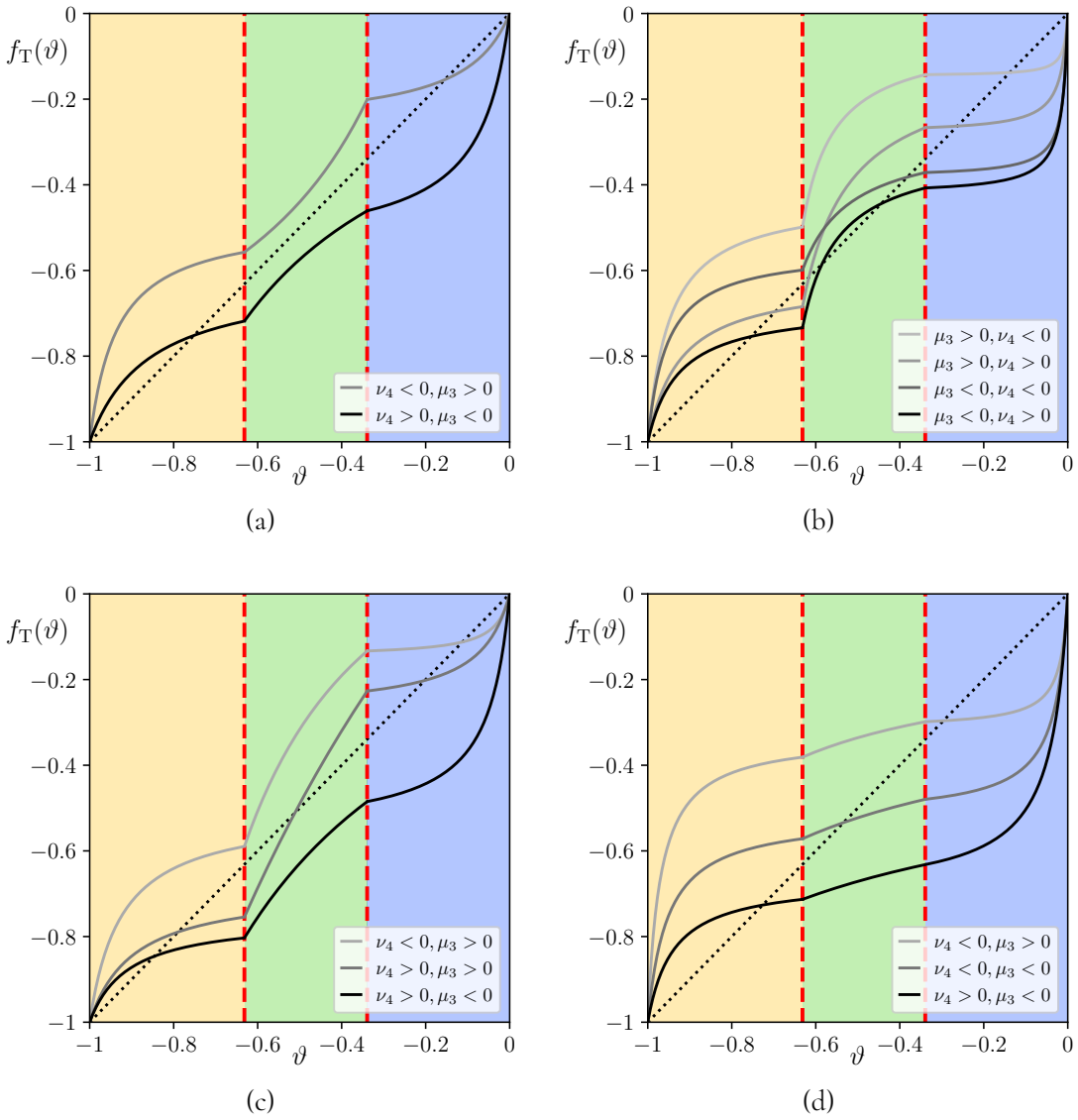

Figure 12.1: Schematic representations of the projected map of the tournament network, for different relations between parameters: (a) $\omega_{34} < 0$, (b) an admissible fold in Θ_{34}, (c) a virtual fold in Θ_3, and (d) a virtual fold in Θ_4, or outside S. In (a), the fixed points ϑ^*_{34} and ϑ^-_{34} do not exist. In (b), (c), and (d), $\omega_{34} > 0$ and so the fixed points exist, and were created in a fold bifurcation. In all plots, $\delta_3 > 1$ and $\delta_4 > 1$. The values of μ_3 and ν_4 are as indicated by the shading of the plot. The regions shaded yellow, green, and blue correspond to Θ_4, Θ_{34}, and Θ_3, respectively. The left dashed red line indicates ϑ^-_s, and the right dashed red line indicates ϑ^+_s. Parameter values for these figures are given in §B.5.4.

1. a subnetwork equivalent to a Kirk–Silber network, $\mathcal{C}_{[3]} \cup \mathcal{C}_{[4]}$; and
2. two subnetworks equivalent to a Δ-clique network: $\mathcal{C}_{[34]} \cup \mathcal{C}_{[4]}$, and $\mathcal{C}_{[3]} \cup \mathcal{C}_{[34]}$.

The tournament network has two switching equilibria: ξ_2 and ξ_3. All trajectories leaving a small neighbourhood of ξ_2 in the direction of ξ_4 cycle around $\mathcal{C}_{[4]}$. Those trajectories that leave ξ_2 in the direction of ξ_3 then leave a small neighbourhood of ξ_3 in the direction of ξ_1 or ξ_4, and therefore cycle around $\mathcal{C}_{[3]}$ or $\mathcal{C}_{[34]}$, respectively. However, all trajectories eventually return to ξ_2 if the network is attracting.

The tournament network was studied in [CFL24] as the Jungle Game. In [CFL24], Castro, Ferreira, and Labouriau make certain assumptions on the parameter values that we do not make here, but the result in [CFL24] that only the $\mathcal{C}_{[4]}$ cycle is stable while the other two are completely unstable agrees with our results where parameter values are equivalent. (This holds, for example, for the parameter values used in Figures 12.1(c) and 12.1(d) when $\nu_4 > 0$ and $\mu_3 < 0$.)

We consider subsets of points in $\mathbf{H}_3^{\mathrm{in},2}$ that give rise to trajectories that cycle around $\mathcal{C}_{[3]}$ or $\mathcal{C}_{[34]}$. We take the pre-image under the basic map $\varphi_{123}\colon \mathbf{H}_2^{\mathrm{in},1} \to \mathbf{H}_3^{\mathrm{in},2}$ of these two domains, and partition $\mathbf{H}_2^{\mathrm{in},1}$ into three domains: Γ_3, Γ_4, and Γ_{34}. These domains correspond to trajectories that, after leaving a small neighbourhood of ξ_2, next cycle around the $\mathcal{C}_{[3]}$, $\mathcal{C}_{[4]}$, or $\mathcal{C}_{[34]}$ cycle. This partition allows us to define three corresponding subsets of S:

$$\Theta_3 = \big(\vartheta_{\mathrm{s}}^{+}, 0\big),$$
$$\Theta_{34} = \big(\vartheta_{\mathrm{s}}^{-}, \vartheta_{\mathrm{s}}^{+}\big),$$

and

$$\Theta_4 = \big(-1, \vartheta_{\mathrm{s}}^{-}\big),$$

where

$$\vartheta_{\mathrm{s}}^{-} = \frac{-1}{1 + \dfrac{e_{24}}{e_{23}}}$$

and

$$\vartheta_{\mathrm{s}}^{+} = \frac{-1}{1 + \left(\dfrac{c_{21}e_{34}}{e_{23}e_{31}} + \dfrac{e_{24}}{e_{23}}\right)}.$$

We can then derive the projected map of the tournament network, $f_{\mathrm{T}}\colon \Theta_3 \cup \Theta_{34} \cup \Theta_4 \to S$:

$$f_{\mathrm{T}}(\vartheta) = \begin{cases} f_3(\vartheta) = \dfrac{-\delta_3\vartheta}{(\delta_3+\rho_3-1)\vartheta - 1}, & \text{if } \vartheta \in \Theta_3, \\ f_{34}(\vartheta) = \dfrac{(\alpha_2-\alpha_1)\vartheta + \alpha_2}{\zeta_{34}\vartheta - \alpha_2 - \alpha_4}, & \text{if } \vartheta \in \Theta_{34}, \\ f_4(\vartheta) = \dfrac{(1-\rho_4)\vartheta - \rho_4}{(\delta_4+\rho_4-1)\vartheta + \delta_4 + \rho_4}, & \text{if } \vartheta \in \Theta_4. \end{cases} \tag{12.1}$$

The expressions for each of the constants in this function are given in §B.1. The complete analysis of this projected map is complicated, and involves many cases. In this section, we do not state a complete description of all dynamics that can be observed near the tournament network, as we did in Theorems 10.1 and 11.1. Instead, we give a qualitative description of how the dynamics can be analysed, and several examples that show interesting dynamics near the network.

The maps f_3, f_{34}, and f_4 are analogous to those studied in Sections 10 and 11, though with differing expressions for some constants used due to the change in the global classification of some eigenvalues. As in the case of the Kirk–Silber and Δ-clique networks, the $\mathcal{C}_{[3]}$ and $\mathcal{C}_{[4]}$ cycles are stable if their corresponding map has an admissible and attracting fixed point. In the case of the $\mathcal{C}_{[34]}$ cycle, for the cycle to be attracting, the fixed point ϑ_{34}^* must be admissible and attracting. However, we must additionally impose $\tau_{34} > \min\{2, 1+\delta_{34}\}$. In all three cases, it is straightforward to verify that admissibility of a fixed point corresponds to all transition matrices satisfying Podvigina's third stability condition in Theorem 6.1, assuming the first two conditions are also satisfied, as in Propositions 10.2 and 11.2.

The stability and admissibility of ϑ_4^* is the same as in Sections 10 and 11. The condition $\nu_3 = 0$ corresponds now to $\vartheta_3^* = \vartheta_{\mathrm{s}}^-$. However, ϑ_3^* is now virtual when $\vartheta_3^* < \vartheta_{\mathrm{s}}^+$, when $\mu_3 < 0$, where

$$\mu_3 = \frac{c_{14}}{e_{12}} - \frac{c_{13}e_{24}}{e_{12}e_{23}} - \frac{c_{13}c_{21}e_{34}}{e_{12}e_{23}e_{31}}.$$

At $\mu_3 = 0$, the eigenvector $w_{\max}$ of $M_1^{(3)}$ has a zero entry, and so does not satisfy Podvigina's third stability condition.

The admissibility of the fixed points ϑ_{34}^* and ϑ_{34}^- is the complicating factor for the analysis of the tournament network's projected map. The projected map of the tournament network, like the Δ-clique network, is continuous (see §12.2). Therefore, border-collision bifurcations of fixed points of f_{34} also occur at $\nu_4 = 0$ and $\mu_3 = 0$. However, which fixed point, ϑ_{34}^* or ϑ_{34}^-, changes admissibility, and which direction it crosses which switching manifold,

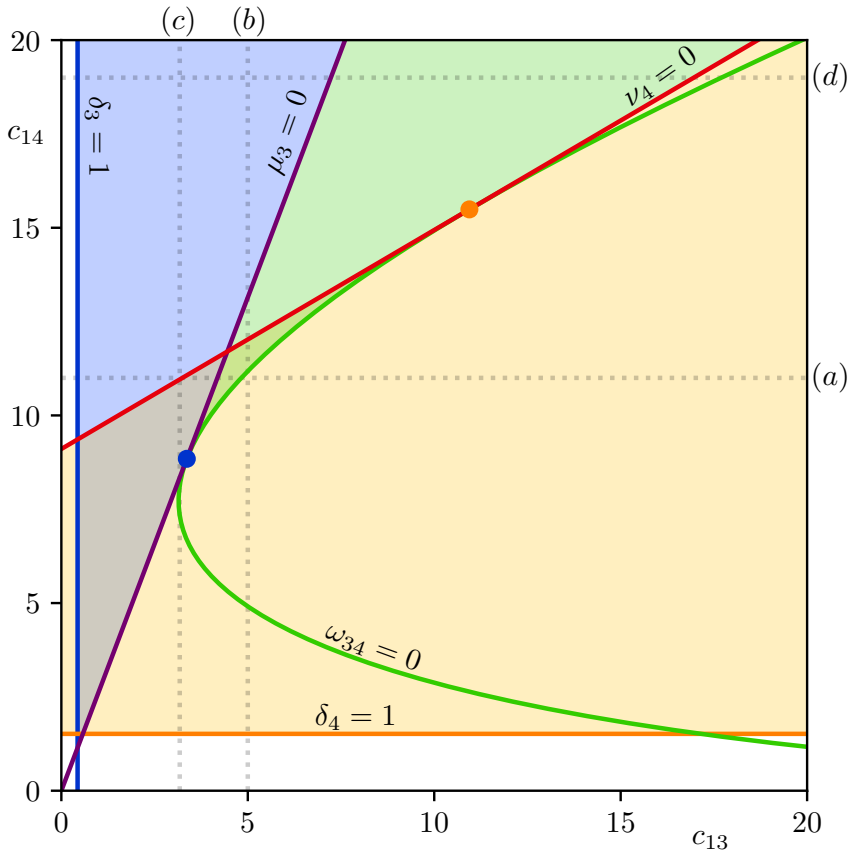

Figure 12.2: A bifurcation set of the tournament network, for $\tau_{34} > \min\{2, 1 + \delta_{34}\}$ and $\zeta_{34} < 0$. Where the set is shaded blue, green, or orange, the $\mathcal{C}_{[3]}$, $\mathcal{C}_{[34]}$, or $\mathcal{C}_{[4]}$ cycle, respectively, is fragmentarily asymptotically stable. Coloured lines correspond to relations between parameter values as indicated. Faint dotted lines correspond as labelled to parameter values of the bifurcation diagrams in Figure 12.3. The blue and orange dots are the location of the codimension-two point where the fold bifurcation of the fixed points of f_{34} occurs on the switching manifolds ϑ_s^+ and ϑ_s^-, respectively. Parameter values for this figure are given in §B.5.4.

depends on whether the fold bifurcation of ϑ_{34}^* and ϑ_{34}^- occurs in Θ_3, Θ_{34}, Θ_4, or outside S, and also depends on the concavity of f_{34} in Θ_{34}; that is, on whether $\zeta_{34} < 0$ or $\zeta_{34} > 0$.

12.1 Overview of analysis

We focus on the case where $\zeta_{34} < 0$, and so the function f_{34} is concave down in Θ_{34}. We assume, when $\omega_{34} > 0$, that $\tau_{34} > \min\{2, 1 + \delta_{34}\}$. We also assume $\delta_3 > 1$ and $\delta_4 > 1$. We show various examples of the projected map of the tournament network in Figure 12.1. For visual clarity, we plot each function only in its domain of definition, and plot multiple examples before and after certain border-collision bifurcations in the same plot, distinguished

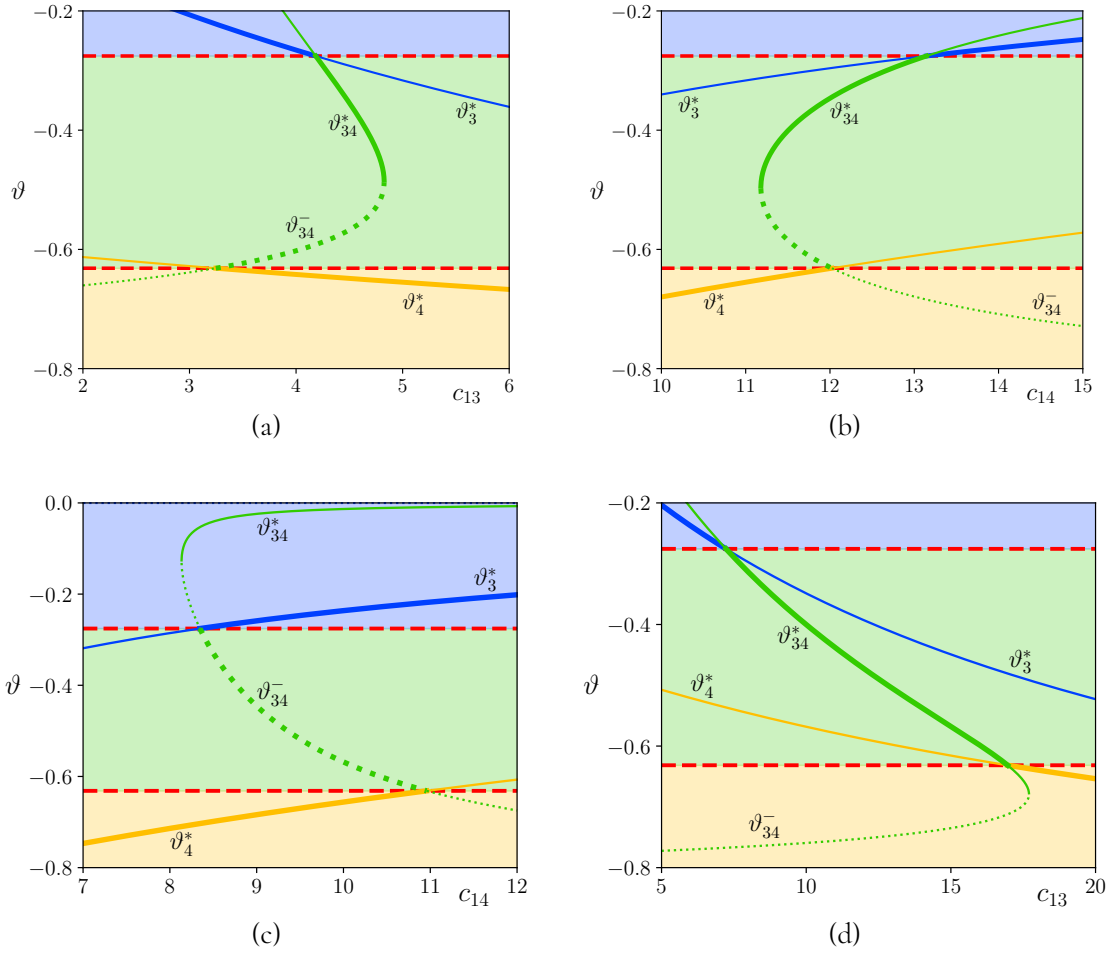

Figure 12.3: Bifurcation diagrams of the fixed points of f_3, f_{34}, and f_4, as labelled, for (a) $c_{14} = 11$, with an admissible fold, (b) $c_{13} = 5$, with an admissible fold, (c) $c_{13} = 3.175$, with a virtual fold in Θ_3, and (d) $c_{14} = 19$, with a virtual fold in Θ_4. In (a) and (b), we observe both persistent and nonsmooth fold border-collisions, in (c), only non smoothfolds, and in (d), only persistent border-collisions. The domain Θ_3, Θ_{34}, and Θ_4 are shaded blue, green, and orange, respectively. Stable fixed points are solid, and unstable dotted. Admissible fixed points are thick lines and virtual fixed points are thin lines. The top and bottom dashed red lines indicate the switching manifolds ϑ_s^+ and ϑ_s^-, respectively. All other parameter values are the same as those in Figure 12.2.

by lines of different shades.

To aid in the understanding of the dynamics we describe below, we present a bifurcation set in Figure 12.2. We also provide four qualitatively different bifurcation diagrams in Figure 12.3, which capture the dynamics we describe here.

Figure 12.1(a) shows the projected map with $\omega_{34} < 0$. We see that, when $\omega_{34} < 0$, only one of the $\mathcal{C}_{[3]}$ or $\mathcal{C}_{[4]}$ cycles is stable, and that all trajectories near the network are asymptotic to this cycle. Trajectories therefore switch between cycles, and can switch from

a length-three cycle to the $\mathcal{C}_{[34]}$ cycle, before switching again to the stable length-three cycle. If parameter values are such that $f_3(\vartheta_s^+) < \vartheta_s^-$, or $f_4(\vartheta_s^-) > \vartheta_s^+$, trajectories may switch from one length-three cycle to the other without cycling around the $\mathcal{C}_{[34]}$ cycle.

Figure 12.1(b) shows the possible dynamics if the fold bifurcation of f_{34} is admissible, and so occurs in Θ_{34}. First, if $\nu_4 < 0$ and $\mu_3 > 0$, all trajectories are asymptotic to the $\mathcal{C}_{[3]}$ cycle, and it is the only stable cycle. If $\nu_4 > 0$ and $\mu_3 > 0$, the length-three cycles are bistable, and Θ_{34} is partitioned by the unstable fixed point ϑ_{34}^- into subsets of points that are mapped into Θ_3 or Θ_4. If $\nu_4 > 0$ and $\mu_3 < 0$, there is bistability of the $\mathcal{C}_{[4]}$ and $\mathcal{C}_{[34]}$ cycles. The $\mathcal{C}_{[3]}$ cycle is unstable, and all trajectories in its domain are asymptotic to the $\mathcal{C}_{[34]}$ cycle. Since $\nu_4 > 0$, ϑ_{34}^- is admissible, and Θ_{34} is partitioned by the unstable fixed point ϑ_{34}^- into subsets of points that are mapped into Θ_4 and those that are asymptotic to the fixed point ϑ_{34}^*. Lastly, if $\nu_4 < 0$ and $\mu_3 < 0$, only the $\mathcal{C}_{[34]}$ cycle is stable, and all trajectories are asymptotic to it. Therefore, under the various cases, trajectories can switch once or twice in total, but only once between two given cycles. These results can be seen in Figures 12.3(a) and 12.3(b), which differ by the admissibility of ϑ_{34}^* between the two border-collision bifurcations. In Figure 12.3(a), between the two border-collisions, $\mathcal{C}_{[3]}$ and $\mathcal{C}_{[4]}$ are bistable, and, in Figure 12.3(b), only $\mathcal{C}_{[34]}$ is stable.

In Figure 12.1(c), we show the possible dynamics if the fold bifurcation of f_{34} is virtual, and occurs in Θ_3. Under these conditions, the $\mathcal{C}_{[34]}$ cycle is always unstable, and there is bistability of the length-three cycles if both $\mu_3 > 0$ and $\nu_4 > 0$. In this case, Θ_{34} is again partitioned into subsets of points that are mapped into Θ_3 or Θ_4. If $\nu_4 < 0$, all trajectories are asymptotic to $\mathcal{C}_{[3]}$, and if $\mu_3 < 0$, all trajectories are asymptotic to $\mathcal{C}_{[4]}$. We can have switching once or twice in total, and again only once between two given cycles. These results can be observed in Figure 12.3(c).

In Figure 12.1(d), we show the possible dynamics if the fold bifurcation of f_{34} is virtual, and occurs in Θ_4, or outside of S. Under these conditions, any cycle can be stable, but at most one cycle is stable for a given set of parameter values. The stable cycle is $\mathcal{C}_{[3]}$ if $\mu_3 > 0$, $\mathcal{C}_{[4]}$ if $\nu_4 > 0$, and it is $\mathcal{C}_{[34]}$ if $\nu_4 < 0$ and $\mu_3 < 0$. All trajectories are asymptotic to the stable cycle, and we again have switching once or twice in total, and only once between two given cycles. These results can be observed in Figure 12.3(d).

A similar analysis can be done in the case of $\zeta_{34} > 0$.[3]

[3] For a visual indication of the results, look at Figure 12.1 upside down, swapping the yellow and blue colours to swap the Θ_3 and Θ_4 domains, and also swapping the captions of (c) and (d).

12.2 Continuity of the projected map of the tournament network at $\vartheta_{\mathrm{s}}^{+}$ and $\vartheta_{\mathrm{s}}^{-}$

In the case of the tournament network, we find at $\vartheta_{\mathrm{s}}^{+}$ that

$$\lim_{\vartheta \searrow \vartheta_{\mathrm{s}}^{+}} f_3(\vartheta) = \frac{-c_{13}}{c_{13}+c_{14}}$$

and

$$\lim_{\vartheta \nearrow \vartheta_{\mathrm{s}}^{+}} f_{34}(\vartheta) = \frac{-c_{13}}{c_{13}+c_{14}},$$

and we find at $\vartheta_{\mathrm{s}}^{-}$ that

$$\lim_{\vartheta \searrow \vartheta_{\mathrm{s}}^{-}} f_{34}(\vartheta) = \frac{-(c_{42}c_{13}+e_{12}c_{43})}{c_{42}(c_{13}+c_{14})+e_{12}c_{43}}$$

and

$$\lim_{\vartheta \nearrow \vartheta_{\mathrm{s}}^{-}} f_{4}(\vartheta) = \frac{-(c_{42}c_{13}+e_{12}c_{43})}{c_{42}(c_{13}+c_{14})+e_{12}c_{43}}.$$

Therefore, the projected map of the tournament network is continuous at both $\vartheta_{\mathrm{s}}^{+}$ and $\vartheta_{\mathrm{s}}^{-}$, as seen in all examples in Figure 12.1.

12.3 Numerical examples

For the tournament network, we consider the system of ODEs

$$\begin{aligned}
\dot{x}_1 &= x_1\big(1-\|x\|_2^2 - c_{21}x_2^2 + e_{31}x_3^2 + e_{41}x_4^2\big),\\
\dot{x}_2 &= x_2\big(1-\|x\|_2^2 + e_{12}x_1^2 - c_{32}x_3^2 - c_{42}x_4^2\big),\\
\dot{x}_3 &= x_3\big(1-\|x\|_2^2 - c_{13}x_1^2 + e_{23}x_2^2 - c_{43}x_4^2\big),\\
\dot{x}_4 &= x_4\big(1-\|x\|_2^2 - c_{14}x_1^2 + e_{24}x_2^2 + e_{34}x_3^2\big),
\end{aligned} \tag{12.2}$$

where c_{jk} and e_{jk} are positive real numbers. System (12.2) is $\mathbb{Z}_2^4$-equivariant, and contains a heteroclinic network equivalent to the tournament network. All four equilibria of the network lie at unit distance from the origin on the four coordinate axes. Again, we assume that the parameters satisfy the contracting condition of the invariant sphere theorem [Fie96].

Again we use the change of coordinates $X_i := \log x_j$, and numerically integrate the resulting ODEs $\dot{X}_j$. We show one example in Figure 12.4. This trajectory has itinerary $(231)^2(2341)^2(241)^\infty$, and therefore switches twice between cycles. The onset of switching from the $\mathcal{C}_{[3]}$ cycle to the $\mathcal{C}_{[34]}$ observed in Figure 12.4 is the result of a border-collision

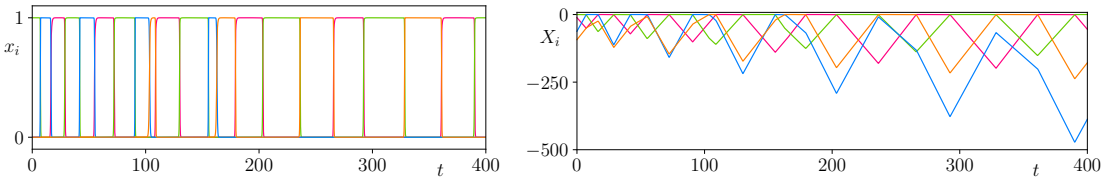

Figure 12.4: An example of a trajectory near the tournament network that switches from the $\mathcal{C}_{[3]}$ cycle to the $\mathcal{C}_{[34]}$ cycle, and then switches to the $\mathcal{C}_{[4]}$ cycle, to which it is asymptotic. For this example, $\omega_{34} < 0$, $\delta_3 > 1$, $\delta_4 > 1$, $\mu_3 < 0$, and $\nu_4 > 0$. Parameter values and initial conditions for these figures are given in §B.5.4.

bifurcation, as $\mu_3 < 0$, whereas the onset of switching from the $\mathcal{C}_{[34]}$ cycle to the $\mathcal{C}_{[4]}$ cycle is a result of a fold bifurcation, as $\omega_{34} < 0$.

IV The projected map in higher dimensions

Parts of the contents of this chapter are adapted from [GKP24, §5].

We now consider the projected map of an arbitrary heteroclinic network. We generalise the process introduced in §13 to heteroclinic networks in higher dimensions. We consider the fixed points of these projected maps. We also present some examples of how the stability conditions listed in Theorem 6.1 may correspond to conditions of bifurcations of the fixed points of the projected map.

We define the projected map of a general heteroclinic network in §13. For simplicity, we make mild simplifying assumptions. We demonstrate the general form of components of the projected map, and show that they are similar to a possible way to generalise Möbius transformations; that is, that they are rational linear transformations. We prove that one-dimensional invariant subspaces of the transition matrices correspond to fixed points of the projected map.

A key result of Chapter III is that the stability of the cycles of the three networks can be determined through the projected map, because Podvigina's third condition for stability in Theorem 6.1 is realised as a border-collision bifurcation. We generalise this result in §14. In particular, we prove that if an eigenvector $w_{\max}$ of a transition matrix lies in the switching subspace of a switching equilibrium, then the cycle is not stable. We relate this to border-collision bifurcations in a general projected map.

In §15, we briefly discuss how Podvigina's first and second stability conditions can affect stability properties of fixed points of the projected map.

§13 Defining the projected map

13.1 Properties of transition matrices

Let $\mathcal{N}$ be a heteroclinic network composed of $n \geq 5$ equilibria, $\xi_1, \ldots, \xi_n$. We assume this network is composed of cycles that are, in the terminology of Garrido da Silva and Castro [GC19], of quasi-simple type, or of type Z as defined by Podvigina [Pod12]. Representing the network as a directed graph and using the simplex realisation of Ashwin and Postlethwaite [AP13] is sufficient to ensure the component cycles are of this type. From here, we assume that the network has been embedded in a system of ODEs with the simplex realisation, and so exists in $\mathbb{R}^n$. This condition implies that transition matrices can be defined, and that Theorem 6.1 holds. Moreover, each equilibrium has one locally expanding and one locally contracting eigenvalue, and also a radial eigenspace of dimension 1. We highlight that the dynamical systems we consider in this chapter therefore do not contain any coordinates that are globally transverse to every component of the network; that is, the network is not contained in a proper subspace of the dynamical system, and each coordinate axis contains an equilibrium of the network.

We assume that ξ_i, ξ_j, and ξ_k are equilibria of the network such that $\xi_i \to \xi_j$ and $\xi_j \to \xi_k$ are orbits of the network and that these three equilibria and two orbits are components of a cycle $\mathcal{C} \subseteq \mathcal{N}$. The eigenvalues of $\mathrm{D}f(\xi_j)$ are therefore the radial eigenvalue $-r_j < 0$, the locally contracting eigenvalue $-c_{ji} < 0$, the locally expanding eigenvalue $e_{jk} > 0$, and the $\ell = n - 3$ locally transverse eigenvalues t_{js} for $1 < s < \ell$. The sign of each t_{js} term is not known *a priori*. However, if the transverse eigenvalue is globally contracting or globally transverse, t_{js} is negative, and if the transverse eigenvalue is globally expanding, t_{js} is positive. A contracting or expanding eigenvalue that is locally transverse can only occur if ξ_j is a switching equilibrium of the network. We do not yet assume that it is or is not a switching equilibrium.

We set $p = n - 2 = \ell + 1$. The results of [Pod12] and [GC19] gives us the form of the $p \times p$ basic transition matrix $m_{ijk} = M(\varphi_{ijk})$. We assume that these basic transition matrices act on vectors composed of the coordinates $X_t \coloneqq \log x_t < 0$, where the x_t are the variables of the dynamical system (3.1), but rescaled so that we are in a neighbourhood of approximate linear flow near ξ_j. For type Z [Pod12] and quasi-simple [GC19] cycles, basic

transition matrices have the form:

$$m_{ijk} = \varrho_j \begin{pmatrix} \frac{c_{ji}}{e_{jk}} & 0 & \dots & 0 & \dots & 0 \\ \frac{t_{j1}}{e_{jk}} & 1 & \dots & 0 & \dots & 0 \\ \vdots & \vdots & \ddots & \vdots & & \vdots \\ \frac{t_{js}}{e_{jk}} & 0 & \dots & 1 & \dots & 0 \\ \vdots & \vdots & & \vdots & \ddots & \vdots \\ \frac{t_{j\ell}}{e_{jk}} & 0 & \dots & 0 & \dots & 1 \end{pmatrix} \tag{13.1}$$

where $\varrho_j \in \mathcal{P}_n \leq \mathrm{GL}_n(\mathbb{R})$ is an $n \times n$ permutation matrix. The matrix ϱ_j relates the eigenvectors of the linearisation of the vector field of those at ξ_j to those at ξ_k, because the right-hand matrix of this product assumes an ordered basis that begins with the expanding direction and then the transverse directions in some particular order, which may change for different equilibria. For example, the matrix ϱ_j maps the coordinate X_t that aligns with the expanding eigenspace at ξ_j to the corresponding eigenspace of ξ_k that also lies in the X_t direction, and similarly for all transverse directions.

We observe that

$$\det m_{ijk} = \det \varrho_j \frac{c_{ji}}{e_{jk}}$$

Since a permutation matrix has a determinant of 1 or -1, the determinant of m_{ijk} is either $\frac{c_{ji}}{e_{jk}}$ or $-\frac{c_{ji}}{e_{jk}}$.

All basic maps of the cycle $\mathcal{C}$ take the form in (13.1), and therefore all full transition matrices M_j of the cycle have determinant

$$\prod_j \det \varrho_j \frac{\prod_j c_{j(j-1)}}{\prod_j e_{j(j+1)}}.$$

The sign of the determinant is determined by the product $\prod_j \det \varrho_j$.

13.1.1 Significant and insignificant subspaces

To aid us in our discussion of bifurcations of a general projected map in §15, we first summarise an additional notion introduced by Podvigina [Pod12]: the *significant subspace* and the *insignificant subspace*.

Let M_1 be the full transition matrix

$$M_1 = m_{(n-1)n1} m_{(n-2)(n-1)n} \dots m_{123} m_{n12}.$$

Let $e_1 = (1, 0, \dots, 0)$ be the first standard basis vector, and similarly for e_ℓ.

Definition 13.1. Let $1 \leq \ell \leq n$. If there exist non-negative integers j and k such that

$$(\varrho_{j-1}\varrho_{j-2} \dots \varrho_2 \varrho_1 \varrho_n \dots \varrho_j)^k \varrho_{j-1} \dots \varrho_1 e_\ell = e_1 \tag{13.2}$$

then the vector e_ℓ is a ***significant vector*** of the transition matrix M_1. If no such j and k exist, then the vector e_ℓ is an ***insignificant vector*** of the transition matrix M_1.

To understand the motivation behind this definition, we note that the first standard basis vector e_1 corresponds to the expanding eigenvector of the linearised vector field $\mathrm{D}f(\xi_j)$, and that the ϱ_i terms relate the eigenvectors of the linearisation of the vector field at one equilibrium in the cycle $\mathcal{C}$ to the next. Therefore, such a j and k exist only if the vector e_ℓ is the locally expanding eigenvector for some other equilibrium in the cycle $\mathcal{C}$. In essence, the equation (13.2) determines those coordinates that contain equilibria that belong to the same cycle as ξ_1.

The span of all significant vectors of M_1 is the ***significant subspace*** of the full transition matrix, denoted V_{sig}. The span of all insignificant vectors is the ***insignificant subspace***, denoted V_{ins}. We refer to eigenvalues with corresponding eigenvectors in V_{ins} as insignificant eigenvalues, and all remaining eigenvalues as significant eigenvalues. These vectors and subspaces are similarly defined for the other full transition matrices of the heteroclinic cycle. Podvigina [Pod12] proves two useful results about the significant and insignificant subspace.

Theorem 13.2 ([Pod12, Theorem 3])**.** *(a) The insignificant subspace V_{ins} is M_1-invariant, and the absolute value of the eigenvalue of any eigenvector that lies in V_{ins} is unity.*

(b) Generically, no component of an eigenvector of M_1 that does not lie in V_{ins} is zero.

For our purposes, these concepts and results can be easily summarised for the networks we consider, as we have assumed they have been constructed with the simplex realisation [AP13]. Consider a cycle $\mathcal{C} \subseteq \mathcal{N}$. Without loss of generality, assume the cycle $\mathcal{C}$ has the structure $\xi_1 \to \xi_2 \to \dots \to \xi_m \to \xi_1$ for some $m \leq n$. Each equilibrium $\xi_i \in \mathcal{C}$ lies on the x_i-axis. For all $1 \leq j \leq m$ such that $j \neq i-1, i$ (that is, excluding the contracting and radial coordinate) the span of the e_j standard basis vectors is the significant subspace of the transition matrix M_i. The complement of V_{sig} in $\mathbb{R}^n$ is the insignificant subspace. For the cycles and networks we consider, the insignificant subspace of the full transition matrix of

all equilibria of the cycle $\mathcal{C}$ coincide. Therefore, we refer to this subspace as the insignificant subspace of $\mathcal{C}$. Moreover, the union of the significant subspaces of the transition matrices of every equilibrium of $\mathcal{C}$ is the smallest subspace that contains $\mathcal{C}$. Therefore, we refer to this subspace at the significant subspace of the cycle $\mathcal{C}$.

We can immediately conclude some information about the eigenvalues and eigenvectors of the linearisation of the vector field at an equilibria ξ_i of a cycle $\mathcal{C} \subseteq \mathcal{N}$. If the cycle $\mathcal{C}$ contains all equilibria of the network $\mathcal{N}$, then no eigenvalue of the linearisation generically has absolute value 1. Moreover, every coordinate of each eigenvector is generically non-zero. However, if the cycle contains $m < n$ equilibria, then there are m eigenvalues that are generically not equal to 1, and all components of the corresponding eigenvectors are generically non-zero. There are also $n - m$ degenerate eigenvalues that have absolute value 1; in fact, in the case of these networks we consider, the $\mathbb{Z}_2^n$-equivariance of the vector field, and each equilibrium of the cycle lying in the positive orthant at unit distance from the origin on a coordinate axis, implies that the insignificant eigenvalues are exactly 1. The corresponding eigenspaces are the $n - m$ coordinate axes that contain equilibria that are not a component of the cycle. The eigenvalue is therefore semisimple, and has algebraic and geometric multiplicity $n - m$.

13.2 Constructing the projected map

We now construct a projected map. Without loss of generality, we assume that ξ_2 is a switching equilibrium of the network. We also assume it only has one incoming heteroclinic orbit $\xi_1 \to \xi_2$, and, for simplicity, we assume it has two outgoing heteroclinic orbits $\xi_2 \to \xi_3$ and $\xi_2 \to \xi_4$. The equilibria ξ_1 and ξ_2 are therefore both components of at least two heteroclinic cycles: $\mathcal{C}_{[3]}$—which also contains ξ_3—and $\mathcal{C}_{[4]}$—which also contains ξ_4. The other equilibria in the network are therefore $\xi_5, \dots, \xi_n$. Thus the eigenvalues of $\mathrm{D}f(\xi_2)$ are $-c_{21}$, e_{23}, e_{24}, $-t_{25}$, …, $-t_{2n}$. Each of these constants is strictly positive, and so only the eigenvalues e_{23} and e_{24} are positive, while all other eigenvalues are negative.

As with the switching equilibrium ξ_2 considered in §9, the incoming cross-section $\mathbf{H}_2^{\mathrm{in},1}$ is partitioned into three components: Γ_3, Γ_4, and Γ_{c}. These sets correspond to initial conditions that give rise to trajectories that cycle around the $\mathcal{C}_{[3]}$ and $\mathcal{C}_{[4]}$ cycle, and the excluded cusp of trajectories that do not remain sufficiently close to the network for the linearisation along the heteroclinic orbits $\xi_2 \to \xi_3$ and $\xi_2 \to \xi_4$ to remain valid. In logarithmic

coordinates, these sets are $\mathcal{D}_3$, $\mathcal{D}_4$, and $\mathcal{D}_c$, defined by

$$\mathcal{D}_3 = \left\{ (X_3, X_4, X_5, \dots, X_n) \mid \log(1+\epsilon) + \frac{e_{24}}{e_{23}} X_3 > X_4, X_k < 0 \text{ for all } 5 \le k \le n \right\},$$
$$\mathcal{D}_4 = \left\{ (X_3, X_4, X_5, \dots, X_n) \mid \log(1+\epsilon) + \frac{e_{23}}{e_{24}} X_4 > X_3, X_k < 0 \text{ for all } 5 \le k \le n \right\},$$

and

$$\mathcal{D}_c = \mathbb{R}^p_- \setminus (\mathcal{D}_3 \cup \mathcal{D}_4).$$

These sets allow us to define a piecewise-linear map $M \colon \mathcal{D}_3 \cup \mathcal{D}_4 \to \mathbb{R}^p_-$

$$M(X) = \begin{cases} M_3(X), & \text{if } X \in \mathcal{D}_3, \\ M_4(X), & \text{if } X \in \mathcal{D}_4. \end{cases} \tag{13.3}$$

The linear maps $M_3 \colon \mathcal{D}_3 \to \mathbb{R}^p_-$ and $M_4 \colon \mathcal{D}_4 \to \mathbb{R}^p_-$ are defined by the transition matrices of the full return maps $\Phi_2^{(3)} \colon \Gamma_3 \subseteq \mathbf{H}_2^{\text{in},1} \to \mathbf{H}_2^{\text{in},1}$ and $\Phi_2^{(4)} \colon \Gamma_4 \subseteq \mathbf{H}_2^{\text{in},1} \to \mathbf{H}_2^{\text{in},1}$. We write α_{ij} for the entries of the transition matrix $M_3 \equiv M_2^{(3)} = M\left(\Phi_2^{(3)}\right)$ and β_{ij} for the entries of the transition matrix $M_4 \equiv M_2^{(4)} = M\left(\Phi_2^{(4)}\right)$.

Let $m = p - 1$. We define an m-simplex S in the negative orthant of $\mathbb{R}^p$ as

$$S = \left\{ (X_3, X_4, X_5, \dots, X_n) \in \mathbb{R}^p_- \mid \sum_k X_k = -1 \right\}.$$

We define the projection $\Pi \colon \mathbb{R}^p_- \to S$ by

$$\Pi \colon X = (X_3, X_4, X_5, \dots, X_n) \mapsto \left(\frac{-X_3}{Q}, \frac{-X_4}{Q}, \dots, \frac{-X_{n-1}}{Q} \right), \tag{13.4}$$

where the denominator is $Q = \sum_k X_k$. We write $\vartheta_1, \dots, \vartheta_m$ for the m coordinates of S, and we can identify S with the subset of $(-1, 0)^m$ defined by:

$$S = \left\{ (\vartheta_1, \dots, \vartheta_m) \in (-1, 0)^m \mid \sum_i \vartheta_i > -1 \right\}.$$

Domains $\Theta_3 \subseteq S$ and $\Theta_4 \subseteq S$ are defined as the projection of the sets $\mathcal{D}_3$ and $\mathcal{D}_4$:

$$\Theta_3 = \{ \vartheta \in S \mid e_{24}\vartheta_1 > e_{23}\vartheta_2 \}$$

and

$$\Theta_4 = \{\vartheta \in S \mid e_{24}\vartheta_1 < e_{23}\vartheta_2\}.$$

We can then define components of the projected map as

$$\begin{aligned} &f_3 \colon \Theta_3 \to S \\ &f_3 \colon \vartheta \mapsto \Pi\left(M_3\left(\vartheta_1, \vartheta_2, \ldots, \vartheta_m, -1 - \sum_i \vartheta_i\right)\right) \end{aligned}$$

and

$$\begin{aligned} &f_4 \colon \Theta_3 \to S \\ &f_4 \colon \vartheta \mapsto \Pi\left(M_4\left(\vartheta_1, \vartheta_2, \ldots, \vartheta_m, -1 - \sum_i \vartheta_i\right)\right). \end{aligned}$$

The projected map is then $f_{\mathcal{N}} \colon \Theta_3 \cup \Theta_4 \to S$, defined by

$$f_{\mathcal{N}}(\vartheta) = \begin{cases} f_3(\vartheta), & \text{if } \vartheta \in \Theta_3, \\ f_4(\vartheta), & \text{if } \vartheta \in \Theta_4. \end{cases}$$

The switching manifold of this piecewise-smooth dynamical system is the codimension-one hyperplane

$$\Theta_{\mathrm{S}} = \{\vartheta \in S \mid e_{24}\vartheta_1 = e_{23}\vartheta_2\}.$$

An argument similar to that in §9.4 shows that the switching manifold is the only subset of S that must be excluded from the domain of the projected map.

We give an explicit example of this process for a network between six equilibria in §19. This construction is also applicable to networks where the switching equilibrium has multiple incoming heteroclinic orbits, such as the bowtie network in [CL16b], although there are some complications. We give an example of how the projected map of such a network can be defined in §20 when studying the Rock–Paper–Scissors–Lizard–Spock network. Moreover, the cycle can have additional switching equilibria, as is the case of the tournament network in §12. In this case, for all trajectories near the network that pass through a neighbourhood of the same switching equilibrium, the pre-image of the domains of each cycle at other switching equilibria can be taken to define one projected map, as we did in §12.

13.3 Properties of the projected map

The general form of these functions is relatively easy to express. In particular, for $\vartheta = (\vartheta_1, \ldots, \vartheta_m)$, and for $1 \leq k \leq m$, the expression for the kth component of f_3, for example, is

$$f_3^{(k)}(\vartheta) = \frac{\alpha_{kp} + \sum_{1\leq i\leq m} (\alpha_{kp} - \alpha_{ki})\vartheta_i}{\sum_{1\leq j\leq p} \sum_{1\leq i\leq m} (\alpha_{ji} - \alpha_{jp})\vartheta_i - \sum_{1\leq j\leq p} \alpha_{jp}}. \tag{13.5}$$

With the quotient rule, it is straightforward to show that, for some $1 \leq t \leq m$, the derivative of $f_3^{(k)}$ with respect to ϑ_t is:

$$\mathrm{D}_{\vartheta_t} f_3^{(k)} = \frac{1}{Q^2}\left(\sum_{1\leq j\leq p} \sum_{1\leq i\leq m} (\alpha_{kp}(\alpha_{ji} - \alpha_{jt}) + \alpha_{kt}(\alpha_{jp} - \alpha_{ji}) + \alpha_{ki}(\alpha_{jt} - \alpha_{jp}))\vartheta_i \right.$$
$$\left. - \sum_{1\leq j\leq p} \alpha_{kt}\alpha_{jp} - \alpha_{kp}\alpha_{jt} \right),$$

where Q is the denominator in (13.5).

With some algebraic substitutions and simplifications, this general form can be seen in the projected maps f_{KS} in (9.9), f_Δ in (11.1), and f_{T} in (12.1). Those three projected maps are Möbius transformations with real coefficients restricted to an open interval of the real line. (It is straightforward to check that they satisfy the nondegeneracy requirement of Möbius transformations, and that this condition is equivalent to the transition matrices that define them having a nonzero determinant, which is always the case.) The general form of each component of these maps is a generalisation of these Möbius transformations, being a rational linear transformation; that is, a map $\mathbb{R}^p \to \mathbb{R}$ defined by

$$\vartheta \mapsto \frac{\zeta \cdot \vartheta + \lambda}{\chi \cdot \vartheta + \gamma},$$

where $\zeta, \chi \in \mathbb{R}^p$ are vectors and $\lambda, \gamma \in \mathbb{R}$ are constants.

Fixed points of a component function of the projected map are also straightforward to determine. They are the projection of all one-dimensional M-invariant subspaces of $\mathbb{R}^n$. In the following propositions, we specifically focus on f_3 for clarity, though the result is readily extendable to f_4.

Proposition 13.3. A point $\vartheta \in S$ is a fixed point of f_3 if and only if the span of the vector

$$\left(\vartheta_1, \vartheta_2, \ldots, \vartheta_m, -1 - \sum_i \vartheta_i\right) \tag{13.6}$$

is an M_3-invariant subspace.

Remark 13.4. In the statement of this result, we have specifically not said that the span of the vector in (13.6) is an eigenspace of M, because the geometric multiplicity of an eigenvalue may be strictly greater than 1. In the case of a type Z cycle with an empty insignificant subspace, the geometric multiplicity of every eigenvalue is generically 1, but the statement in Proposition 13.3 applies to a wider class of heteroclinic cycles.

Proof. Write

$$w = \left(\vartheta_1, \vartheta_2, \ldots, \vartheta_m, -1 - \sum_i \vartheta_i\right).$$

Suppose that $\vartheta \in S$ is a fixed point of f_3. With the definition of Π in (13.4), we first observe that $\vartheta = \Pi(tw)$ for all real numbers t. Next

$$\Pi(tw) = \vartheta = f(\vartheta) = \Pi(M_3 w).$$

Therefore, there is some $\kappa \in \mathbb{R}$ such that $M_3 w = \kappa t w$. Therefore, the span of w is M_3-invariant.

Now suppose that the span of w is M_3-invariant. Then $M_3 w = \kappa w$ for some $\kappa \in \mathbb{R}$, and also $\Pi(tw) = \vartheta$ for all $t \in \mathbb{R}$. Lastly,

$$f_3(\vartheta) = \Pi(M_3 w) = \Pi(\kappa w) = \Pi(w) = \vartheta.$$

■

Assuming that all eigenvalues of M_3 are simple is sufficient to change the statement of Proposition 13.3 to

Proposition 13.5. A point $\vartheta \in S$ is a fixed point of f_3 if and only if the span of the vector

$$\left(\vartheta_1, \vartheta_2, \ldots, \vartheta_m, -1 - \sum_i \vartheta_i\right)$$

is an eigenspace of M_3.

In fact, assuming that each eigenvalue is non-degenerate is also sufficient and less restrictive, though this condition could imply that the transition matrix is not diagonalisable.

§14 Generalised border-collision bifurcations

In this section, we generalise the analysis presented in §10.2 to investigate border-collision bifurcations in the projected map. We assume the network $\mathcal{N}$ has the same structure as in §13 above.

We now consider the basic maps $\varphi_{123}\colon \Gamma_3 \subseteq \mathbf{H}_2^{\text{in},1} \to \mathbf{H}_3^{\text{in},2}$ and $\varphi_{124}\colon \Gamma_4 \subseteq \mathbf{H}_2^{\text{in},1} \to \mathbf{H}_4^{\text{in},2}$. The basic transition matrices $m_{123} = M(\varphi_{123})$ and $m_{124} = M(\varphi_{124})$ using the ordered basis $(X_3, X_4, X_5, \ldots, X_n)$ are

$$m_{123} = \begin{pmatrix} \frac{c_{21}}{e_{23}} & 0 & 0 & \cdots & 0 \\ -\frac{e_{24}}{e_{23}} & 1 & 0 & \cdots & 0 \\ \frac{t_{25}}{e_{23}} & 0 & 1 & \cdots & 0 \\ \vdots & \vdots & \vdots & \ddots & \vdots \\ \frac{t_{2n}}{e_{23}} & 0 & 0 & \cdots & 1 \end{pmatrix}$$

and

$$m_{124} = \begin{pmatrix} 1 & -\frac{e_{23}}{e_{24}} & 0 & \cdots & 0 \\ 0 & \frac{c_{21}}{e_{24}} & 0 & \cdots & 0 \\ 0 & \frac{t_{25}}{e_{24}} & 1 & \cdots & 0 \\ \vdots & \vdots & \vdots & \ddots & \vdots \\ 0 & \frac{t_{2n}}{e_{24}} & 0 & \cdots & 1 \end{pmatrix}.$$

Note that the topology of the rest of the network does not affect these matrices. Furthermore, unlike in (13.1), there are no permutation matrices $\varrho_3, \varrho_4 \in \mathcal{P}_p$ multiplying these matrices on the left, since fixing the order of the basis incorporates the required permutations. In particular, the expression for m_{124} is not the same as the right-hand matrix in the product in (13.1).

The domains of these matrices as linear maps acting on $\mathbf{H}_2^{\text{in},1}$ in logarithmic coordinates are $\mathcal{D}_3$ and $\mathcal{D}_4$, separated by the excluded subspace $\mathcal{D}_c$, defined around the codimension-one switching subspace

$$W_{\text{s}} = \{(X_3, X_4, X_5, \ldots, X_n) \in \mathbb{R}^p_- \mid e_{24}X_3 = e_{23}X_4\}.$$

As we did in §10.2, we consider the image of a vector in the switching subspace under

m_{123} and m_{124}, which gives

$$m_{123}w_{\rm s} = \begin{pmatrix} \frac{c_{21}}{e_{23}} & 0 & 0 & \cdots & 0 \\ -\frac{e_{24}}{e_{23}} & 1 & 0 & \cdots & 0 \\ \frac{t_{25}}{e_{23}} & 0 & 1 & \cdots & 0 \\ \vdots & \vdots & & \ddots & \\ \frac{t_{2n}}{e_{23}} & 0 & 0 & \cdots & 1 \end{pmatrix} \begin{pmatrix} -1 \\ -\frac{e_{24}}{e_{23}} \\ X_5 \\ \vdots \\ X_n \end{pmatrix} = \begin{pmatrix} -\frac{c_{21}}{e_{23}} \\ 0 \\ -\frac{t_{25}}{e_{23}} + X_5 \\ \vdots \\ -\frac{t_{2n}}{e_{23}} + X_n \end{pmatrix}.$$

Note that the image has a 0 entry, and it is straightforward to check that the image under m_{124} also has a 0 entry. Furthermore, the vectors $m_{123}w$ and $m_{124}w$ have a zero entry for *any* vector w in the switching subspace $W_{\rm s}$. Therefore, if the eigenvector $w_{\max}$ of M_3 lies in $W_{\rm s}$, the eigenvector $w_{\max}$ of $M_3^{(3)}$ has a zero entry, and so does not satisfy Podvigina's third condition for fragmentary asymptotic stability in Theorem 6.1. The corresponding cycle $\mathcal{C}_{[3]}$ is therefore not fragmentarily asymptotically stable. The same result holds if the eigenvector $w_{\max}$ of M_4 lies in $W_{\rm s}$. In general, we have the following result.

Theorem 14.1. *If the eigenvector $w_{\max}$ of a full transition matrix M_j defined at a switching equilibrium ξ_j lies in the switching subspace $W_{\rm s}$, then the corresponding heteroclinic cycle is not fragmentarily asymptotically stable.*

In the projected map $f_{\mathcal{N}}$, the projection of $W_{\rm s}$ is the codimension-one switching manifold $\Theta_{\rm s}$. A border-collision bifurcation occurs if a fixed point ϑ^* of $f_{\mathcal{N}}$ that corresponds to an eigenvector w of M_j lies in $\Theta_{\rm s}$. Hence, assuming that Podvigina's first two conditions for stability are satisfied, a border-collision bifurcation of the fixed point that corresponds to $w_{\max}$ corresponds to a change in stability of the heteroclinic cycle.

However, a border-collision bifurcation in the projected map need not correspond to a loss of stability of the heteroclinic cycle. For example, in Figure 11.3(a) we see a border-collision bifurcation of ϑ_{34}^- that does not correspond to stability loss of the $\mathcal{C}_{[34]}$ cycle because this fixed point does not correspond to $w_{\max}$ in Theorem 6.1. In §10.5, a border-collision bifurcation of ϑ_3^* also does not cause stability loss because the cycle does not satisfy the second condition in Theorem 6.1; in particular, the cycle has already lost stability in a resonance bifurcation. In both cases, however, these border-collision bifurcations do affect switching near the network.

Note that, as in the case of the tournament network, a cycle may have additional switching equilibria. If so, the cycle may lose stability through a border-collision bifurcation in the switching subspace of a different switching equilibrium. Assuming all trajectories near the network pass through a neighbourhood of the same switching equilibrium, the pre-image of

the domains of each cycle at other switching equilibria can be taken, allowing for all border-collision bifurcations to be analysed on a single cross-section, as we did in §12.

Lastly, a result analogous to Theorem 14.1 holds in the case of positive transverse eigenvalues, but these bifurcations do not result in the switching of trajectories near the network, as positive transverse eigenvalues only shrink the basin of attraction of the network. In this thesis, however, we assume that all transverse eigenvalues are negative.

§15 Other bifurcations

From Theorem 14.1, we conclude that a breaking of Podvigina's third condition for stability in Theorem 6.1 corresponds to a border-collision bifurcation. In the remainder of this chapter, we present a discussion of how Podvigina's first and second stability conditions can affect stability properties of fixed points of the projected map. We present a few examples. These examples are not exhaustive of all possible ways these conditions can be broken.

Podvigina's first and second stability conditions both concern the eigenvalue $\lambda_{\max}$ of the full transition matrix M_j. Since all full transition matrices of a cycle have the same spectrum, any changes to these conditions occurs for all matrices simultaneously, and so is realised in the projected map. As such, let $\{\lambda_1, \lambda_2, \ldots, \lambda_p\}$ be the spectrum of the $p \times p$ full transition matrices, where $p \geq 3$. We generally assume that all eigenvalues are simple, and we explicitly highlight when the eigenvalues are not simple. We assume that all significant eigenvalues are non-degenerate. We explicitly highlight in §15.2 which eigenvalues are significant and which are insignificant, and the consequences of the insignificant eigenvalues being semisimple. We further suppose that $\mu \in \mathbb{R}$ is some parameter of the dynamical system on which the eigenvalues depend.

15.1 Breaking $\lambda_{\max} \in \mathbb{R}$

We first consider the projected map under two different scenarios in which Podvigina's first stability condition is broken. This condition is that $\lambda_{\max} \in \mathbb{R}$.

First, we assume, without loss of generality in this example, that $\lambda_i \in \mathbb{R}$ for all $2 < i \leq p$. For this example, we assume that all eigenvalues are non-degenerate. Suppose that λ_1 and λ_2 have the following dependence on μ and some specific critical value μ^*:

1. If $\mu < \mu^*$, then $\lambda_1, \lambda_2 \in \mathbb{R}$ and $|\lambda_1| > |\lambda_2|$.

2. If $\mu = \mu^*$, then $\lambda_1, \lambda_2 \in \mathbb{R}$ and $\lambda_1 = \lambda_2$.

3. If $\mu > \mu^*$, then $\lambda_1, \lambda_2 \in \mathbb{C}$, with $\lambda_1 = \overline{\lambda_2}$.

Since we assume that all eigenvalues are non-degenerate, at $\mu = \mu^*$, $w_1 = w_2$. For $\mu > \mu^*$, these eigenvectors form a complex-conjugate pair. Therefore, assuming certain genericity conditions on $\mathrm{D}f_{\mathcal{N}}$, there is a fold bifurcation of the fixed points $\Pi(w_1)$ and $\Pi(w_2)$ of $f_{\mathcal{N}}$. A fold bifurcation is observed in the fixed points ϑ_{34}^* and ϑ_{34}^- of the map f_{34} for the projected map of both the Δ-clique and tournament networks in Sections 11 and 12, respectively.

Second, we consider a change in which eigenvalue has greatest absolute value. For this scenario, we assume that $\lambda_1 \in \mathbb{R}$ and $\lambda_2, \lambda_3 \in \mathbb{C}$, with $\lambda_2 = \overline{\lambda_3}$. Without loss of generality for this example, we assume that $\lambda_i \in \mathbb{R}$ for all $3 < i \leq p$, and that $|\lambda_i| < \min\{|\lambda_1|, |\lambda_2|, |\lambda_3|\}$, again for all $3 < i \leq p$. Suppose that λ_1, λ_2, and λ_3 have the following dependence on μ and some specific critical value μ^*:

1. If $\mu < \mu^*$, then $|\lambda_1| > |\lambda_2| = |\lambda_3|$.
2. If $\mu = \mu^*$, then $|\lambda_1| = |\lambda_2| = |\lambda_3|$.
3. If $\mu > \mu^*$, then $|\lambda_1| < |\lambda_2| = |\lambda_3|$.

In this case, a change in which eigenvalue has greatest absolute value occurs. The fixed point $\Pi(w_1)$ therefore loses stability, even though no eigenvalue is at a critical value. It is not evident what type of bifurcation occurs for the fixed point $\Pi(w_1)$ at μ^*. However, the plane of rotation defined by the eigenvectors w_2 and w_3 is now attracting under iteration of the matrix M_j. In §20, we show that this bifurcation can lead to what appears to be a strange attractor.

15.2 Breaking $\lambda_{\max} > 1$

We now consider several scenarios in which Podvigina's second stability condition is broken. This condition is that $\lambda_{\max} > 1$, and therefore we assume that $\lambda_{\max} \in \mathbb{R}$.

We first consider a scenario that can occur if a subcycle of the network contains all equilibria of the network, and so the cycle has an empty insignificant subspace. In this case, no eigenvalue of the transition matrix is generically 1. We assume in this example that $|\lambda_1| > |\lambda_i|$ for all $1 < i \leq p$ and for all μ. Suppose that λ_1 has the following dependence on μ and some specific critical value μ^*:

1. If $\mu < \mu^*$, then $\lambda_1 > 1$.
2. If $\mu = \mu^*$, then $\lambda_1 = 1$.
3. If $\mu > \mu^*$, then $0 < \lambda_1 < 1$.

Under these conditions, the cycle loses stability in a resonance bifurcation [SC92] at $\mu = \mu^*$. However, $\lambda_1 = \lambda_{\max}$ for all values of μ. Therefore, there is no stability change to any of the fixed points. We discussed a similar set of conditions in §11.1, and these conditions must be accounted for to ensure that the projected map is being correctly used to analyse the dynamics of trajectories near a heteroclinic network.

We now suppose that the cycle $\mathcal{C}$ does not contain all equilibria of the network, and therefore that the full transition matrices have an insignificant subspace. In this scenario, there are eigenvalues that are generically 1. Moreover, their eigenvectors align with the coordinate axes that contain the equilibria not in the cycle $\mathcal{C}$. Therefore, we cannot assume that an insignificant eigenvalue is non-degenerate: if multiple eigenvalues are generically 1, they are degenerate, though we assume that this eigenvalue is semisimple. See, for example, the transition matrices $M_3^{(3)}$ and $M_4^{(4)}$ of the Kirk–Silber network at the start of §10, or the transition matrices M_{L} and M_{R} of Podvigina's two-cycle network in §19 below. Without loss of generality, we assume that $\lambda_2 = 1$. Suppose that λ_1 has the following dependence on μ and some specific critical value μ^*:

1. If $\mu < \mu^*$, then $\lambda_1 > 1$.
2. If $\mu = \mu^*$, then $\lambda_1 = 1$.
3. If $\mu > \mu^*$, then $0 < \lambda_1 < 1$.

Then at $\mu = \mu^*$, the fixed point $\Pi(w_1)$ of $f_{\mathcal{N}}$ loses stability. If λ_2 is the only insignificant eigenvalue of the full transition matrices, then the fixed point $\Pi(w_2)$—which does not lie in S, as ϑ_3^- and ϑ_4^- in Sections 10 to 12—is attracting for $\mu > \mu^*$. Moreover, at $\mu = \mu^*$, $w_1 = w_2$, and so the fixed points $\Pi(w_1)$ and $\Pi(w_2)$ of $f_{\mathcal{N}}$ also coincide. Assuming certain genericity conditions on $\mathrm{D}f_{\mathcal{N}}$, a transcritical bifurcation occurs at $\mu = \mu^*$. This bifurcation occurs in both f_3 and f_4 of all three projected maps in Chapter III. However, if λ_2 is not the only insignificant eigenvalue of the full transition matrices, it is not apparent what bifurcation occurs in the projected map. In particular, suppose without loss of generality that $\lambda_2, \ldots, \lambda_s$ for some $s < p$ are all insignificant eigenvalues of the cycle. Then all vectors in $\operatorname{span}\{w_2, \ldots, w_s\}$ project to fixed points of $f_{\mathcal{N}}$—though again that do not lie in S.

Another way by which this condition can be broken is for an eigenvalue with a negative real value to become the eigenvalue of greatest absolute value. We consider an example of such a change numerically when studying the Rock–Paper–Scissors–Lizard–Spock network in §20. We do not consider this change in more detail here, nor any of the other changes that can occur.

V Continuity of the projected map of heteroclinic networks in $\mathbb{R}^4$

The contents of this chapter are being prepared for publication as [GPR25].

In Sections 10.3, 11.2, and 12.2, we observed that the projected map of a heteroclinic network in $\mathbb{R}^4$ may be continuous on its switching manifold or generically discontinuous. In this chapter, we examine the dynamical origin of this continuity or discontinuity. We focus on the Kirk–Silber and Δ-clique networks, as the analysis of the Δ-clique network is readily extended to the tournament network.

In §16, we define the two dynamical systems we study that contain a Kirk–Silber and a Δ-clique network. These are equivalent to those in Chapter III, but we make some additional observations and assumptions about structures in the dynamical system that are not a part of the two heteroclinic networks. These structures, which are not a part of the networks but exist in dynamical systems containing these networks, are important to understanding the (dis)continuity. We also make certain notational changes to ease analysis.

We then construct a *completed full return map* in §17. This return map is constructed similarly to the return maps in Sections 6 and 9.1, except it is defined for all points in the cross-section used to define the projected map. In particular, there is no excluded cusp in the domain of this completed full return map. The return map is constructed by defining cross-sections that are transverse to the entire unstable manifold of the switching equilibrium. Therefore, all trajectories that begin sufficiently close to the network are in the domain of the map, even if they do not stay sufficiently close to the heteroclinic orbits that are contained in the two-dimensional coordinate planes. This process provides us with a single map that describes the behaviour of all trajectories near the network, and that is not defined in a piecewise manner. However, not all components of this return map can be written explicitly. Nevertheless, we can derive sufficient information about the map and its components to anal-

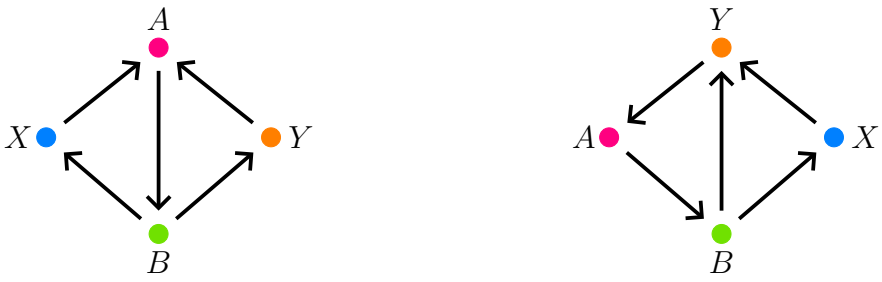

Figure 16.1: Diagrammatic representations of (a) the Kirk–Silber network and (b) the Δ-clique network, with the equilibria relabelled for the purposes of this chapter.

yse the origin of the continuity or the discontinuity. In the case of the Kirk–Silber network, we find that certain components of this map have a discontinuity in the limit as a trajectory approaches the network. This discontinuity emerges from the presence of a separatrix near the network, which exists because of the stable and unstable manifolds of certain invariant sets that are not part of the network. In comparison, no component of completed return map of the Δ-clique network has a discontinuity in the limit as a trajectory approaches the network.

In §18, we analyse this completed return map for trajectories that begin near the switching manifold of the projected map. We define this completed map in logarithmic coordinates, and show how a projected map can then be defined. Unlike the projected maps in Chapters III and IV, this projected map depends on the location of the simplex, since the action of the completed full return map in logarithmic coordinates is not linear. We then apply the projection to trajectories that begin near the switching manifold. We show that, when evaluating the limit as these trajectories approach the network, the presence of a separatrix creates a discontinuity in the projected map of the Kirk–Silber network, but that no such discontinuity emerges in the projected map of the Δ-clique network.

§16 Problem statement

In this chapter, we consider the Kirk–Silber and Δ-clique networks, as defined in §8. However, for notational convenience, we relabel the equilibria as $A \equiv \xi_1$, $B \equiv \xi_2$, $X \equiv \xi_3$, and $Y \equiv \xi_4$. These equilibria form three cycles: $\mathcal{C}_{[\mathrm{X}]} = A \to B \to X \to A$, $\mathcal{C}_{[\mathrm{Y}]} = A \to B \to Y \to A$, and $\mathcal{C}_{[\mathrm{XY}]} = A \to B \to X \to Y \to A$. The two networks are then $\mathcal{N}_{\mathrm{KS}} = \mathcal{C}_{[\mathrm{X}]} \cup \mathcal{C}_{[\mathrm{Y}]}$ and $\mathcal{N}_{\Delta} = \mathcal{C}_{[\mathrm{XY}]} \cup \mathcal{C}_{[\mathrm{Y}]}$. We show these two networks with relabelled equilibria in Figure 16.1.

Table 16.1: The eigenvalues of $\mathrm{D}f$ evaluated at the four equilibria of the two networks.

(a) Kirk–Silber network

Eigen-space	Equilibrium A	B	X	Y
x_1	$-r_{\mathrm{A}}$	$-c_{\mathrm{B}}$	e_{XA}	e_{YA}
x_2	e_{A}	$-r_{\mathrm{B}}$	$-c_{\mathrm{XB}}$	$-c_{\mathrm{YB}}$
x_3	$-c_{\mathrm{AX}}$	e_{BX}	$-r_{\mathrm{X}}$	$-c_{\mathrm{YX}}$
y_3	$-c_{\mathrm{AY}}$	e_{BY}	$-c_{\mathrm{XY}}$	$-r_{\mathrm{Y}}$

(b) Δ-clique network

Eigen-space	Equilibrium A	B	X	Y
x_1	$-r_{\mathrm{A}}$	$-c_{\mathrm{B}}$	$-c_{\mathrm{XA}}$	e_{YA}
x_2	e_{A}	$-r_{\mathrm{B}}$	$-c_{\mathrm{XB}}$	$-c_{\mathrm{YB}}$
x_3	$-c_{\mathrm{AX}}$	e_{BX}	$-r_{\mathrm{X}}$	$-c_{\mathrm{YX}}$
y_3	$-c_{\mathrm{AY}}$	e_{BY}	e_{XY}	$-r_{\mathrm{Y}}$

We consider these networks as realised by the system of ODEs

$$\begin{aligned}
\dot{x}_1 &= x_1\bigl(1 - \|x\|_2^2 + \alpha_{21}x_2^2 + \alpha_{31}x_3^2 + \alpha_{41}y_3^2\bigr),\\
\dot{x}_2 &= x_2\bigl(1 - \|x\|_2^2 + \alpha_{12}x_1^2 + \alpha_{32}x_3^2 + \alpha_{42}y_3^2\bigr),\\
\dot{x}_3 &= x_3\bigl(1 - \|x\|_2^2 + \alpha_{13}x_1^2 + \alpha_{23}x_2^2 + \alpha_{43}y_3^2\bigr),\\
\dot{y}_3 &= y_3\bigl(1 - \|x\|_2^2 + \alpha_{14}x_1^2 + \alpha_{24}x_2^2 + \alpha_{34}x_3^2\bigr).
\end{aligned} \tag{16.1}$$

Specific choices of the signs of the α_{jk} terms ensure the existence of certain heteroclinic orbits in the two-dimensional coordinate planes, and the choices can be made in such a way as to give either of the two networks we consider. We list the eigenvalues of each equilibrium, along with the corresponding coordinate axis that is its eigenspace, in Table 16.1. The entries in the row corresponding to x_k, excluding the $-r$ radial eigenvalue, can be substituted into the α_{jk} terms in the equation for $\dot{x}_j$ in (16.1) to derive ODEs that contain the respective network. (See (A.1.1) and (A.1.2) in §A.1). Note that each constant in Table 16.1 represents a positive value, and so a negative eigenvalue is indicated with a minus sign. We also do not explicitly label transverse eigenvalues as $-t$, but instead as $-c$, as this provides more consistency between the two networks. Since we assume in this thesis that all transverse eigenvalues are negative, this relabelling does not affect our calculations. These eigenvalues ensure the existence of the necessary heteroclinic orbits needed to form the Kirk–Silber and Δ-clique networks.

In the case of the Kirk–Silber network, we assume that there is an additional hyperbolic saddle equilibrium P in the (x_3, y_3)-plane, and that there are robust heteroclinic orbits $P \to X$ and $P \to Y$ in this plane, and $B \to P$ in the $x_1 = 0$ subspace. The equilibrium P and these additional orbits are themselves not components of the Kirk–Silber network, but their existence is needed for the analysis presented in Sections 17 and 18.

With both networks, we consider the dynamics near a flow-invariant curve that exists in the (x_3, y_3)-plane. In both cases, we label this curve C. With the relabelling of the equilibria,

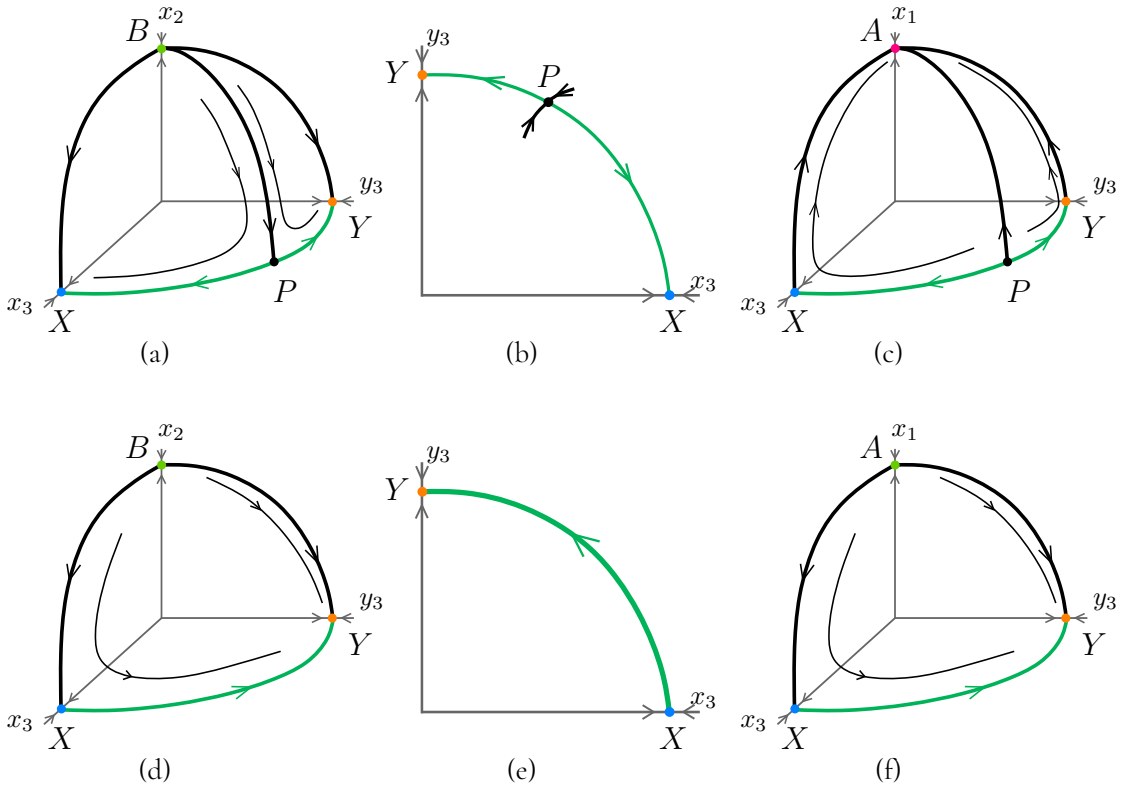

Figure 16.2: Dynamics within various subspaces of the two dynamical systems being considered. Equilibria are given by solid dots. The equilibria that are components of the network are coloured the same as in Figure 1.3; the equilibrium P of the Kirk–Silber network is black. Heteroclinic orbits are thick lines. The orbits that are part of the flow-invariant curve C are coloured green, and all other orbits are coloured black. Example trajectories are thin black lines, and the flow-invariant coordinate axes are thin grey lines. (a) Kirk–Silber and (d) Δ-clique: the $x_1 = 0$ subspace, showing the two dimensional unstable manifold of B and the curve C, and how these structures interact. (b) Kirk–Silber and (e) Δ-clique: the (x_3, y_3)-plane and details of the invariant curve C. (c) Kirk–Silber and (f) Δ-clique: the $x_2 = 0$ subspace, showing the two dimensional stable manifold of A and how it interacts with C.

both networks can now be described as $A \to B \to C \to A$.

For the Kirk–Silber network, the curve C is the union of the three equilibria X, Y, and P, and the two orbits $P \to X$ and $P \to Y$. For the Δ-clique network, the curve C is the union of the two equilibria X and Y, and the orbit $X \to Y$. We assume that the curve C can be parametrised by an angle θ_3, defined by $\tan\theta_3 = y_3/x_3$. For both networks, the angle of the equilibria X and Y are $\theta_3^{\mathrm{X}} = 0$ and $\theta_3^{\mathrm{Y}} = \frac{\pi}{2}$, respectively. For the Kirk–Silber network, the angle of the equilibrium P is θ_3^{P}.

We present diagrammatic representations of the dynamics in relevant subspaces in Figure 16.2. For the Δ-clique network, we make no particular assumptions about the dynamics in the (x_1, x_3)-plane, other than the sign of the eigenvalue $-c_{\mathrm{AX}}$ at A in the x_3-direction, and the sign of the eigenvalue $-c_{\mathrm{XA}}$ at X in the x_1-direction. For this reason, we have shown only a portion of the dynamics in this subspace, locally near A and X.

In terms of these relabelled equilibria, the cross-section $\mathbf{H}_{\mathrm{B}}^{\mathrm{in,A}}$ is defined in a small neighbourhood of B, transverse to the incoming heteroclinic orbit to B, $A \to B$:

$$\mathbf{H}_{\mathrm{B}}^{\mathrm{in,A}} = \big\{(x_1, x_2, x_3, y_3) \in \mathbb{R}^4 \mid x_1 = h, |x_2 - 1| < h, 0 \leq x_3, y_3 < h\big\}.$$

As in previous chapters, we disregard two coordinates, as one coordinate is fixed in the definition of the section, and the radial coordinate again does not affect our analysis. Therefore, we employ in the remainder of this chapter an abuse of notation and only consider the coordinates (x_3, y_3). When constructing a return map to $\mathbf{H}_{\mathrm{B}}^{\mathrm{in,A}}$ following the usual methodology—as outlined in Sections 6.1 and 9.1—the cross-section is partitioned into three subsets, Γ_{X}, Γ_{Y}, and Γ_{c}. We then have a map $\Phi_{\mathrm{B}} \colon \Gamma_{\mathrm{X}} \cup \Gamma_{\mathrm{Y}} \subsetneq \mathbf{H}_{\mathrm{B}}^{\mathrm{in,A}} \to \mathbf{H}_{\mathrm{B}}^{\mathrm{in,A}}$, defined in a piecewise manner:

$$\Phi_{\mathrm{B}}(x_3, y_3) = \begin{cases} \Phi_{\mathrm{X}}(x_3, y_3), & \text{if } (x_3, y_3) \in \Gamma_{\mathrm{X}}, \\ \Phi_{\mathrm{Y}}(x_3, y_3), & \text{if } (x_3, y_3) \in \Gamma_{\mathrm{Y}}. \end{cases} \tag{16.2}$$

Transition matrices can be defined from these return maps, resulting in a piecewise-linear map

$$M_{\mathrm{B}}(X_3, Y_3) = \begin{cases} M_{\mathrm{X}}(X_3, Y_3), & \text{if } (X_3, Y_3) \in \mathcal{D}_{\mathrm{X}}, \\ M_{\mathrm{Y}}(X_3, Y_3), & \text{if } (X_3, Y_3) \in \mathcal{D}_{\mathrm{Y}}. \end{cases} \tag{16.3}$$

We note that the sets $\mathcal{D}_{\mathrm{X}}$ and $\mathcal{D}_{\mathrm{Y}}$ are subsets of $\mathcal{D} = \{(X_3, Y_3) \in \mathbb{R}^2_- \mid X_3, Y_3 < \log h\} \subsetneq \mathbb{R}^2_-$.

From these transition matrices, the projected maps of the networks are defined, $f_{\mathrm{KS}} \colon \Theta_{\mathrm{X}} \cup$

$\Theta_{\mathrm{Y}} \to S$ and $f_\Delta \colon \Theta_{\mathrm{XY}} \cup \Theta_{\mathrm{Y}} \to S$:

$$f_{\mathrm{KS}}(\vartheta) = \begin{cases} f_{\mathrm{X}}(\vartheta), & \text{if } \vartheta \in \Theta_{\mathrm{X}}, \\ f_{\mathrm{Y}}(\vartheta), & \text{if } \vartheta \in \Theta_{\mathrm{Y}}, \end{cases}$$

and,

$$f_\Delta(\vartheta) = \begin{cases} f_{\mathrm{XY}}(\vartheta), & \text{if } \vartheta \in \Theta_{\mathrm{XY}}, \\ f_{\mathrm{Y}}(\vartheta), & \text{if } \vartheta \in \Theta_{\mathrm{Y}}. \end{cases}$$

The domains of definition of each component of the map are

$$\begin{aligned} \Theta_{\mathrm{X}} &= (\vartheta_s, 0), \\ \Theta_{\mathrm{Y}} &= (-1, \vartheta_s), \end{aligned}$$

and

$$\Theta_{\mathrm{XY}} = (\vartheta_s, 0),$$

where

$$\vartheta_{\mathrm{s}} = \frac{-1}{1 + \dfrac{e_{\mathrm{BY}}}{e_{\mathrm{BX}}}}.$$

Note that the subscripts on the domains of the projected map refer to the *cycle*, whereas the subscripts on the domains of the return maps and transition matrices refer to the next *equilibrium* that the trajectory visits.

With the above information, we now proceed to explain the dynamical origin of the discontinuity of the projected map f_{KS} at its switching manifold ϑ_{s}, and explain why the projected map f_Δ is continuous at its switching manifold. This discontinuity and continuity was first presented in Sections 10.3 and 11.2. Since we have relabelled the equilibria and eigenvalues of the linearised flow near the equilibria, the values of these limits are now

$$\lim_{\vartheta \searrow \vartheta_{\mathrm{s}}} f_{\mathrm{KS}}(\vartheta) = \lim_{\vartheta \searrow \vartheta_{\mathrm{s}}} f_{\mathrm{X}}(\vartheta) = \frac{-c_{\mathrm{XB}} c_{\mathrm{AX}}}{c_{\mathrm{XB}}(c_{\mathrm{AX}} + c_{\mathrm{AY}}) + e_{\mathrm{A}} c_{\mathrm{XY}}} \tag{16.4}$$

and

$$\lim_{\vartheta \nearrow \vartheta_{\mathrm{s}}} f_{\mathrm{KS}}(\vartheta) = \lim_{\vartheta \nearrow \vartheta_{\mathrm{s}}} f_{\mathrm{Y}}(\vartheta) = \frac{-(c_{\mathrm{YB}} c_{\mathrm{AX}} + e_{\mathrm{A}} c_{\mathrm{YX}})}{c_{\mathrm{YB}}(c_{\mathrm{AX}} + c_{\mathrm{AY}}) + e_{\mathrm{A}} c_{\mathrm{YX}}} \tag{16.5}$$

in the case of the Kirk–Silber network, and

$$\lim_{\vartheta\to\vartheta_{\mathrm{s}}} f_{\Delta}(\vartheta) = \lim_{\vartheta\searrow\vartheta_{\mathrm{s}}} f_{\mathrm{XY}}(\vartheta) = \lim_{\vartheta\nearrow\vartheta_{\mathrm{s}}} f_{\mathrm{Y}}(\vartheta) = \frac{-(c_{\mathrm{YB}}c_{\mathrm{AX}} + e_{\mathrm{A}}c_{\mathrm{YX}})}{c_{\mathrm{YB}}(c_{\mathrm{AX}} + c_{\mathrm{AY}}) + e_{\mathrm{A}}c_{\mathrm{YX}}} \tag{16.6}$$

in the case of the Δ-clique network.

Given (16.4)–(16.6), we consider the projected map of the Kirk–Silber network to be generically discontinuous, and the projected map of the Δ-clique network to be continuous. However, we recall that the projected maps are not defined at ϑ_{s}, due to the mechanism by which the map was constructed, excluding Γ_c from the domain of Φ. (See §9.)

We highlight that the limit in (16.6) is the same as in (16.5). Both of these limits are calculated from the component of the projected map f_{Y} or f_{XY}, which corresponds to the $\mathcal{C}_{[\mathrm{Y}]}$ cycle. Therefore, both of these limits are calculated from the part of the projected map that describes the dynamics of trajectories that leave a neighbourhood of the curve C near the equilibrium Y, with θ_3 close to $\frac{\pi}{2}$. The limit in (16.4), however, is calculated from the component of the projected map f_{X}, which corresponds to trajectories that leave C near X, with θ_3 close to 0. This difference provides us with an initial indication of the dynamical properties of the system that produce the discontinuity in the case of the Kirk–Silber network. In particular, all trajectories sufficiently close to the Δ-clique network leave a neighbourhood of the invariant curve C near the equilibrium Y, even if they have first visited X and so are in the domain of f_{XY}. In contrast, trajectories sufficiently close to the Kirk–Silber network can leave a small neighbourhood of C near either X or Y. The limit from below of the Kirk–Silber network—which corresponds to trajectories that leave near Y—is equal to the limit of the Δ-clique network. However, the limit from above differs, and corresponds to trajectories that leave near X. We can see in Figure 16.2(a) that there is a separatrix that divides trajectories near the Kirk–Silber network into those that pass close to X and those that pass close to Y. In Figure 16.2(d), we see for the Δ-clique network that there is a surface of orbits from B to Y, with some passing close to X.

§17 Constructing a completed return map

We now construct for both networks a *completed return map*—that is, one that captures all trajectories near the network. We follow the standard procedure to analyse the dynamics of trajectories near a heteroclinic network, which is to construct cross-sections transverse to the flow near the network, and construct maps between these sections. We adapt the methodology presented in [KLP10, KPR12] to construct the parts of the map that differ from

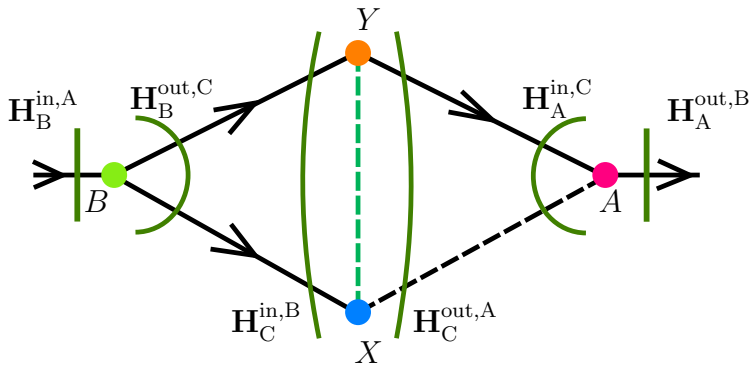

Figure 17.1: A diagrammatic representation of both the Kirk–Silber and Δ-clique networks, and the sections we define near them, showing how they capture all trajectories sufficiently close to the network. Because certain features differ between the two networks, the curve C is shown as a dashed line between X and Y, as is the connection between X and A. For visual clarity, we have not shown the entire heteroclinic orbit $A \to B$.

the more straightforward calculations in Sections 6 and 9.1. We compose these maps to derive a completed full return map for each network and, in the next section, we analyse these maps to explain the (dis)continuity.

For convenience, we sometimes work in polar coordinates in the (x_3, y_3)-plane, giving us coordinates $(x_1, x_2, r_3, \theta_3)$, where r_3 and θ_3 are defined by

$$r_3^2 = x_3^2 + y_3^2$$

and

$$\tan\theta_3 = \frac{y_3}{x_3}.$$

We also, when convenient, consider the angle $\varphi_3 = \frac{\pi}{2} - \theta_3$.

We use the following six cross-sections in our construction of the completed return map. Let h be a sufficiently small positive constant, so that all six of the following cross-sections are defined in a neighbourhood of approximate linear flow. First, near B, we have

$$\begin{aligned}
\mathbf{H}_{\mathrm{B}}^{\mathrm{in,A}} &= \{(x_1, x_2, x_3, y_3) \mid x_1 = h, |x_2 - 1| < h, 0 \le x_3, y_3 < h\},\\
\mathbf{H}_{\mathrm{B}}^{\mathrm{out,C}} &= \left\{(x_1, x_2, r_3, \theta_3) \mid 0 < x_1 < h, |x_2 - 1| < h, r_3 = h, 0 \le \theta_3 \le \frac{\pi}{2}\right\}.
\end{aligned}$$

Second, near C,

$$\begin{aligned}
\mathbf{H}_{\mathrm{C}}^{\mathrm{in,B}} &= \left\{(x_1, x_2, r_3, \theta_3) \mid 0 < x_1 < h, x_2 = h, |r_3 - 1| < h, 0 \le \theta_3 \le \frac{\pi}{2}\right\},\\
\mathbf{H}_{\mathrm{C}}^{\mathrm{out,A}} &= \left\{(x_1, x_2, r_3, \theta_3) \mid x_1 = h, 0 < x_2 < h, r_3 = h, 0 \le \theta_3 \le \frac{\pi}{2}\right\}.
\end{aligned}$$

Last, near A,

$$\mathbf{H}_{\mathrm{A}}^{\mathrm{in,C}} = \left\{(x_1, x_2, r_3, \theta_3) \mid |x_1 - 1| < h, 0 < x_2 < h, r_3 = h, 0 \le \theta_3 \le \frac{\pi}{2}\right\},$$
$$\mathbf{H}_{\mathrm{A}}^{\mathrm{out,B}} = \{(x_1, x_2, x_3, y_3) \mid |x_1 - 1| < h, x_2 = h, 0 \le x_3, y_3 < h\}.$$

Figure 17.1 gives a diagrammatic representation of these sections. We note that these sections have not been defined in terms of any rescaled coordinates, as we do in Chapters III and VI.

We construct three completed local maps, which approximate the dynamics in small neighbourhoods of the equilibria A and B and the curve C. These maps are

$$\widehat{\psi}_{\mathrm{B}} \colon \mathbf{H}_{\mathrm{B}}^{\mathrm{in,A}} \to \mathbf{H}_{\mathrm{B}}^{\mathrm{out,C}},$$
$$\widehat{\psi}_{\mathrm{C}} \colon \mathbf{H}_{\mathrm{C}}^{\mathrm{in,B}} \to \mathbf{H}_{\mathrm{C}}^{\mathrm{out,A}},$$
$$\widehat{\psi}_{\mathrm{A}} \colon \mathbf{H}_{\mathrm{A}}^{\mathrm{in,C}} \to \mathbf{H}_{\mathrm{A}}^{\mathrm{out,B}}.$$

We also construct three completed global maps, which approximate the dynamics along the unstable manifolds of the equilibria A and B, and the curve C:

$$\widehat{\Psi}_{\mathrm{BC}} \colon \mathbf{H}_{\mathrm{B}}^{\mathrm{out,C}} \to \mathbf{H}_{\mathrm{C}}^{\mathrm{in,B}},$$
$$\widehat{\Psi}_{\mathrm{CA}} \colon \mathbf{H}_{\mathrm{C}}^{\mathrm{out,A}} \to \mathbf{H}_{\mathrm{A}}^{\mathrm{in,C}},$$
$$\widehat{\Psi}_{\mathrm{AB}} \colon \mathbf{H}_{\mathrm{A}}^{\mathrm{out,B}} \to \mathbf{H}_{\mathrm{B}}^{\mathrm{in,A}}.$$

The completed full return map $\widehat{\Phi}_{\mathrm{B}} \colon \mathbf{H}_{\mathrm{B}}^{\mathrm{in,A}} \to \mathbf{H}_{\mathrm{B}}^{\mathrm{in,A}}$ is then the composition

$$\widehat{\Phi}_{\mathrm{B}} = \widehat{\Psi}_{\mathrm{AB}}\widehat{\psi}_{\mathrm{A}}\widehat{\Psi}_{\mathrm{CA}}\widehat{\psi}_{\mathrm{C}}\widehat{\Psi}_{\mathrm{BC}}\widehat{\psi}_{\mathrm{B}},$$

and we write $\widehat{\Phi}_{\mathrm{B}} \colon \left(x_3^{\mathrm{in,B}}, y_3^{\mathrm{in,B}}\right) \mapsto (x_3', y_3')$.

For clarity, we say the map $\widehat{\Phi}_{\mathrm{B}}$ is *full* in the sense that it applies to trajectories that make one full excursion around the network. (This terminology is the same as in §6.) Moreover, we say all local, global, and full return maps are *complete* in the sense that they account for all trajectories sufficiently close to the network, and do not require removing from their domain of definition an excluded cusp or its image. We represent completion of a map with a hat above it, in contrast to the maps in Chapters II and III.

In many cases, because we want our maps to account for all trajectories near the network, we are unable to derive an explicit form for most of the above maps. However, we know enough about the dynamics in relevant subspaces to derive sufficient information about the components of this map for our analysis. By the invariant sphere theorem [Fie96], we know

we can exclude the radial component from each step of our analysis. With an abuse of notation, in the remainder of this chapter, we work with only two relevant coordinates for each map, disregarding the radial coordinate and the coordinate fixed in the definition of each cross-section.

17.1 The local map $\widehat{\psi}_{\mathrm{B}}\colon \mathbf{H}_{\mathrm{B}}^{\mathrm{in,A}} \to \mathbf{H}_{\mathrm{B}}^{\mathrm{out,C}}$

We begin with a point $\left(x_3^{\mathrm{in,B}}, y_3^{\mathrm{in,B}}\right) \in \mathbf{H}_{\mathrm{B}}^{\mathrm{in,A}}$. Near B, the linearised flow is

$$\dot{x}_1 = -c_{\mathrm{B}} x_1, \quad \dot{x}_3 = e_{\mathrm{BX}} x_3, \quad \dot{y}_3 = e_{\mathrm{BY}} y_3.$$

Integrating these ODEs gives solutions $x_1(t)$, $x_3(t)$, and $y_3(t)$, which can also be used to find expressions for $r_3(t)$ and $\theta_3(t)$. The trajectory crosses $\mathbf{H}_{\mathrm{B}}^{\mathrm{out,C}}$ when $r_3(t) = h$, and so although the residence time T_{B} cannot be solved for exactly, it satisfies the equation

$$\begin{aligned} h^2 &= x_3^2\, \mathrm{e}^{2e_{\mathrm{BX}}T_{\mathrm{B}}} + y_3^2\, \mathrm{e}^{2e_{\mathrm{BY}}T_{\mathrm{B}}} \\ &= r_3^2 \cos^2\theta_3\, \mathrm{e}^{2e_{\mathrm{BX}}T_{\mathrm{B}}} + r_3^2 \sin^2\theta_3\, \mathrm{e}^{2e_{\mathrm{BY}}T_{\mathrm{B}}}, \end{aligned} \tag{17.1}$$

and we see that

$$\lim_{r_3^{\mathrm{in,B}} \to 0} T_{\mathrm{B}} = \infty. \tag{17.2}$$

Thus, the local map $\widehat{\psi}_{\mathrm{B}}\colon \mathbf{H}_{\mathrm{B}}^{\mathrm{in,A}} \to \mathbf{H}_{\mathrm{B}}^{\mathrm{out,C}}$ is defined by

$$\widehat{\psi}_{\mathrm{B}}\left(x_3^{\mathrm{in,B}}, y_3^{\mathrm{in,B}}\right) = \left(x_1^{\mathrm{out,B}}, \theta_3^{\mathrm{out,B}}\right),$$

where

$$x_1^{\mathrm{out,B}} = h\, \mathrm{e}^{-c_{\mathrm{B}}T_{\mathrm{B}}}$$

and

$$\begin{aligned} \tan\theta_3^{\mathrm{out,B}} &= \tan\theta_3\, \mathrm{e}^{(e_{\mathrm{BY}}-e_{\mathrm{BX}})T_{\mathrm{B}}} \\ &= \frac{y_3^{\mathrm{in,B}}}{x_3^{\mathrm{in,B}}}\, \mathrm{e}^{(e_{\mathrm{BY}}-e_{\mathrm{BX}})T_{\mathrm{B}}}. \end{aligned} \tag{17.3}$$

17.2 The global map $\widehat{\Psi}_{\mathrm{BC}}\colon \mathbf{H}_{\mathrm{B}}^{\mathrm{out,C}} \to \mathbf{H}_{\mathrm{C}}^{\mathrm{in,B}}$

The two-dimensional unstable manifold of B intersects $\mathbf{H}_{\mathrm{B}}^{\mathrm{out,C}}$ at $(x_1, r_3, \theta_3) = (0, h, \theta_3)$, and intersects $\mathbf{H}_{\mathrm{C}}^{\mathrm{in,B}}$ at $(x_1, x_2, \theta_3) = \big(0, h, \bar{\theta}_{\mathrm{C}}(\theta_3)\big)$, where $\bar{\theta}_{\mathrm{C}}$ is an $\mathcal{O}(1)$ function of θ_3.

Therefore, the effect of the global map $\widehat{\Psi}_{\mathrm{BC}}$ is, to leading order, to rescale x_1 by a θ_3-dependent $\mathcal{O}(1)$ amount, and to map the outgoing angle to an incoming angle, and so we have

$$\widehat{\Psi}_{\mathrm{BC}}\Big(x_1^{\mathrm{out,B}}, \theta_3^{\mathrm{out,B}}\Big) = \Big(x_1^{\mathrm{in,C}}, \theta_3^{\mathrm{in,C}}\Big) = \Big(E_{\mathrm{C}}\Big(\theta_3^{\mathrm{out,B}}\Big)x_1^{\mathrm{out,B}}, \bar{\theta}_{\mathrm{C}}\Big(\theta_3^{\mathrm{out,B}}\Big)\Big).$$

Here, E_{C} is an $\mathcal{O}(1)$ function of θ_3. We know little about the function $\bar{\theta}_{\mathrm{C}}$. However, due to the invariance of the x_3- and y_3-axes, we know that $\bar{\theta}_{\mathrm{C}}(0) = 0$ and $\bar{\theta}_{\mathrm{C}}\big(\frac{\pi}{2}\big) = \frac{\pi}{2}$.

17.3 The local map $\widehat{\psi}_{\mathrm{C}}\colon \mathbf{H}_{\mathrm{C}}^{\mathrm{in,B}} \to \mathbf{H}_{\mathrm{C}}^{\mathrm{out,A}}$

The local map $\widehat{\psi}_{\mathrm{C}}$ is the most difficult to construct, and is the only map that differs between the two networks. We need to construct this map in such a way that it captures all trajectories that begin on $\mathbf{H}_{\mathrm{B}}^{\mathrm{in,A}}$, noting that, for any part of the curve C, there exists initial conditions on $\mathbf{H}_{\mathrm{B}}^{\mathrm{in,A}}$ that give rise to trajectories that pass arbitrarily close to that part of C. As such, we cannot simply consider the linear flow near each equilibrium that lies in C, as we usually do when constructing return maps near heteroclinic cycles. Here, we follow the methodology in [KLP10, KPR12].

We assumed that the curve C could be parametrised by the angle θ_3. We also know, by the invariant sphere theorem, that in the (x_3, y_3)-plane there is strong contraction onto the curve C. Therefore, the evolution of θ_3 can be described by a θ_3-dependent function. The local flow near C is thus given by

$$\dot{x}_1 = g_{\mathrm{A}}(\theta_3)x_1, \quad \dot{x}_2 = -g_{\mathrm{B}}(\theta_3)x_2, \quad \dot{\theta}_3 = g_\theta(\theta_3),$$

where $g_{\mathrm{A}}, g_{\mathrm{B}}, g_\theta\colon \big[0, \frac{\pi}{2}\big] \to \mathbb{R}$ are functions of θ_3, and depend on the particular network being considered. A diagrammatic representation of the flow near the curve C is shown in Figure 17.2.

We have little precise information about the functions g_{A}, g_{B}, and g_θ. However, in the case of the Kirk–Silber network, we know the following:

(a) x_1 expands for all values of θ_3, and so $g_{\mathrm{A}}(\theta_3) > 0$ for all $\theta_3 \in \big[0, \frac{\pi}{2}\big]$. The only known values of g_{A} are $g_{\mathrm{A}}(0) = e_{\mathrm{XA}}$ and $g_{\mathrm{A}}\big(\frac{\pi}{2}\big) = e_{\mathrm{YA}}$.

(b) x_2 contracts for all values of θ_3, and so $g_{\mathrm{B}}(\theta_3) > 0$ for all $\theta_3 \in \big[0, \frac{\pi}{2}\big]$. The only known values of g_{B} are $g_{\mathrm{B}}(0) = c_{\mathrm{XB}}$ and $g_{\mathrm{B}}\big(\frac{\pi}{2}\big) = c_{\mathrm{YB}}$.

(c) The invariance of the x_3- and y_3-axes implies that $g_\theta(0) = g_\theta\big(\frac{\pi}{2}\big) = 0$. Moreover, the existence of the equilibrium P implies that $g_\theta\big(\theta_3^P\big) = 0$. The heteroclinic orbits

$P \to X$ and $P \to Y$ imply that, respectively, $g_\theta(\theta_3) < 0$ for all $\theta_3 \in \left(0, \theta_3^P\right)$, and $g_\theta(\theta_3) > 0$ for all $\theta_3 \in \left(\theta_3^P, \frac{\pi}{2}\right)$.

(d) The linearisation of the vector field about X and Y implies that $\mathrm{D}g_\theta(0) = -c_{\mathrm{XY}} < 0$ and $\mathrm{D}g_\theta\left(\frac{\pi}{2}\right) = -c_{\mathrm{YX}} < 0$. It follows that, for small $|\theta_3|$, $\dot{\theta}_3 \approx -c_{\mathrm{XY}}\theta_3$, and that for small $\left|\frac{\pi}{2} - \theta_3\right|$, $\dot{\varphi}_3 \approx -c_{\mathrm{YX}}\varphi_3$, where we recall that we set $\varphi_3 = \frac{\pi}{2} - \theta_3$.

The following, mostly similar, properties are known in the case of the Δ-clique network:

(a) There exists an angle θ_3^* such that x_1 contracts for all $\theta_3 \in [0, \theta_3^*)$, and expands for all $\theta_3 \in \left(\theta_3^*, \frac{\pi}{2}\right]$. (See Figure 16.2(f) and Figure 17.2(b)). Therefore, $g_{\mathrm{A}}(\theta_3) < 0$ for all $\theta_3 \in [0, \theta_3^*)$ and $g_{\mathrm{A}}(\theta_3) > 0$ for all $\theta_3 \in \left(\theta_3^*, \frac{\pi}{2}\right]$. The only known values of g_{A} are $g_{\mathrm{A}}(0) = -c_{\mathrm{XA}}$ and $g_{\mathrm{A}}\left(\frac{\pi}{2}\right) = e_{\mathrm{YA}}$.

(b) x_2 contracts for all values of θ_3, and so $g_{\mathrm{B}}(\theta_3) > 0$ for all $\theta_3 \in \left[0, \frac{\pi}{2}\right]$. The only known values of g_{B} are $g_{\mathrm{B}}(0) = c_{\mathrm{XB}}$ and $g_{\mathrm{B}}\left(\frac{\pi}{2}\right) = c_{\mathrm{YB}}$.

(c) The invariance of the x_3- and y_3-axes implies that $g_\theta(0) = g_\theta\left(\frac{\pi}{2}\right) = 0$. Moreover, the heteroclinic orbit $X \to Y$ implies that $g_\theta(\theta_3) > 0$ for all $\theta_3 \in \left(0, \frac{\pi}{2}\right)$.

(d) The linearisation of the vector field about X and Y implies that $\mathrm{D}g_\theta(0) = e_{\mathrm{XY}} > 0$ and $\mathrm{D}g_\theta\left(\frac{\pi}{2}\right) = -c_{\mathrm{YX}} < 0$. It follows that, for small $|\theta_3|$, $\dot{\theta}_3 \approx e_{\mathrm{XY}}\theta_3$, and that for small $\left|\frac{\pi}{2} - \theta_3\right|$, $\dot{\varphi}_3 \approx -c_{\mathrm{YX}}\varphi_3$.

To derive the local map $\widehat{\psi}_{\mathrm{C}}$, we first use separation of variables to solve $\dot{\theta}_3$, and find $\theta_3^{\mathrm{C}}(t)$ implicitly:

$$t = \int_{\theta_3^{\mathrm{C}}(0)}^{\theta_3^{\mathrm{C}}(t)} \frac{1}{g_\theta(\theta)}\,\mathrm{d}\,\theta. \tag{17.4}$$

Next, the trajectory crosses $\mathbf{H}_{\mathrm{C}}^{\mathrm{out,A}}$ when $x_1(t) = h$, and so although we again cannot solve for the residence time T_{C} explicitly, it satisfies the equation

$$\int_0^{T_{\mathrm{C}}} g_{\mathrm{A}}(\theta_3(\tau))\,\mathrm{d}\,\tau = -\log\left(\frac{x_1(0)}{h}\right) = -\log\left(E_{\mathrm{C}}\left(\theta_3^{\mathrm{out,B}}\right)\right) + c_{\mathrm{B}}T_{\mathrm{B}}.$$

From this relationship we see that

$$\lim_{x_1^{\mathrm{in,C}} \to 0} T_{\mathrm{C}} = \infty. \tag{17.5}$$

We write $\theta_3^{\mathrm{in,C}} \equiv \theta_3^{\mathrm{C}}(0)$ and $\theta_3^{\mathrm{out,C}} \equiv \theta_3^{\mathrm{C}}(T_{\mathrm{C}})$, and we note that $\theta_3^{\mathrm{out,C}}$ is a function of both $\theta_3^{\mathrm{in,C}}$ and T_{C}: $\theta_3^{\mathrm{out,C}}\left(\theta_3^{\mathrm{in,C}}, T_{\mathrm{C}}\right)$.

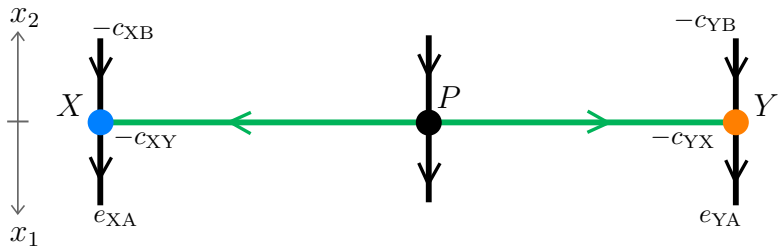

(a)

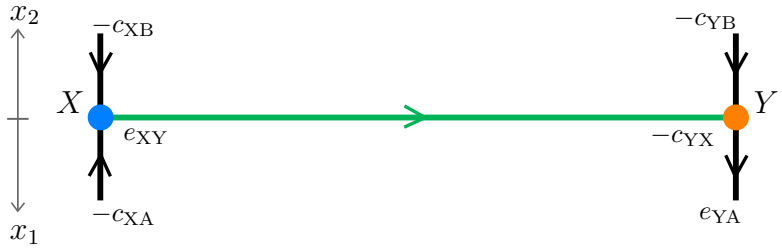

(b)

Figure 17.2: A schematic representation of the dynamics near the curve C for (a) the Kirk–Silber network, and (b) the Δ-clique network, showing the difference in how trajectories pass near the curve C. We use the positive vertical axis to represent the coordinate x_2, and assume that x_1 is small. We use the negative vertical axis to represent the coordinate x_1, and assume that x_2 is small. The (x_2, x_3, y_3)-subspace is thus represented above the curve C, and the (x_1, x_3, y_3)-subspace below.

In the case of the Δ-clique network, we know that $g_\theta(\theta_3) > 0$ for all $\theta_3 \in \left(0, \frac{\pi}{2}\right)$. Therefore, we know that, for a fixed initial condition $\theta_3^{\mathrm{in,C}}$,

$$\lim_{T_{\mathrm{C}} \to \infty} \theta_3^{\mathrm{out,C}}\left(\theta_3^{\mathrm{in,C}}, T_{\mathrm{C}}\right) = \frac{\pi}{2}.$$

However, since $g_{\mathrm{A}}\left(\theta_3^{\mathrm{C}}\right) < 0$ for all $\theta_3 < \theta_3^*$, $\theta_3^{\mathrm{out,C}}$ is bounded below, regardless of T_{C}: $\theta_3^{\mathrm{out,C}} > \theta_3^*$.

In the case of the Kirk–Silber network, since $g_\theta(\theta_3) < 0$ for all $\theta_3 \in \left(0, \theta_3^P\right)$, we know that for a fixed initial condition $\theta_3^{\mathrm{in,C}} \in \left(0, \theta_3^P\right)$,

$$\lim_{T_{\mathrm{C}} \to \infty} \theta_3^{\mathrm{out,C}}\left(\theta_3^{\mathrm{in,C}}, T_{\mathrm{C}}\right) = 0,$$

and since $g_\theta(\theta_3) > 0$ for all $\theta_3 \in \left(\theta_3^P, \frac{\pi}{2}\right)$, we know that for a fixed initial condition $\theta_3^{\mathrm{in,C}} \in \left(\theta_3^P, \frac{\pi}{2}\right)$,

$$\lim_{T_{\mathrm{C}} \to \infty} \theta_3^{\mathrm{out,C}}\left(\theta_3^{\mathrm{in,C}}, T_{\mathrm{C}}\right) = \frac{\pi}{2}.$$

Since $g_\theta\left(\theta_3^P\right) = 0$, then, if $\theta_3^{\mathrm{in,C}} = \theta_3^P$, $\theta_3^{\mathrm{out,C}} = \theta_3^P$, regardless of T_{C}.

From these relationships, we have our first indication of the origin of the discontinuity of the projected map in the case of the Kirk–Silber network. In particular, considering the outgoing angle $\theta_3^{\mathrm{out,C}} \equiv \theta_3^{\mathrm{C}}(T_{\mathrm{C}})$ as a function of the incoming angle $\theta_3^{\mathrm{in,C}} \equiv \theta_3^{\mathrm{C}}(0)$, where we take the $x_1^{\mathrm{in,C}}$-dependent expression T_{C} as a parameter, we have, in the case of the Kirk–Silber network,

$$\lim_{x_1^{\mathrm{in,C}} \to 0} \theta_3^{\mathrm{out,C}}\left(\theta_3^{\mathrm{in,C}}\right) = \begin{cases} 0, & \text{if } \theta_3^{\mathrm{in,C}} < \theta_3^P, \\ \theta_3^P, & \text{if } \theta_3^{\mathrm{in,C}} = \theta_3^P, \\ \frac{\pi}{2}, & \text{if } \theta_3^{\mathrm{in,C}} > \theta_3^P, \end{cases} \tag{17.6}$$

and, for the Δ-clique network,

$$\lim_{x_1^{\mathrm{in,C}} \to 0} \theta_3^{\mathrm{out,C}}\left(\theta_3^{\mathrm{in,C}}\right) = \frac{\pi}{2}. \tag{17.7}$$

The function $\theta_3^{\mathrm{out,C}}\left(\theta_3^{\mathrm{in,C}}\right)$ is a continuous function for both networks, noting that $x_1^{\mathrm{in,C}} \neq 0$ for all trajectories that pass near C. However, in the limit as the trajectory approaches the network, the function is continuous for the Δ-clique network—being a constant function—and discontinuous for the Kirk–Silber network, being a step function. In the case of the Kirk–Silber network, a separatrix is formed by the stable manifold of P, and is defined as the surface of trajectories that satisfy $\theta_3^{\mathrm{out,C}} = \theta_3^{\mathrm{in,C}}$. No such separatrix exists near the Δ-clique network.

Although we cannot analytically derive the function $\theta_3^{\mathrm{out,C}}\left(\theta_3^{\mathrm{in,C}}\right)$, we can, with numerical computation, observe the limits in (17.6) and (17.7). We show in Figure 17.3 plots of these functions for various values of $x_1^{\mathrm{in,C}}$, where we can observe the convergence to a constant or step function. In §A.2, we describe how these figures were computed.

With assumptions about the functions g_{A}, g_{B} and g_θ, we could derive exact expressions for components of this local map. In [KPR12], for example, they assumed that $g_\theta(\theta_3) = -\frac{\lambda}{4}\sin 4\theta_3$ for the Kirk–Silber network. However, we do not need to make such assumptions here, as the asymptotic behaviour of these components is sufficient for our purposes.

In summary, we write the local map as

$$\widehat{\psi}_{\mathrm{C}}\left(x_1^{\mathrm{in,C}}, \theta_3^{\mathrm{in,C}}\right) = \left(x_2^{\mathrm{out,C}}, \theta_3^{\mathrm{C}}(T_{\mathrm{C}})\right),$$

where

$$x_2^{\mathrm{out,C}} = h \exp\left(-\int_0^{T_{\mathrm{C}}} g_{\mathrm{B}}(\theta_3^{\mathrm{C}}(\tau))\,\mathrm{d}\,\tau\right).$$

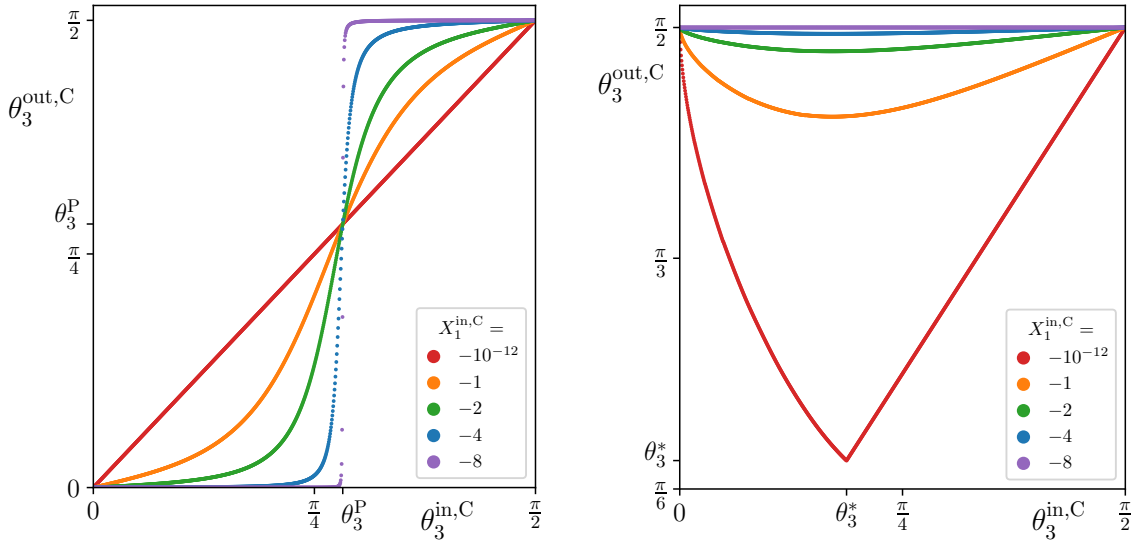

(a) (b)

Figure 17.3: Plots of the outgoing angle $\theta_3^{\text{out,C}}$ as a function of $\theta_3^{\text{in,C}}$ for both (a) the Kirk–Silber network and (b) the Δ-clique network. The relationship is computed for various values of $x_1^{\text{in,C}}$, given as $X_1^{\text{in,C}} := \log x_1^{\text{in,C}}$. These plots were computed numerically by integrating ODEs that contain the heteroclinic networks. We see that the function in the case of the Kirk–Silber network begins as an identity function and converges to a step function, while the function in the case of the Δ-clique case is initially more complicated but converges to a constant function as $x_1^{\text{in,C}} \to 0$. Parameter values for these figures are given in Tables B.6.1 and B.6.2.

17.4 The global map $\widehat{\Psi}_{\text{CA}} : \mathbf{H}_{\text{C}}^{\text{out,A}} \to \mathbf{H}_{\text{A}}^{\text{in,C}}$

The two-dimensional unstable manifold of C intersects $\mathbf{H}_{\text{C}}^{\text{out,A}}$ at $(x_1, x_2, \theta_3) = (h, 0, \theta_3)$ and intersects $\mathbf{H}_{\text{A}}^{\text{in,C}}$ at $(x_2, r_3\theta_3) = \big(0, h, \bar{\theta}_{\text{A}}(\theta_3)\big)$. Again, we know that the effect of the global map $\widehat{\Psi}_{\text{CA}}$ is, to leading order, to rescale x_2 by a θ_3-dependent $\mathcal{O}(1)$ amount, and to map the outgoing angle to an incoming angle, and so we have

$$\widehat{\Psi}_{\text{CA}}\left(x_2^{\text{out,C}}, \theta_3^{\text{out,C}}\right) = \left(x_2^{\text{in,A}}, \theta_3^{\text{in,A}}\right) = \left(E_{\text{A}}\left(\theta_3^{\text{out,C}}\right) x_2^{\text{out,C}}, \bar{\theta}_{\text{A}}\left(\theta_3^{\text{out,C}}\right)\right).$$

As for the global map $\widehat{\Psi}_{\text{BC}}$, E_{A} is an $\mathcal{O}(1)$ function of θ_3. We know little about the function $\bar{\theta}_{\text{A}}$, except again that $\bar{\theta}_{\text{A}}(0) = 0$ and $\bar{\theta}_{\text{A}}\left(\frac{\pi}{2}\right) = \frac{\pi}{2}$.

17.5 The local map $\widehat{\psi}_{\text{A}} : \mathbf{H}_{\text{A}}^{\text{in,C}} \to \mathbf{H}_{\text{A}}^{\text{out,B}}$

The local map $\widehat{\psi}_{\text{A}}$ is the most straightforward to compute. The flow linearised about A is

$$\dot{x}_2 = e_{\text{A}} x_2, \quad \dot{x}_3 = -c_{\text{AX}} x_3, \quad \dot{y}_3 = -c_{\text{AY}} y_3.$$

The trajectory crosses $\mathbf{H}_{\mathrm{A}}^{\mathrm{out,B}}$ when $x_2(t) = h$, and therefore the residence time T_{A} can be found explicitly:

$$T_{\mathrm{A}} = -\frac{1}{e_{\mathrm{A}}} \log\Big(\frac{x_2}{h}\Big).$$

Thus, the local map is

$$\widehat{\psi}_{\mathrm{A}}\Big(x_2^{\mathrm{in,A}}, \theta_3^{\mathrm{in,A}}\Big) = \Big(x_3^{\mathrm{out,A}}, y_3^{\mathrm{out,A}}\Big) = \left(h\cos\theta_3^{\mathrm{in,A}}\left(\frac{x_2^{\mathrm{in,A}}}{h}\right)^{\frac{c_{\mathrm{AX}}}{e_{\mathrm{A}}}}, h\sin\theta_3^{\mathrm{in,A}}\left(\frac{x_2^{\mathrm{in,A}}}{h}\right)^{\frac{c_{\mathrm{AY}}}{e_{\mathrm{A}}}}\right).$$

17.6 The global map $\widehat{\Psi}_{\mathrm{AB}}\colon \mathbf{H}_{\mathrm{A}}^{\mathrm{out,B}} \to \mathbf{H}_{\mathrm{B}}^{\mathrm{in,A}}$

The heteroclinic orbit from A to B intersects $\mathbf{H}_{\mathrm{A}}^{\mathrm{out,B}}$ at $(x_2, x_3, y_3) = (h, 0, 0)$, and intersects $\mathbf{H}_{\mathrm{B}}^{\mathrm{in,A}}$ at $(x_1, x_3, y_3) = (h, 0, 0)$. The effect of the global map $\widehat{\Phi}_{AB}$ is thus, to leading order, to multiply the coordinates x_3 and y_3 by an $\mathcal{O}(1)$ amount. The expression for this map is therefore

$$\widehat{\Psi}_{\mathrm{AB}}\Big(x_3^{\mathrm{out,A}}, y_3^{\mathrm{out,A}}\Big) = \Big(x_3^{\mathrm{in,B}\prime}, y_3^{\mathrm{in,B}\prime}\Big) = \Big(E_{\mathrm{BX}} x_3^{\mathrm{out,A}}, E_{\mathrm{BY}} y_3^{\mathrm{out,A}}\Big).$$

17.7 Composing the maps

Composing these maps, we can write the completed full return map $\widehat{\Phi}_{\mathrm{B}}\colon \mathbf{H}_{\mathrm{B}}^{\mathrm{in,A}} \to \mathbf{H}_{\mathrm{B}}^{\mathrm{in,A}}$ as

$$\widehat{\Phi}_{\mathrm{B}}\Big(x_3^{\mathrm{in,B}}, y_3^{\mathrm{in,B}}\Big) = (x_3', y_3'), \tag{17.8}$$

where

$$x_3' = E_{\mathrm{BX}} h \cos\big(\bar{\theta}_{\mathrm{A}}\big(\theta_3^{\mathrm{C}}(T_{\mathrm{C}})\big)\big)\left(E_{\mathrm{A}}\big(\theta_3^{\mathrm{C}}(T_{\mathrm{C}})\big)\exp\left(-\int_0^{T_{\mathrm{C}}} g_{\mathrm{B}}(\theta_3^{\mathrm{C}}(\tau))\,\mathrm{d}\,\tau\right)\right)^{\frac{c_{\mathrm{AX}}}{e_{\mathrm{A}}}} \tag{17.9}$$

and

$$y_3' = E_{\mathrm{BY}} h \sin\big(\bar{\theta}_{\mathrm{A}}\big(\theta_3^{\mathrm{C}}(T_{\mathrm{C}})\big)\big)\left(E_{\mathrm{A}}\big(\theta_3^{\mathrm{C}}(T_{\mathrm{C}})\big)\exp\left(-\int_0^{T_{\mathrm{C}}} g_{\mathrm{B}}(\theta_3^{\mathrm{C}}(\tau))\,\mathrm{d}\,\tau\right)\right)^{\frac{c_{\mathrm{AY}}}{e_{\mathrm{A}}}}. \tag{17.10}$$

The value of $\theta_3^{\mathrm{C}}(T_{\mathrm{C}})$ is found by integrating $\dot{\theta}_3$ with initial condition

$$\theta_3^{\mathrm{C}}(0) = \bar{\theta}_{\mathrm{C}}\left(\frac{y_3^{\mathrm{in,B}}}{x_3^{\mathrm{in,B}}}\,\mathrm{e}^{(e_{\mathrm{BY}} - e_{\mathrm{BX}})T_{\mathrm{B}}}\right).$$

These expressions for x_3' and y_3' are valid for both the Kirk–Silber and Δ-clique networks. However, each network has a different definition of g_{A}, g_{B}, and g_θ, and of the $\mathcal{O}(1)$ components of the global maps. Therefore, the actual evaluation of these two expressions differs between the two networks.

This return map $\widehat{\Phi}_{\mathrm{B}}$ is defined on the entirety of the incoming cross-section $\mathbf{H}_{\mathrm{B}}^{\mathrm{in,A}}$, including inside the cusp Γ_{c} excluded from the domain of Φ_{B} in (16.2). Therefore, it is also defined on the switching curve Σ_{s} defined by $x_3^{e_{\mathrm{BY}}} = y_3^{e_{\mathrm{BX}}}$, which corresponds to the switching manifold ϑ_{s} of the projected maps f_{KS} and f_Δ. Moreover, it is a continuous map.

§18 Analysing the continuity of the projected map

We now analyse the completed return map $\widehat{\Phi}_{\mathrm{B}}$ to determine the continuity of the projected maps f_{KS} and f_Δ on ϑ_{s}.

From the expressions in (17.9) and (17.10), we calculate the action of the completed full return map in logarithmic coordinates:

$$\begin{aligned} X_3' &\coloneqq \log x_3' \\ &= \log E_{\mathrm{BX}} + \log h + \log\cos\bar{\theta}_{\mathrm{A}}\big(\theta_3^{\mathrm{C}}(T_{\mathrm{C}})\big) \\ &\qquad + \frac{c_{\mathrm{AX}}}{e_{\mathrm{A}}}\left(\log E_{\mathrm{A}}\big(\theta_3^{\mathrm{C}}(T_{\mathrm{C}})\big) - \int_0^{T_{\mathrm{C}}} g_{\mathrm{B}}(\theta_3^{\mathrm{C}}(\tau))\,\mathrm{d}\,\tau\right) \end{aligned} \tag{18.1}$$

and

$$\begin{aligned} Y_3' &\coloneqq \log y_3' \\ &= \log E_{\mathrm{BY}} + \log h + \log\sin\bar{\theta}_{\mathrm{A}}\big(\theta_3^{\mathrm{C}}(T_{\mathrm{C}})\big) \\ &\qquad + \frac{c_{\mathrm{AY}}}{e_{\mathrm{A}}}\left(\log E_{\mathrm{A}}\big(\theta_3^{\mathrm{C}}(T_{\mathrm{C}})\big) - \int_0^{T_{\mathrm{C}}} g_{\mathrm{B}}(\theta_3^{\mathrm{C}}(\tau))\,\mathrm{d}\,\tau\right) \end{aligned} \tag{18.2}$$

These expressions allow us to define a map $M_{\mathrm{B}}\colon \mathcal{D} \to \mathcal{D}$:

$$\widehat{M}_{\mathrm{B}}(X_3, Y_3) = (X_3', Y_3').$$

The domain of this map is

$$\mathcal{D} = \big\{(X_3, Y_3) \in \mathbb{R}^2 \mid X_3, Y_3 < \log h\big\} \subsetneq \mathbb{R}^2_-.$$

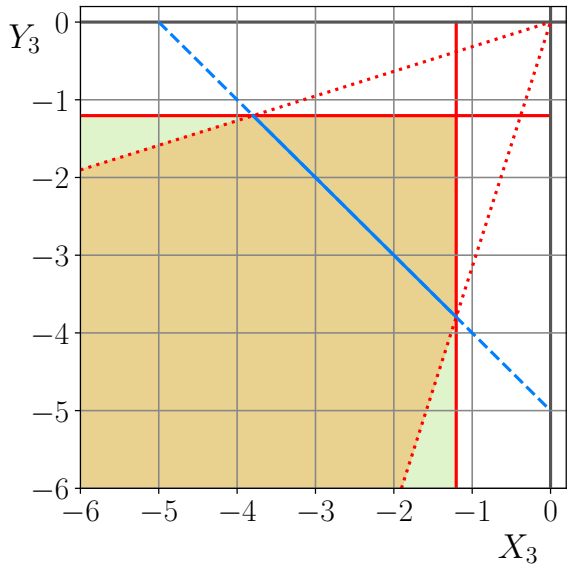

Figure 18.1: A representation of the domain of the map $\widehat{M}_{\mathrm{B}}$ and of the projection $\Pi^{(k)}$, and the set $T^{(k)}$. We show a subset of $\mathbb{R}^2_-$. The solid red lines are $X_3 = \log h$ and $Y_3 = \log h$. The lower-left region bounded by these lines, shaded green and orange, is the domain $\mathcal{D}$ of $\widehat{M}_{\mathrm{B}}$. The solid blue line is the set $T^{(k)}$, and the set $\mathcal{D}^{(k)}$ of all points that project onto a point in $T^{(k)}$ that are in $\mathcal{D}$ is shaded orange.

18.1 Projection of the completed full return map

Just as the projected maps f_{KS} and f_Δ are defined from the transition matrices in (16.3), we can define a projected map from the map $\widehat{M}$. To do so, we follow the methodology in §9.3. Let $k > 0$ be a positive real number. We define the line $T^{(k)}$ in the negative orthant of $\mathbb{R}^2$ by

$$T^{(k)} := \{(X_3, Y_3) \in \mathcal{D} \mid X_3 + Y_3 = -k\}.$$

Note that in the definition given in (9.5), the set S, which is the domain of both f_{KS} and f_Δ, is the straight line from the point $(-1, 0)$ to the point $(0, -1)$. The line $T^{(k)}$ is instead a subset of $\mathcal{D}$, and so does not extend to the coordinate axes, as all points (X_3, Y_3) on the line $T^{(k)}$ must satisfy $X_3 < \log h$ and $Y_3 < \log h$. We can identify this line with the open interval $(-k - \log h, \log h)$.

We can rescale this set by k to define the open interval

$$S^{(k)} = \left(-1 - \frac{\log h}{k}, \frac{\log h}{k}\right).$$

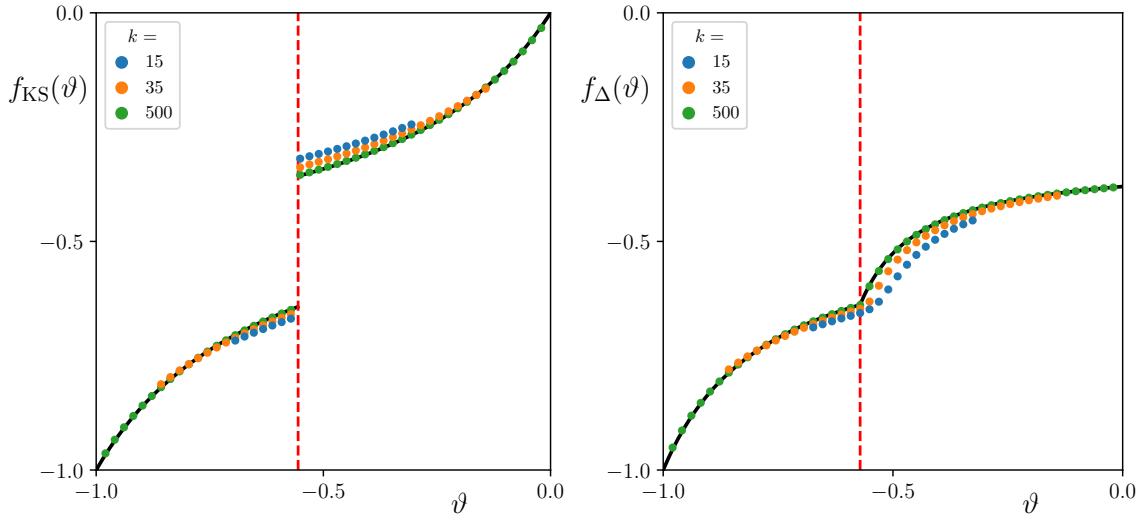

(a) (b)

Figure 18.2: Numerical approximations of the projected maps (a) $f_{\mathrm{KS}}^{(k)}$ and (b) $f_{\Delta}^{(k)}$, for various values of k, as indicated. The projected maps f_{KS} and f_{Δ} are plotted as solid black lines. As k increases, $f_{\mathrm{KS}}^{(k)}$ and $f_{\Delta}^{(k)}$ converge to f_{KS} and f_{Δ}, respectively. Note that, for larger k, the domains of the maps widen. See Figure 18.3 for more detailed plots near the switching manifold. See §A.3 for an explanation of how these approximations are calculated. For visual clarity, we plot only the components of the projected map within their domain of definition, and we do not shade these domains. The dashed red line indicates ϑ_{s}. Parameter values for these figures are given in Tables B.6.3 and B.6.4.

We then have $\lim_{k\to\infty} S^{(k)} = S$. We can define a projection $\Pi^{(k)} \colon \mathcal{D}^{(k)} \to S^{(k)}$ by

$$\Pi^{(k)} \colon (X_3, Y_3) \mapsto \frac{-X_3}{X_3 + Y_3}.$$

The domain of this projection is

$$\mathcal{D}^{(k)} = \left\{ (X_3, Y_3) \in \mathcal{D} \;\middle|\; Y_3 < \frac{-\log h}{k + \log h} X_3 \text{ and } X_3 < \frac{-\log h}{k + \log h} Y_3 \right\}.$$

This set is the set all points in $\mathbb{R}^2_-$ that project onto a point in $T^{(k)}$ that are in the domain of definition of $\widehat{M}_{\mathrm{B}}$. We show a visual representation of this domain in Figure 18.1.

We can now define a projected map $f^{(k)} \colon S^{(k)} \to S^{(k)}$:

$$f^{(k)} \colon \vartheta \mapsto \Pi^{(k)}\Big(\widehat{M}_{\mathrm{B}}(\vartheta, -k - \vartheta)\Big).$$

The map $f^{(k)}$ is continuous. Since the map $\widehat{M}_{\mathrm{B}}$ is not linear, the value of $f^{(k)}(\vartheta)$ depends on the value of k; that is, if $\ell > k$, then for any point $\vartheta \in S^{(k)} \subsetneq S^{(\ell)}$, $f^{(\ell)}(\vartheta) \neq f^{(k)}(\vartheta)$.

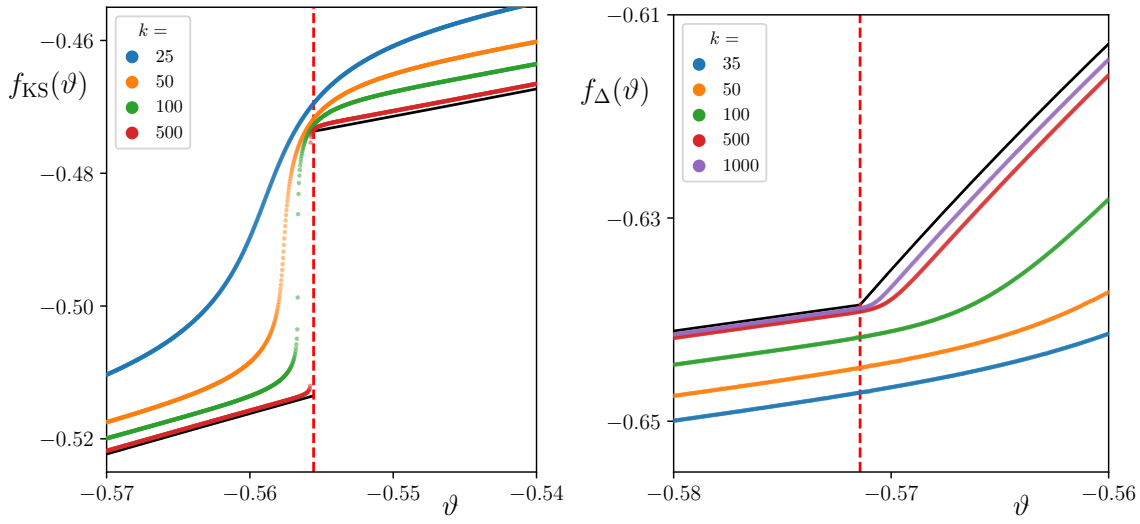

(a) (b)

Figure 18.3: Numerical approximations of the projected maps (a) $f_{\mathrm{KS}}^{(k)}$ and (b) $f_{\Delta}^{(k)}$ near the switching manifold ϑ_{s} for various values of k, as indicated. The projected maps f_{KS} and f_{Δ} are plotted as solid black lines. As k increases, we see that the functions converge to f_{KS} and f_{Δ}. More importantly, however, we see a discontinuity emerge in the case of $f_{\mathrm{KS}}^{(k)}$. See §A.3 for an explanation of how these approximations are calculated. For visual clarity, we plot only the components of the projected map within their domain of definition, and we do not shade these domains. The dashed red line indicates ϑ_{s}. Parameter values for these figures are given in Tables B.6.3 and B.6.4.

We show numerical approximations of this projected map for both networks in Figure 18.2. We observe that, as $k \to \infty$, the function $f^{(k)}$ appears to converge to the projected maps f_{KS} and f_{Δ}, and we conjecture that they do in fact converge, though we do not prove that here. In Figure 18.2(a), the map $f_{\mathrm{KS}}^{(k)}$ appears to be discontinuous at ϑ_{s}, though only because of the discretisation of the numerical calculations. In Figure 18.3, we show the same calculations in a small neighbourhood of the switching manifold ϑ_{s}. We see that the projected maps $f^{(k)}$ are continuous at $\vartheta = \vartheta_{\mathrm{s}}$ for both the Kirk–Silber and Δ-clique networks, though a discontinuity emerges in the limit $k \to \infty$ for the Kirk–Silber network. We observe a similar discontinuity emerge in the function $\theta_3^{\mathrm{out,C}}\left(\theta_3^{\mathrm{out,C}}\right)$.

18.2 Calculating the completed full return map

We begin with the Kirk–Silber network. We assume we have some point

$$\left(x_3^{\mathrm{in,B}}, y_3^{\mathrm{in,B}}\right) \in \mathbf{H}_{\mathrm{B}}^{\mathrm{in,A}}.$$

Applying the basic map defined by the composition $\widehat{\Psi}_{\mathrm{BC}}\widehat{\psi}_{\mathrm{B}}$ to this point, we calculate

$$\left(\theta_3^{\mathrm{in,C}}, x_1^{\mathrm{in,C}}\right) = \left(\widehat{\Psi}_{\mathrm{BC}}\widehat{\psi}_{\mathrm{B}}\right)\left(x_3^{\mathrm{in,B}}, y_3^{\mathrm{in,B}}\right).$$

We assume that the trajectory beginning at $\left(x_3^{\mathrm{in,B}}, y_3^{\mathrm{in,B}}\right)$ strikes $\mathbf{H}_{\mathrm{C}}^{\mathrm{in,B}}$ in a small neighbourhood of the equilibrium P, and close to the heteroclinic orbit $P \to X$. This condition is $\theta_3^{\mathrm{P}} - h < \theta_3^{\mathrm{in,C}} < \theta_3^{\mathrm{P}}$. This assumption requires the point $\left(x_3^{\mathrm{in,B}}, y_3^{\mathrm{in,B}}\right)$ to be close to the switching curve Σ_{s}, defined by $x_3^{e_{\mathrm{BY}}} = y_3^{e_{\mathrm{BX}}}$. Therefore, this point is inside the cusp Γ_{c} that is excluded from the domain of the return map Φ_{B} in (16.2). For $\theta_3^{\mathrm{in,C}} < \theta_3^{\mathrm{P}}$, we require $x_3^{e_{\mathrm{BY}}} > y_3^{e_{\mathrm{BX}}}$.

We also assume that the trajectory strikes $\mathbf{H}_{\mathrm{C}}^{\mathrm{out,A}}$ in a small neighbourhood of the equilibrium X. This condition is $0 < \theta_3^{\mathrm{out,C}} < \theta_3^{\mathrm{X}} + h$, and requires T_{B} to be sufficiently large. We quantify this requirement explicitly in the inequality (18.4) below.

The flow linearised about P is given by

$$\begin{aligned}
\dot{x}_1 &= g_{\mathrm{A}}\left(\theta_3^{\mathrm{P}}\right)x_1,\\
\dot{x}_2 &= -g_{\mathrm{B}}\left(\theta_3^{\mathrm{P}}\right)x_2,\\
\dot{\theta}_3 &= -\lambda_{\mathrm{P}}\left(\theta_3^{\mathrm{P}} - \theta_3\right),
\end{aligned}$$

for some real number $\lambda_{\mathrm{P}} > 0$.

Our assumption that $\theta_3^{\mathrm{out,C}} < \theta_3^{\mathrm{X}} + h$ implies that there is some time $T_{\mathrm{C}}^{(\mathrm{P})}$ such that $\theta_3^{\mathrm{C}}\left(T_{\mathrm{C}}^{(\mathrm{P})}\right) = \theta_3^{\mathrm{P}} - h$. Solving $\dot{\theta}_3$ with initial condition $\theta_3(0) = \theta_3^{\mathrm{in,C}}$, we find

$$T_C^{(P)} = \frac{-1}{\lambda_{\mathrm{P}}}\log\left(\frac{\theta_3^{\mathrm{P}} - \theta_3^{\mathrm{in,C}}}{h}\right).$$

Solving both $\dot{x}_1$ and $\dot{x}_2$ with initial conditions

$$x_1(0) = x_1^{\mathrm{in,C}} = E_{\mathrm{C}}\left(\theta_3^{\mathrm{out,B}}\right)he^{-c_{\mathrm{B}}T_{\mathrm{B}}},$$

and $x_2(0) = h$, we find that

$$x_1\left(T_{\mathrm{C}}^{(\mathrm{P})}\right) = E_{\mathrm{C}}\left(\theta_3^{out,B}\right)he^{-c_{\mathrm{B}}T_{\mathrm{B}}}\left(\frac{\theta_3^{\mathrm{P}} - \theta_3^{\mathrm{in,C}}}{h}\right)^{-\frac{g_A\left(\theta_3^{\mathrm{P}}\right)}{\lambda_{\mathrm{P}}}}$$

and

$$x_2\left(T_{\mathrm{C}}^{(\mathrm{P})}\right) = h\left(\frac{\theta_3^{\mathrm{P}} - \theta_3^{\mathrm{in,C}}}{h}\right)^{\frac{g_{\mathrm{B}}\left(\theta_3^{\mathrm{P}}\right)}{\lambda_{\mathrm{P}}}}.$$

There is then a jump from P to X as the trajectory follows the heteroclinic orbit $P \to X$. In this transition, both x_1 and x_2 are scaled by an h-dependent $\mathcal{O}(1)$ amount, $E_{\mathrm{PX}}^{(1)}$ and $E_{\mathrm{PX}}^{(2)}$, respectively. Therefore, at $\theta_3 = \theta_3^{\mathrm{X}} + h$, the value of x_1 is

$$E_{\mathrm{PX}}^{(1)} E_{\mathrm{C}}\left(\theta_3^{out,B}\right) h e^{-c_{\mathrm{B}} T_{\mathrm{B}}} \left(\frac{\theta_3^{\mathrm{P}} - \theta_3^{\mathrm{in,C}}}{h}\right)^{-\frac{g_A\left(\theta_3^{\mathrm{P}}\right)}{\lambda_{\mathrm{P}}}} \tag{18.3}$$

and the value of x_2 is

$$E_{\mathrm{PX}}^{(2)} h \left(\frac{\theta_3^{\mathrm{P}} - \theta_3^{\mathrm{in,C}}}{h}\right)^{\frac{g_{\mathrm{B}}\left(\theta_3^{\mathrm{P}}\right)}{\lambda_{\mathrm{P}}}}.$$

Our assumption that the trajectory strikes $\mathbf{H}_{\mathrm{C}}^{\mathrm{out,A}}$ in a small neighbourhood of X means that we require the value of x_1 in (18.3) to be strictly less than h. Solving this inequality for T_{B} shows that we require

$$T_{\mathrm{B}} > \frac{1}{c_{\mathrm{B}}}\left(\log\left(E_{\mathrm{PX}}^{(1)} E_{\mathrm{C}}\left(\theta_3^{\mathrm{out,B}}\right)\right) - \frac{g_{\mathrm{A}}\left(\theta_3^{\mathrm{P}}\right)}{\lambda_{\mathrm{P}}} \log\left(\frac{\theta_3^{\mathrm{P}} - \theta_3^{\mathrm{in,C}}}{h}\right)\right). \tag{18.4}$$

Therefore, our assumption that the trajectory strikes $\mathbf{H}_{\mathrm{C}}^{\mathrm{in,B}}$ near P and then strikes $\mathbf{H}_{\mathrm{C}}^{\mathrm{out,A}}$ near X requires $T_{\mathrm{B}} \to \infty$ as $\theta_3^{\mathrm{in,C}} \to \theta_3^{\mathrm{P}}$.

Near X, the linearised flow is

$$\begin{aligned}
\dot{x}_1 &= e_{\mathrm{XA}} x_1, \\
\dot{x}_2 &= -c_{\mathrm{XB}} x_2, \\
\dot{\theta}_3 &= -c_{XY} \theta_3.
\end{aligned}$$

We solve for the residence time $T_{\mathrm{C}}^{(\mathrm{X})}$ near X by solving $x_1(T_{\mathrm{C}}^{(\mathrm{X})}) = h$ with the initial condition of x_1 given in (18.3):

$$T_{\mathrm{C}}^{(\mathrm{X})} = -\frac{1}{e_{\mathrm{XA}}}\left(\log\left(E_{\mathrm{PX}}^{(1)} E_{\mathrm{C}}\left(\theta_3^{\mathrm{out,B}}\right)\right) - \frac{g_{\mathrm{A}}\left(\theta_3^{\mathrm{P}}\right)}{\lambda_{\mathrm{P}}} \log\left(\frac{\theta_3^{\mathrm{P}} - \theta_3^{\mathrm{in,C}}}{h}\right) - c_{\mathrm{B}} T_{\mathrm{B}}\right).$$

Therefore, the value of x_2 on $\mathbf{H}_{\mathrm{C}}^{\mathrm{out,A}}$ is

(18.5)
$$x_2^{\mathrm{out,C}} = E_{\mathrm{PX}}^{(2)} h \left(\frac{\theta_3^{\mathrm{P}} - \theta_3^{\mathrm{in,C}}}{h} \right)^{\frac{g_{\mathrm{B}}\left(\theta_3^{\mathrm{P}}\right)}{\lambda_{\mathrm{P}}}} \left(E_{\mathrm{PX}}^{(1)} E_{\mathrm{C}}\left(\theta_3^{\mathrm{out,B}}\right) e^{-C_{\mathrm{B}} T_{\mathrm{B}}} \left(\frac{\theta_3^{\mathrm{P}} - \theta_3^{\mathrm{in,C}}}{h} \right)^{-\frac{g_{\mathrm{A}}\left(\theta_3^{\mathrm{P}}\right)}{\lambda_{\mathrm{P}}}} \right)^{\frac{c_{\mathrm{XB}}}{e_{\mathrm{XA}}}}$$

and the value of $\theta_3^{\mathrm{out,C}} \equiv \theta_3^{\mathrm{C}}(T_{\mathrm{C}})$ is

$$\theta_3^{\mathrm{out,C}} = h \left(E_{\mathrm{PX}}^{(1)} E_{\mathrm{C}}\left(\theta_3^{\mathrm{out,B}}\right) e^{-c_{\mathrm{B}} T_{\mathrm{B}}} \left(\frac{\theta_3^{\mathrm{P}} - \theta_3^{\mathrm{in,C}}}{h} \right)^{-\frac{g_{\mathrm{A}}\left(\theta_3^{\mathrm{P}}\right)}{\lambda_{\mathrm{P}}}} \right)^{\frac{c_{\mathrm{XY}}}{e_{\mathrm{XA}}}} . \tag{18.6}$$

A similar analysis can be completed in the case of the Kirk–Silber network when a trajectory strikes $\mathbf{H}_{\mathrm{C}}^{\mathrm{in,B}}$ in a small neighbourhood of the equilibrium P, and close to the heteroclinic orbit $P \to Y$. This condition is $\theta_3^{\mathrm{P}} < \theta_3^{\mathrm{in,C}} < \theta_3^{\mathrm{P}} + h$. In this case, the value of x_2 on $\mathbf{H}_{\mathrm{C}}^{\mathrm{out,A}}$ is

(18.7)
$$x_2^{\mathrm{out,C}} = E_{\mathrm{PY}}^{(2)} h \left(\frac{\theta_3^{\mathrm{P}} - \theta_3^{\mathrm{in,C}}}{h} \right)^{\frac{g_{\mathrm{B}}\left(\theta_3^{\mathrm{P}}\right)}{\lambda_{\mathrm{P}}}} \left(E_{\mathrm{PY}}^{(1)} E_{\mathrm{C}}\left(\theta_3^{\mathrm{out,B}}\right) e^{-C_{\mathrm{B}} T_{\mathrm{B}}} \left(\frac{\theta_3^{\mathrm{P}} - \theta_3^{\mathrm{in,C}}}{h} \right)^{-\frac{g_{\mathrm{A}}\left(\theta_3^{\mathrm{P}}\right)}{\lambda_{\mathrm{P}}}} \right)^{\frac{c_{\mathrm{YB}}}{e_{\mathrm{YA}}}}$$

and the value of $\varphi_3^{\mathrm{out,C}}$, where we recall $\varphi_3 = \frac{\pi}{2} - \theta_3$, is

$$\theta_3^{\mathrm{out,C}} = h \left(E_{\mathrm{PY}}^{(1)} E_{\mathrm{C}}\left(\theta_3^{\mathrm{out,B}}\right) e^{-c_{\mathrm{B}} T_{\mathrm{B}}} \left(\frac{\theta_3^{\mathrm{P}} - \theta_3^{\mathrm{in,C}}}{h} \right)^{-\frac{g_{\mathrm{A}}\left(\theta_3^{\mathrm{P}}\right)}{\lambda_{\mathrm{P}}}} \right)^{\frac{c_{\mathrm{YX}}}{e_{\mathrm{YA}}}} . \tag{18.8}$$

A lower bound similar to (18.4) exists for T_{B}.

Finally, in the case of the Δ-clique network, there is no equilibrium P. Any trajectory that begins in the cusp that is excluded from the cross-section $\mathbf{H}_{\mathrm{B}}^{\mathrm{in,A}}$ strikes $\mathbf{H}_{\mathrm{C}}^{\mathrm{in,B}}$ along the heteroclinic connection $X \to Y$, and not in a small neighbourhood of X or Y. Therefore, the initial conditions on $\mathbf{H}_{\mathrm{C}}^{\mathrm{in,A}}$ are $x_1 = E_{\mathrm{C}}\left(\theta_3^{\mathrm{out,B}}\right) h e^{-c_{\mathrm{B}} T_{\mathrm{B}}}$, $x_2 = h$, and $\theta_3^{\mathrm{X}} + h < \theta_3^{\mathrm{in,C}} < \theta_3^{\mathrm{Y}} - h$. We assume that the trajectory leaves C near Y, and thus we can again compute a lower bound for T_{B} similar to (18.4).

The transition of the trajectory along the heteroclinic orbit $X \to Y$ rescales x_1 and x_2

by h-dependent $\mathcal{O}(1)$ amounts, $E^{(1)}_{\mathrm{XY}}$ and $E^{(2)}_{\mathrm{XY}}$, respectively. Near Y, the linearised flow is

$$\begin{aligned}\dot{x}_1 &= e_{\mathrm{YA}}x_1,\\ \dot{x}_2 &= -c_{\mathrm{YB}}x_2,\\ \dot{\varphi}_3 &= -c_{YX}\varphi_3.\end{aligned}$$

Solving for $x_1\Big(T^{(\mathrm{Y})}_{\mathrm{C}}\Big) = h$ and then integrating the above linear system gives $x_2^{\mathrm{out,C}}$

$$x_2^{\mathrm{out,C}} = E^{(2)}_{\mathrm{XY}}h\Big(E^{(1)}_{\mathrm{XY}}E_{\mathrm{C}}\Big(\theta_3^{\mathrm{out,B}}\Big)e^{-c_{\mathrm{B}}T_{\mathrm{B}}}\Big)^{\frac{c_{\mathrm{YB}}}{e_{\mathrm{YA}}}} \tag{18.9}$$

and the value of $\theta_3^{\mathrm{out,C}}$ is

$$\theta_3^{\mathrm{out,C}} = h\Big(E^{(1)}_{\mathrm{XY}}E_{\mathrm{C}}\Big(\theta_3^{\mathrm{out,B}}\Big)e^{-c_{\mathrm{B}}T_{\mathrm{B}}}\Big)^{\frac{c_{\mathrm{YX}}}{e_{\mathrm{YA}}}}. \tag{18.10}$$

18.3 Applying the projection

We now use the values for $\theta_3^{\mathrm{out,C}}$ and $x_2^{\mathrm{out,C}}$ in the expressions for X_3' and Y_3' in (18.1) and (18.2), respectively.

For the Kirk–Silber network with $\theta_3^{\mathrm{in,C}} < \theta_3^{\mathrm{P}}$, $\theta_3^{\mathrm{out,C}} \equiv \theta_3^{\mathrm{C}}(T_{\mathrm{C}}) < \theta_3^{\mathrm{X}} + h \ll 1$. Therefore, we Taylor expand $\bar{\theta}_{\mathrm{A}}$ about the fixed point $\bar{\theta}_A(0) = 0$ to derive the leading order expansion

$$\bar{\theta}_A\big(\theta_3^{\mathrm{C}}(T_{\mathrm{C}})\big) = K_1\theta_3^{\mathrm{C}}(T_{\mathrm{C}}) + \mathcal{O}\big(\theta_3^{\mathrm{C}}(T_{\mathrm{C}})^2\big),$$

for some $\mathcal{O}(1)$ constant K_1. We can then apply a leading order Taylor expansion to the trigonometric terms in (18.1) and (18.2). The resulting expressions are rather long and cumbersome, and are the sums of terms involving T_{B}, $\log\Big(\frac{\theta_3^{\mathrm{P}}-\theta_3^{\mathrm{in,C}}}{h}\Big)$, and the logarithm of constant terms. Since we have assumed that $T_{\mathrm{B}} \gg 1$ and $\theta_3^{\mathrm{P}} - \theta_3^{\mathrm{in,C}} \ll h$, we can ignore the logarithm of the constant terms as they do not affect the asymptotic behaviour of the expressions of interest in the limit $T_{\mathrm{B}} \to \infty$ or $\theta_3^{\mathrm{in,C}} \to \theta_3^{\mathrm{P}}$. We then substitute the expressions in (18.5) and (18.6) into (18.1) and (18.2), and the resulting expressions into the projection $\Pi^{(k)}$, and rearrange to derive

(18.11)

$$\Pi^{(k)}(X_3', Y_3') = \frac{-c_{\mathrm{AX}}\Big(-\frac{e_{\mathrm{XA}}}{c_{\mathrm{B}}\lambda_{\mathrm{P}}}\Big(g_{\mathrm{B}}(\theta_3^{\mathrm{P}}) - \frac{g_{\mathrm{A}}(\theta_3^{\mathrm{P}})c_{\mathrm{XB}}}{e_{\mathrm{XA}}}\Big)\frac{\log\delta}{T_{\mathrm{B}}} + c_{\mathrm{XB}}\Big)}{(c_{\mathrm{AX}} + c_{\mathrm{AY}})\Big(-\frac{e_{\mathrm{XA}}}{c_{\mathrm{B}}\lambda_{\mathrm{P}}}\Big(g_{\mathrm{B}}(\theta_3^{\mathrm{P}}) - \frac{g_{\mathrm{A}}(\theta_3^{\mathrm{P}})c_{\mathrm{XB}}}{e_{\mathrm{XA}}}\Big)\frac{\log\delta}{T_{\mathrm{B}}} + c_{\mathrm{XB}}\Big) + e_{\mathrm{A}}\Big(\frac{g_{\mathrm{A}}(\theta_3^{\mathrm{P}})c_{\mathrm{XY}}}{c_{\mathrm{B}}\lambda_{\mathrm{P}}}\frac{\log\delta}{T_{\mathrm{B}}} + c_{\mathrm{XY}}\Big)}.$$

In this expressions, we have written

$$\delta = \frac{\theta_3^{\mathrm{P}} - \theta_3^{\mathrm{in,C}}}{h}.$$

In §10.3, to evaluate the limit of the projected map f_{KS} as $\vartheta \searrow \vartheta_{\mathrm{s}}$, we must follow the definition of the projected map outlined in §9.4, and calculate the projection of the action of the transition matrix M_{X} on points on the line $Y_3 = \log(1-\epsilon) + \frac{e_{\mathrm{BY}}}{e_{\mathrm{BX}}} X_3$. Recall from (9.2) and (9.3) in §9.1 that ϵ was a positive constant used in the definition of the excluded cusp. The limit $\vartheta \searrow \vartheta_{\mathrm{s}}$ is then the limit $X_3 \to -\infty$.

On $\mathbf{H}_{\mathrm{B}}^{\mathrm{in,A}}$, curves of constant angle $\theta_3^{\mathrm{in,B}}$ have the form $x_3 = a y_3$. Therefore, in logarithmic coordinates, curves of constant $\theta_3^{\mathrm{in,B}}$ in $\mathcal{D}$ are $X_3 = \log a + Y_3$. We see from the action of the local map $\widehat{\psi}_{\mathrm{B}}$ in (17.3) that curves of constant angle $\theta_3^{\mathrm{out,B}}$ in $\mathcal{D}$ have the form $X_3 = \log a + \frac{e_{\mathrm{BX}}}{e_{\mathrm{BY}}} Y_3$.

For any $0 > \log a > \log(1-\epsilon)$, the line $X_3 = \log a + \frac{e_{\mathrm{BX}}}{e_{\mathrm{BY}}} Y_3$ lies inside the region corresponding to the excluded cusp. Moreover, the expression in (18.11) is valid, and can be evaluated, at any point on the line $X_3 = \log a + \frac{e_{\mathrm{BX}}}{e_{\mathrm{BY}}} Y_3$, whereas the transition matrix M_{X} cannot. For any point along this line, $\theta_3^{\mathrm{in,C}}$, and therefore also δ, is fixed, but as $X_3 \to -\infty$, we see from (17.1) that $T_{\mathrm{B}} \to \infty$ and thus $\frac{\log \delta}{T_{\mathrm{B}}} \to 0$. Therefore, the expression in (18.11) simplifies to

$$\Pi^{(k)}(X_3', Y_3') = \frac{-c_{\mathrm{XB}} c_{\mathrm{AX}}}{c_{\mathrm{XB}}(c_{\mathrm{AX}} + c_{\mathrm{AY}}) + e_{\mathrm{A}} c_{\mathrm{XY}}},$$

which is the value of the limit $\lim_{\vartheta \searrow \vartheta_{\mathrm{s}}} f_{\mathrm{KS}}(\vartheta)$ in (16.4). This limit applies for all $0 > \log a > \log(1-\epsilon)$, and so $\theta_3^{\mathrm{P}} - \theta_3^{\mathrm{in,C}}$ can be chosen to be arbitrarily close to 0, and thus the trajectory is arbitrarily close to the switching manifold.

In the case of the Kirk–Silber network with $\theta_3^{\mathrm{P}} < \theta_3^{\mathrm{in,C}} < \theta_3^{\mathrm{P}} + h$, substituting the expressions in (18.7) and (18.8) into (18.1) and (18.2), disregarding the logarithm of $\mathcal{O}(1)$ constant terms, which do not affect the dynamics in the limit $T_{\mathrm{B}} \to \infty$, and applying the projection, gives

(18.12)

$$\Pi^{(k)}(X_3', Y_3') = \frac{-c_{\mathrm{AX}}\left(-\frac{e_{\mathrm{YA}}}{c_{\mathrm{B}}\lambda_{\mathrm{P}}}\left(g_{\mathrm{B}}(\theta_3^{\mathrm{P}}) - \frac{g_{\mathrm{A}}(\theta_3^{\mathrm{P}})c_{\mathrm{YB}}}{e_{\mathrm{YA}}}\right)\frac{\log\delta}{T_{\mathrm{B}}} + c_{\mathrm{YB}}\right) - e_{\mathrm{A}}\left(\frac{g_{\mathrm{A}}(\theta_3^{\mathrm{P}})c_{\mathrm{YX}}}{c_{\mathrm{B}}\lambda_{\mathrm{P}}}\frac{\log\delta}{T_{\mathrm{B}}} + c_{\mathrm{YX}}\right)}{(c_{\mathrm{AX}} + c_{\mathrm{AY}})\left(-\frac{e_{\mathrm{YA}}}{c_{\mathrm{B}}\lambda_{\mathrm{P}}}\left(g_{\mathrm{B}}(\theta_3^{\mathrm{P}}) - \frac{g_{\mathrm{A}}(\theta_3^{\mathrm{P}})c_{\mathrm{YB}}}{e_{\mathrm{YA}}}\right)\frac{\log\delta}{T_{\mathrm{B}}} + c_{\mathrm{YB}}\right) + e_{\mathrm{A}}\left(\frac{g_{\mathrm{A}}(\theta_3^{\mathrm{P}})c_{\mathrm{YX}}}{c_{\mathrm{B}}\lambda_{\mathrm{P}}}\frac{\log\delta}{T_{\mathrm{B}}} + c_{\mathrm{YX}}\right)}.$$

We note that the additional term in the numerator compared to (18.11) is a result of the fact that the leading order Taylor expansion of $\log\cos\bar{\theta}_{\mathrm{A}}(\theta)$ around the point $\frac{\pi}{2}$ is $\log\theta$, as opposed to $\log 1$ when the Taylor expansion is evaluated around 0.

For any $0 < \log a < \log\left(\frac{1}{1-\epsilon}\right)$, the line $X_3 = \log a + \frac{e_{\mathrm{BX}}}{e_{\mathrm{BY}}} Y_3$ lies inside the region corresponding to the excluded cusp, and the expression in (18.12) is valid, and the expression can be evaluated, at any point on that line. In the limit of $X_3 \to -\infty$, we find

$$\Pi^{(k)}(X_3', Y_3') = \frac{-(c_{\mathrm{YB}} c_{\mathrm{AX}} + e_{\mathrm{A}} c_{\mathrm{YX}})}{c_{\mathrm{YB}}(c_{\mathrm{AX}} + c_{\mathrm{AY}}) + e_{\mathrm{A}} c_{\mathrm{YX}}},$$

which is the value of the limit $\lim_{\vartheta \nearrow \vartheta_{\mathrm{s}}} f_{\mathrm{KS}}(\vartheta)$ in (16.5).

We note that, since the map $\widehat{\Phi}_{\mathrm{B}}$ is defined for all points in $\mathbf{H}_{\mathrm{B}}^{\mathrm{in,A}}$, we can evaluate this map at any point on the line $x_3^{e_{\mathrm{BY}}} = y_3^{e_{\mathrm{BX}}}$, and we can therefore also evaluate $\widehat{M}_{\mathrm{B}}$ at any point on the line $e_{\mathrm{BY}} X_3 = e_{\mathrm{BX}} Y_3$. Therefore, for all $k > 0$, we can evaluate $f^{(k)}(\vartheta_{\mathrm{s}})$. We cannot, however, determine the value of this expression since we do not know the value of $\bar{\theta}_{\mathrm{A}}\left(\theta_3^{\mathrm{P}}\right)$. However, evaluating the map $f^{(k)}$ at ϑ_{s} for any $k > 0$ does not tell us about the limiting behaviour of f_{KS} at ϑ_{s}, since the components of these functions are defined only for trajectories that leave C near X or Y.

In the case of the Δ-clique network, the expressions for X_3' and Y_3' differ on either side of the switching manifold by only an $\mathcal{O}(1)$ global constant, since, in both cases, the trajectory follows the connection $X \to Y$ but does not strike $\mathbf{H}_{\mathrm{C}}^{\mathrm{in,B}}$ near X. Therefore, in both cases, applying the projection gives

$$\Pi^{(k)}(X_3', Y_3') = \frac{-c_{\mathrm{AX}}\left(-\frac{e_{\mathrm{YA}}}{c_{\mathrm{B}}}\frac{1}{T_{\mathrm{B}}} + c_{\mathrm{YB}}\right) - e_{\mathrm{A}}\left(\frac{c_{\mathrm{YX}}}{c_{\mathrm{B}}}\frac{1}{T_{\mathrm{B}}} + c_{\mathrm{YX}}\right)}{(c_{\mathrm{AX}} + c_{\mathrm{AY}})\left(-\frac{e_{\mathrm{YA}}}{c_{\mathrm{B}}}\frac{1}{T_{\mathrm{B}}} + c_{\mathrm{YB}}\right) + e_{\mathrm{A}}\left(\frac{c_{\mathrm{YX}}}{c_{\mathrm{B}}}\frac{1}{T_{\mathrm{B}}} + c_{\mathrm{YX}}\right)}. \tag{18.13}$$

The expression is valid, and can be evaluated, at any point on the line $X_3 = \log a + \frac{e_{\mathrm{BX}}}{e_{\mathrm{BY}}} Y_3$ for $0 > \log a > \log(1-\epsilon)$ and $0 < \log a < \log\left(\frac{1}{1-\epsilon}\right)$. Any such value of $\log a$ ensures the line lies inside the region corresponding to the excluded cusp. In both cases, δ is again fixed and $T_{\mathrm{B}} \to \infty$, giving us, in both cases,

$$\Pi^{(k)}(X_3', Y_3') = \frac{-(c_{\mathrm{YB}} c_{\mathrm{AX}} + e_{\mathrm{A}} c_{\mathrm{YX}})}{c_{\mathrm{YB}}(c_{\mathrm{AX}} + c_{\mathrm{AY}}) + e_{\mathrm{A}} c_{\mathrm{YX}}},$$

which is the value of the limit $\lim_{\vartheta \to \vartheta_{\mathrm{s}}} f_{\Delta}(\vartheta)$ in (16.6).

In summary, we find that the discontinuity of f_{KS} at ϑ_{s} is a result of two factors: first, that evaluating the limit $\vartheta \to \vartheta_{\mathrm{s}}$ requires us to evaluate the flow in the limit as a trajectory approaches the network; and, second, that there is a separatrix near the network that creates a discontinuity in the flow in the limit as a trajectory approaches the network. In the case of the Δ-clique network, however, although the first of these two factors is still required,

no discontinuity emerges in the flow in the limit as a trajectory approaches the network. Therefore, the projected map f_Δ is continuous at ϑ_s.

In §12, we also studied the tournament network, which is the union $\mathcal{C}_{[X]} \cup \mathcal{C}_{[Y]} \cup \mathcal{C}_{[XY]}$. Although the tournament network also contains a subnetwork whose graph representation is equivalent to the Kirk–Silber network, the nearby dynamics does not contain a structure equivalent to the equilibrium P, and so also does not contain the separatrix formed by its stable and unstable manifolds. It instead contains two Δ-cliques, with trajectories leaving a neighbourhood containing the Δ-clique near a common equilibrium. A small extension of the map derived in §17 and the analysis in this section shows that the projected map of the tournament network is continuous on both of its two switching manifolds.

VI Dynamics near networks in higher dimensions

In this chapter, we present investigations of two heteroclinic networks with $n \geq 5$ equilibria, embedded in $\mathbb{R}^n$ with the simplex realisation of Ashwin and Postlethwaite [AP13].

We begin in §19 with a detailed description of a network between 6 equilibria studied by Podvigina [Pod23], composed of two cycles of four equilibria each, joined along one common heteroclinic orbit. This network is a natural extension of the Kirk–Silber network [KS94]. We first summarise the results obtained by Podvigina [Pod23], and present examples of time-series that complement Podvigina's findings that suggest that more complicated behaviour is observed in trajectories near this network than the Kirk–Silber network and other networks in $\mathbb{R}^4$. We then compute in §19.1 a partial bifurcation set of regular cycling near this network. We make numerous observations about the structures and patterns in this bifurcation set, and make conjectures about the structure of regions of fragmentarily asymptotically stable root sequences in the complete bifurcation set. In §19.2, we construct the network's projected map, and relate periodic orbits of this projected map to regular cycling near the network. We present in §19.3 a numerical investigation of some of these periodic orbits and how they relate to the bifurcation structure of regular cycling near the network. We consider the continuity of the projected map on the map's switching manifold in §19.4

Next we consider in §20 the Rock–Paper–Scissors–Lizard–Spock network, studied by Postlethwaite and Rucklidge [PR22]. In this network, the heteroclinic orbits are grouped into two different classes, A and B. We present a bifurcation set of regular cycling near this network in §20.1. In the case of this heteroclinic network, itineraries and root sequences of

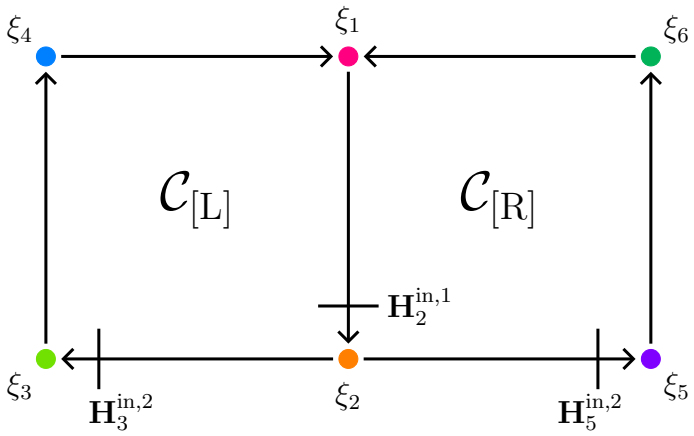

Figure 19.1: A diagrammatic representation of Podvigina's two-cycle network [Pod23], and the location of the three cross-sections relevant to the analysis of the network.

eventually periodic itineraries are not defined by the equilibria a trajectory visits but instead by the classes of the orbits a trajectory follows when transitioning between equilibria. We review the work of Postlethwaite and Rucklidge to construct return maps near the network in §20.2, and then in §20.3 we construct the projected map of the heteroclinic network. Since the switching equilibria of this network have multiple incoming heteroclinic orbits, the projected map is not straightforward to define. We therefore present a method to overcome these complications and construct a single projected map on a connected domain. We analyse regular cycling near the network in the projected map in §20.4, and irregular cycling near the network, in what appears to be a strange attractor, in §20.5. Lastly, we again consider the continuity of the projected map on the map's switching manifolds in §20.6.

§19 Podvigina's two-cycle network

We begin by considering a network in $\mathbb{R}^6$ that was studied by Podvigina in [Pod23], which we refer to as *Podvigina's two-cycle network*. This network is composed of six equilibria, $\xi_1, \ldots, \xi_6$, that are each at unit distance from the origin in the positive orthant on each of the six coordinate axes, and seven heteroclinic orbits that are contained in specific two-dimensional flow-invariant subspaces. These equilibria and orbits form two cycles:[1] $\mathcal{C}_{[\mathrm{L}]} = \xi_1 \to \xi_2 \to \xi_3 \to \xi_4 \to \xi_1$ and $\mathcal{C}_{[\mathrm{R}]} = \xi_1 \to \xi_2 \to \xi_5 \to \xi_6 \to \xi_1$. The network is the union $\mathcal{N}_{\mathrm{Pod}} = \mathcal{C}_{[\mathrm{L}]} \cup \mathcal{C}_{[\mathrm{R}]}$. A diagrammatic representation of this network is shown in Figure 19.1. As in the case of the networks in Chapter III, the equilibrium ξ_2 has a two-dimensional unstable manifold, and

[1] of type C_4^- [KM04]

so there in fact exists a continuum of heteroclinic orbits $\xi_2 \to \xi_3$ and $\xi_2 \to \xi_5$. However, all but one of these orbits are not contained in a two-dimensional subspace. We do not consider any of these heteroclinic orbits to be part of the network, only the orbit that is contained in the (x_2, x_3)-plane and the orbit that is contained in the (x_2, x_5)-plane.

Truncated at third-degree, the general form of the equations (3.2) that contains Podvigina's two-cycle network is

$$
\begin{aligned}
\dot{x}_1 &= x_1\Big(1 - \|x\|_2^2 - c_{21}x_2^2 - t_{31}x_3^2 + e_{41}x_4^2 - t_{51}x_5^2 + e_{51}x_6^2\Big),\\
\dot{x}_2 &= x_2\Big(1 - \|x\|_2^2 + e_{12}x_1^2 - c_{32}x_3^2 - t_{42}x_4^2 - c_{52}x_5^2 - c_{62}x_6^2\Big),\\
\dot{x}_3 &= x_3\Big(1 - \|x\|_2^2 - t_{13}x_1^2 + e_{\mathrm{L}}x_2^2 - c_{43}x_4^2 - t_{53}x_5^2 - t_{63}x_6^2\Big),\\
\dot{x}_4 &= x_4\Big(1 - \|x\|_2^2 - c_{\mathrm{L}}x_1^2 - t_{24}x_2^2 + e_{34}x_3^2 - t_{54}x_5^2 - t_{64}x_6^2\Big),\\
\dot{x}_5 &= x_5\Big(1 - \|x\|_2^2 - t_{15}x_1^2 + e_{\mathrm{R}}x_2^2 - t_{35}x_3^2 - t_{45}x_4^2 - c_{65}x_6^2\Big),\\
\dot{x}_6 &= x_6\Big(1 - \|x\|_2^2 - c_{\mathrm{R}}x_1^2 - t_{26}x_6^2 - t_{36}x_3^2 - t_{46}x_4^2 + e_{56}x_5^2\Big),
\end{aligned}
\tag{19.1}
$$

where all e_{ij}, c_{ij}, t_{ij} are strictly positive real constants. Note that, to simplify the presentation of some results in the remainder of this section, we have made the identifications $c_{\mathrm{L}} \equiv c_{14}$, $c_{\mathrm{R}} \equiv c_{16}$, $e_{\mathrm{L}} \equiv e_{23}$, and $e_{\mathrm{R}} \equiv e_{25}$.

In their paper, Podvigina [Pod23] considered root sequences (see §5) corresponding to the two cycles, $\mathcal{C}_{[\mathrm{L}]}$ and $\mathcal{C}_{[\mathrm{R}]}$, and of a trajectory that makes one excursion around one cycle before switching to the other, then switches back again after one excursion around the second cycle, and repeats this process. These root sequences are $L = (1234)$, $R = (1256)$, and $LR = (12341256)$. A trajectory which is asymptotic to either cycle has an itinerary that is eventually periodic with root sequence either L or R, and a trajectory which regularly switches back and forth between the two cycles after one excursion around each has an itinerary that is eventually periodic with root sequence LR. We show in Figure 19.2(a) an example of a trajectory which regularly cycles between $\mathcal{C}_{[\mathrm{L}]}$ and $\mathcal{C}_{[\mathrm{R}]}$, with root sequence LR. Podvigina [Pod23] proves that the LR root sequence is fragmentarily asymptotically stable for certain parameter values. (Podvigina uses the term *omnicycle* and *trail stability* for the concepts of a root sequence and its stability, respectively.) Therefore, for certain parameter values, there is an open set of initial conditions that are asymptotic to the entire network $\mathcal{N}_{\mathrm{Pod}}$, and not to a proper subset of the network. These properties are in direct contrast to the three networks considered in Chapter III: for those three networks, a trajectory asymptotic

to the network is asymptotic to a proper subset of the network.

Podvigina's proof of the stability of the LR root sequence relies on assuming that many of the eigenvalues of the linearisation of the vector field at each equilibrium vanish. Since the eigenvalues and eigenvectors of a matrix depend continuously on its entries, there is an open set of values for each of these eigenvalues around 0 for which the conditions in Theorem 6.1 continue to hold. To simplify the analysis, Podvigina additionally assumes the system has additional symmetry, namely a $\mathbb{Z}_2$ symmetry generated by

$$(x_1, x_2, x_3, x_4, x_5, x_6) \mapsto (x_1, x_2, x_5, x_6, x_3, x_4).$$

We do not make these assumptions concerning vanishing eigenvalues and additional symmetries of the system.

19.1 Regular cycling

In their paper, Podvigina [Pod23] proved the fragmentary asymptotic stability of the root sequence LR. They also provided some preliminary numerical examples of more complicated root sequences, such as L^2R^4, L^3R, and L^5R^5, among others. In Figure 19.2, we present similar example timeseries of trajectories near this network. We observe, as Podvigina did, that these trajectories are asymptotic to the network, and not a proper subset of it—that is, $\omega(x) = \mathcal{N}_{\text{Pod}}$. In addition to the LR root sequence, the trajectories in Figure 19.2 have itineraries that are eventually periodic with root sequences LR^3, L^3R^2, and L^2RLR. These root sequences were not observed or considered by Podvigina. We therefore ask what other root sequences can be fragmentarily asymptotically stable, for what parameter values are they fragmentarily asymptotically stable, and what relationships exist between these root sequences? In the remainder of this chapter, we sometimes shorten fragmentarily asymptotically stable to *stable* for brevity. The definition of stability of a root sequence is given in Definitions 5.6 and 5.7, and necessary and sufficient conditions for stability are given in Theorem 6.2.

19.1.1 Constructing a bifurcation set

To answer these questions, we construct a bifurcation set of fragmentarily asymptotically stable root sequences. We determine for what parameter values the transition matrices that correspond to certain root sequences satisfy the three conditions in Theorem 6.2. We define

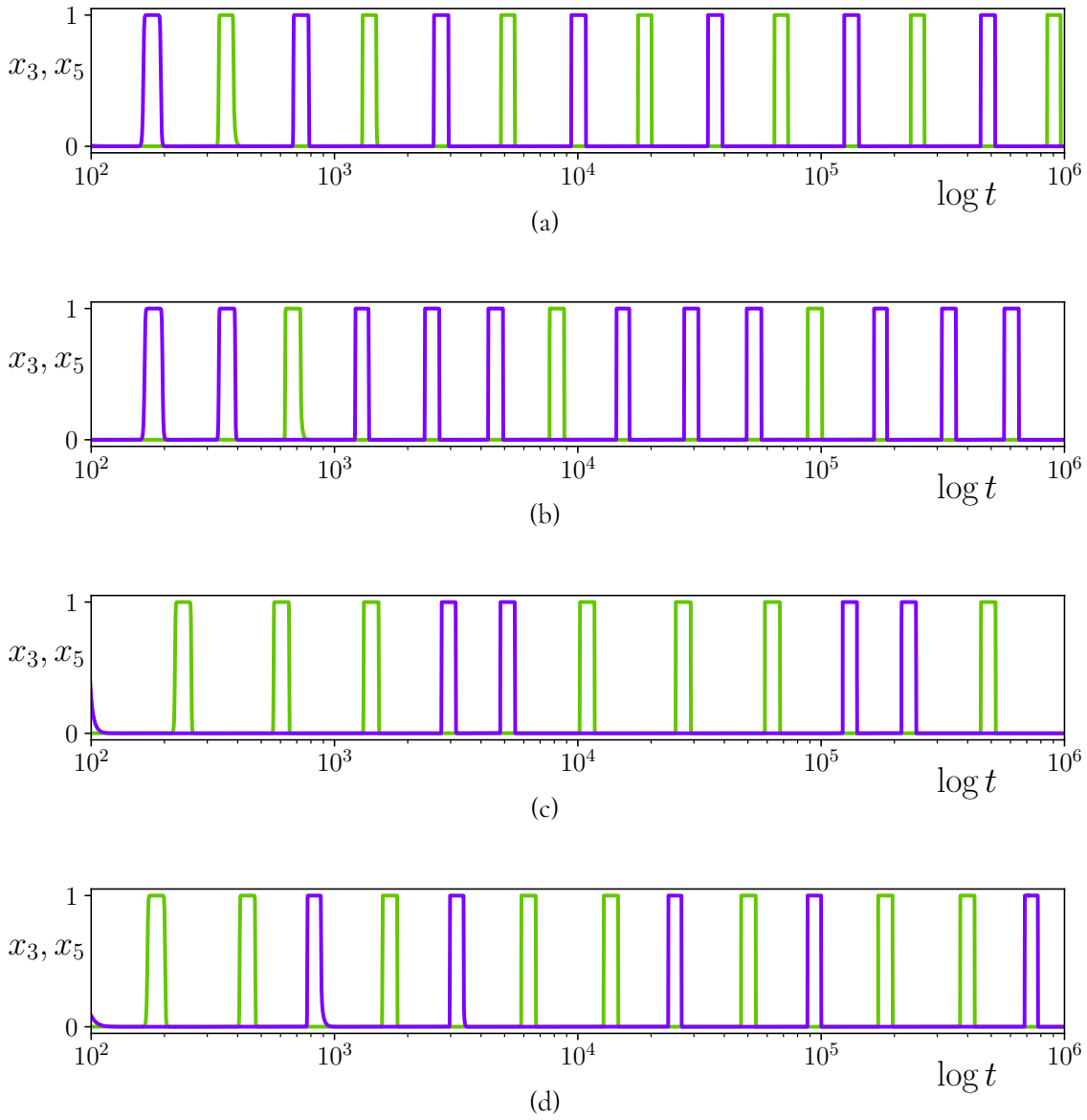

Figure 19.2: Various example timeseries of trajectories near Podvigina's two-cycle network. The values of c_{L} and c_{R} vary between examples, while all other parameters remain the same. For visual clarity, we plot only the x_3- and x_5-coordinates: when x_3, coloured green, is close to 1, all other coordinates are close to 0 and the trajectory is in a small neighbourhood of ξ_3. Similarly, when x_5, coloured purple, is close to 1, all other coordinates are close to 0 and the trajectory is in a small neighbourhood of ξ_5. Time is plotted on a logarithmic scale, to aid visual clarity. We see a regular pattern in these timeseries, and their root sequences are readily deduced: (a) LR, (b) LR^3, (c) L^3R^2, and (d) L^2RLR. Parameter values and initial conditions for these figures are given in §B.7.

the transition matrices M_{L} and M_{R} by

$$M_{\mathrm{L}} \equiv M_2^{(\mathrm{L})} = m_{412}m_{341}m_{234}m_{123} = \begin{pmatrix} \alpha_{11} & \alpha_{12} & 0 & 0 \\ \alpha_{21} & \alpha_{22} & 0 & 0 \\ \alpha_{31} & \alpha_{32} & 1 & 0 \\ \alpha_{41} & \alpha_{42} & 0 & 1 \end{pmatrix} \tag{19.2}$$

and

$$M_{\mathrm{R}} \equiv M_2^{(\mathrm{R})} = m_{612}m_{561}m_{256}m_{125} = \begin{pmatrix} 1 & 0 & \beta_{13} & \beta_{14} \\ 0 & 1 & \beta_{23} & \beta_{24} \\ 0 & 0 & \beta_{33} & \beta_{34} \\ 0 & 0 & \beta_{43} & \beta_{44} \end{pmatrix}. \tag{19.3}$$

The expressions for the α_{jk} and β_{jk} terms are given in §B.2, along with the basic transition matrices. These transition matrices act on the coordinates (X_3, X_4, X_5, X_6), where $X_i \coloneqq \log x_i$, and where we have rescaled the coordinates x_i so that we are in a neighbourhood of approximate linear flow of ξ_2.

In theory, we might have to consider every cyclic permutation of these two products to determine when the $\mathcal{C}_{[\mathrm{L}]}$ and $\mathcal{C}_{[\mathrm{R}]}$ cycles are stable. However, because ξ_2 is the only equilibrium with positive locally transverse eigenvalues, the only basic transition matrices with negative entries are m_{123} and m_{125}. Therefore, the only transition matrices that must be checked to determine the stability of each cycle are $M_3^{(\mathrm{L})} = m_{123}M_{\mathrm{L}}m_{123}^{-1}$ and $M_5^{(\mathrm{R})} = m_{125}M_{\mathrm{R}}m_{125}^{-1}$. Having to check only these matrices is equivalent to having to check only $M_3^{(3)}$ and $M_4^{(4)}$ when studying the Kirk–Silber network in §10.

Fixing all parameter values but c_{L} and c_{R} to those specified in Table B.7.1, we construct a bifurcation set for the parameter values $c_{\mathrm{L}} \in (0, 2.75]$ and $c_{\mathrm{R}} \in (0, 2]$. Due to the difficulty of evaluating the eigenvalues and eigenvectors of the matrices M_{L} and M_{R}—these difficulties being the motivation behind Podvigina's assumptions in [Pod23]—we calculate this bifurcation set numerically, which can be done, for example, by following the process outlined in [PR22], or by discretely sampling parameter space and evaluating the transition matrices M_{L} and M_{R} at these parameter values.

In Figure 19.3, the blue shaded region, labelled L, is the set of all parameter values for which the $M_3^{(\mathrm{L})}$ matrix satisfies these conditions. This region is therefore the set of all parameter values for which the $\mathcal{C}_{[\mathrm{L}]}$ cycle, and thus also the L root sequence, is fragmentarily asymptotically stable. The orange shaded region, labelled R, is the set of all parameter values for which the R root sequence is fragmentarily asymptotically stable.

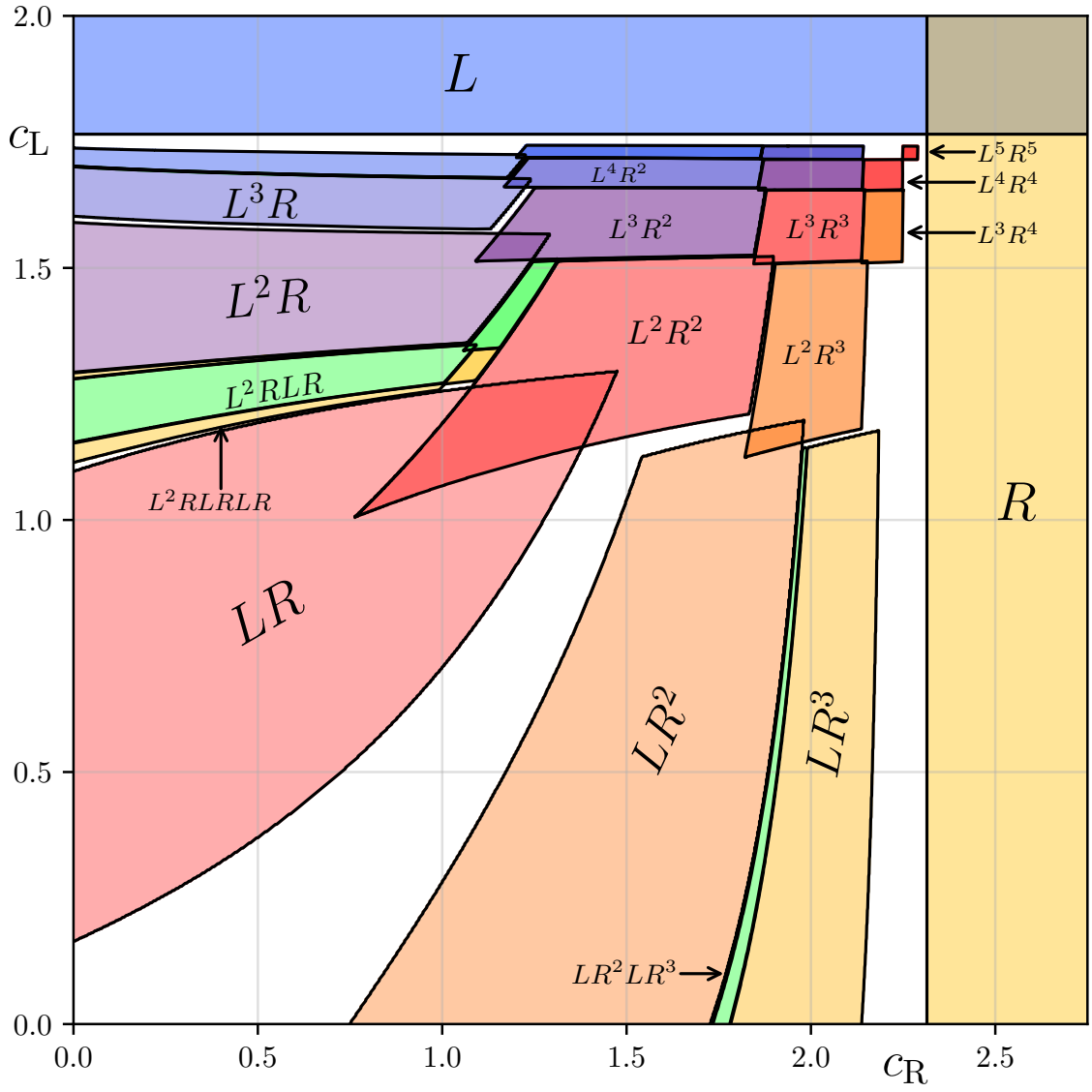

Figure 19.3: A partial bifurcation set of stable root sequences of regular cycling near Podvigina's two-cycle network. Each shaded region is the subset of parameter space for which the labelled root sequence is fragmentarily asymptotically stable; that is, there exists an open set of initial conditions that give rise to trajectories that are asymptotic to the network and with an itinerary that is eventually periodic with that given root sequence. Where two regions overlap, there exist two such open sets, disjoint from each other, each corresponding to one of the root sequences. In this bifurcation set, the contracting eigenvalues at ξ_1 are varied, while all other eigenvalues are fixed. We have calculated only finitely many stability regions, and conjecture that the remaining white space is filled with similar stability regions. All root sequences that are shown here and the links between them are presented in Figure 19.4. Parameter values for these figures are given in Table B.7.1.

For the LR root sequence, we repeat the same process. We begin with the matrix[2]

$$M_{\mathrm{LR}} = M_{\mathrm{R}}M_{\mathrm{L}} = m_{612}m_{561}m_{256}m_{125}m_{412}m_{341}m_{234}m_{123}.$$

We consider the two cyclic permutations of this product that are the transition matrix of full return maps defined on $\mathbf{H}_3^{\mathrm{in},2}$ and $\mathbf{H}_5^{\mathrm{in},2}$. These permutations are

$$m_{123}m_{612}m_{561}m_{256}m_{125}m_{412}m_{341}m_{234} = m_{123}M_{\mathrm{R}}M_{\mathrm{L}}m_{123}^{-1} \tag{19.4}$$

and

$$m_{125}m_{412}m_{341}m_{234}m_{123}m_{612}m_{561}m_{256} = m_{125}M_{\mathrm{L}}M_{\mathrm{R}}m_{125}^{-1} \tag{19.5}$$

The light red region in Figure 19.3, labelled LR, is the set of parameter values for which the LR root sequence is fragmentarily asymptotically stable; that is, there is an open set of initial conditions that give rise to trajectories that are asymptotic to the network and that have itineraries that are eventually periodic with root sequence LR.

In general, for a root sequence $\mathcal{X} = (\mathcal{X}_i)_{i=1}^{k}$ of minimal period k, where $\mathcal{X}_i \in \{L, R\}$ and k is some positive integer, we consider the transition matrix $M_{\mathcal{X}}$ defined by

$$M_{\mathcal{X}} = \prod_{i=0}^{k-1} M_{\mathcal{X}_{k-i}},$$

which is a product of the matrices M_{L} and M_{R}. To determine for which parameter values the root sequence $\mathcal{X}$ is stable, we need only verify Podvigina's conditions for stability for the permutations of this product that are the transition matrices of full return maps defined on $\mathbf{H}_3^{\mathrm{in},2}$ and $\mathbf{H}_5^{\mathrm{in},2}$.

19.1.2 Observations of patterns

In Figure 19.3, we present a partial bifurcation set which consists of 34 stability regions corresponding to different root sequences. In each shaded region, the labelled root sequence is fragmentarily asymptotically stable. Since we can only compute the stability region for finitely many root sequences, this bifurcation set is only partially complete. This bifurcation set has several particularly interesting properties. Many of these properties are similar to the bifurcation set of the Rock–Paper–Scissors–Lizard–Spock network first considered by

[2]We note that, since function composition is applied right-to-left, with the operators written to the left of the operand, the order of the subscripts differs between the terms of the product—which is read right-to-left—and the matrix that represents that order of excursions around each cycle—which is read left-to-right.

Postlethwaite and Rucklidge [PR22], presented in Figure 20.2, and in §20 we compare and contrast these similarities in detail.

First, there is a Farey-like concatenation of certain root sequences. For example, we observe that, in the region of parameter space bounded by the stability boundaries of L and R, there is a region of stability of their concatenation, LR. Between the regions of stability of L and LR, we observe the region of stability of their concatenation, $(L)(LR) = L^2R$. Moreover, between the regions of stability of L and L^2R, we observe their concatenation L^3R. As a final example, between L^2R and LR, we observe L^2RLR.

In general, every stable root sequence that is formed by concatenation appears to concatenate with both of its parent root sequences to form two new stable root sequences. More explicitly, if the stable root sequences $\mathcal{X}$ and $\mathcal{Y}$ concatenate to form $\mathcal{XY}$, then there exists a region of parameter space in which the root sequence $\mathcal{X}^2\mathcal{Y}$ is stable, and a region in which $\mathcal{XY}^2$ is stable.

The second interesting property of this bifurcation set is that the regions of stability of stable root sequences form chains, and it is the root sequences at the beginning of these chains that follow the above Farey-like concatenation. For example, the root sequence LR appears as the first stable root sequence in a sequence of stable root sequences of the form L^nR^n, of which we have computed five. We have also computed the first few root sequences in eight other chains. To aid in understanding the bifurcation set, we present in Figure 19.4 a diagrammatic representation of all stable root sequences in Figure 19.3 and the relationship between these root sequences. Note that many of the stability regions of the root sequences shown in Figure 19.4 are too small to be visible in Figure 19.3. Solid arrows represent the Farey-like concatenation of two root sequences, and dashed arrows represent the transition from one root sequence to the next in the same chain. For all chains of root sequences, we observe that the transition from one root sequence to the next occurs via replacing an LR with L^2R^2, or an RL with R^2L^2—which, up to a cyclic permutation of the root sequence, are equivalent. We also notice that each chain appears to converge to the codimension-two point where both the $\mathcal{C}_{[\mathrm{L}]}$ cycle and the $\mathcal{C}_{[\mathrm{R}]}$ cycle lose stability.

Successive stable roots sequences in a chain have stability regions that overlap. For all parameter values in these overlapping areas, both root sequences are fragmentarily asymptotically stable. Thus, there exists two disjoint open sets of initial conditions, each giving rise to trajectories that are asymptotic to the network and that have an itinerary that is eventually periodic with one of the two given sequences as a root sequence. However, different chains appear to always be disjoint. Moreover, for two stable root sequences $\mathcal{X}$ and $\mathcal{Y}$ that concatenate to form the stable root sequence $\mathcal{XY}$, we can consider the boundary of the chains that begin at the stability regions of $\mathcal{X}$, $\mathcal{Y}$, and $\mathcal{XY}$. We observe that these boundaries are all

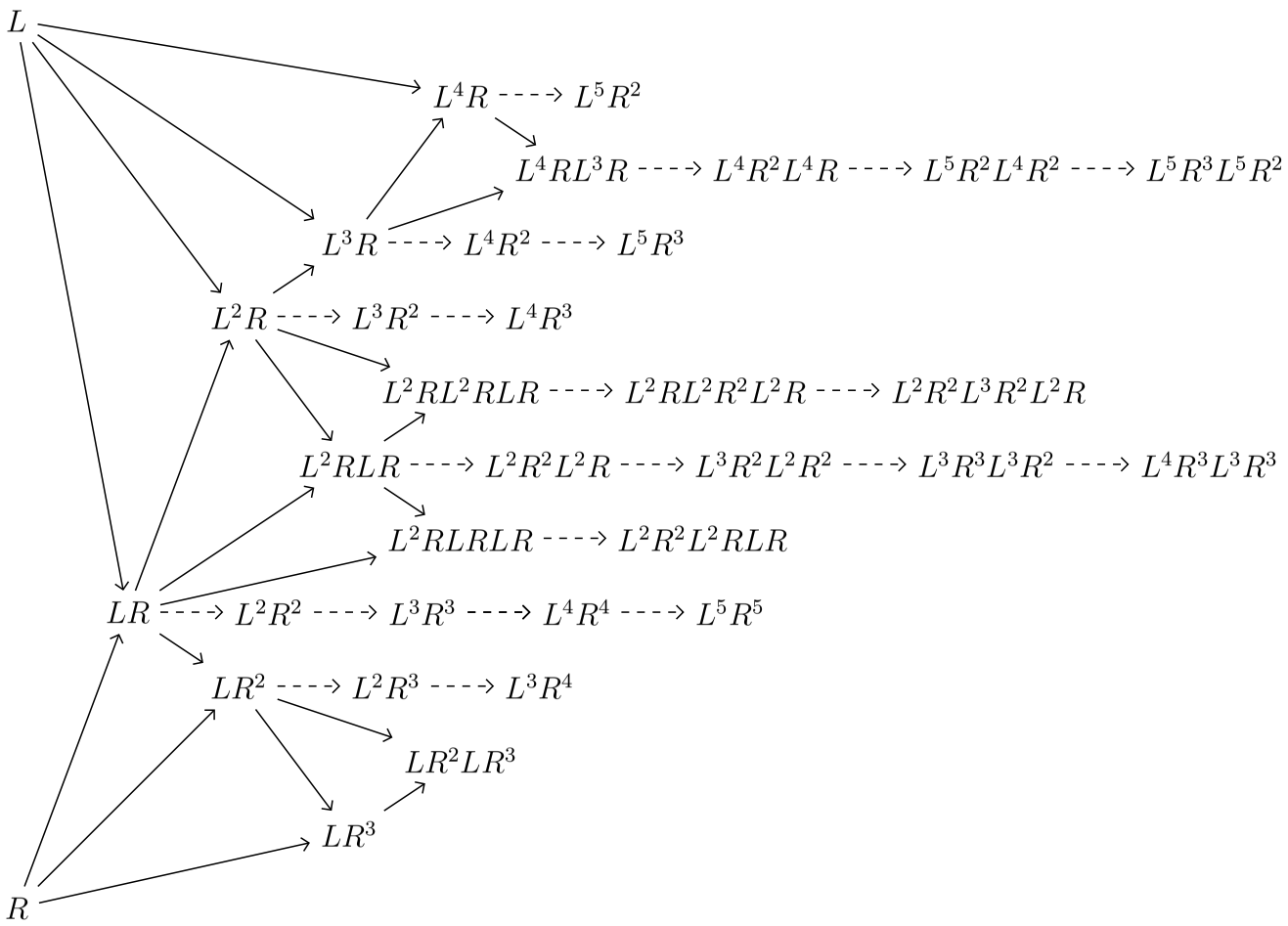

Figure 19.4: A diagram of the root sequences that appear in the bifurcation set in Figure 19.3 and the relationship between them. Solid lines show the Farey-like concatenation between root sequences, and dashed lines link root sequences in the same chain.

disjoint. In a less precise sense, there is always sufficient space in this bifurcation set between two chains for the chain of their concatenation.

Lastly, for every root sequence shown in Figure 19.3, the boundary of the stability region corresponds to a breaking of Podvigina's third condition for stability—that all entries of the eigenvector $w_{\max}$ are non-zero and have the same sign. Applying the consequences of Theorem 14.1, we can therefore conclude that stability loss corresponds to a border-collision bifurcation of the eigenvector $w_{\max}$ of the transition matrix of the return map with domain $\mathbf{H}_2^{\text{in},1}$. For a given stability region, each of its boundaries corresponds to a different permutation of the product that defines the transition matrices failing the admissibility condition.

Lastly, we note that we have not yet found any numerical evidence of irregular cycling near Podvigina's two-cycle network, though we have no reason beyond these numerical results to expect that such irregular cycling does not exist.

19.1.3 Conjectures

These properties allow us to form a series of conjectures about the regular cycling of trajectories near Podvigina's two-cycle network. Our main claim is the following.

Conjecture 19.1. There are infinitely many stable root sequences in the completed bifurcation set, which fill the remaining white space of Figure 19.3.

We expect that the concatenation of each root sequence with both of its parent root sequences continues. This process gives root sequences of the form $L^m R$ and LR^m for all positive integers m. It also gives root sequences of the form $L^{m+1}RL^mR$ and LR^mLR^{m+1} for all positive integers m, and so on, as the concatenation of these root sequences continues.

We make the following additional conjectures about the stability regions of root sequences.

Conjecture 19.2. Each of these root sequences formed through concatenation is the first root sequence in a chain of stable root sequences.

Conjecture 19.3. The stability region of two consecutive root sequences in a chain overlap. However, different chains are disjoint.

Conjecture 19.4. The transition from one root sequence in a chain to the next occurs via an LR being replaced by an L^2R^2

We have as yet no explanation of why this replacement occurs in terms of the dynamics of the flow generated by (19.1).

For root sequences that have the L and R root sequence as a parent, it is straightforward to conjecture the pattern of the resulting chain. In particular, these root sequences have the form $L^m R$ or LR^m, for some positive integer m. We expect the k-th root sequence in the chain that begins at $L^m R$ or LR^m to be of the form $L^{m+k}R^k$ or $L^k R^{m+k}$, respectively. For root sequences which are not of this form, we do not yet know a general way to express all root sequences in a given chain.

19.2 Constructing the projected map

To further our understanding of the bifurcation set in Figure 19.3 and present a method by which we might prove the above conjectures about its structure, we now construct the projected map of Podvigina's two-cycle network.

We follow an identical process to that presented in Chapters III and IV, and consider the induced action of the transition matrices M_{L} and M_{R} on a simplex defined in the negative orthant of $\mathbb{R}^4$. We therefore begin by considering the simplex

$$\left\{ (X_3, X_4, X_5, X_6) \in \mathbb{R}^4_- \middle| \sum_i X_i = -1 \right\}.$$

We can, without ambiguity, represent each point in this simplex by its first three coordinates, and so we define the set

$$S = \left\{ (\vartheta_1, \vartheta_2, \vartheta_3) \in (-1, 0)^3 \mid \vartheta_1 + \vartheta_2 + \vartheta_3 > -1 \right\} \subsetneq (-1, 0)^3.$$

Since the domains of the transition matrices M_{L} and M_{R} are subsets of $\mathbb{R}^4_-$, we adapt the definition of the projection Π to $\Pi\colon \mathbb{R}^4_- \to S$:

$$\begin{aligned} \Pi\colon X = (X_3, X_4, X_5, X_6) \mapsto & \frac{-1}{(1,1,1,1)\cdot X}(e_1 \cdot X, e_2 \cdot X, e_3 \cdot X) \\ & = \frac{-1}{X_3 + X_4 + X_5 + X_6}(X_3, X_4, X_5), \end{aligned}$$

where $e_1 = (1, 0, 0, 0)$, $e_2 = (0, 1, 0, 0)$, and $e_3 = (0, 0, 1, 0)$.

The switching subspace $\Sigma_{\mathrm{s}} \subseteq \mathbf{H}_2^{\mathrm{in},1}$ is defined by

$$\Sigma_{\mathrm{s}} = \left\{ x \in \mathbf{H}_2^{\mathrm{in},1} \mid x_3^{e_{\mathrm{R}}} = x_5^{e_{\mathrm{L}}} \right\}$$

and, therefore, the switching manifold of projected map is

$$\Theta_{\mathrm{S}} = \{(\vartheta_1, \vartheta_2, \vartheta_3) \in S \mid e_{\mathrm{R}}\vartheta_1 = e_{\mathrm{L}}\vartheta_3\}.$$

When analysing return maps defined on $\mathbf{H}_2^{\mathrm{in},1}$, there is, of course, a subset of the cross-section which must be excluded from the domain of definition of the return map, equivalent to Γ_{c} in §9. However, an argument similar to that in §9.4 allows us to conclude that the only subset of S which must be excluded from the domain of the projected map is the codimension-one switching manifold Θ_{S}. Therefore, we define the domains

$$\Theta_{\mathrm{L}} = \{(\vartheta_1, \vartheta_2, \vartheta_3) \in S \mid e_{\mathrm{R}}\vartheta_1 > e_{\mathrm{L}}\vartheta_3\}$$

and

$$\Theta_{\mathrm{R}} = \{(\vartheta_1, \vartheta_2, \vartheta_3) \in S \mid e_{\mathrm{R}}\vartheta_1 < e_{\mathrm{L}}\vartheta_3\}$$

On each of these domains, we define a component of the projected map by

$$f_{\mathrm{L}}(\vartheta_1, \vartheta_2, \vartheta_3) = \Pi(M_{\mathrm{L}}(\vartheta_1, \vartheta_2, \vartheta_3, -1 - \vartheta_1 - \vartheta_2 - \vartheta_3))\colon \Theta_{\mathrm{L}} \to S$$

if $(\vartheta_1, \vartheta_2, \vartheta_3) \in \Theta_{\mathrm{L}}$, and

$$f_{\mathrm{R}}(\vartheta_1, \vartheta_2, \vartheta_3) = \Pi(M_{\mathrm{R}}(\vartheta_1, \vartheta_2, \vartheta_3, -1 - \vartheta_1 - \vartheta_2 - \vartheta_3))\colon \Theta_{\mathrm{R}} \to S$$

if $(\vartheta_1, \vartheta_2, \vartheta_3) \in \Theta_{\mathrm{R}}$. We compose these two maps to define the projected map of Podvigina's two-cycle network $f_{\mathrm{Pod}}\colon \Theta_{\mathrm{L}} \cup \Theta_{\mathrm{R}} \to S$:

$$f_{\mathrm{Pod}} = \begin{cases} f_{\mathrm{L}}(\vartheta) = (f_{\mathrm{L}}^1(\vartheta), f_{\mathrm{L}}^2(\vartheta), f_{\mathrm{L}}^3(\vartheta)), & \text{if } \vartheta \in \Theta_{\mathrm{L}}, \\ f_{\mathrm{R}}(\vartheta) = (f_{\mathrm{R}}^1(\vartheta), f_{\mathrm{R}}^2(\vartheta), f_{\mathrm{R}}^3(\vartheta)), & \text{if } \vartheta \in \Theta_{\mathrm{R}}. \end{cases} \tag{19.6}$$

The expressions for the three components of the map f_{L} are

$$f_{\mathrm{L}}^{(1)}(\vartheta_1, \vartheta_2, \vartheta_3) = \frac{-(\alpha_{11}\vartheta_1 + \alpha_{12}\vartheta_2)}{D_{\mathrm{L}}(\vartheta)},$$

$$f_{\mathrm{L}}^{(2)}(\vartheta_1, \vartheta_2, \vartheta_3) = \frac{-(\alpha_{21}\vartheta_1 + \alpha_{22}\vartheta_2)}{D_{\mathrm{L}}(\vartheta)},$$

$$f_{\mathrm{L}}^{(3)}(\vartheta_1, \vartheta_2, \vartheta_3) = \frac{-(\alpha_{31}\vartheta_1 + \alpha_{32}\vartheta_2 + \vartheta_3)}{D_{\mathrm{L}}(\vartheta)},$$

where the denominator is

$$D_{\mathrm{L}}(\vartheta) = (\alpha_{11}+\alpha_{21}+\alpha_{31}+\alpha_{41}-1)\vartheta_1 + (\alpha_{12}+\alpha_{22}+\alpha_{32}+\alpha_{42}-1)\vartheta_2 + 1.$$

The expressions for the three components of the map f_{R} are

$$f_{\mathrm{R}}^{(1)}(\vartheta_1,\vartheta_2,\vartheta_3) = \frac{(\beta_{12}-1)\vartheta_1 + \beta_{12}\vartheta_2 + (\beta_{12}-\beta_{11})\vartheta_3 - \beta_{12}}{D_{\mathrm{R}}(\vartheta)},$$

$$f_{\mathrm{R}}^{(2)}(\vartheta_1,\vartheta_2,\vartheta_3) = \frac{\beta_{22}\vartheta_1 + (\beta_{22}-1)\vartheta_2 + (\beta_{22}-\beta_{21})\vartheta_3 - \beta_{22}}{D_{\mathrm{R}}(\vartheta)},$$

$$f_{\mathrm{R}}^{(3)}(\vartheta_1,\vartheta_2,\vartheta_3) = \frac{\beta_{32}\vartheta_1 + \beta_{32}\vartheta_2 + (\beta_{32}-\beta_{31})\vartheta_3 - \beta_{32}}{D_{\mathrm{R}}(\vartheta)}.$$

where the denominator is

$$D_{\mathrm{R}}(\vartheta) = \vartheta_1+\vartheta_2+(\beta_{11}+\beta_{21}+\beta_{31}+\beta_{41})\vartheta_3-(\beta_{12}+\beta_{22}+\beta_{32}+\beta_{42})(\vartheta_1+\vartheta_2+\vartheta_3-1).$$

As in Chapter III, fixed points of these maps correspond to eigenvectors of the transition matrices, and the stability and admissibility of certain fixed points corresponds to the stability of the component heteroclinic cycles. Since we have assumed in (19.1) that there are no positive transverse eigenvalues, it is straightforward to generalise the results in Proposition 10.2 and Proposition 11.2, using Theorem 14.1, to prove that all stability conditions of the two component cycles of the network are realised as conditions on $\mathbf{H}_2^{\mathrm{in},1}$, and therefore as bifurcations in the projected map. First, the first two stability conditions in Theorem 6.1—that $\lambda_{\max} \in \mathbb{R}$ and $\lambda_{\max} > 1$—are always realised for all transition matrices, and so correspond to existence and stability conditions, respectively, for the fixed points. If the first two conditions are satisfied, then the third condition, as a consequence of Theorem 6.1 and Theorem 14.1, corresponds to admissibility of the fixed points of f_{Pod}.

The transition matrix M_{L} clearly has eigenvectors $(0,0,1,0)$ and $(0,0,0,1)$, both with eigenvalue 1. These two eigenvectors lie in the X_5- and X_6-axes, and therefore correspond to the $\mathcal{C}_{[\mathrm{R}]}$ cycle. The span of these eigenvectors is the cycle's insignificant subspace. (See §13.1.1 for the definition of the significant subspace and insignificant subspace.) These eigenvectors are analogous to the eigenvectors $(1,0)$ and $(0,1)$ of the transition matrices of the $\mathcal{C}_{[3]}$ and $\mathcal{C}_{[4]}$ cycles observed in Chapter III. In all cases, they are a consequence of the fact that the cycle is contained in a proper subspace of the system. (See [Pod12, § 4.2] for full details.) The transition matrix M_{R} similarly has eigenvectors $(1,0,0,0)$ and $(0,1,0,0)$ for the same

reason. The existence of these eigenvectors immediately provides us with information about the fixed points of the projected map f_{Pod}.

First, we can immediately conclude that $(0,0,0)$ and $(0,0,-1)$ are fixed points of the map f_{L}. Strictly speaking, these fixed points do not lie in the domain of f_{L}. However, as with the fixed points ϑ_3^- and ϑ_4^- of the projected map of the Kirk–Silber network in §10.1, they have significance in the analysis of the projected map, as they represent the insignificant subspace of the $\mathcal{C}_{[\text{L}]}$ cycle.

Second, if the cycle loses stability through a resonance bifurcation—which has the algebraic condition that $\lambda_{\max} = 1$—then, after the bifurcation, $\lambda_{\max}$ remains equal to 1, but the eigenvalue with greatest absolute value has changed, and now $w_{\max} = (0,0,1,0)$ and $w_{\max} = (0,0,0,1)$. Therefore, the fixed points that are the projections of these two vectors are asymptotically stable. Moreover, the fixed points that correspond to the other two eigenvectors of $w_{\max}$ lose stability, as their eigenvalues have values strictly less than 1. Therefore, there is no need to impose any additional conditions on the analysis of the projected map f_{Pod}, as there was in §11 and §12 when studying the $\mathcal{C}_{[XY]}$ cycle, which did not have an insignificant subspace. The corresponding results are true for the component map f_{R}, with fixed points $(-1,0,0)$ and $(0,-1,0)$.

We now consider how regular cycling is realised in the projected map. We consider regular LR cycling as a simple but illustrative example. To determine if this root sequence is stable, we must verify if the transition matrices defined in (19.4) and (19.5) satisfy Podvigina's three conditions for stability in Theorem 6.1. However, Theorem 14.1 tells us we can instead study the matrices $M_{\text{LR}} = M_{\text{R}}M_{\text{L}}$ and $M_{\text{RL}} = M_{\text{L}}M_{\text{R}}$, respectively, and, assuming the first two conditions of Theorem 6.1 are satisfied, verify that their respective eigenvectors $w_{\max}^{(\text{LR})}$ and $w_{\max}^{(\text{RL})}$ are admissible.

If both eigenvectors are admissible, then since,

$$M_{\text{LR}}w_{\max}^{(\text{LR})} = (M_{\text{R}}M_{\text{L}})w_{\max}^{(\text{LR})} = \lambda_{\max}w_{\max}^{(\text{LR})},$$

we observe that

$$M_{\text{RL}}\big(M_{\text{L}}w_{\max}^{(\text{LR})}\big) = (M_{\text{L}}M_{\text{R}})\big(M_{\text{L}}w_{\max}^{(\text{LR})}\big) = M_{\text{L}}(M_{\text{R}}M_{\text{L}})w_{\max}^{(\text{LR})} = \lambda_{\max}\big(M_{\text{L}}w_{\max}^{(\text{LR})}\big).$$

Therefore, $w_{\max}^{(\text{RL})} = M_{\text{L}}w_{\max}^{(\text{LR})}$, and similar reasoning allows us to prove that $w_{\max}^{(\text{LR})} = M_{\text{R}}w_{\max}^{(\text{RL})}$. Thus, the eigenvectors of M_{LR} and M_{RL} are mapped to each other under the action of M_{L} and M_{R}. (See §6.2 for a more general explanation.)

Write $\vartheta^*_{\mathrm{LR}} = \Pi\Big(w^{(\mathrm{LR})}_{\max}\Big)$ and $\vartheta^*_{\mathrm{RL}} = \Pi\Big(w^{(\mathrm{RL})}_{\max}\Big)$. Then

$$f_{\mathrm{Pod}}(\vartheta^*_{\mathrm{LR}}) = f_{\mathrm{L}}(\vartheta^*_{\mathrm{LR}}) = \Pi\big(M_{\mathrm{L}}\big(w^{(\mathrm{LR})}_{\max}\big)\big) = \Pi\big(\lambda_{\max} w^{(\mathrm{RL})}_{\max}\big) = \vartheta^*_{\mathrm{RL}}$$

and, similarly, $f_{\mathrm{Pod}}(\vartheta^*_{\mathrm{RL}}) = f_{\mathrm{R}}(\vartheta^*_{\mathrm{RL}}) = \vartheta^*_{\mathrm{LR}}$. These two points thus form a period-two periodic orbit. Expanding this reasoning allows us to form a more general conclusion: that stable regular cycling is realised in the projected map as a stable and admissible *periodic orbit*. We next consider explicit numerical examples of such periodic orbits.

19.3 Numerical investigation of the projected map of Podvigina's two-cycle network

A direct analysis of the map f_{Pod}—like the analyses presented in §10, §11, and §12—would be incredibly challenging. For example, simply deriving closed-form expressions for fixed points of these maps is equivalent to determining the eigenvectors of M_{L} and M_{R}. These algebraic expressions are difficult to produce, and it was for this reason that Podvigina made certain simplifying assumptions in [Pod23]. Therefore, we present here a numerical investigation of this projected map.

We begin by showing in Figure 19.5 some examples of the action of the projected map. Parameter values and initial conditions vary between each of the four panels. All parameter values that are not c_{L} and c_{R} are identical to those in Figures 19.2 and 19.3. In each of the four panels, points of the same orbit have the same colour.

In Figure 19.5(a), we choose $c_{\mathrm{L}} = 1.9$ and $c_{\mathrm{R}} = 2.5$; that is, we are in the upper right-hand corner of Figure 19.3, where both the $\mathcal{C}_{[\mathrm{L}]}$ cycle and the $\mathcal{C}_{[\mathrm{R}]}$ cycle are stable. We plot three different orbits in Figure 19.5(a) with different initial conditions. First, the orbit represented by the magenta points has initial condition $(-0.08, -0.15, -0.12) \in \Theta_{\mathrm{L}}$, and we see that it is asymptotic to the fixed point $\vartheta^*_{\mathrm{L}} \in \Theta_{\mathrm{L}}$. Next, the orbit represented by the green points has initial condition $(-0.12, -0.02, -0.08) \in \Theta_{\mathrm{R}}$ and it is asymptotic to the fixed point $\vartheta^*_{\mathrm{R}} \in \Theta_{\mathrm{R}}$. The third orbit represented in Figure 19.5(a) is the most interesting: it has initial condition $(-0.11, -0.02, -0.12) \in \Theta_{\mathrm{L}}$, but after one iteration it is mapped into Θ_{R}, and the orbit is asymptotic to $\vartheta^*_{\mathrm{R}} \in \Theta_{\mathrm{R}}$. Therefore, the trajectories near Podvigina's two-cycle network that this orbit in the projected map represents switch from the $\mathcal{C}_{[\mathrm{L}]}$ cycle to the $\mathcal{C}_{[\mathrm{R}]}$ cycle, to which they are then asymptotic. There are also orbits that are mapped from Θ_{R} to Θ_{L}. These orbits correspond to trajectories that switch from the $\mathcal{C}_{[\mathrm{R}]}$ cycle to the $\mathcal{C}_{[\mathrm{L}]}$ cycle. We do not represent these orbits in Figure 19.5(a) for visual clarity. This mapping of orbits between domains of the projected map is analogous to what was observed in §11 and §12 when studying the $\mathcal{C}_{[34]}$ cycle. Both the $\mathcal{C}_{[\mathrm{L}]}$ and the $\mathcal{C}_{[\mathrm{R}]}$ cycle are of type C_4^- when

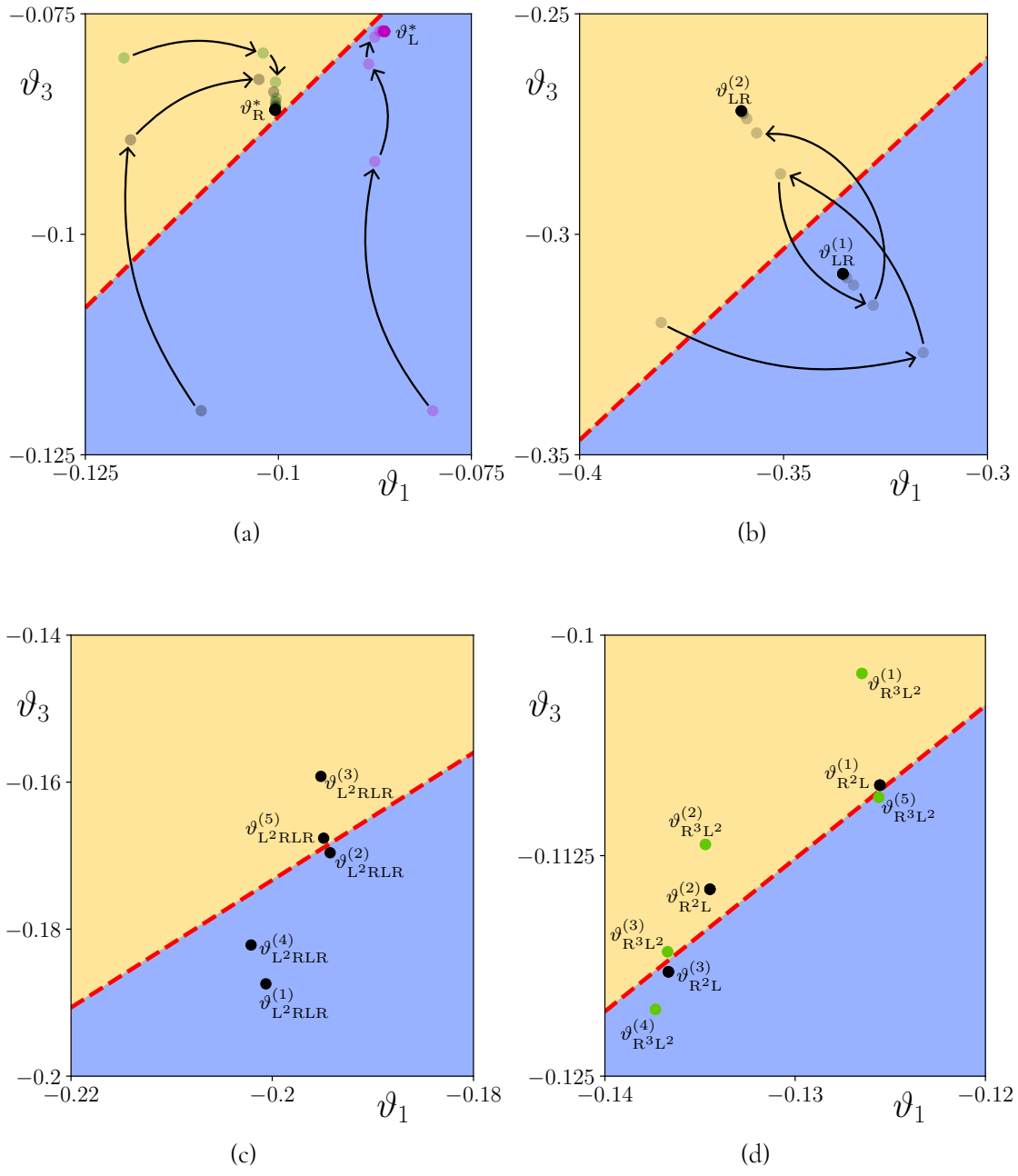

Figure 19.5: Various examples of the action of the projected map f_{Pod} for different parameter values and initial conditions, plotted in the $(\vartheta_1, \vartheta_3)$-plane. We do not represent the ϑ_2-coordinate. In each figure, the dashed red line indicates the switching manifold Θ_{S}, the orange region is Θ_{R}, and the blue region is Θ_{L}. Points from the same orbit are shaded the same colour, and each point is plotted slightly transparent, so that the attracting set appears darker. The attracting set in each case is: (a) the fixed point ϑ^*_{L} or ϑ^*_{R}, (b) a period-two LR-orbit, (c) a period-five L^2RLR-orbit, and (d) a period-three R^2L-orbit or a period-five R^3L^2-orbit. Further details are given in the text. In (a) and (b), we join successive points to indicate the dynamics. In all panels, we label attracting points.

restricted to the four-dimensional subspace that contains them. Therefore, they each have two fixed points that are created in a saddle-node bifurcation. The stable and unstable manifolds of these fixed points divide Θ_{L} and Θ_{R} into sets of points that are eventually mapped into the other domain. However, because an attracting fixed point remains admissible in each domain, there is no sustained switching between these two domains and, therefore, no regular cycling between these cycles.

In Figure 19.5(b), we set $c_{\mathrm{L}} = 0.5$ and $c_{\mathrm{R}} = 0.1$, and so LR cycling is stable. In this region of parameter space, both ϑ_{L}^* and ϑ_{R}^* have lost admissibility in border-collision bifurcations, and so the $\mathcal{C}_{[\mathrm{L}]}$ and $\mathcal{C}_{[\mathrm{R}]}$ cycles are both unstable. We choose initial conditions $(-0.38, -0.3, -0.32) \in \Theta_{\mathrm{R}}$, and observe that the orbit is asymptotic to a periodic orbit. We observe that this orbit is composed of two points: $\vartheta_{\mathrm{LR}}^{(1)} \in \Theta_{\mathrm{L}}$, and $\vartheta_{\mathrm{LR}}^{(2)} \in \Theta_{\mathrm{R}}$, and $f_{\mathrm{L}}\left(\vartheta_{\mathrm{LR}}^{(1)}\right) = \vartheta_{\mathrm{LR}}^{(2)}$ and $f_{\mathrm{R}}\left(\vartheta_{\mathrm{LR}}^{(2)}\right) = \vartheta_{\mathrm{LR}}^{(1)}$. Therefore, the symbol sequence of this orbit is LR, and so this periodic orbit is an admissible LR-orbit. (See §7 for the definition of an admissible $\mathcal{X}$-orbit in a piecewise-smooth dynamical system.) The admissibility and stability of this periodic orbit corresponds to the fragmentary asymptotic stability of the LR root sequence of trajectories asymptotic to the network.

Next, in Figure 19.5(c), we choose $c_{\mathrm{L}} = 1.27$ and $c_{\mathrm{R}} = 0.5$, and initial conditions $(-0.21, -0.02, -0.16) \in \Theta_{\mathrm{R}}$. For these parameter values, the L^2RLR root sequence is stable. We observe that this orbit is asymptotic to a period-five orbit. We have not presented the initial transient dynamics for visual clarity. Three points of this orbit lie in Θ_{L} and two lie in Θ_{R}. Similar to the LR-orbit above, this orbit is therefore a stable and admissible L^2RLR-orbit that corresponds to the L^2RLR root sequence. In Figure 19.5(c), we can see two points that lie quite close to the switching manifold. If we were to increase c_{L}, we would observe the upper of these two points cross Θ_{S} from Θ_{R} into Θ_{L}, in which case the periodic orbit would lose admissibility. If we were to decrease c_{L}, we would observe the lower point cross Θ_{S} from Θ_{L} into Θ_{R}. Again, the periodic orbit would lose admissibility. In both cases, there would be a border-collision bifurcation of the periodic orbit, corresponding to a certain cyclic permutation of the product that defines the matrix $M_{\mathcal{X}}$ no longer satisfying Podvigina's third condition for stability. In the former case, this product corresponds to the transition matrix of the return map with domain $\mathbf{H}_5^{\mathrm{in},2}$, and in the latter case this return map has domain $\mathbf{H}_3^{\mathrm{in},2}$. That both these periodic points are close to the switching manifold is simply due to how thin the stability region of the L^2RLR root sequence is in Figure 19.3 along the c_{L}-axis.

Lastly, we consider Figure 19.5(d). We set $c_{\mathrm{L}} = 1.165$ and $c_{\mathrm{R}} = 1.9$, which in Figure 19.3 is located in the region of parameter space where both the $\mathcal{X} = LR^2$ and $\mathcal{Y} = L^2R^3$ root sequences are stable. In this panel, we plot two different periodic orbits, but not any initial

transient dynamics. We observe that the periodic orbit represented by the black points is of period-three, and has one point that lies in Θ_{L} and two points that lie in Θ_{R}. The periodic orbit represented by the green points has two points in Θ_{L} and three points in Θ_{R}. With a similar explanation to that in the proceeding paragraphs, the black points form an admissible LR^2-orbit, and the green points form an admissible L^2R^3-orbit. We notice that there are four points in total that are close to the switching manifold. Similar to the L^2RLR-orbit, if we were to vary either c_{L} or c_{R}, we would observe a border-collision bifurcation and a loss of admissibility of the periodic orbit. If the periodic point that crossed Θ_{S} began in Θ_{R}, then the permutation of the product that defines $M_{\mathcal{X}}$ or $M_{\mathcal{Y}}$ that no longer satisfies Podvigina's third stability condition would have domain $\mathbf{H}_5^{\mathrm{in},2}$, and vice-versa for Θ_{L} and $\mathbf{H}_3^{\mathrm{in},2}$. This region of parameter space where the root sequences are bistable is quite small in the direction of both c_{L} and c_{R}, and so we are close to all four edges that define this region, two from each root sequence. Therefore, we observe that we are close to the parameter values of four different border-collision bifurcations, again, two from each periodic orbit.

In general, if we were to continue this process, we would observe a stable and admissible $\mathcal{X}$-orbit for each of the root sequences we have shown in Figure 19.3. We expect that bifurcations of fixed points and periodic orbits of f_{Pod} would occur at the same parameter values as stability boundaries of stable regular cycling near the network. In piecewise-smooth dynamical systems theory, a region of parameter space in which a periodic orbit is admissible and stable is referred to as a *mode-locking region*. There have been many studies of the bifurcation structure of periodic orbits in piecewise-smooth dynamical systems. These have mostly focussed on continuous piecewise-linear maps, where the so-called "strings-of-sausages" [YH87] emerge, and which we discuss further when considering the Rock–Paper–Scissors–Lizard–Spock network below in §20. The structure in Figure 19.3 bears some resemblance to the bifurcation sets presented in [Sim20], which concerns two-dimensional, discontinuous piecewise-linear maps. The map in (19.6) is certainly not linear, though as explained in §13.3, it is a rational linear transformation, and as we show next it is generically discontinuous.

Therefore, to prove the existence of the bifurcation structure we observe in Figure 19.3 and also prove the conjectures we make in §19.1.3 concerning how the root sequences relate to each other, we would need to establish the bifurcation structure of periodic orbits of f_{Pod}. The required analysis, however, would require some significant advances in the theory of piecewise-smooth dynamical systems, since these structures have not been studied in detail for maps that are not piecewise-linear. Moreover, the root sequences of regular cycling in Figure 19.3 do not correspond to any of the various families of symbol sequences studied in the literature, such as *rotational symbol sequences* [Sim16]. However, the work of Dullin, Meiss, and

Sterling [DMS05] may provide an appropriate starting point, as it considers symbol sequences of a more general type. The root sequences at the base of each chain formed by the Farey-like concatenation are the same as those studied in [GAK17], which considered discontinuous circle maps. The mode-locking regions of these discontinuous circle maps, however, do not form chains. Therefore, a clear first step needed to analyse the structure of regular cycling near Podvigina's two-cycle network is to understand the structure of the symbol sequences that form its stable root sequences. This understanding would then allow us to study the bifurcation structure of these periodic orbits, and prove the existence of the structure we conjecture completes the bifurcation set in Figure 19.3.

19.4 Continuity of the projected map

We lastly make a brief comment on the continuity of f_{Pod}, to compare with the results we identified in Chapter V. We find that generically, for a point $\vartheta_{\text{s}} = \left(\vartheta_1, \vartheta_2, \dfrac{e_{\text{L}}}{e_{\text{R}}}\vartheta_1\right) \in \Theta_{\text{S}}$,

$$f_{\text{L}}(\vartheta_{\text{s}}) \neq f_{\text{R}}(\vartheta_{\text{s}}).$$

Therefore, the projected map f_{Pod} is discontinuous. The actual expressions for these terms are quite long, and so we give them in §B.3.

We note that, restricted to the (x_2, x_3, x_5)-subspace, the dynamics of the system is equivalent to that of the Kirk–Silber network restricted to the (x_2, x_3, x_4)-subspace, a representation of which is presented in Figure 16.2(a). Thus, we suspect that a simple extension to the argument presented in in Chapter V explains the origin of this discontinuity, again as the effect of a separatrix near the network resulting in a discontinuity of the completed full return map, in the limit as the network is approached.

§20 The Rock-Paper-Scissors-Lizard-Spock network

We now consider the Rock–Paper–Scissors–Lizard–Spock network in $\mathbb{R}^5$, a comprehensive study of which is presented in [PR22]. This network is composed of five equilibria, $\xi_1, \ldots, \xi_5$, which we again assume are at unit distance from the origin in the positive orthant on each of the five coordinate axes. A diagrammatic representation of this network is shown in Figure 20.1. Like Postlethwaite and Rucklidge [PR22], we assume that all equilibria of the network lie in the same group orbit, where the symmetry is an order-5 cyclic permutation of the

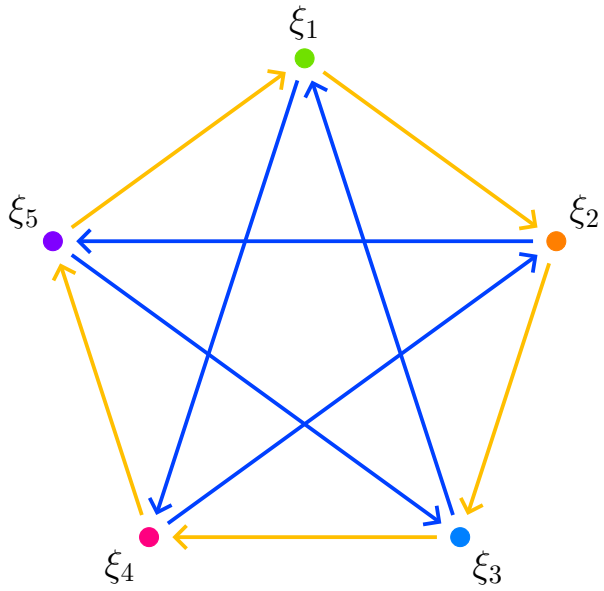

Figure 20.1: A diagrammatic representation of the Rock–Paper–Scissors–Lizard–Spock network [PR22]. The directed edges coloured amber represent the heteroclinic orbits of class A, which form the $\mathcal{C}_{[A]}$ cycle, and the blue directed edges represent the heteroclinic orbits of class B, which from the $\mathcal{C}_{[B]}$ cycle. An example of a $\mathcal{C}_{[T]}$ cycle, of which there are five in total, is the length-three cycle $\xi_1 \to \xi_2 \to \xi_3 \to \xi_1$. An example of the length-four $\mathcal{C}_{[Q]}$ cycle is $\xi_1 \to \xi_2 \to \xi_5 \to \xi_3 \to \xi_1$.

coordinates axes:

$$(x_1, x_2, x_3, x_4, x_5) \mapsto (x_2, x_3, x_4, x_5, x_1) \tag{20.1}$$

This symmetry simplifies the analysis of the behaviour of trajectories near this network.

Along with the five equilibria, the network contains ten heteroclinic orbits, which are of one of two different classes. The first, known as class A orbits, connect ξ_j to ξ_{j+1} for all $1 \leq j \leq 5$, and so lie in the (x_j, x_{j+1})-plane, where all operations are taken modulo 5. The second, known as class B orbits, connect ξ_j to ξ_{j+3} for all $1 \leq j \leq 5$, and so lie in the (x_j, x_{j+3})-plane. (Note that the labelling of orbits as being of class A or B is entirely unrelated to the classification of heteroclinic cycles as type A, B, or C [CKM97, KM04], and how this classification is extended to heteroclinic orbits. In fact, all ten of these orbits are of type C in the sense of Krupa and Melbourne [KM04, Definition 5.4]. To avoid confusion, we refer to the orbits as being of *class* A or B here, not as *type* A or B, as is used by Postlethwaite and Rucklidge [PR22].) The orbits of class A and B form two different cycles:[3] $\mathcal{C}_{[A]} = \xi_1 \to \xi_2 \to \xi_3 \to \xi_4 \to \xi_5 \to \xi_1$ and $\mathcal{C}_{[B]} = \xi_1 \to \xi_4 \to \xi_2 \to \xi_5 \to \xi_3 \to \xi_1$. The network is

[3] Both of which are type C in the sense of Krupa and Melbourne [KM04]

then $\mathcal{N}_{\text{RPSLS}} = \mathcal{C}_{[\text{A}]} \cup \mathcal{C}_{[\text{B}]}$.

We note that this network contains other subcycles. For example, there is the cycle $\mathcal{C} = \xi_1 \to \xi_2 \to \xi_3 \to \xi_1$, which is equivalent to the Guckenheimer–Holmes cycle without the additional $\mathbb{Z}_3$-symmetry. There are five subcycles equivalent to the Guckenheimer–Holmes cycle, found by applying powers of the symmetry in (20.1). We label all five of these cycles as $\mathcal{C}_{[\text{T}]}$. There are also five cycles that can be found by applying powers of the symmetry in (20.1) to the cycle $\xi_1 \to \xi_2 \to \xi_5 \to \xi_3 \to \xi_1$. We label these five equivalent cycles $\mathcal{C}_{[\text{Q}]}$.

This network also contains five equivalent Δ-clique structures, formed, for example, by the orbits $\xi_1 \to \xi_2$ and $\xi_1 \to \xi_4 \to \xi_2$, and those related by the symmetry (20.1). In the (x_1, x_2, x_4)-subspace, there is a continuum of orbits $\xi_1 \to \xi_2$, only one of which is contained in the (x_1, x_2)-plane. As before, we consider only this orbit to be part of the network, and similarly for the other four Δ-cliques.

Truncated at third-degree, the general form of the equations (3.2) that contains a Rock–Paper–Scissors–Lizard–Spock network is

$$\begin{aligned}
\dot{x}_1 &= x_1\Big(1 - \|x\|_2^2 - c_{\text{A}}x_2^2 - c_{\text{B}}x_4^2 + e_{\text{A}}x_5^2 + e_{\text{B}}x_3^2\Big),\\
\dot{x}_2 &= x_2\Big(1 - \|x\|_2^2 - c_{\text{A}}x_3^2 - c_{\text{B}}x_5^2 + e_{\text{A}}x_1^2 + e_{\text{B}}x_4^2\Big),\\
\dot{x}_3 &= x_3\Big(1 - \|x\|_2^2 - c_{\text{A}}x_4^2 - c_{\text{B}}x_1^2 + e_{\text{A}}x_2^2 + e_{\text{B}}x_5^2\Big),\\
\dot{x}_4 &= x_4\Big(1 - \|x\|_2^2 - c_{\text{A}}x_5^2 - c_{\text{B}}x_2^2 + e_{\text{A}}x_3^2 + e_{\text{B}}x_1^2\Big),\\
\dot{x}_5 &= x_5\Big(1 - \|x\|_2^2 - c_{\text{A}}x_1^2 - c_{\text{B}}x_3^2 + e_{\text{A}}x_4^2 + e_{\text{B}}x_2^2\Big),
\end{aligned}$$

where $c_{\text{A}}, c_{\text{B}}, e_{\text{A}}, e_{\text{B}}$ are positive real constants.

Every equilibrium in this network has two outgoing heteroclinic orbits within the network, one of each class, and therefore every equilibrium is a switching equilibrium. A significant difference between this network and the other networks we have considered until now is that the switching equilibria have two incoming heteroclinic orbits within the network, again, one of each class. This difference complicates the construction of return maps near the network, and in turn complicates the construction of the projected map.

20.1 Stability of regular cycling

A key realisation of Postlethwaite and Rucklidge [PR22] is that a trajectory asymptotic to the network makes a series of transitions between successive equilibria that either follow close

to an orbit of class A or an orbit of class B. Therefore, we refer to these transitions as also being either of class A or class B. In particular, if a trajectory leaves a small neighbourhood of ξ_j and next visits ξ_k, then if $k - j \equiv 1 \mod 5$, we say the transition is of class A, and if $k - j \equiv 3 \mod 5$, we say the transition is of class B. Moreover, since all equilibria of the network are equivalent under the symmetry (20.1), a trajectory's itinerary is more meaningfully defined, not by the sequence of equilibria it visits, but by the sequence of transitions it makes, which is then a sequence of As and Bs, rather than the indices $1, \ldots, 5$. We do not give explicit definitions of such an itinerary, as these can be readily found in [PR22, §4, pp. 1713–1714]. Postlethwaite and Rucklidge [PR22] present a bifurcation set of stable root sequences composed of As and Bs; we present a similar bifurcation set in Figure 20.2, calculated similarly to the bifurcation set of Podvigina's two-cycle network in Figure 19.3. To calculate this bifurcation set, four transition matrices are needed. See §20.2 below for the derivation and expressions of these matrices.

Like the bifurcation set of Podvigina's two-cycle network, this bifurcation set has many interesting features. These observations were all first made by Postlethwaite and Rucklidge [PR22], and see therein for further observations and conjectures.

First, we note that there are no parameter values for which more than one of the cycles $\mathcal{C}_{[A]}$, $\mathcal{C}_{[B]}$, and $\mathcal{C}_{[T]}$ is stable. The cycle $\mathcal{C}_{[Q]}$ does not appear to be stable for any parameter values. Next, we observe many regions of stability of root sequences that do not correspond to subcycles of the network. A series of these root sequences emerge from the boundary of the stability region of the A root sequence. Some of these root sequences have the form T^nD or TD^n, and can be found in the region of parameter space bounded in part by the stability regions of $T \equiv AAB$ and $D \equiv BB$. Thus, these root sequences are all formed by a Farey-like concatenation. These root sequences are similar to the L^nR and LR^n root sequences in Figure 19.3. Between the stability regions of these root sequences are the stability regions of their concatenations, such as $TDTD^2$, T^2DTD, and T^3DT^2D. Again, this process repeats, with every root sequence being observed to concatenate with both of its parent root sequences, forming, for example, T^2DT^2DTD and T^2DTDTD.

Root sequences that are not of the form TD^n for positive integers n appear to be the first stable sequence in a chain of stable sequences. In contrast to Podvigina's two-cycle network, there is overlap of different chains of stable root sequences regions. The successive stability regions in a given chain do not overlap, like they do in the case of Podvigina's two-cycle network. However, their boundaries meet at a codimension-two point, known as a *shrinking point* [SM09]. (We note that many successive regions in the chains in Figure 20.2 appear to have a small gap between them, which is simply a consequence of the numerical discretisation of the bifurcation set.) These chains—which are referred to as chains of mode-locking regions

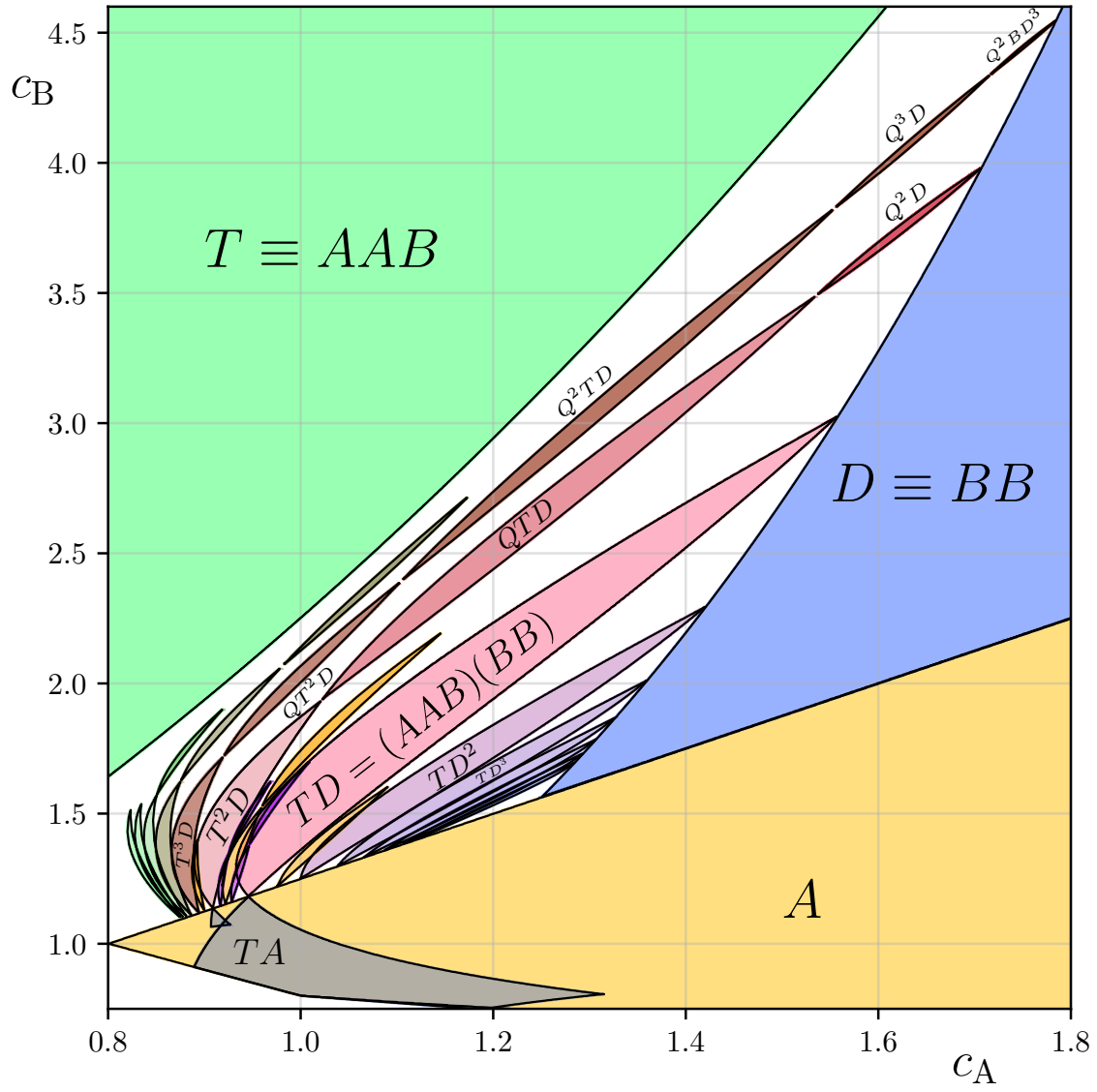

Figure 20.2: A partial bifurcation set of stable root sequences of regular cycling near the Rock–Paper–Scissors–Lizard–Spock network. Each shaded region is the subset of parameter space for which the labelled root sequence is fragmentarily asymptotically stable; that is, there exists an open set of initial conditions that give rise to trajectories that are asymptotic to the network and with an itinerary that is eventually periodic with the labelled root sequence. Where two regions overlap, there exist two such open sets, disjoint from each other, each corresponding to one of the root sequences. In this bifurcation set, the contracting eigenvalues c_A and c_B are varied, while the two other eigenvalues are fixed at $e_A = 1$ and $e_B = 0.8$. We have calculated only finitely many stability regions, and, like Postlethwaite and Rucklidge [PR22], conjecture the remaining white space is filled with further chains of stability regions of stable root sequences.

in literature concerning piecewise-smooth dynamical systems [Sim16]—are known as strings-of-sausages [YH87] when they take this particular form. Strings-of-sausages are typical in continuous piecewise-linear maps, because these maps admit periodic orbits contained in invariant polygons [Sim17]. As observed by Postlethwaite and Rucklidge, all boundaries of stability regions in these strings-of-sausages correspond to the eigenvector $w_{\max}$ of a certain transition matrix having a 0 in its third component.

These chains of stability regions of root sequences all appear to terminate on the boundary of the stability region of the $D \equiv BB$ root sequence. The TD^n root sequences themselves have a shrinking point that lies on this boundary, and for this reason they do not appear to form a string-of-sausages-like chain. The transition from one root sequence to the next in a chain corresponds to a replacement of an A by a BB. For example, the stability region of $T^2D = (AAB)(AAB)(BB)$ meets at a shrinking point the stability region of $QTD = (ABBB)(AAB)(BB)$. This change of $A \to BB$ occurs at all shrinking points that have been calculated. We highlight that an A and a BB form the two "routes" around a Δ-clique. Therefore, this change represents a change in a trajectory's path from a small neighbourhood of one equilibrium to another equilibrium, without the equilibria changing. We lastly observe that the cycle $\mathcal{C}_{[Q]}$, which does not appear to be stable for any parameter values in Figure 20.2, corresponds to the root sequence $Q \equiv ABBB$, which is obtained from $T \equiv AAB$ after the transition $A \to BB$.

As with Podvigina's two-cycle network, we expect that the projected map we construct below will be able to explain the intricate patterns that exist in the bifurcation set, though, again, certain advancements in the theory of piecewise-smooth dynamical systems are likely to be required.

20.2 Return maps and transitions matrices of the network

We first review the construction of the return map near the Rock–Paper–Scissors–Lizard–Spock network, as understanding this process is necessary to understand the construction of its projected map. This process was originally presented by Postlethwaite and Rucklidge in [PR22], and the presentation below is adapted from [PR22]. We give only as much detail as needed to understand how the projected map is constructed, and so do not give expressions for every step in the process. Full details can be found in [PR22, §4.1–5.2.4], though we employ different notation here.

Since all equilibria of $\mathcal{N}_{\text{RPSLS}}$ are equivalent under the symmetry (20.1), we consider an arbitrary equilibrium ξ. The flow linearised about ξ is defined by two expanding coordinates x_{A}^{e} and x_{B}^{e}, which grow at the rate of e_{A} and e_{B} respectively, two contracting coordinates x_{A}^{c} and x_{B}^{c}, which decay at the rate of $-c_{\text{A}}$ and $-c_{\text{B}}$ respectively, and a radial coordinate. As a

consequence of the invariant sphere theorem [Fie96], we ignore the radial coordinate.

We define an incoming cross-section using polar coordinates (r, θ) defined in terms of the contracting coordinates, such that $r^2 = (x_{\mathrm{A}}^{\mathrm{c}})^2 + (x_{\mathrm{B}}^{\mathrm{c}})^2$ and

$$\tan\theta = \frac{x_{\mathrm{B}}^{\mathrm{c}}}{x_{\mathrm{A}}^{\mathrm{c}}}.$$

From here, we use these polar coordinates, and so for simplicity we remove the e superscript from the expanding coordinates, and write $x_{\mathrm{A}} \equiv x_{\mathrm{A}}^{\mathrm{e}}$ and $x_{\mathrm{B}} \equiv x_{\mathrm{B}}^{\mathrm{e}}$. We refer to θ as the contracting angle. The incoming cross-section is then

$$\mathbf{H}^{\mathrm{in}} = \left\{(x_{\mathrm{A}}, x_{\mathrm{B}}, r, \theta) \mid r = h, 0 < x_{\mathrm{A}}, x_{\mathrm{B}} < h, 0 \leq \theta \leq \frac{\pi}{2}\right\}.$$

Since the radius r is fixed, it can be ignored in our calculations. Therefore, in an abuse of notation, we present only the three coordinates on $\mathbf{H}^{\mathrm{in}}$ that are relevant to our analysis, which are $(x_{\mathrm{A}}, x_{\mathrm{B}}, \theta)$.

For a given initial condition $x_0 = (x_{\mathrm{A}}, x_{\mathrm{B}}, \theta)$, if $(1-\epsilon)x_{\mathrm{A}}^{e_{\mathrm{B}}} > x_{\mathrm{B}}^{e_{\mathrm{A}}}$, then the trajectory beginning at x_0 leaves a small neighbourhood of ξ along a class A orbit, and therefore makes a class A transition. If $(1-\epsilon)x_{\mathrm{B}}^{e_{\mathrm{A}}} > x_{\mathrm{A}}^{e_{\mathrm{B}}}$, then the trajectory makes a class B transition. Postlethwaite and Rucklidge [PR22] calculate two different basic maps, one for each class of transition:

$$\Phi_{\mathrm{A}}\colon \mathbf{H}^{\mathrm{in}} \to \mathbf{H}^{\mathrm{in}}, \qquad \Phi_{\mathrm{B}}\colon \mathbf{H}^{\mathrm{in}} \to \mathbf{H}^{\mathrm{in}},$$

$$\Phi_{\mathrm{A}}\colon \begin{pmatrix} x_{\mathrm{A}} \\ x_{\mathrm{B}} \\ \theta \end{pmatrix} \mapsto \begin{pmatrix} D_{\mathrm{A}} \cos\theta x_{\mathrm{A}}^{\frac{c_{\mathrm{B}}}{e_{\mathrm{A}}}} \\ D_{\mathrm{B}} \sin\theta x_{\mathrm{A}}^{\frac{c_{\mathrm{A}}}{e_{\mathrm{A}}}} \\ \frac{\pi}{2} - D_\theta x_{\mathrm{B}} x_{\mathrm{A}}^{-\frac{e_{\mathrm{B}}}{e_{\mathrm{A}}}} \end{pmatrix}, \qquad \Phi_{\mathrm{B}}\colon \begin{pmatrix} x_{\mathrm{A}} \\ x_{\mathrm{B}} \\ \theta \end{pmatrix} \mapsto \begin{pmatrix} C_{\mathrm{A}} \sin\theta x_{\mathrm{B}}^{\frac{c_{\mathrm{A}}}{e_{\mathrm{B}}}} \\ C_{\mathrm{B}} x_{\mathrm{A}} x_{\mathrm{B}}^{-\frac{e_{\mathrm{A}}}{e_{\mathrm{B}}}} \\ C_\theta \cos\theta x_{\mathrm{B}}^{\frac{c_{\mathrm{B}}}{e_{\mathrm{B}}}} \end{pmatrix},$$

where $C_{\mathrm{A}}, C_{\mathrm{B}}, C_\theta, D_{\mathrm{A}}, D_{\mathrm{B}}$, and D_θ are $\mathcal{O}(1)$ positive constants. Technically, the domain of definition of each map is restricted to a subset of $\mathbf{H}^{\mathrm{in}}$, which we could label Γ_{A} and Γ_{B}, that is defined by the relative sizes of e_{A} and e_{B}. There is also an excluded subset Γ_{c}. However, to lighten the notational burden in what follows, we do not make these domains of definition explicit.

These maps cannot be expressed as transition matrices, due to the trigonometric terms. However, as Postlethwaite and Rucklidge [PR22] observed, if the previous transition is of class A, then the angle θ is close to $\frac{\pi}{2}$, and if the previous transition is of class B, then θ is

small. We thus define $\varphi \coloneqq \frac{\pi}{2} - \theta$, and define two cross-sections that are subsets of $\mathbf{H}^{\text{in}}$:

$$\mathbf{H}^{\text{in}}_{\theta} = \{(x_{\text{A}}, x_{\text{B}}, \theta) \mid 0 < x_{\text{A}}, x_{\text{B}} < h \text{ and } 0 \leq \theta < h\} \subseteq \mathbf{H}^{\text{in}}$$

and

$$\mathbf{H}^{\text{in}}_{\varphi} = \{(x_{\text{A}}, x_{\text{B}}, \varphi) \mid 0 < x_{\text{A}}, x_{\text{B}} < h \text{ and } 0 \leq \varphi < h\} \subseteq \mathbf{H}^{\text{in}}.$$

Substituting leading order Taylor expansions of the trigonometric terms in Φ_{A} and Φ_{B} for small θ and φ, Postlethwaite and Rucklidge [PR22] define four different basic maps, each of which depends both on the previous and current class of transition. These maps are, to leading order,

$$\Phi_{\text{A}\to\text{A}} \colon \mathbf{H}^{\text{in}}_{\varphi} \to \mathbf{H}^{\text{in}}_{\varphi}, \qquad \Phi_{\text{A}\to\text{B}} \colon \mathbf{H}^{\text{in}}_{\varphi} \to \mathbf{H}^{\text{in}}_{\theta},$$

$$\Phi_{\text{A}\to\text{A}} \colon \begin{pmatrix} x_{\text{A}} \\ x_{\text{B}} \\ \varphi \end{pmatrix} \mapsto \begin{pmatrix} D_{\text{A}}\varphi x_{\text{A}}^{\frac{c_{\text{B}}}{e_{\text{A}}}} \\ D_{\text{B}} x_{\text{A}}^{\frac{c_{\text{A}}}{e_{\text{A}}}} \\ D_{\theta} x_{\text{B}} x_{\text{A}}^{-\frac{e_{\text{B}}}{e_{\text{A}}}} \end{pmatrix}, \qquad \Phi_{\text{A}\to\text{B}} \colon \begin{pmatrix} x_{\text{A}} \\ x_{\text{B}} \\ \varphi \end{pmatrix} \mapsto \begin{pmatrix} C_{\text{A}} x_{\text{B}}^{\frac{c_{\text{A}}}{e_{\text{B}}}} \\ C_{\text{B}} x_{\text{A}} x_{\text{B}}^{-\frac{e_{\text{A}}}{e_{\text{B}}}} \\ C_{\theta}\varphi x_{\text{B}}^{\frac{c_{\text{B}}}{c_{\text{A}}}} \end{pmatrix},$$

$$\Phi_{\text{B}\to\text{A}} \colon \mathbf{H}^{\text{in}}_{\theta} \to \mathbf{H}^{\text{in}}_{\varphi}, \qquad \Phi_{\text{B}\to\text{B}} \colon \mathbf{H}^{\text{in}}_{\theta} \to \mathbf{H}^{\text{in}}_{\theta},$$

$$\Phi_{\text{B}\to\text{A}} \colon \begin{pmatrix} x_{\text{A}} \\ x_{\text{B}} \\ \theta \end{pmatrix} \mapsto \begin{pmatrix} D_{\text{A}} x_{\text{A}}^{\frac{c_{\text{B}}}{e_{\text{A}}}} \\ D_{\text{B}}\theta x_{\text{A}}^{\frac{c_{\text{A}}}{e_{\text{A}}}} \\ D_{\theta} x_{\text{B}} x_{\text{A}}^{-\frac{e_{\text{B}}}{e_{\text{A}}}} \end{pmatrix}, \qquad \Phi_{\text{B}\to\text{B}} \colon \begin{pmatrix} x_{\text{A}} \\ x_{\text{B}} \\ \theta \end{pmatrix} \mapsto \begin{pmatrix} C_{\text{A}}\theta x_{\text{B}}^{\frac{c_{\text{A}}}{e_{\text{B}}}} \\ C_{\text{B}} x_{\text{A}} x_{\text{B}}^{-\frac{e_{\text{A}}}{e_{\text{B}}}} \\ C_{\theta} x_{\text{B}}^{\frac{c_{\text{B}}}{e_{\text{B}}}} \end{pmatrix}.$$

In each of these maps, the domain of the map depends on the class of the *previous* transition, while the codomain depends on the *current* transition. Again, the domain of definition of each map is technically a subset of each cross-section, with an excluded cusp removed. We emphasise that when the previous and current class of transition are identical, then the relevant $\Phi_{X\to X}$ maps between the same cross-section, and if they differ, $\Phi_{X\to Y}$ maps between different cross-sections. Recognising that there is a difference between these cross-sections is important for the construction of the projected map, which is why we present the results here as we have done so, more explicitly than in [PR22]. (Note that these expressions correct minor typographical errors made by Postlethwaite and Rucklidge [PR22].)

These maps can be written as transition matrices. To do so, we recall that the transition matrix represents the map written in logarithmic coordinates, and so we define $X_{\text{A}} \coloneqq \log x_{\text{A}} - \log h$, $X_{\text{B}} \coloneqq \log x_{\text{B}} - \log h$, $\Theta \coloneqq \log\theta - \log h$, and $\Phi \coloneqq \log\varphi - \log h$. (The

$-\log h$ term is a rescaling by h). The transition matrices of $\Phi_{\mathrm{A}\to\mathrm{A}}$ and $\Phi_{\mathrm{A}\to\mathrm{B}}$ therefore act on a point $(X_{\mathrm{A}}, X_{\mathrm{B}}, \Phi)$, and so we define the set

$$V_\Phi = \left\{(X_{\mathrm{A}}, X_{\mathrm{B}}, \Phi) \in \mathbb{R}^3_-\right\}.$$

For the transition matrices of $\Phi_{\mathrm{B}\to\mathrm{A}}$ and $\Phi_{\mathrm{B}\to\mathrm{B}}$, we define the set

$$V_\Theta = \left\{(X_{\mathrm{A}}, X_{\mathrm{B}}, \Theta) \in \mathbb{R}^3_-\right\}.$$

Although both of these sets are equivalent to $\mathbb{R}^3_-$, they represent different subsets of the original phase space: in particular, they represent the set of points near ξ that previously made a class A or B transition. We then have the four transition matrices

$$M_{\mathrm{A}\to\mathrm{A}}\colon V_\Phi \to V_\Phi, \qquad M_{\mathrm{A}\to\mathrm{B}}\colon V_\Phi \to V_\Theta,$$

$$M_{\mathrm{A}\to\mathrm{A}} = \begin{pmatrix} \frac{c_{\mathrm{B}}}{e_{\mathrm{A}}} & 0 & 1 \\ \frac{c_{\mathrm{A}}}{e_{\mathrm{A}}} & 0 & 0 \\ -\frac{e_{\mathrm{B}}}{e_{\mathrm{A}}} & 1 & 0 \end{pmatrix}, \qquad M_{\mathrm{A}\to\mathrm{B}} = \begin{pmatrix} 0 & \frac{c_{\mathrm{A}}}{e_{\mathrm{B}}} & 0 \\ 1 & -\frac{e_{\mathrm{A}}}{e_{\mathrm{B}}} & 0 \\ 0 & \frac{c_{\mathrm{B}}}{e_{\mathrm{B}}} & 1 \end{pmatrix},$$

$$M_{\mathrm{B}\to\mathrm{A}}\colon V_\Theta \to V_\Phi, \qquad M_{\mathrm{B}\to\mathrm{B}}\colon V_\Theta \to V_\Theta,$$

$$M_{\mathrm{B}\to\mathrm{A}} = \begin{pmatrix} \frac{c_{\mathrm{B}}}{e_{\mathrm{A}}} & 0 & 0 \\ \frac{c_{\mathrm{A}}}{e_{\mathrm{A}}} & 0 & 1 \\ -\frac{e_{\mathrm{B}}}{e_{\mathrm{A}}} & 1 & 0 \end{pmatrix}, \qquad M_{\mathrm{B}\to\mathrm{B}} = \begin{pmatrix} 0 & \frac{c_{\mathrm{A}}}{e_{\mathrm{B}}} & 1 \\ 1 & -\frac{e_{\mathrm{A}}}{e_{\mathrm{B}}} & 0 \\ 0 & \frac{c_{\mathrm{B}}}{e_{\mathrm{B}}} & 0 \end{pmatrix}.$$

20.3 Constructing the projected map

We now build on the work of Postlethwaite and Rucklidge [PR22] and construct the projected map of the Rock–Paper–Scissors–Lizard–Spock network. This map requires a slightly different process to define than used before. The complication arises from the fact that there are two different spaces, V_Θ and V_Φ, on which the transition matrices act. First, we define a set of projected maps that act on these spaces separately, and then we "glue" them together to form the projected map of the Rock–Paper–Scissors–Lizard–Spock network. This process could also be used to construct the projected map of other heteroclinic networks where the unique switching equilibria has multiple incoming heteroclinic orbits, such as the bowtie network studied in [CL16b], shown in Figure 1.5(a). This process could also be used to con-

struct a projected map for a network that has multiple switching equilibria in different parts of the network, such as the network studied in [PR23].

In both of the spaces V_Θ and V_Φ, we define a simplex:

$$T_\Theta = \{(X_\mathrm{A}, X_\mathrm{B}, \Theta) \in V_\Theta \mid X_\mathrm{A} + X_\mathrm{B} + \Theta = -1\} \tag{20.2}$$

and

$$T_\Phi = \{(X_\mathrm{A}, X_\mathrm{B}, \Phi) \in V_\Phi \mid X_\mathrm{A} + X_\mathrm{B} + \Phi = -1\}. \tag{20.3}$$

Since both of these simplices are two-dimensional, we can, without ambiguity, identify any point on either with the first two coordinates of that point, which we write as ϑ_1 and ϑ_2. We can thus identify both of these simplices with subsets of $(-1,0)^2$:

$$T_\Theta \equiv \left\{(\vartheta_1, \vartheta_2) \in (-1,0)^2 \mid \vartheta_1 + \vartheta_2 > -1\right\} \subsetneq (-1,0)^2$$

and

$$T_\Phi \equiv \left\{(\vartheta_1, \vartheta_2) \in (-1,0)^2 \mid \vartheta_1 + \vartheta_2 > -1\right\} \subsetneq (-1,0)^2.$$

Again, we highlight that, as with V_Θ and V_Φ, although these sets have identical definitions, they represent different subsets of the original phase space. We note that, as subsets of $(-1,0)^2$—and therefore excluding the X_3- and X_4-axes—the boundary of both of these sets is the line $\vartheta_1 + \vartheta_2 = -1$. Given the definition in (20.2) and (20.3), a point on this line represents a trajectory for which $\Theta = 0$ or $\Phi = 0$, respectively, and thus that the angle θ or φ is no longer small, but is now $\mathcal{O}(1)$.

The projection Π is now defined by

$$\Pi\colon X \in \mathbb{R}^3_- \mapsto \frac{-1}{(1,1,1)\cdot X}(e_1 \cdot X, e_2 \cdot X),$$

where $e_1 = (1,0,0)$ and $e_2 = (0,1,0)$. Note that this definition applies when the codomain is T_Θ or T_Φ.

We now consider the subsets of the simplices T_Θ and T_Φ that correspond to trajectories that make a certain class of transition. To do so, we define first

$$\Omega_{\mathrm{A}\to\mathrm{A}} = \{(\vartheta_1, \vartheta_2) \in T_\Phi \mid e_\mathrm{B}\vartheta_1 > e_\mathrm{A}\vartheta_2\} \subseteq T_\Phi,$$
$$\Omega_{\mathrm{A}\to\mathrm{B}} = \{(\vartheta_1, \vartheta_2) \in T_\Phi \mid e_\mathrm{B}\vartheta_1 < e_\mathrm{A}\vartheta_2\} \subseteq T_\Phi,$$

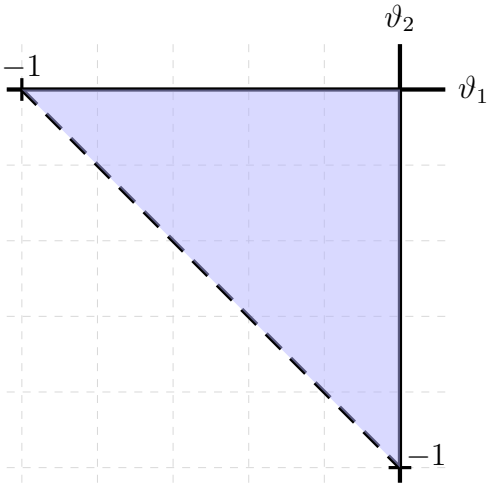

Figure 20.3: The sets T_Θ and T_Φ represented as a subset of $\mathbb{R}^2_-$, shaded blue. The dashed line represents the condition $\Theta = 0$ or $\Phi = 0$, for T_Θ and T_Φ respectively, where the contracting angle is no longer close to 0 or $\frac{\pi}{2}$.

and

$$\Omega_{\mathrm{S}} = \{(\vartheta_1, \vartheta_2) \in T_\Phi \mid e_{\mathrm{B}}\vartheta_1 = e_{\mathrm{A}}\vartheta_2\} \subseteq T_\Phi.$$

We similarly define

$$\Xi_{\mathrm{B}\to\mathrm{A}} = \{(\vartheta_1, \vartheta_2) \in T_\Theta \mid e_{\mathrm{B}}\vartheta_1 > e_{\mathrm{A}}\vartheta_2\} \subseteq T_\Theta,$$
$$\Xi_{\mathrm{B}\to\mathrm{B}} = \{(\vartheta_1, \vartheta_2) \in T_\Theta \mid e_{\mathrm{B}}\vartheta_1 < e_{\mathrm{A}}\vartheta_2\} \subseteq T_\Theta,$$

and

$$\Xi_{\mathrm{S}} = \{(\vartheta_1, \vartheta_2) \in T_\Theta \mid e_{\mathrm{B}}\vartheta_1 = e_{\mathrm{A}}\vartheta_2\} \subseteq T_\Theta.$$

These sets represent, respectively, trajectories that next make a transition of class A or of class B, and the switching manifold, depending on if the previous transition is of class A or B. As with Podvigina's two-cycle network, the results of §9.4 can be generalised here to prove that only the switching subspace defined by $x_{\mathrm{A}}^{e_{\mathrm{B}}} = x_{\mathrm{B}}^{e_{\mathrm{A}}}$ needs to be excluded from the domain of the projected map.

The four components of the projected map are thus

$$g_{\mathrm{A}\to\mathrm{A}} \colon \Omega_{\mathrm{A}\to\mathrm{A}} \to T_\Phi,$$
$$g_{\mathrm{A}\to\mathrm{A}} \colon (\vartheta_1, \vartheta_2) \mapsto \Pi(M_{\mathrm{A}\to\mathrm{A}}(\vartheta_1, \vartheta_2, -1 - \vartheta_1 - \vartheta_2)),$$
$$g_{\mathrm{A}\to\mathrm{A}} \colon (\vartheta_1, \vartheta_2) \mapsto \left(\frac{(c_{\mathrm{B}} - e_{\mathrm{A}})\vartheta_1 - e_{\mathrm{A}}(\vartheta_2 + 1)}{(e_{\mathrm{A}} + e_{\mathrm{B}} - c_{\mathrm{A}} - c_{\mathrm{B}})\vartheta_1 + e_{\mathrm{A}}}, \frac{c_{\mathrm{A}}\vartheta_1}{(e_{\mathrm{A}} + e_{\mathrm{B}} - c_{\mathrm{A}} - c_{\mathrm{B}})\vartheta_1 + e_{\mathrm{A}}} \right),$$

$$g_{\mathrm{A}\to\mathrm{B}}\colon \Omega_{\mathrm{A}\to\mathrm{B}} \to T_\Theta,$$
$$g_{\mathrm{A}\to\mathrm{B}}\colon (\vartheta_1,\vartheta_2) \mapsto \Pi(M_{\mathrm{A}\to\mathrm{B}}(\vartheta_1,\vartheta_2,-1-\vartheta_1-\vartheta_2)),$$
$$g_{\mathrm{A}\to\mathrm{B}}\colon (\vartheta_1,\vartheta_2) \mapsto \left(\frac{c_\mathrm{A}\vartheta_2}{(e_\mathrm{A}+e_\mathrm{B}-c_\mathrm{A}-c_\mathrm{B})\vartheta_2+e_\mathrm{B}}, \frac{e_\mathrm{B}\vartheta_1-e_\mathrm{A}\vartheta_2}{(e_\mathrm{A}+e_\mathrm{B}-c_\mathrm{A}-c_\mathrm{B})\vartheta_2+e_\mathrm{B}}\right),$$

$$g_{\mathrm{B}\to\mathrm{A}}\colon \Xi_{\mathrm{B}\to\mathrm{A}} \to T_\Phi,$$
$$g_{\mathrm{B}\to\mathrm{A}}\colon (\vartheta_1,\vartheta_2) \mapsto \Pi(M_{\mathrm{B}\to\mathrm{A}}(\vartheta_1,\vartheta_2,-1-\vartheta_1-\vartheta_2)),$$
$$g_{\mathrm{B}\to\mathrm{A}}\colon (\vartheta_1,\vartheta_2) \mapsto \left(\frac{c_\mathrm{B}\vartheta_1}{(e_\mathrm{A}+e_\mathrm{B}-c_\mathrm{A}-c_\mathrm{B})\vartheta_1+e_\mathrm{A}}, \frac{(c_\mathrm{A}-e_\mathrm{A})\vartheta_1-e_\mathrm{A}(\vartheta_2+1)}{(e_\mathrm{A}+e_\mathrm{B}-c_\mathrm{A}-c_\mathrm{B})\vartheta_1+e_\mathrm{A}}\right),$$

and

$$g_{\mathrm{B}\to\mathrm{B}}\colon \Xi_{\mathrm{B}\to\mathrm{B}} \to T_\Theta,$$
$$g_{\mathrm{B}\to\mathrm{B}}\colon (\vartheta_1,\vartheta_2) \mapsto \Pi(M_{\mathrm{B}\to\mathrm{B}}(\vartheta_1,\vartheta_2,-1-\vartheta_1-\vartheta_2)),$$
$$g_{\mathrm{B}\to\mathrm{B}}\colon (\vartheta_1,\vartheta_2) \mapsto \left(\frac{(c_\mathrm{A}-e_\mathrm{B})\vartheta_2-e_\mathrm{B}(\vartheta_1+1)}{(e_\mathrm{A}+e_\mathrm{B}-c_\mathrm{A}-c_\mathrm{B})\vartheta_2+e_\mathrm{B}}, \frac{e_\mathrm{B}\vartheta_1-e_\mathrm{A}\vartheta_2}{(e_\mathrm{A}+e_\mathrm{B}-c_\mathrm{A}-c_\mathrm{B})\vartheta_2+e_\mathrm{B}}\right).$$

In each case, if the previous transition is of class A, then the domain of the map $g_{X\to Y}$ is a subset of T_Φ, and if it is of class B, then the domain is a subset of T_Θ. The codomain similarly depends on the class of the current transition.

These four component maps can then be used to define a projected map

$$g\colon (\Omega_{\mathrm{A}\to\mathrm{A}} \cup \Omega_{\mathrm{A}\to\mathrm{B}}) \sqcup (\Xi_{\mathrm{B}\to\mathrm{A}} \cup \Xi_{\mathrm{B}\to\mathrm{B}}) \to T_\Phi \sqcup T_\Theta.$$

Both the domain and the codomain of this map require the *disjoint* union to be taken, so that we can keep track of the sequence of transitions that a trajectory makes. We therefore require some way to modify the domain and codomain of this map to build a single connected domain while preserving the ability to identify the previous and current class of transition. We now present a method to construct such a projected map.

Both T_Θ and T_Φ are subsets of $(-1,0)^2$, and, as we can see in Figure 20.3, we can visually describe them as the upper right-hand triangle of this space which is bounded by a square region. The lower left-hand triangle is disjoint from these domains and not used in the definition of the map. It is, however, the equivalent to both T_Θ and T_Φ, but reflected across the line $\vartheta_1+\vartheta_2=-1$, and so we can make it the domain of one of the component maps, while leaving the other domain unchanged.

Therefore, we define $S=(-1,0)^2$. With the identity map, we embed the set T_Φ into

S as the subset

$$S_{\mathrm{A}} = \{(\vartheta_1, \vartheta_2) \in S \mid \vartheta_1 + \vartheta_2 > -1\}.$$

Next, we use a reflection across the line $\vartheta_1 + \vartheta_2 = -1$ defined by

$$\begin{aligned} P\colon S &\to S \\ \colon (\vartheta_1, \vartheta_2) &\mapsto (-1 - \vartheta_2, -1 - \vartheta_1) \end{aligned}$$

to embed the set T_Θ into S as the subset

$$S_{\mathrm{B}} = \{(\vartheta_1, \vartheta_2) \in S \mid \vartheta_1 + \vartheta_2 < -1\}.$$

The embedding of the sets $\Omega_{\mathrm{A}\to\mathrm{A}}$ and $\Omega_{\mathrm{A}\to\mathrm{B}}$ gives us the sets

$$\Theta_{\mathrm{A}\to\mathrm{A}} = \{(\vartheta_1, \vartheta_2) \in S \mid \vartheta_1 + \vartheta_2 > -1 \text{ and } e_{\mathrm{B}}\vartheta_1 > e_{\mathrm{A}}\vartheta_2\} \subseteq S_{\mathrm{A}}$$

and

$$\Theta_{\mathrm{A}\to\mathrm{B}} = \{(\vartheta_1, \vartheta_2) \in S \mid \vartheta_1 + \vartheta_2 > -1 \text{ and } e_{\mathrm{B}}\vartheta_1 < e_{\mathrm{A}}\vartheta_2\} \subseteq S_{\mathrm{A}}.$$

For $\Xi_{\mathrm{A}\to\mathrm{A}}$ and $\Xi_{\mathrm{A}\to\mathrm{B}}$, we have

$$\Theta_{\mathrm{B}\to\mathrm{A}} = \{(\vartheta_1, \vartheta_2) \in S \mid \vartheta_1 + \vartheta_2 < -1 \text{ and } e_{\mathrm{B}}(-1 - \vartheta_2) > e_{\mathrm{A}}(-1 - \vartheta_1)\} \subseteq S_{\mathrm{B}}$$

and

$$\Theta_{\mathrm{B}\to\mathrm{B}} = \{(\vartheta_1, \vartheta_2) \in S \mid \vartheta_1 + \vartheta_2 < -1 \text{ and } e_{\mathrm{B}}(-1 - \vartheta_2) < e_{\mathrm{A}}(-1 - \vartheta_1)\} \subseteq S_{\mathrm{B}}.$$

These sets allow us to define the four components of the projected map, where we set $\eta \coloneqq c_{\mathrm{A}} + c_{\mathrm{B}} - e_{\mathrm{A}} - e_{\mathrm{B}}$:

$$\begin{aligned} &f_{\mathrm{A}\to\mathrm{A}} = g_{\mathrm{A}\to\mathrm{A}}\colon \Theta_{\mathrm{A}\to\mathrm{A}} \to S, \\ &f_{\mathrm{A}\to\mathrm{A}}\colon (\vartheta_1, \vartheta_2) \mapsto \left(\frac{(e_{\mathrm{A}} - c_{\mathrm{B}})\vartheta_1 + e_{\mathrm{A}}(\vartheta_2 + 1)}{\eta\vartheta_1 - e_{\mathrm{A}}}, \frac{-c_{\mathrm{A}}\vartheta_1}{\eta\vartheta_1 - e_{\mathrm{A}}}\right), \end{aligned}$$

$$\begin{aligned} &f_{\mathrm{A}\to\mathrm{B}} = Pg_{\mathrm{A}\to\mathrm{B}}\colon \Theta_{\mathrm{A}\to\mathrm{B}} \to S, \\ &f_{\mathrm{A}\to\mathrm{B}}\colon (\vartheta_1, \vartheta_2) \mapsto \left(\frac{e_{\mathrm{B}}(\vartheta_1 + 1) + (e_{\mathrm{B}} - c_{\mathrm{A}} - c_{\mathrm{B}})\vartheta_2}{\eta\vartheta_2 - e_{\mathrm{B}}}, \frac{(e_{\mathrm{A}} + e_{\mathrm{B}} - c_{\mathrm{B}})\vartheta_2 + e_{\mathrm{B}}}{\eta\vartheta_2 - e_{\mathrm{B}}}\right), \end{aligned}$$

$$f_{\mathrm{B}\to\mathrm{A}} = g_{\mathrm{B}\to\mathrm{A}}P\colon \Theta_{\mathrm{B}\to\mathrm{A}} \to S,$$
$$f_{\mathrm{B}\to\mathrm{A}}\colon (\vartheta_1,\vartheta_2) \mapsto \left(\frac{-c_{\mathrm{B}}(\vartheta_2+1)}{\eta\vartheta_2+(c_{\mathrm{A}}+c_{\mathrm{B}}-e_{\mathrm{B}})}, \frac{e_{\mathrm{A}}(\vartheta_1+1)+(e_{\mathrm{A}}-c_{\mathrm{A}})\vartheta_2-c_{\mathrm{A}}}{\eta\vartheta_2+(c_{\mathrm{A}}+c_{\mathrm{B}}-e_{\mathrm{B}})}\right),$$

and

$$f_{\mathrm{B}\to\mathrm{B}} = Pg_{\mathrm{B}\to\mathrm{B}}P\colon \Theta_{\mathrm{B}\to\mathrm{B}} \to S,$$
$$f_{\mathrm{B}\to\mathrm{B}}\colon (\vartheta_1,\vartheta_2) \mapsto \left(\frac{(e_{\mathrm{B}}-c_{\mathrm{A}}-c_{\mathrm{B}})\vartheta_1+e_{\mathrm{B}}(\vartheta_2+1)-c_{\mathrm{A}}-c_{\mathrm{B}}}{\eta\vartheta_1+(c_{\mathrm{A}}+c_{\mathrm{B}}-e_{\mathrm{A}})}, \frac{(e_{\mathrm{A}}-c_{\mathrm{B}})\vartheta_1-e_{\mathrm{B}}\vartheta_2+(e_{\mathrm{A}}-e_{\mathrm{B}}-c_{\mathrm{B}})}{\eta\vartheta_1+(c_{\mathrm{A}}+c_{\mathrm{B}}-e_{\mathrm{A}})}\right).$$

With these functions, we finally define the projected map of the Rock–Paper–Scissors–Lizard–Spock network, $f_{\mathrm{RPSLS}}\colon \Theta_{\mathrm{A}\to\mathrm{A}} \cup \Theta_{\mathrm{B}\to\mathrm{A}} \cup \Theta_{\mathrm{A}\to\mathrm{B}} \cup \Theta_{\mathrm{B}\to\mathrm{B}} \to S$:

$$f_{\mathrm{RPSLS}}(\vartheta) = \begin{cases} f_{\mathrm{A}\to\mathrm{A}}(\vartheta), & \text{if } \vartheta \in \Theta_{\mathrm{A}\to\mathrm{A}}, \\ f_{\mathrm{A}\to\mathrm{B}}(\vartheta), & \text{if } \vartheta \in \Theta_{\mathrm{A}\to\mathrm{B}}, \\ f_{\mathrm{B}\to\mathrm{A}}(\vartheta), & \text{if } \vartheta \in \Theta_{\mathrm{B}\to\mathrm{A}}, \\ f_{\mathrm{B}\to\mathrm{B}}(\vartheta), & \text{if } \vartheta \in \Theta_{\mathrm{B}\to\mathrm{B}}. \end{cases} \tag{20.4}$$

As a two-dimensional piecewise-smooth map, this projected map has a one-dimensional switching manifold, Θ_{S}, which for this map is piecewise-linear and defined as the union of three different components. First, there is the embedding of Ω_{S}, the switching manifold between the maps $g_{\mathrm{A}\to\mathrm{A}}$ and $g_{\mathrm{A}\to\mathrm{B}}$:

$$\Theta_{\mathrm{S}}^{\mathrm{A}\to} = \{(\vartheta_1,\vartheta_2) \in S \mid e_{\mathrm{B}}\vartheta_1 = e_{\mathrm{A}}\vartheta_2 \text{ and } \vartheta_1+\vartheta_2 > -1\} = \partial_S\Theta_{\mathrm{A}\to\mathrm{A}} \cap \partial_S\Theta_{\mathrm{A}\to\mathrm{B}},$$

where $\partial_S X$ represents the topological boundary of the set X *as a subspace of* S. Next, there is the embedding of Ξ_{S} with the reflection P:

$$\begin{aligned}\Theta_{\mathrm{S}}^{\mathrm{B}\to} &= \{(\vartheta_1,\vartheta_2) \in S \mid e_{\mathrm{B}}(-1-\vartheta_2) = e_{\mathrm{A}}(-1-\vartheta_1) \text{ and } \vartheta_1+\vartheta_2 < -1\} \\ &= \partial_S\Theta_{\mathrm{B}\to\mathrm{A}} \cap \partial_S\Theta_{\mathrm{B}\to\mathrm{B}}.\end{aligned}$$

These two switching manifolds represent trajectories that begin in the excluded cusp Γ_{c}, and thus that do not remain sufficiently close to the network to be captured by the return map. They divide trajectories according to the current transition, and thus crossing one of these lines generically represents a change in the current transition of a trajectory, without a change to the previous transition of that trajectory.

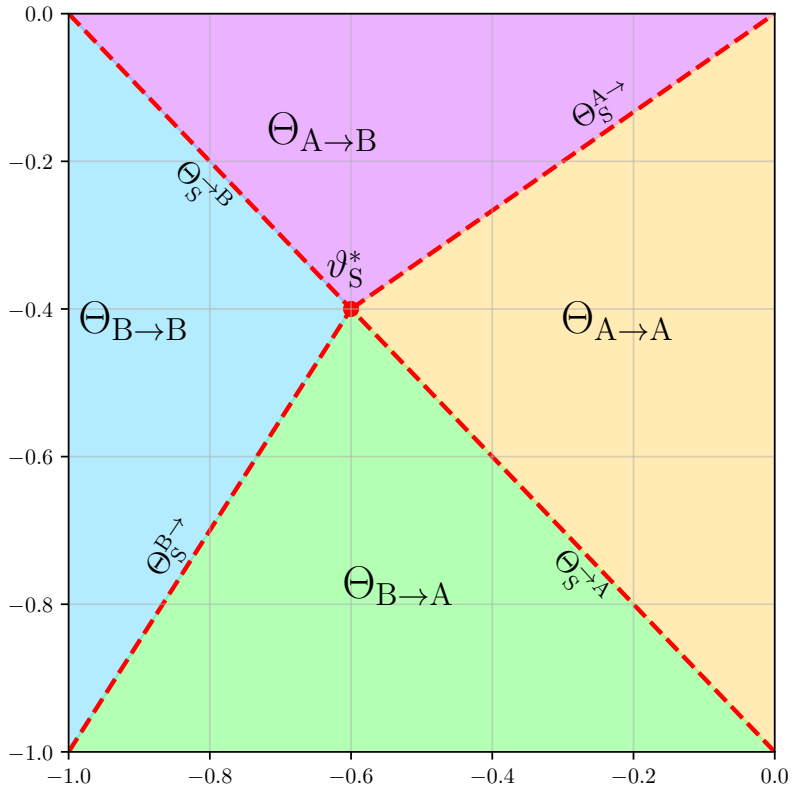

Figure 20.4: A representation of the set $S = (-1, 0)^2$ and its components. The four shaded regions represent the domains $\Theta_{X\to Y}$ of the component functions $f_{X\to Y}$, as labelled, where $X, Y \in \{A, B\}$. The dashed red lines represent the components of the piecewise-linear switching manifold, as labelled. The point ϑ^*_{S} is highlighted as the labelled red dot, where all four component lines of the switching manifold meet.

Lastly, there is the line $\vartheta_1 + \vartheta_2 = -1$, which is the separation of the embeddings of T_Θ and T_Φ. Since this line is fixed by the reflection P, for both S_{A} and S_{B} this line corresponds to the contracting angle θ no longer being close to 0 or $\frac{\pi}{2}$. Therefore, crossing this line generically represents a trajectory that changes whether it strikes $\mathbf{H}^{\mathrm{in}}_{\varphi}$ or $\mathbf{H}^{\mathrm{in}}_{\theta}$ when it enters a small neighbourhood of ξ, and so represents a change in the class of the previous transition, without a change to the class of the current transition.

It is convenient to decompose the line $\vartheta_1 + \vartheta_2 = -1$ into two lines and one point. The first of these lines is

$$\Theta_{\mathrm{S}}^{\to\mathrm{A}} = \{(\vartheta_1, \vartheta_2) \in S \mid \vartheta_1 + \vartheta_2 = -1 \text{ and } e_{\mathrm{B}}\vartheta_1 > e_{\mathrm{A}}\vartheta_2\} = \partial_S\Theta_{\mathrm{A}\to\mathrm{A}} \cap \partial_S\Theta_{\mathrm{B}\to\mathrm{A}}$$

and the second is

$$\Theta_{\mathrm{S}}^{\to\mathrm{B}} = \{(\vartheta_1, \vartheta_2) \in S \mid \vartheta_1 + \vartheta_2 = -1 \text{ and } e_{\mathrm{B}}\vartheta_1 < e_{\mathrm{A}}\vartheta_2\} = \partial_S\Theta_{\mathrm{A}\to\mathrm{B}} \cap \partial_S\Theta_{\mathrm{B}\to\mathrm{B}}.$$

Finally, there is the point ϑ_{S}^*, which is the unique limit point of all four of $\Theta_{\mathrm{S}}^{\mathrm{A}\to}$, $\Theta_{\mathrm{S}}^{\mathrm{B}\to}$, $\Theta_{\mathrm{S}}^{\to\mathrm{A}}$, and $\Theta_{\mathrm{S}}^{\to\mathrm{B}}$:

$$\vartheta_{\mathrm{S}}^* = \left(\frac{-e_{\mathrm{A}}}{e_{\mathrm{A}}+e_{\mathrm{B}}}, \frac{-e_{\mathrm{B}}}{e_{\mathrm{A}}+e_{\mathrm{B}}}\right) = \partial_S\Theta_{\mathrm{A}\to\mathrm{A}} \cap \partial_S\Theta_{\mathrm{A}\to\mathrm{B}} \cap \partial_S\Theta_{\mathrm{B}\to\mathrm{A}} \cap \partial_S\Theta_{\mathrm{B}\to\mathrm{B}}.$$

Crossing the point ϑ_{S}^* generically results in a change in both the current and previous class of transition.

The entire switching manifold thus is $\Theta_{\mathrm{S}} = \Theta_{\mathrm{A}\to} \cup \Theta_{\mathrm{B}\to} \cup \Theta_{\to\mathrm{A}} \cup \Theta_{\to\mathrm{B}} \cup \vartheta_{\mathrm{S}}^*$. We represent the entire domain S in Figure 20.4.

20.4 Regular cycling in the projected map

As with Podvigina's two-cycle network, stable regular cycling with root sequence $\mathcal{X}$ is represented in the projected map with an attracting and admissible $\mathcal{X}$-orbit. We present four examples in Figure 20.5. In all four examples, $e_{\mathrm{A}} = 1$ and $e_{\mathrm{B}} = 0.8$. The initial condition used in all four examples is $(-0.1, -0.1)$, though we do not plot this point, beginning instead from the first iterate.

The cycles $\mathcal{C}_{[\mathrm{A}]}$ and $\mathcal{C}_{[\mathrm{B}]}$ are represented in the projected map with stable and admissible fixed points $\vartheta_{\mathrm{A}}^* \in \Theta_{\mathrm{A}\to\mathrm{A}}$ and $\vartheta_{\mathrm{B}}^* \in \Theta_{\mathrm{B}\to\mathrm{B}}$, respectively. Examples of an orbit attracted to each fixed point are shown in Figures 20.5(a) and 20.5(b), which have $c_{\mathrm{A}} = 1.6$ and $c_{\mathrm{B}} = 1.1$, and $c_{\mathrm{A}} = 1.8$ and $c_{\mathrm{B}} = 3$, respectively. We note, however, that these cycles are represented as fixed points because they represent trajectories always making the same class of transition, either of class A or B.

The five $\mathcal{C}_{[\mathrm{T}]}$ cycles are not represented in the projected map as a fixed point, because such a cycle does not correspond to a trajectory making the same class of transition, but rather the sequence of transitions AAB. Therefore, these $\mathcal{C}_{[\mathrm{T}]}$ cycles are represented by an admissible and attracting period-three periodic orbit, specifically a T-orbit, where we recall $T = AAB$. See Figure 20.5(c), where $c_{\mathrm{A}} = 1.1$ and $c_{\mathrm{B}} = 3.05$. We also observe initial transient cycling around the $\mathcal{C}_{[\mathrm{B}]}$ cycle before the trajectory is asymptotic to the $\mathcal{C}_{[\mathrm{T}]}$ cycle. More complicated behaviour of trajectories near the network includes examples where a trajectory has an eventually periodic itinerary, but where the root sequence is not the root sequence of a subcycle. For example, trajectories that have the root sequence $TD = (AAB)(BB)$, where we recall $D \equiv BB$. Such cycling behaviour is represented with an attracting and admissible period-five TD-orbit. See Figure 20.5(d), where $c_{\mathrm{A}} = 1$ and $c_{\mathrm{B}} = 1.5$

In Figure 20.6, we present admissible $\mathcal{X}$-orbits close to parameter values of border-collision bifurcations. In these figures, we colour periodic points two colours: the outer edge colour represents the class of the previous transition, and the inner colour represents the class

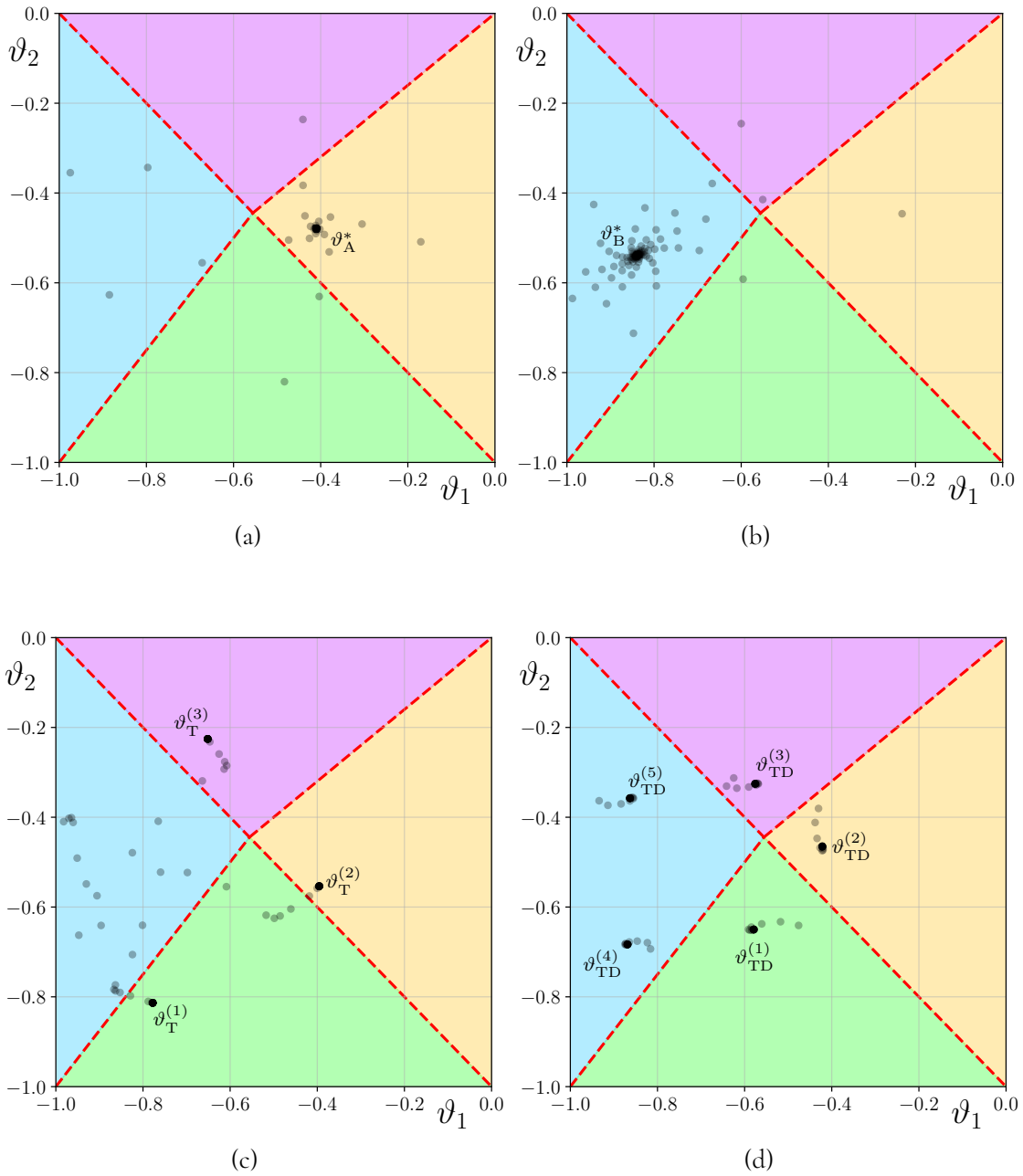

Figure 20.5: Various examples of the action of the projected map f_{RPSLS} for different parameter values and initial conditions. In each figure, the dashed red line indicates the switching manifold, and the four domains are coloured the same as in Figure 20.4. Each point is plotted slightly transparent, so that the attracting set appears darker. The attracting set in each case is: (a) the fixed point ϑ^*_{A}, (b) the fixed point ϑ^*_{B}, (c) a period-three $T \equiv AAB$-orbit, and (d) a period-five $TD \equiv (AAB)(BB)$-orbit. Further details are given in the text. In all panels, we label attracting sets.

of the current transition. For both, amber represents class A, and blue class B.

In Figures 20.6(a) and 20.6(b), we present an admissible T-orbit and TD-orbit, respectively. In these panels, we set $c_{\mathrm{A}} = 1.2$ and $c_{\mathrm{B}} = 2.945$, and $c_{\mathrm{A}} = 1.2$ and $c_{\mathrm{B}} = 2.23$, respectively. We see that, in both panels, there are two periodic points that are near to a component of the switching manifold. In both cases, one periodic point is close to $\Theta_{\mathrm{S}}^{\mathrm{A}\rightarrow} \cup \Theta_{\mathrm{S}}^{\mathrm{B}\rightarrow}$. This component of the switching manifold corresponds to the excluded cusps that separate trajectories that next make a class A or B transition at a certain equilibrium of the network. Therefore, by Theorem 14.1, we expect that, at the next equilibrium, there is a 0 entry in $w_{\max}$. For all stability boundaries observed in Figure 20.2, all 0 entries are the third component of $w_{\max}$, which corresponds to the logarithm of the contracting angle θ.

However, under the symmetry (20.1), the two equilibria are equivalent, and the conditions $\Theta = 0$ and $\Phi = 0$ are represented in the domain of the projected map along the line defined by $\vartheta_1 + \vartheta_2 = -1$. Therefore, the other periodic point that can be observed in both Figures 20.6(a) and 20.6(b) to be near a border-collision is near the line $\vartheta_1 + \vartheta_2 = -1$. Moreover, this periodic point is the next periodic point in the periodic orbit.

In general, near any stability boundary in Figure 20.2, we expect two border-collision bifurcations. The first is a point near $\Theta_{\mathrm{S}}^{X\rightarrow}$, where $X \in \{A, B\}$. This border-collision is equivalent to all other border-collision bifurcations we have until now considered, and represents trajectories passing through the excluded cusp Γ_{c} of initial conditions that do not remain sufficiently close to the network under the flow of the dynamical system. The second is a point near $\Theta_{\mathrm{S}}^{\rightarrow X}$, where $X \in \{A, B\}$, and represents the change in the contracting angle as the class of the previous transition changes. However, there are exceptions to this phenomenon.

In Figures 20.6(c) and 20.6(d), we present an admissible period-eight T^2D-orbit and an admissible period-nine QTD-orbit, respectively. In these panels, we set $c_{\mathrm{A}} = 1.0216$ and $c_{\mathrm{B}} = 1.935$, and $c_{\mathrm{A}} = 1.02185$ and $c_{\mathrm{B}} = 1.93555$, respectively. The parameter values in these panels are either side of the shrinking point that joins the stability regions of these two root sequences. The shrinking point is the codimension-two point where the chain of stability regions has zero width, and is where the two stability boundaries of the root sequence meet. Therefore, at the parameter values for these panels, there is a total of four periodic points near a border-collision bifurcation. Since the transition $T^2D \equiv (AAB)(AAB)(BB)$ to $QTD \equiv (ABBB)(AAB)(BB)$ corresponds to the exchange $A \rightarrow BB$, the QTD-orbit has one additional periodic point, which lies in the $\Theta_{\mathrm{B}\rightarrow\mathrm{B}}$ domain.

Comparing Figures 20.6(c) and 20.6(d), we see that the periodic points all undergo persistent border-collision bifurcations; that is, an admissible periodic point lies either side of the critical parameter value of the border-collision bifurcation. However, unlike in the per-

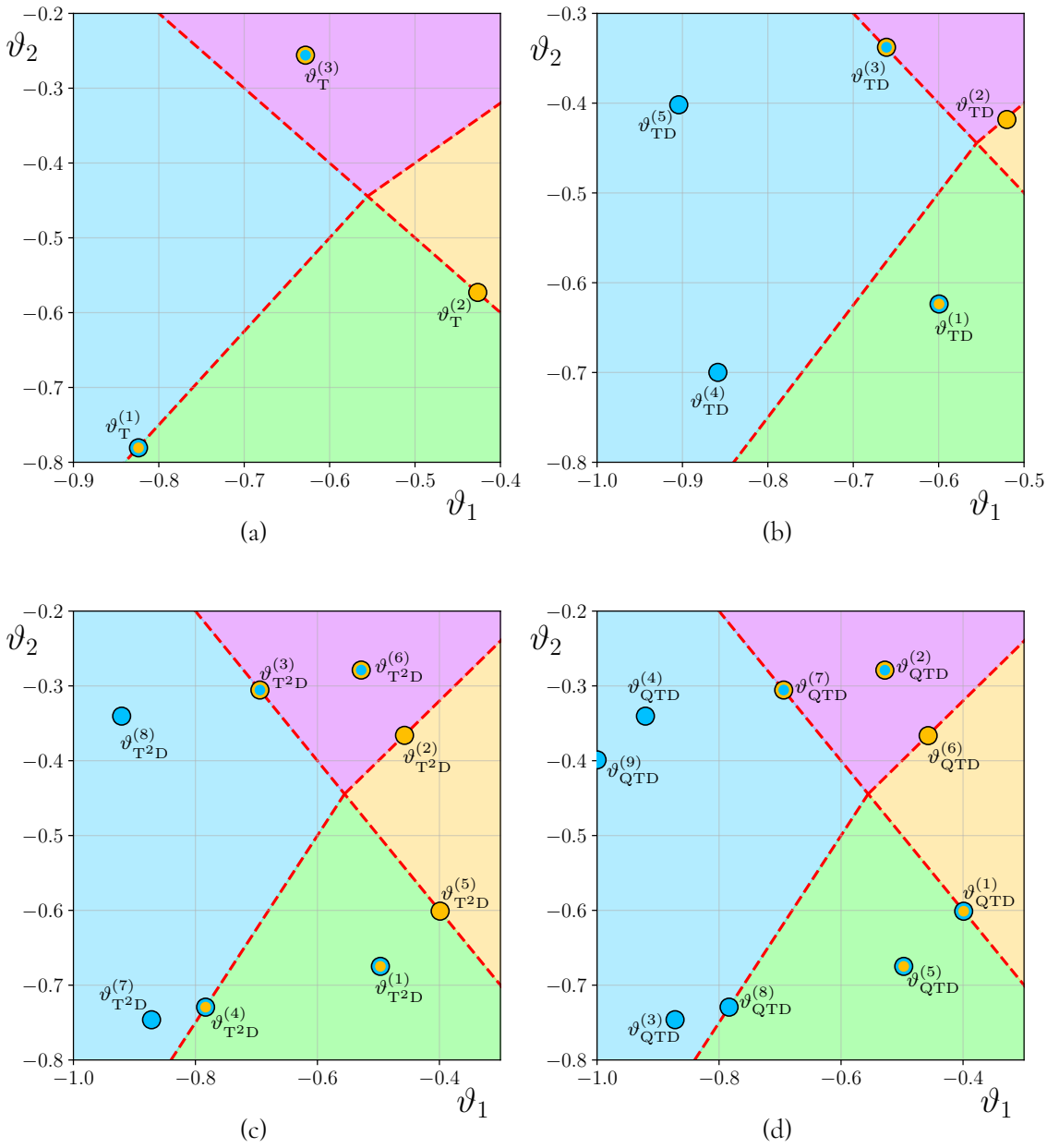

Figure 20.6: Various examples of admissible $\mathcal{X}$-orbits for different parameter values that are near the point of a border-collision bifurcation. In each panel, the dashed red lines indicate the components of the switching manifold, and the four domains are coloured the same as in Figure 20.4. We do not plot any initial transient dynamics, and each point has two colours: the outer edge colour represents the class of the previous transition, and the inner colour represents the class of the current transition. For both, amber represents class A, and blue class B. The attracting set in each case is: (a) a period-three T-orbit near a border-collision bifurcation, (b) a period-five TD-orbit near a border-collision bifurcation, (c) a period-eight T^2D-orbit near a codimension-two shrinking point, and (d) a period-nine QTD-orbit near the same codimension-two shrinking point. Further details are given in the text. In all panels, we label attracting sets.

sistent border-collisions of fixed points observed in Figures 11.3 and 12.3, the admissible periodic points may not exist in different domains on either side of the bifurcation. For example, the points $\vartheta^{(2)}_{\mathrm{T}^2D}$ and $\vartheta^{(6)}_{\mathrm{QTD}}$ undergo a persistent border-collision bifurcation on $\Theta_{\mathrm{S}}^{\mathrm{A}\rightarrow}$, since there exists a periodic point either side of the critical parameter value. However, these points both lie in $\Theta_{\mathrm{A}\rightarrow\mathrm{A}}$. The same holds for their respective forward images $\vartheta^{(3)}_{\mathrm{T}^2D}$ and $\vartheta^{(7)}_{\mathrm{QTD}}$, which undergo a persistent border-collision bifurcation on $\Theta_{\mathrm{S}}^{\rightarrow\mathrm{B}}$ but both lie in $\Theta_{\mathrm{A}\rightarrow\mathrm{B}}$.

In the border-collision bifurcation of $\vartheta^{(4)}_{\mathrm{T}^2\mathrm{D}}$ and $\vartheta^{(8)}_{\mathrm{QTD}}$, we see that the domain in which the admissible periodic orbit lies differs either side of the critical parameter value, going from $\Theta_{\mathrm{B}\rightarrow\mathrm{A}}$ to $\Theta_{\mathrm{B}\rightarrow\mathrm{B}}$. The domain for points that cross the switching manifold $\Theta_{\rightarrow\mathrm{A}}$ also changes, from $\Theta_{\mathrm{A}\rightarrow\mathrm{A}}$ to $\Theta_{\mathrm{B}\rightarrow\mathrm{A}}$. However, in this case, the point colliding with $\Theta_{\rightarrow\mathrm{A}}$ is not the next periodic point on the orbit, as after the bifurcation, the point $\vartheta^{(9)}_{\mathrm{QTD}}$ is now admissible. We show below in §20.6 that $f_{\mathrm{B}\rightarrow\mathrm{A}} = f_{\mathrm{B}\rightarrow\mathrm{B}}f_{\mathrm{B}\rightarrow\mathrm{B}}$, and thus we still expect a border-collision bifurcation of $\vartheta^{(1)}_{\mathrm{QTD}}$ on $\Theta_{\mathrm{S}}^{\rightarrow\mathrm{A}}$, by continuity.

As noted, the strings-of-sausages structure seen in Figure 20.2 are typically found in the bifurcation sets of periodic orbits in continuous piecewise-linear systems. The functions in (20.4) are clearly not linear. However, as we noted in §13.3, they are the ratios of linear maps. Moreover, as we show below in §20.6, the functions are not continuous on all switching manifolds. Moreover, the symbol sequences of the periodic orbits are always of a certain class, known as *rotational symbol sequences* [Sim16]. In continuous piecewise-linear systems, the symbol sequence of successive stable periodic orbits in a given chain are of the same length, whereas the root sequences in Figure 20.2 increase in length by one as the first root sequence transitions to the next through the shrinking point.

Therefore, although there is a clear understanding of these structures in the piecewise-smooth dynamical systems literature [Sim16], considerable additional work is still needed to apply the results of continuous piecewise-linear systems to the projected map of the Rock–Paper–Scissors–Lizard–Spock network, and to account for the different nature of the root sequences of stable cycling near the network. Nevertheless, we expect that the projected map f_{RPSLS} can be used to explain the structure in Figure 20.2 and prove the conjectures made by Postlethwaite and Rucklidge in [PR22].

20.5 Irregular cycling in the projected map

We now present numerical examples of the projected map for parameter values that correspond to numerical observations by Postlethwaite and Rucklidge [PR22] of irregular cycling near the Rock–Paper–Scissors–Lizard–Spock network. For these parameter values, trajectories remain asymptotic to the network, but their itinerary is not eventually periodic. Therefore, in the projected map, we do not expect to find a periodic orbit.

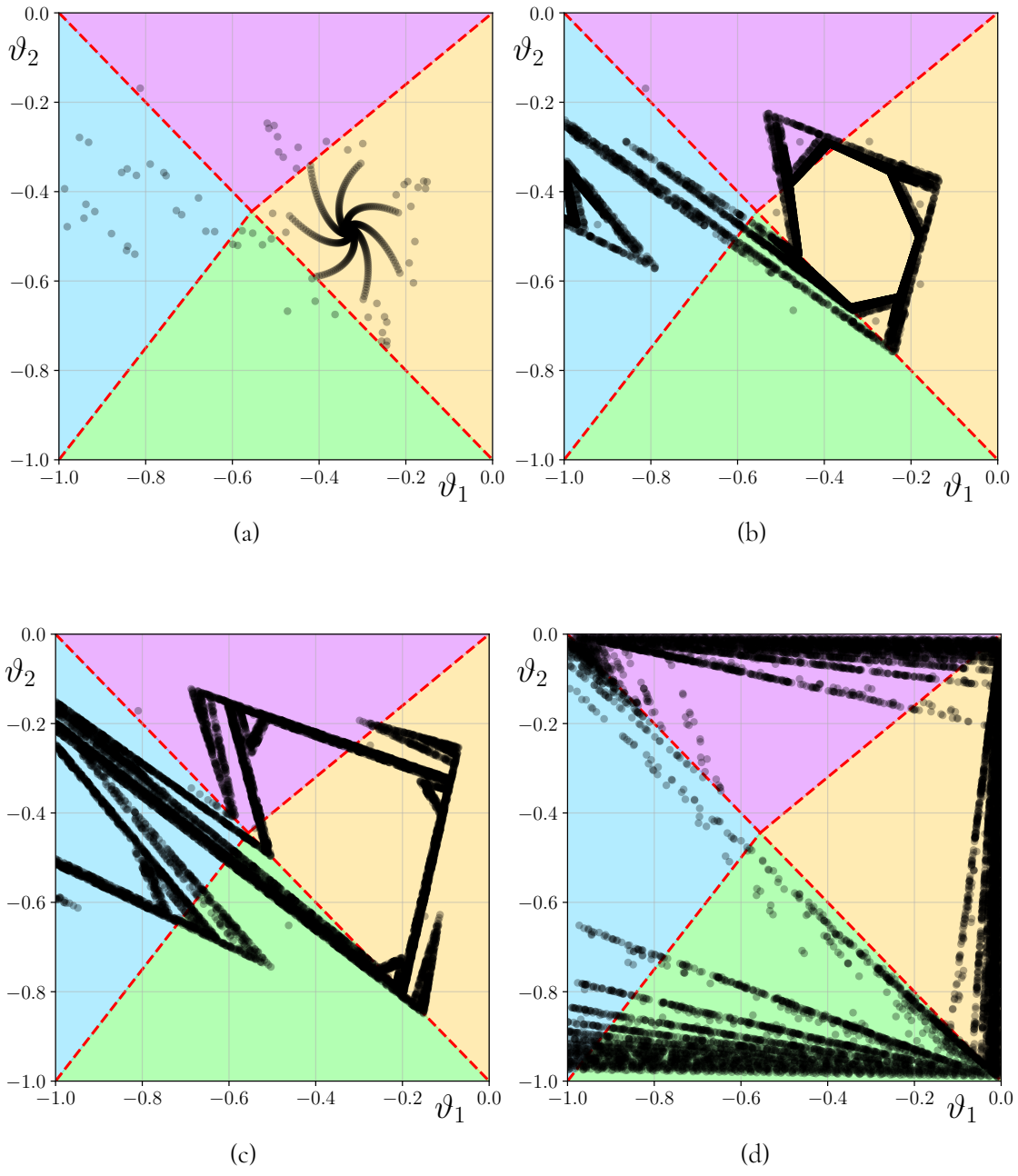

Figure 20.7: Various stages of the evolution of an attractor of f_{RPSLS} for different parameter values, which we expect is a strange attractor. The orbit in each panel begins at the same initial condition, and we plot each point in this orbit with slight transparency, so that both initial transient behaviour and the long-term attractor is apparent. In (b) to (d), the plotted orbits are calculated in regions of parameter space for which Postlethwaite and Rucklidge [PR22] observed irregular cycling near the network. In each figure, the dashed red line indicates the switching manifold, and the four domains are coloured the same as in Figure 20.4. See the text for further details. See [Gro25b] for an animated bifurcation set of the birth, evolution, and destruction of this attractor.

We present in Figure 20.7(a) the projected map for the parameter values $c_{\mathrm{A}} = 1.8$ and $c_{\mathrm{B}} = 0.671$. These parameter values are slightly larger than for the lower stability boundary of the A root sequence. We see in Figure 20.7(a) that the fixed point ϑ^*_{A} is weakly attracting, and that there is considerable initial transient dynamics.

In Figure 20.7(b), with $c_{\mathrm{B}} = 0.65$, ϑ^*_{A} has lost stability. In [PR22], Postlethwaite and Rucklidge calculate that the loss of stability of the $\mathcal{C}_{[\mathrm{A}]}$ cycle occurs in a bifurcation that corresponds to a breaking of Podvigina's first stability condition in Theorem 6.1. In particular, a complex-conjugate pair of eigenvalues now has greatest absolute value. We observe in Figure 20.7(b) that, under iteration of the projected map, the orbit is asymptotic to what appears to be a strange attractor. This attractor bears some resemblance to the attractor observed in the piecewise-affine Lozi map [Loz78]. Comparing the shape of the attracting structure in Figure 20.7(b) to the initial transient dynamics in Figure 20.7(a), we see that there are traces of this attractor, suggesting that it possibly is of saddle-type for the parameter values used in Figure 20.7(a).

In Figure 20.7(c), with $c_{\mathrm{B}} = 0.5$, we see that the strange attractor now appears larger in phase space, and has gained additional structure. Additional self-similar components of this attractor appear to form after border-collision bifurcations of the attractor. In Figure 20.7(d), we can see the beginning of the break-up of this attractor, as the network as a whole loses stability. Orbits are attracted to the boundaries of the domain S, which represent $X_{\mathrm{A}} = 0$ and $X_{\mathrm{B}} = 0$. Therefore, the expanding coordinates x_{A} and x_{B} are growing and become $\mathcal{O}(1)$, and the network is unstable.

We expect that an analysis similar to that in [SG24] will be able to prove that there exists a chaotic attractor for the region of parameter space below the region of stability of A cycling in Figure 20.2. Such a proof would in turn confirm Postlethwaite and Rucklidge's conjecture that there exists irregular cycling near the Rock–Paper–Scissors–Lizard–Spock network.

20.6 Continuity of the projected map

We conclude our study of the projected map of the Rock–Paper–Scissors–Lizard–Spock network by considering the continuity of the projected map at its switching manifold.

Recall that we set $\eta \coloneqq c_{\mathrm{A}} + c_{\mathrm{B}} + e_{\mathrm{A}} + e_{\mathrm{B}}$. First, for a point $\vartheta = (\vartheta_1, -1 - \vartheta_1) \in \Theta_{\mathrm{S}}^{\to \mathrm{A}}$, we find that

$$f_{\mathrm{A}\to\mathrm{A}}(\vartheta) = \left(\frac{-c_{\mathrm{B}}\vartheta_1}{\eta\vartheta_1 - e_{\mathrm{A}}}, \frac{-c_{\mathrm{A}}\vartheta_1}{\eta\vartheta_1 - e_{\mathrm{A}}} \right) = f_{\mathrm{B}\to\mathrm{A}}(\vartheta),$$

and for a point $\vartheta = (\vartheta_1, -1 - \vartheta_1) \in \Theta_{\mathrm{S}}^{\to \mathrm{B}}$, we find that,

$$f_{\mathrm{A}\to\mathrm{A}}(\vartheta) = \left(\frac{-(c_{\mathrm{A}} + c_{\mathrm{B}})(\vartheta_1 + 1)}{\eta(\vartheta_1 + 1) + e_{\mathrm{B}}}, \frac{(e_{\mathrm{A}} + e_{\mathrm{B}} - c_{\mathrm{B}})(\vartheta_1 + 1) - e_{\mathrm{B}}}{\eta(\vartheta_1 + 1) + e_{\mathrm{B}}} \right) = f_{\mathrm{B}\to\mathrm{A}}(\vartheta).$$

Thus, the projected map has the following continuity:[4]

$$f_{\mathrm{A}\to\mathrm{A}} \restriction \Theta_{\mathrm{S}}^{\to\mathrm{A}} = f_{\mathrm{B}\to\mathrm{A}} \restriction \Theta_{\mathrm{S}}^{\to\mathrm{A}}$$

and

$$f_{\mathrm{A}\to\mathrm{B}} \restriction \Theta_{\mathrm{S}}^{\to\mathrm{B}} = f_{\mathrm{B}\to\mathrm{B}} \restriction \Theta_{\mathrm{S}}^{\to\mathrm{B}}.$$

In Sections 11 and 12, we observed that there was continuity on a switching manifold that corresponds to an excluded cusp that divides trajectories that transition between each of the two ways around a Δ-clique. The components of the switching manifold $\Theta_{\mathrm{S}}^{\mathrm{A}\to}$ and $\Theta_{\mathrm{S}}^{\mathrm{B}\to}$ also correspond to such an excluded cusp. Therefore, we might naïvely expect that we also have continuity along the $\Theta_{\mathrm{S}}^{\mathrm{A}\to}$ and $\Theta_{\mathrm{S}}^{\mathrm{B}\to}$ switching manifolds; that is, that the following two conditions hold:

$$f_{\mathrm{A}\to\mathrm{A}} \restriction \Theta_{\mathrm{S}}^{A\to} = f_{\mathrm{A}\to\mathrm{B}} \restriction \Theta_{\mathrm{S}}^{A\to}$$

and

$$f_{\mathrm{B}\to\mathrm{A}} \restriction \Theta_{\mathrm{S}}^{B\to} = f_{\mathrm{B}\to\mathrm{B}} \restriction \Theta_{\mathrm{S}}^{A\to}.$$

These conditions, however, generically do not hold. In fact, for a point $\left(\vartheta_1, \dfrac{e_{\mathrm{A}}}{e_{\mathrm{B}}}\vartheta_1\right) \in \Theta_{\mathrm{S}}^{\mathrm{A}\to}$, we find that

$$f_{\mathrm{A}\to\mathrm{A}}(\vartheta) = \left(\frac{-(c_{\mathrm{B}} - e_{\mathrm{A}} - e_{\mathrm{B}})\vartheta_1 + e_{\mathrm{A}}}{\eta\vartheta_1 - e_A}, \frac{-c_{\mathrm{A}}\vartheta_1}{\eta\vartheta_1 - e_A}\right),$$

while

$$f_{\mathrm{A}\to\mathrm{B}}(\vartheta) = \left(-1, \frac{(c_{\mathrm{B}} - e_{\mathrm{A}} - e_{\mathrm{B}})\vartheta_1 - e_{\mathrm{A}}}{e_{\mathrm{A}} - \eta\vartheta_1}\right).$$

Moreover, for a point $\left(\vartheta_1, -1 + \dfrac{e_{\mathrm{A}}}{e_{\mathrm{B}}}(1+\vartheta_1)\right) \in \Theta_{\mathrm{S}}^{\mathrm{B}\to}$, we find that

$$f_{\mathrm{B}\to\mathrm{A}}(\vartheta) = \left(\frac{-c_{\mathrm{B}}(\vartheta_1+1)}{\eta(\vartheta_1+1) + e_B}, \frac{-\eta(\vartheta_1+1) + c_{\mathrm{B}} - e_{\mathrm{B}}}{\eta(\vartheta_1+1) + e_{\mathrm{B}}}\right),$$

while

$$f_{\mathrm{B}\to\mathrm{B}}(\vartheta) = \left(-1, \frac{-c_{\mathrm{B}}(\vartheta_1+1)}{\eta(\vartheta_1+1) - e_{\mathrm{B}}}\right).$$

In the case of the Δ-clique network in $\mathbb{R}^4$, once a trajectory has made the equivalent of a class B transition, it must then make another class B transition, as $\xi_3 \to \xi_4$ is the only outgoing heteroclinic orbit of ξ_3. However, in the case of the Rock–Paper–Scissors–Lizard–Spock network, after one B transition, a trajectory need not make another B transition and

[4] Since the notation in this section is rather involved, we write the function restriction as $f \restriction \Theta$, without the subset of the domain as a subscript for typographical clarity.

traverse the Δ-clique, but can instead make a class A transition. Only for those trajectories that do make another B transition should we expect continuity of the projected map. For a point $\left(\vartheta_1, \frac{e_{\mathrm{A}}}{e_{\mathrm{B}}}\vartheta_1\right) \in \Theta_{\mathrm{S}}^{\mathrm{A}\to}$, we find that

$$f_{\mathrm{A}\to\mathrm{A}}(\vartheta) = \left(\frac{-(c_{\mathrm{B}} - e_{\mathrm{A}} - e_{\mathrm{B}})\vartheta_1 + e_{\mathrm{A}}}{\eta\vartheta_1 - e_A}, \frac{-c_{\mathrm{A}}\vartheta_1}{\eta\vartheta_1 - e_A}\right) = (f_{\mathrm{B}\to\mathrm{B}} \circ f_{\mathrm{A}\to\mathrm{B}})(\vartheta),$$

and for a point $\left(\vartheta_1, -1 + \frac{e_{\mathrm{A}}}{e_{\mathrm{B}}}(1+\vartheta_1)\right) \in \Theta_{\mathrm{S}}^{\mathrm{B}\to}$, we find that

$$f_{\mathrm{B}\to\mathrm{A}}(\vartheta) = \left(\frac{-c_{\mathrm{B}}(\vartheta_1+1)}{\eta(\vartheta_1+1) + e_B}, \frac{-\eta(\vartheta_1+1) + c_{\mathrm{B}} - e_{\mathrm{B}}}{\eta(\vartheta_1+1) + e_{\mathrm{B}}}\right) = (f_{\mathrm{B}\to\mathrm{B}} \circ f_{\mathrm{B}\to\mathrm{B}})(\vartheta).$$

Therefore, we instead have a certain compatibility condition. Namely, the following two conditions hold

$$f_{\mathrm{A}\to\mathrm{A}} \restriction \Theta_{\mathrm{S}}^{A\to} = (f_{\mathrm{B}\to\mathrm{B}} \circ f_{\mathrm{A}\to\mathrm{B}}) \restriction \Theta_{\mathrm{S}}^{A\to}$$

and

$$f_{\mathrm{B}\to\mathrm{A}} \restriction \Theta_{\mathrm{S}}^{B\to} = (f_{\mathrm{B}\to\mathrm{B}} \circ f_{\mathrm{B}\to\mathrm{B}}) \restriction \Theta_{\mathrm{S}}^{A\to}.$$

As in the case of Podvigina's two-cycle network, we expect that an extension of the ideas in Chapter V will allow us to explain the dynamical origin behind these continuity and compatibility conditions, since there is no separatrix present like there is in the case of the Kirk–Silber network and Podvigina's two-cycle network.

VII | Discussion

Since they were first observed in 1975, the study of heteroclinic cycles and networks in dynamical systems theory has provided many interesting and challenging problems, the resolution of which has led to the development of new techniques and produced many novel results. There are many interesting questions to ask about isolated heteroclinic cycles—that is, after identifying all cycles in the same group orbit, heteroclinic cycles that are not embedded in a heteroclinic network—particularly concerning their classification and stability. Nevertheless, a trajectory's path near an attracting isolated heteroclinic cycle is always the same: all trajectories that are asymptotic to a cycle have the same itinerary, regardless of any nuances in the cycle's stability. Near a heteroclinic network, however, a trajectory's itinerary can be more complicated, and the possible itineraries that trajectories can have can vary intricately with changes in parameter values. This thesis has focussed on the dynamics of trajectories near heteroclinic networks.

In Chapter III, we introduced an extension to the study of heteroclinic networks by defining the piecewise-smooth *projected map* of a network as the induced action of the transition matrices on a codimension-one simplex. This map is defined on a cross-section near a *switching equilibrium* of the network. The primary idea of this projected map is that the analysis of a network is simplified by identifying all trajectories that are equivalent in a certain sense, even though these trajectories are disjoint orbits in phase space. The projected map allowed us to completely classify the dynamics of trajectories near the three heteroclinic networks in $\mathbb{R}^4$ with four equilibria: the Kirk–Silber, Δ-clique, and tournament networks. This analysis resolved a claim by Brannath [Bra94] that there is no regular or irregular cycling near these three networks. In particular, it is straightforward to show that, for the three net-

works we studied in Chapter III, the projected map of each network is injective and strictly increasing, and so cannot contain periodic orbits. This result confirms Brannath's conjecture *"…that there should be a quite general (but non-trivial) argument…"* [Bra94] to prove complicated switching cannot occur near these three networks. To complete this analysis, it was necessary to show that the breaking of Podvigina's stability conditions is apparent at the switching equilibrium, which is not *a priori* known to be the case. We proved that stability of a component cycle can be determined at the switching equilibrium, in particular because Podvigina's third condition for stability manifests as a *border-collision bifurcation* in the projected map.

We generalised this result in Chapter IV, and proved that if the eigenvector $w_{\max}$ of a transition matrix lies in the switching subspace, then the heteroclinic cycle is not stable; that is, a border-collision bifurcation causes stability loss of a heteroclinic cycle. This result is particularly significant, as it relates stability loss of a cycle that corresponds to the breaking of Podvigina's third stability condition to changes in the unstable manifold of an invariant structure near the network.

We focussed on the continuity or discontinuity of the projected map on its switching manifold in Chapter V. We showed that, in the case of the Kirk–Silber network, the projected map is discontinuous because a separatrix exists near the network that creates a discontinuity in the flow in the limit as a trajectory approaches the network. This discontinuity emerges at the switching manifold because evaluating the limit $\vartheta \to \vartheta_s$ requires taking the limit as a trajectory approaches the network. For the Δ-clique network, no such separatrix exists, and so the projected map is continuous at its switching manifold. We note that, as we proved in Chapter III, a trajectory is asymptotic to at most one component cycle. As such, for the three networks in $\mathbb{R}^4$ composed of only four equilibria, the continuity or discontinuity of the projected map at the switching manifold does not correspond to a qualitative difference in the long-term dynamics observed near these networks.

In Chapter VI, we considered two heteroclinic networks composed of more than four equilibria: Podvigina's two-cycle network and the Rock–Paper–Scissors–Lizard–Spock network. For both networks, we constructed a partial bifurcation set of the regions of fragmentary asymptotic stability of root sequences of regular cycling near the network. These bifurcation sets have many interesting features, most notably the presence of a Farey-like concatenation of stable root sequences, and that the stability regions of root sequences form chains in parameter space. For both networks, we constructed their projected map. In the case of the Rock–Paper–Scissors–Lizard–Spock network, this process required additional steps, due to the increased complexity of analysing the dynamics near this network. We then considered regular cycling of trajectories in these maps and observed that this cycling is realised as periodic orbits. We also considered border-collision bifurcations of these orbits. For the Rock–

Paper–Scissors–Lizard–Spock network, we observed that irregular cycling near this network appears to manifest as a strange attractor in the projected map. For both networks, we considered their continuity, observing that the projected map of Podvigina's two-cycle network is generically discontinuous. The projected map of the Rock–Paper–Scissors–Lizard–Spock network, however, is continuous on a subset of its switching manifold, and satisfies a certain compatibility condition of continuity of certain compositions that correspond to trajectories that follow a Δ-clique.

This work has allowed us to establish a future course for studying the dynamics of higher-dimensional heteroclinic networks.

For example, as a straightforward extension of the work in Chapter III, we could investigate the dynamics of the projected maps of the three networks in $\mathbb{R}^4$ that we have considered with positive transverse eigenvalues. This work would allow us to determine the nature of regular and irregular cycling near these networks which was initially considered in [CL16b].

A complete understanding of the possible dynamics of the projected map is a desirable extension of the work in Chapter IV, particularly all possible bifurcations of fixed points of the projected map. Transition matrices have a particular form, and these matrices are defined with many of the same parameters. However, it is not yet apparent what the consequences of this form are on the eigenvalues and eigenvectors of these matrices, and the resulting dynamics under iteration of the matrix. This work would require determining all possible ways in which Podvigina's stability conditions can be broken, and all other possible values of the remaining eigenvalues and eigenvectors—that is, those other than $\lambda_{\max}$ and $w_{\max}$—after such changes. It would also be desirable to understand the possible invariant structures the projected map admits. For example, it is not readily apparent what properties of the transition matrices of the Rock–Paper–Scissors–Lizard–Spock network allow for the apparent strange attractor in §20.5. A further extension of this work could involve the analysis of the projected map of a heteroclinic network that is contained in a proper subspace of a dynamical system.

A particularly exciting direction of future work is an understanding of the bifurcation structure of regular cycling near Podvigina's two-cycle network and the Rock–Paper–Scissors–Lizard–Spock network, allowing us to resolve the conjectures made about these networks. We expect to accomplish this analysis by investigating the bifurcations of periodic orbits in the projected map, for which we expect the continuity of the projected map to be important. However, as noted, this analysis requires certain advances in the theory of piecewise-smooth dynamical systems. These advances could then allow us to prove more general results regarding heteroclinic networks in higher dimensions.

With the general methodology used to construct a projected map, we could construct the projected map of many heteroclinic networks that have been studied in the literature,

such as the house network studied in [CL16b]. Moreover, with the methodology used to create the projected map of the Rock–Paper–Scissors–Lizard–Spock network, we could also define the projected map of the bowtie network [CL16b], and other networks where the switching equilibria have multiple incoming heteroclinic orbits. There are many ways to form general classes of heteroclinic networks. For example, the house network and Podvigina's network both generalise the Kirk–Silber network. We could therefore ask if there are any common features to the bifurcation sets of networks that are the union of two cycles, possibly of a different number of equilibria, joined along one—or possibly even more than one—heteroclinic orbit. We could ask if all such networks have the same bifurcation structure as Podvigina's two-cycle network, or if this structure is affected by the length of the network's component cycles and the common connections.

The continuity or discontinuity of a piecewise-smooth map on its switching manifold can greatly affect the resulting dynamics seen in the system [ZM03, BBC08, Sim10, AGS19]. For example, in piecewise-linear *continuous* maps, we often find the so-called "strings-of-sausages" [YH87, Sim17]. However, in a piecewise-smooth *discontinuous* map, the rotation numbers of periodic orbits can form a devil's staircase in parameter space. With our analysis in Chapter V, we expect that we can determine more generally the properties of a heteroclinic network that results in a discontinuous projected map, and thus how these properties also affect the nature of regular and irregular cycling near the network.

With an understanding of the dynamics possible in the projected map, how the topology of the network affects the transition matrices and therefore also the projected map, and how the topology of the network affects the continuity and more general compatibility conditions of the projected map on its switching manifold, we expect it will be possible to understand more generally the possible dynamics of trajectories near many broad classes of heteroclinic networks.

A | Numerical calculations

In this appendix, we describe in §A.2 the numerics used to produce Figure 17.3, and in §A.3 the numerics used to produce Figures 18.2 and 18.3.

§A.1 Systems of ODEs

For reference, the ODEs (16.1) with the necessary constant terms to ensure the existence of a Kirk–Silber network are

$$\begin{aligned}
\dot{x}_1 &= x_1\big(1 - \|x\|_2^2 - c_{\mathrm{B}}x_2^2 + e_{\mathrm{XA}}x_3^2 + e_{\mathrm{YA}}y_3^2\big),\\
\dot{x}_2 &= x_2\big(1 - \|x\|_2^2 + e_{\mathrm{A}}x_1^2 - c_{\mathrm{XB}}x_3^2 - c_{\mathrm{YB}}y_3^2\big),\\
\dot{x}_3 &= x_3\big(1 - \|x\|_2^2 - c_{\mathrm{AX}}x_1^2 + e_{\mathrm{BX}}x_2^2 - c_{\mathrm{YX}}y_3^2\big),\\
\dot{y}_3 &= y_3\big(1 - \|x\|_2^2 - c_{\mathrm{AY}}x_1^2 + e_{\mathrm{BY}}x_2^2 - c_{\mathrm{XY}}x_3^2\big),
\end{aligned} \tag{A.1.1}$$

where each constant is a positive real number.

The ODEs (16.1) with the necessary constant terms to ensure the existence of a Δ-clique network are

$$\begin{aligned}
\dot{x}_1 &= x_1\big(1 - \|x\|_2^2 - c_{\mathrm{B}}x_2^2 - c_{\mathrm{XA}}x_3^2 + e_{\mathrm{YA}}y_3^2\big),\\
\dot{x}_2 &= x_2\big(1 - \|x\|_2^2 + e_{\mathrm{A}}x_1^2 - c_{\mathrm{XB}}x_3^2 - c_{\mathrm{YB}}y_3^2\big),\\
\dot{x}_3 &= x_3\big(1 - \|x\|_2^2 - c_{\mathrm{AX}}x_1^2 + e_{\mathrm{BX}}x_2^2 - c_{\mathrm{YX}}y_3^2\big),\\
\dot{y}_3 &= y_3\big(1 - \|x\|_2^2 - c_{\mathrm{AY}}x_1^2 + e_{\mathrm{BY}}x_2^2 + e_{\mathrm{XY}}x_3^2\big),
\end{aligned} \tag{A.1.2}$$

where each constant is a positive real number.

§A.2 Approximation of $\theta_3^{\mathrm{out,C}}\left(\theta_3^{\mathrm{in,C}}\right)$

To derive a numerical approximation of $\theta_3^{\mathrm{out,C}}\left(\theta_3^{\mathrm{in,C}}\right)$, we begin with a point $x(0) \in \mathbf{H}_{\mathrm{C}}^{\mathrm{in,B}}$, which implies that $x_2(0) = h$ and $x_1(0) < h$. As such, $x_1(0), x_2(0) \ll 1$. To minimise round-off error when computing $\dot{x}_1$ and $\dot{x}_2$, we use the change of coordinates $X_1 \coloneqq \log x_1$ and $X_2 \coloneqq \log x_2$, and compute $\dot{X}_1$ and $\dot{X}_2$. Since $x_1(t), x_2(t) \ll 1$ while the trajectory is in a small neighbourhood of C, we can ignore them from the right-hand side of the ODEs. Thus, we have the following system of ODEs for the Kirk–Silber network

$$\begin{aligned}
\dot{X}_1 &= 1 - \left(x_3^2 + y_3^2\right) + e_{\mathrm{XA}} x_3^2 + e_{\mathrm{YA}} y_3^2, \\
\dot{X}_2 &= 1 - \left(x_3^2 + y_3^2\right) - c_{\mathrm{XB}} x_3^2 - c_{\mathrm{YB}} y_3^2, \\
\dot{x}_3 &= x_3\left(1 - \left(x_3^2 + y_3^2\right) - c_{\mathrm{YX}} y_3^2\right), \\
\dot{y}_3 &= y_3\left(1 - \left(x_3^2 + y_3^2\right) - c_{\mathrm{XY}} x_3^2\right),
\end{aligned} \tag{A.2.1}$$

and the following system of ODES for the Δ-clique network

$$\begin{aligned}
\dot{X}_1 &= 1 - \left(x_3^2 + y_3^2\right) - c_{\mathrm{XA}} x_3^2 + e_{\mathrm{YA}} y_3^2, \\
\dot{X}_2 &= 1 - \left(x_3^2 + y_3^2\right) - c_{\mathrm{XB}} x_3^2 - c_{\mathrm{YB}} y_3^2, \\
\dot{x}_3 &= x_3\left(1 - \left(x_3^2 + y_3^2\right) - c_{\mathrm{YX}} y_3^2\right), \\
\dot{y}_3 &= y_3\left(1 - \left(x_3^2 + y_3^2\right) + e_{\mathrm{XY}} x_3^2\right).
\end{aligned} \tag{A.2.2}$$

For an initial condition $(X_1(0), \log h, x_3(0), y_3(0)) \in \mathbf{H}_{\mathrm{C}}^{\mathrm{in,B}}$, with $X_1(0) < 0$, these ODEs can be integrated until $X_1 = 0$, at which time $(X_1(t), X_2(t), x_3(t), y_3(t)) \in \mathbf{H}_{\mathrm{C}}^{\mathrm{out,A}}$.

To produce Figure 17.3, we integrated (A.2.1) and (A.2.2) with a range of initial conditions. In particular, we chose first $X_1(0) \in \{-10^{-12}, -1, -2, -4, -8\}$. For each value of $X_1(0)$, we then sampled 1000 values of the angle θ_3 from the open interval $\left(\frac{\pi}{2} \cdot \frac{1}{1001}, \frac{\pi}{2} - \frac{\pi}{2} \cdot \frac{1}{1001}\right)$, in particular, setting $\theta_3^{(\ell)} = \ell \frac{\pi}{2} \cdot \frac{1}{1001}$ for all positive integers $1 \leq \ell \leq 1001$. (Note we deliberately exclude $\theta_3(0) = 0, \frac{\pi}{2}$, as we trivially know the angle on $\mathbf{H}_{\mathrm{C}}^{\mathrm{out,A}}$ in these cases.) We then used as initial conditions $x_3(0) = \cos\theta_3^{(\ell)}$ and $y_3(0) = \sin\theta_3^{(\ell)}$.

We used the eighth-order Dormand-Prince method [HNW08, § II.5] of the Python scientific computing library SciPy [VGO20] to integrate the ODES (A.2.1) and (A.2.2) with these initial conditions until the solver detected that $X_1(t) = 0$ at $t = T_C$. We then calculated $\theta_3(T_C) \coloneqq \arctan \frac{y_3(T_C)}{x_3(T_C)}$. The results, plotting $\theta_3(T_C)$ against the initial angle $\theta_3^{(\ell)}$, are

shown in Figure 17.3.

§A.3 Approximations of $f_{\mathrm{KS}}^{(k)}$ and $f_{\Delta}^{(k)}$

For a given $k > 1$, we begin with a subset of 50 equispaced points in $S^{(k)}$ defined by

$$\left\{ X_3^{(\ell)} = \frac{k}{51}\ell \;\middle|\; 1 \leq \ell \leq 50 \right\}.$$

The point $\left(X_3^{(\ell)}, Y_3^{(\ell)}\right) \in S^{(k)}$, where $Y_3^{(\ell)} = -k - X_3^{(\ell)}$, lies on $\mathbf{H}_{\mathrm{B}}^{\mathrm{in,A}}$ expressed in logarithmic coordinates. Therefore, as an initial condition, we know for that point that $x_1(0) = h$ and $|x_2(0) - h| = 0$. For Figure 18.2, we used $h = 10^{-2}$, and, for simplicity, we chose $x_2(0) = 1$.

To minimise round-off error, we integrate the ODEs (A.1.1) and (A.1.2) in logarithmic coordinates, with the initial condition $X(0) = \left(\log 10^{-2}, 0, X_3^{(\ell)}, Y_3^{(\ell)}\right)$. Again, we used the eighth-order Dormand-Prince method of SciPy until the solver detected that the trajectory intersected $\mathbf{H}_{\mathrm{B}}^{\mathrm{in,A}}$ again. This intersection point is a numerical approximation of (X_3', Y_3'). The projection $\Pi^{(k)}$ of this point was then calculated. This projection provided a numerical approximation of $f_{\mathrm{KS}}^{(k)}$ or $f_{\Delta}^{(k)}$ at the point $\vartheta = X_3^{(\ell)}$. We last rescaled the set $S^{(k)}$ to unit length. These numerical approximations are presented in Figures 18.2 and 18.3.

We note that a point $\left(X_3^{(\ell)}, Y_3^{(\ell)}\right) \in S^{(k)}$ may satisfy either $\exp X_3^{(\ell)} > \log h$ or $\exp Y_3^{(\ell)} > \log h$, in which case the point is not actually in $\mathbf{H}_{\mathrm{B}}^{\mathrm{in,A}}$. If this is the case, we exclude the point from consideration as they are not in the set $T^{(k)}$. For this reason, the domain of $f^{(k)}$ lengthens as k increases.

B | Expressions and parameter values

§B.1 Transition matrices of heteroclinic networks in $\mathbb{R}^4$

We list all basic transition matrices and relevant full transition matrices used in the analysis of the three networks we study. Recall that the basic transition matrices have the notation $m_{ijk} = M(\varphi_{ijk})$, and the full transition matrices have the notation $M_j^{(k)} = M(\Phi_j^{(k)})$. The basic maps $\varphi_{ijk} \colon \mathbf{H}_j^{\text{in},i} \to \mathbf{H}_k^{\text{in},j}$ are the maps between successive incoming cross-sections in a cycle, and the full return maps $\Phi_j^{(k)} \colon \mathbf{H}_j^{\text{in},i} \to \mathbf{H}_j^{\text{in},i}$ are the maps from the incoming cross-section of an equilibrium ξ_j to itself, around the $\mathcal{C}_{[k]}$ cycle. The full return maps are the composition of basic maps, and so the full transition matrices are the product of basic transition matrices.

B.1.1 The Kirk–Silber network

The basic transition matrices of the Kirk–Silber network are

$$m_{312} = \begin{pmatrix} \frac{c_{13}}{e_{12}} & 0 \\ \frac{c_{14}}{e_{12}} & 1 \end{pmatrix}, \qquad m_{123} = \begin{pmatrix} \frac{c_{21}}{e_{23}} & 0 \\ -\frac{e_{24}}{e_{23}} & 1 \end{pmatrix}, \qquad m_{231} = \begin{pmatrix} \frac{c_{32}}{e_{31}} & 0 \\ \frac{t_{34}}{e_{31}} & 1 \end{pmatrix},$$

$$m_{412} = \begin{pmatrix} \frac{c_{13}}{e_{12}} & 1 \\ \frac{c_{14}}{e_{12}} & 0 \end{pmatrix}, \qquad m_{124} = \begin{pmatrix} 0 & \frac{c_{21}}{e_{24}} \\ 1 & -\frac{e_{23}}{e_{24}} \end{pmatrix}, \qquad m_{241} = \begin{pmatrix} \frac{c_{42}}{e_{41}} & 0 \\ \frac{t_{43}}{e_{41}} & 1 \end{pmatrix}.$$

The relevant full transition matrices of the Kirk–Silber network are

$$M_3 \equiv M_2^{(3)} = m_{312}m_{231}m_{123} = \begin{pmatrix} \delta_3 & 0 \\ \rho_3 & 1 \end{pmatrix},$$

and

$$M_4 \equiv M_2^{(4)} = m_{412}m_{241}m_{124} = \begin{pmatrix} 1 & \rho_4 \\ 0 & \delta_4 \end{pmatrix},$$

where

$$\begin{aligned} \delta_3 =& \frac{c_{13}c_{21}c_{32}}{e_{12}e_{23}e_{31}} > 0, \\ \delta_4 =& \frac{c_{14}c_{21}c_{42}}{e_{12}e_{24}e_{41}} > 0, \\ \rho_3 =& -\frac{e_{24}}{e_{23}} + \frac{c_{21}t_{34}}{e_{23}e_{31}} + \frac{c_{14}c_{21}c_{32}}{e_{12}e_{23}e_{31}}, \end{aligned}$$

and

$$\rho_4 = -\frac{e_{23}}{e_{24}} + \frac{c_{21}t_{43}}{e_{24}e_{41}} + \frac{c_{13}c_{21}c_{42}}{e_{12}e_{24}e_{41}}.$$

From the full transition matrices

$$M_3^{(3)} = m_{123}m_{312}m_{231}$$

and

$$M_4^{(4)} = m_{124}m_{412}m_{241}$$

we derive

$$\nu_3 = \frac{t_{34}}{e_{31}} + \frac{c_{14}c_{32}}{e_{12}e_{31}} - \frac{c_{13}c_{32}e_{24}}{e_{12}e_{23}e_{31}}$$

and

$$\nu_4 = \frac{t_{43}}{e_{41}} + \frac{c_{13}c_{42}}{e_{12}e_{41}} - \frac{c_{14}c_{42}e_{23}}{e_{12}e_{24}e_{41}}.$$

The remaining full transition matrices are the products

$$M_1^{(3)} = m_{231}m_{123}m_{312}$$

and

$$M_1^{(4)} = m_{241}m_{124}m_{412}$$

B.1.2 The Δ-clique network

The basic transition matrices of the Δ-clique network are

$$m_{412} = \begin{pmatrix} \frac{t_{13}}{e_{12}} & 1 \\ \frac{c_{14}}{e_{12}} & 0 \end{pmatrix}, \qquad m_{123} = \begin{pmatrix} \frac{c_{21}}{e_{23}} & 0 \\ -\frac{e_{24}}{e_{23}} & 1 \end{pmatrix}, \qquad m_{124} = \begin{pmatrix} 0 & -\frac{e_{23}}{e_{24}} \\ 1 & \frac{c_{21}}{e_{24}} \end{pmatrix},$$

$$m_{234} = \begin{pmatrix} 1 & \frac{t_{31}}{e_{34}} \\ 0 & \frac{c_{32}}{e_{34}} \end{pmatrix}, \qquad m_{241} = \begin{pmatrix} \frac{c_{42}}{e_{41}} & 0 \\ \frac{c_{43}}{e_{41}} & 1 \end{pmatrix}, \qquad m_{341} = \begin{pmatrix} \frac{c_{42}}{e_{41}} & 1 \\ \frac{c_{43}}{e_{41}} & 0 \end{pmatrix}.$$

The relevant full transition matrices of the Δ-clique network are

$$M_{34} \equiv M_2^{(34)} = m_{412}m_{341}m_{234}m_{123} = \begin{pmatrix} \alpha_1 & \alpha_2 \\ \alpha_3 & \alpha_4 \end{pmatrix},$$

and

$$M_4 \equiv M_2^{(4)} = m_{412}m_{241}m_{124} = \begin{pmatrix} 1 & \rho_4 \\ 0 & \delta_4 \end{pmatrix},$$

where

$$\begin{aligned}
\alpha_1 &= \frac{c_{21}c_{43}}{e_{23}e_{41}} + \frac{c_{21}c_{42}t_{13}}{e_{23}e_{41}e_{12}} - \frac{c_{32}e_{24}t_{13}}{e_{34}e_{23}e_{12}} - \frac{c_{43}e_{24}t_{31}}{e_{41}e_{23}e_{34}} - \frac{c_{42}e_{24}t_{13}t_{31}}{e_{41}e_{23}e_{12}e_{34}}, \\
\alpha_2 &= \frac{c_{32}t_{13}}{e_{34}e_{12}} + \frac{c_{43}t_{31}}{e_{41}e_{34}} + \frac{c_{42}t_{13}t_{31}}{e_{41}e_{12}e_{34}}, \\
\alpha_3 &= \frac{c_{14}c_{21}c_{42}}{e_{12}e_{23}e_{41}} - \frac{c_{14}c_{32}e_{24}}{e_{12}e_{34}e_{23}} - \frac{c_{14}c_{42}e_{24}t_{31}}{e_{12}e_{41}e_{23}e_{34}}, \\
\alpha_4 &= \frac{c_{14}c_{32}}{e_{12}e_{34}} + \frac{c_{14}c_{42}t_{31}}{e_{12}e_{41}e_{34}},
\end{aligned}$$

and

$$\rho_4 = -\frac{e_{23}}{e_{24}} + \frac{c_{21}c_{43}}{e_{24}e_{41}} + \frac{c_{21}c_{42}t_{13}}{e_{24}e_{41}e_{12}},$$

and δ_4 is the same as for the Kirk–Silber network. The remaining full transition matrices of the Δ-clique network can be found by evaluating the following products:

$$\begin{aligned} M_1^{(34)} &= m_{341}m_{234}m_{123}m_{412}, \\ M_3^{(34)} &= m_{123}m_{412}m_{341}m_{234}, \\ M_4^{(34)} &= m_{234}m_{123}m_{412}m_{341}, \\ M_1^{(4)} &= m_{241}m_{124}m_{412}, \end{aligned}$$

and

$$M_4^{(4)} = m_{124}m_{412}m_{241}.$$

From $M_4^{(4)}$, we obtain the expression

$$\nu_4 = \frac{c_{43}}{e_{41}} + \frac{c_{42}t_{13}}{e_{41}e_{12}} - \frac{c_{14}c_{42}e_{23}}{e_{12}e_{41}e_{24}}.$$

B.1.3 The tournament network

The basic transition matrices of the tournament network are

$$m_{312} = \begin{pmatrix} \frac{c_{13}}{e_{12}} & 0 \\ \frac{c_{14}}{e_{12}} & 1 \end{pmatrix}, \; m_{123} = \begin{pmatrix} \frac{c_{21}}{e_{23}} & 0 \\ -\frac{e_{24}}{e_{23}} & 1 \end{pmatrix}, \; m_{231} = \begin{pmatrix} \frac{c_{32}}{e_{31}} & 0 \\ -\frac{e_{34}}{e_{31}} & 1 \end{pmatrix}, \; m_{234} = \begin{pmatrix} 1 & \frac{c_{32}}{e_{31}} \\ 0 & -\frac{e_{34}}{e_{31}} \end{pmatrix},$$

$$m_{412} = \begin{pmatrix} \frac{c_{13}}{e_{12}} & 1 \\ \frac{c_{14}}{e_{12}} & 0 \end{pmatrix}, \; m_{124} = \begin{pmatrix} 0 & \frac{c_{21}}{e_{24}} \\ 1 & -\frac{c_{23}}{e_{24}} \end{pmatrix}, \; m_{241} = \begin{pmatrix} \frac{c_{42}}{e_{41}} & 0 \\ \frac{c_{43}}{e_{41}} & 1 \end{pmatrix}, \; m_{341} = \begin{pmatrix} \frac{c_{42}}{e_{41}} & 1 \\ \frac{c_{43}}{e_{41}} & 0 \end{pmatrix}.$$

The relevant full transition matrices of the tournament network are

$$M_3 \equiv M_2^{(3)} = m_{312}m_{231}m_{123} = \begin{pmatrix} \delta_3 & 0 \\ \rho_3 & 1 \end{pmatrix},$$

$$M_{34} \equiv M_2^{(34)} = m_{412}m_{341}m_{234}m_{123} = \begin{pmatrix} \alpha_1 & \alpha_2 \\ \alpha_3 & \alpha_4 \end{pmatrix},$$

and

$$M_4 \equiv M_2^{(4)} = m_{412}m_{241}m_{124} = \begin{pmatrix} 1 & \rho_4 \\ 0 & \delta_4 \end{pmatrix},$$

where

$$\begin{aligned}
\alpha_1 &= \frac{c_{21}c_{43}}{e_{23}e_{41}} + \frac{c_{13}c_{21}c_{42}}{e_{12}e_{23}e_{41}} + \frac{c_{43}e_{24}e_{31}}{e_{41}e_{23}e_{34}} + \frac{c_{13}c_{42}e_{24}e_{31}}{e_{12}e_{41}e_{23}e_{34}} - \frac{c_{13}c_{32}e_{24}}{e_{12}e_{34}e_{23}},\\
\alpha_2 &= \frac{c_{32}c_{13}}{e_{12}e_{34}} - \frac{c_{43}e_{31}}{e_{41}e_{34}} - \frac{c_{13}c_{42}e_{31}}{e_{12}e_{41}e_{34}},\\
\alpha_3 &= \frac{c_{14}c_{21}c_{42}}{e_{12}e_{23}e_{41}} + \frac{c_{14}c_{42}e_{24}e_{31}}{e_{12}e_{41}e_{23}e_{34}} - \frac{c_{14}c_{32}e_{24}}{e_{12}e_{34}e_{23}},\\
\alpha_4 &= \frac{c_{14}c_{32}}{e_{12}e_{34}} - \frac{c_{14}c_{42}e_{31}}{e_{12}e_{41}e_{34}},\\
\rho_3 &= -\frac{e_{23}}{e_{23}} - \frac{c_{21}c_{34}}{e_{24}e_{31}} + \frac{c_{14}c_{21}c_{32}}{e_{12}e_{23}e_{31}},
\end{aligned}$$

and

$$\rho_4 = -\frac{e_{23}}{e_{24}} + \frac{c_{21}c_{43}}{e_{24}e_{41}} + \frac{c_{13}c_{21}c_{42}}{e_{12}e_{24}e_{41}},$$

and δ_3 and δ_4 are the same as for the Kirk–Silber network. The remaining full transition matrices of the tournament network can be found by evaluating the following products:

$$\begin{aligned}
M_1^{(3)} &= m_{123}m_{312}m_{231},\\
M_3^{(3)} &= m_{123}m_{312}m_{231},\\
M_1^{(34)} &= m_{341}m_{234}m_{123}m_{412},\\
M_3^{(34)} &= m_{123}m_{412}m_{341}m_{234},\\
M_4^{(34)} &= m_{234}m_{123}m_{412}m_{341},\\
M_1^{(4)} &= m_{241}m_{124}m_{412},
\end{aligned}$$

and

$$M_4^{(4)} = m_{124}m_{412}m_{241}.$$

From $M_1^{(3)}$ and $M_4^{(4)}$, we obtain, respectively, the expressions,

$$\mu_3 = \frac{c_{14}}{e_{12}} - \frac{c_{13}e_{24}}{e_{12}e_{23}} - \frac{c_{13}c_{21}e_{34}}{e_{12}e_{23}e_{34}},$$

and

$$\nu_4 = \frac{c_{43}}{e_{41}} + \frac{c_{13}c_{42}}{e_{12}e_{41}} - \frac{c_{14}c_{42}e_{23}}{e_{12}e_{41}e_{24}}.$$

§B.2 Transition matrices of Podvigina's two-cycle network

The basic transition matrices for Podvigina's two-cycle network are:

$$m_{123} = \begin{pmatrix} \frac{t_{24}}{e_{23}} & 1 & 0 & 0 \\ \frac{c_{21}}{e_{23}} & 0 & 0 & 0 \\ -\frac{e_{25}}{e_{23}} & 0 & 1 & 0 \\ \frac{t_{26}}{e_{23}} & 0 & 0 & 1 \end{pmatrix}, \qquad m_{125} = \begin{pmatrix} 0 & 0 & \frac{t_{26}}{e_{25}} & 1 \\ 0 & 0 & \frac{c_{21}}{e_{25}} & 0 \\ 1 & 0 & -\frac{e_{23}}{e_{25}} & 0 \\ 0 & 1 & \frac{t_{24}}{e_{25}} & 0 \end{pmatrix},$$

$$m_{234} = \begin{pmatrix} \frac{t_{31}}{e_{34}} & 1 & 0 & 0 \\ \frac{c_{32}}{e_{34}} & 0 & 0 & 0 \\ \frac{t_{35}}{e_{34}} & 0 & 1 & 0 \\ \frac{t_{36}}{e_{34}} & 0 & 0 & 1 \end{pmatrix}, \qquad m_{256} = \begin{pmatrix} \frac{t_{51}}{e_{56}} & 1 & 0 & 0 \\ \frac{c_{52}}{e_{56}} & 0 & 0 & 0 \\ \frac{t_{53}}{e_{56}} & 0 & 1 & 0 \\ \frac{t_{54}}{e_{56}} & 0 & 0 & 1 \end{pmatrix},$$

$$m_{341} = \begin{pmatrix} \frac{t_{42}}{e_{41}} & 1 & 0 & 0 \\ \frac{c_{43}}{e_{41}} & 0 & 0 & 0 \\ \frac{t_{45}}{e_{41}} & 0 & 1 & 0 \\ \frac{t_{46}}{e_{41}} & 0 & 0 & 1 \end{pmatrix}, \qquad m_{561} = \begin{pmatrix} \frac{t_{62}}{e_{61}} & 1 & 0 & 0 \\ \frac{t_{63}}{e_{61}} & 0 & 1 & 0 \\ \frac{t_{64}}{e_{61}} & 0 & 0 & 1 \\ \frac{c_{65}}{e_{61}} & 0 & 0 & 0 \end{pmatrix},$$

$$m_{412} = \begin{pmatrix} \frac{t_{13}}{e_{12}} & 1 & 0 & 0 \\ \frac{c_{14}}{e_{12}} & 0 & 0 & 0 \\ \frac{t_{15}}{e_{12}} & 0 & 1 & 0 \\ \frac{c_{16}}{e_{12}} & 0 & 0 & 1 \end{pmatrix}, \qquad m_{614} = \begin{pmatrix} \frac{t_{13}}{e_{12}} & 1 & 0 & 0 \\ \frac{c_{14}}{e_{12}} & 0 & 1 & 0 \\ \frac{t_{15}}{e_{12}} & 0 & 0 & 1 \\ \frac{c_{16}}{e_{12}} & 0 & 0 & 0 \end{pmatrix}.$$

The full transition matrices of the network are then:

$$
\begin{aligned}
M_1^{(\mathrm{L})} &= m_{341}m_{234}m_{123}m_{412}, & M_1^{(\mathrm{R})} &= m_{561}m_{256}m_{125}m_{612},\\
M_2^{(\mathrm{L})} &= m_{412}m_{341}m_{234}m_{123}, & M_2^{(\mathrm{R})} &= m_{612}m_{561}m_{256}m_{125},\\
M_3^{(\mathrm{L})} &= m_{123}m_{412}m_{341}m_{234}, & M_5^{(\mathrm{R})} &= m_{125}m_{612}m_{561}m_{256},\\
M_4^{(\mathrm{L})} &= m_{234}m_{123}m_{412}m_{341}, & M_6^{(\mathrm{R})} &= m_{256}m_{125}m_{612}m_{561}.
\end{aligned}
$$

The expressions for the α_{jk} of $M_{\mathrm{L}} \equiv M_2^{(\mathrm{L})}$ in (19.2) are:

$$
\begin{aligned}
\alpha_{11} &= \frac{c_{21}c_{43}e_{12}e_{34} + c_{21}e_{34}t_{13}t_{42} + c_{32}e_{41}t_{13}t_{24} + c_{43}e_{12}t_{24}t_{31} + t_{13}t_{24}t_{31}t_{42}}{e_{12}e_{23}e_{34}e_{41}},\\
\alpha_{12} &= \frac{c_{32}e_{41}t_{13} + c_{43}e_{12}t_{31} + t_{13}t_{31}t_{42}}{e_{12}e_{34}e_{41}},\\
\alpha_{21} &= \frac{c_{14}(c_{21}e_{34}t_{42} + c_{32}e_{41}t_{24} + t_{24}t_{31}t_{42})}{e_{12}e_{23}e_{34}e_{41}},\\
\alpha_{22} &= \frac{c_{14}(c_{32}e_{41} + t_{31}t_{42})}{e_{12}e_{34}e_{41}},\\
\alpha_{31} &= \frac{A_{31}}{e_{12}e_{23}e_{34}e_{41}},
\end{aligned}
$$

where

$$
\begin{aligned}
A_{31} &= c_{21}e_{12}e_{34}t_{45} + c_{21}e_{34}t_{15}t_{42} + c_{32}e_{41}t_{15}t_{24} - e_{12}e_{25}e_{34}e_{41} + e_{12}e_{41}t_{24}t_{35} +\\
&\quad e_{12}t_{24}t_{31}t_{45} + t_{15}t_{24}t_{31}t_{42},\\
\alpha_{32} &= \frac{c_{32}e_{41}t_{15} + e_{12}e_{41}t_{35} + e_{12}t_{31}t_{45} + t_{15}t_{31}t_{42}}{e_{12}e_{34}e_{41}},\\
\alpha_{41} &= \frac{A_{41}}{e_{12}e_{23}e_{34}e_{41}},
\end{aligned}
$$

where

$$
\begin{aligned}
A_{41} &= c_{16}c_{21}e_{34}t_{42} + c_{16}c_{32}e_{41}t_{24} + c_{16}t_{24}t_{31}t_{42} + c_{21}e_{12}e_{34}t_{46} + e_{12}e_{34}e_{41}t_{26} +\\
&\quad e_{12}e_{41}t_{24}t_{36} + e_{12}t_{24}t_{31}t_{46},\\
\alpha_{41} &= \frac{c_{16}c_{32}e_{41} + c_{16}t_{31}t_{42} + e_{12}e_{41}t_{36} + e_{12}t_{31}t_{46}}{e_{12}e_{34}e_{41}}.
\end{aligned}
$$

The expressions for the β_{jk} of $M_{\rm R} \equiv M_2^{(\rm R)}$ in (19.3) are:

$$\beta_{13} = \frac{B_{13}}{e_{12}e_{25}e_{56}e_6},$$

where

$$\begin{aligned} B_{13} &= c_{21}e_{12}e_{56}t_{63} + c_{21}e_{56}t_{13}t_{62} + c_{52}e_{61}t_{13}t_{26} - e_{12}e_{23}e_{56}e_{61} + e_{12}e_{61}t_{26}t_{53} + \\ &\quad e_{12}t_{26}t_{51}t_{63} + t_{13}t_{26}t_{51}t_{62}, \\ \beta_{14} &= \frac{c_{52}e_{61}t_{13} + e_{12}e_{61}t_{53} + e_{12}t_{51}t_{63} + t_{13}t_{51}t_{62}}{e_{12}e_{56}e_{61}}, \\ \beta_{23} &= \frac{B_{23}}{e_{12}e_{25}e_{56}e_{61}}, \end{aligned}$$

where

$$\begin{aligned} B_{23} &= c_{14}c_{21}e_{56}t_{62} + c_{14}c_{52}e_{61}t_{26} + c_{14}t_{26}t_{51}t_{62} + c_{21}e_{12}e_{56}t_{64} + e_{12}e_{56}e_{61}t_{24} + \\ &\quad e_{12}e_{61}t_{26}t_{54} + e_{12}t_{26}t_{51}t_{64}, \\ \beta_{24} &= \frac{c_{14}c_{52}e_{61} + c_{14}t_{51}t_{62} + e_{12}e_{61}t_{54} + e_{12}t_{51}t_{64}}{e_{12}e_{56}e_{61}}, \\ \beta_{33} &= \frac{c_{21}c_{65}e_{12}e_{56} + c_{21}e_{56}t_{15}t_{62} + c_{52}e_{61}t_{15}t_{26} + c_{65}e_{12}t_{26}t_{51} + t_{15}t_{26}t_{51}t_{62}}{e_{12}e_{25}e_{56}e_{61}}, \\ \beta_{34} &= \frac{c_{52}e_{61}t_{15} + c_{65}e_{12}t_{51} + t_{15}t_{51}t_{62}}{e_{12}e_{56}e_{61}}, \\ \beta_{43} &= \frac{c_{16}(c_{21}e_{56}t_{62} + c_{52}e_{61}t_{26} + t_{26}t_{51}t_{62})}{e_{12}e_{25}e_{56}e_{61}}, \\ \beta_{44} &= \frac{c_{16}(c_{52}e_{61} + t_{51}t_{62})}{e_{12}e_{56}e_{61}}. \end{aligned}$$

§B.3 Continuity of the projected map of Podvigina's two-cycle network

For a point $\vartheta_{\mathrm{s}} = \left(\vartheta_1, \vartheta_2, \dfrac{e_{\mathrm{L}}}{e_{\mathrm{R}}}\vartheta_1\right) \in \Theta_{\mathrm{S}}$, we have the following expressions for each component of each piece of the projected map f_{Pod}:

$$
\begin{aligned}
f_{\mathrm{L}}^{(1)}(\vartheta_{\mathrm{s}}) = &-(c_{21}c_{43}e_{12}e_{34}\vartheta_1 + c_{32}e_{23}e_{41}t_{13}\vartheta_2 + c_{43}e_{12}e_{23}t_{31}\vartheta_2 + c_{21}e_{34}t_{13}t_{42}\vartheta_1 + \\
&c_{32}e_{41}t_{13}t_{24}\vartheta_1 + c_{43}e_{12}t_{24}t_{31}\vartheta_1 + e_{23}t_{13}t_{31}t_{42}\vartheta_2 + t_{13}t_{24}t_{31}t_{42}\vartheta_1),\\
f_{\mathrm{L}}^{(2)}(\vartheta_{\mathrm{s}}) = &-c_{14}(c_{32}e_{23}e_{41}\vartheta_2 + c_{21}e_{34}t_{42}\vartheta_1 + c_{32}e_{41}t_{24}\vartheta_1 + e_{23}t_{31}t_{42}\vartheta_2 + t_{24}t_{31}t_{42}\vartheta_1),\\
f_{\mathrm{L}}^{(3)}(\vartheta_{\mathrm{s}}) = &-(c_{21}e_{12}e_{34}t_{45}\vartheta_1 + c_{32}e_{23}e_{41}t_{15}\vartheta_2 + e_{12}e_{23}e_{41}t_{35}\vartheta_2 + c_{21}e_{34}t_{15}t_{42}\vartheta_1 + \\
&c_{32}e_{41}t_{15}t_{24}\vartheta_1 + e_{12}e_{23}t_{31}t_{45}\vartheta_2 + e_{12}e_{41}t_{24}t_{35}\vartheta_1 + e_{12}t_{24}t_{31}t_{45}\vartheta_1 + \\
&e_{23}t_{15}t_{31}t_{42}\vartheta_2 + t_{15}t_{24}t_{31}t_{42}\vartheta_1),
\end{aligned}
$$

where

$$
\begin{aligned}
D_{\mathrm{L}}(\vartheta_{\mathrm{s}}) = {} & c_{21}c_{43}e_{12}e_{34}\vartheta_1 - e_{12}e_{23}e_{34}e_{41} + c_{14}c_{32}e_{23}e_{41}\vartheta_2 + c_{16}c_{32}e_{23}e_{41}\vartheta_2 - \\
& e_{12}e_{23}e_{34}e_{41}\vartheta_1 - e_{12}e_{23}e_{34}e_{41}\vartheta_2 - e_{12}e_{25}e_{34}e_{41}\vartheta_1 + c_{14}c_{21}e_{34}t_{42}\vartheta_1 + c_{14}c_{32}e_{41}t_{24}\vartheta_1 + \\
& c_{16}c_{21}e_{34}t_{42}\vartheta_1 + c_{16}c_{32}e_{41}t_{24}\vartheta_1 + c_{32}e_{23}e_{41}t_{13}\vartheta_2 + c_{43}e_{12}e_{23}t_{31}\vartheta_2 + c_{21}e_{12}e_{34}t_{45}\vartheta_1 + \\
& c_{32}e_{23}e_{41}t_{15}\vartheta_2 + c_{21}e_{12}e_{34}t_{46}\vartheta_1 + e_{12}e_{23}e_{41}t_{35}\vartheta_2 + e_{12}e_{23}e_{41}t_{36}\vartheta_2 + e_{12}e_{34}e_{41}t_{26}\vartheta_1 + \\
& c_{21}e_{34}t_{13}t_{42}\vartheta_1 + c_{32}e_{41}t_{13}t_{24}\vartheta_1 + c_{43}e_{12}t_{24}t_{31}\vartheta_1 + c_{14}e_{23}t_{31}t_{42}\vartheta_2 + c_{21}e_{34}t_{15}t_{42}\vartheta_1 + \\
& c_{32}e_{41}t_{15}t_{24}\vartheta_1 + c_{16}e_{23}t_{31}t_{42}\vartheta_2 + e_{12}e_{23}t_{31}t_{45}\vartheta_2 + e_{12}e_{41}t_{24}t_{35}\vartheta_1 + e_{12}e_{23}t_{31}t_{46}\vartheta_2 + \\
& e_{12}e_{41}t_{24}t_{36}\vartheta_1 + c_{14}t_{24}t_{31}t_{42}\vartheta_1 + c_{16}t_{24}t_{31}t_{42}\vartheta_1 + e_{23}t_{13}t_{31}t_{42}\vartheta_2 + e_{12}t_{24}t_{31}t_{45}\vartheta_1 + \\
& e_{23}t_{15}t_{31}t_{42}\vartheta_2 + e_{12}t_{24}t_{31}t_{46}\vartheta_1 + t_{13}t_{24}t_{31}t_{42}\vartheta_1 + t_{15}t_{24}t_{31}t_{42}\vartheta_1.
\end{aligned}
$$

However,

$$
\begin{aligned}
f_{\mathrm{R}}^{(1)}(\vartheta_{\mathrm{s}}) = -(&c_{52}e_{23}e_{61}t_{13} + e_{12}e_{23}e_{61}t_{53} + e_{12}e_{23}t_{51}t_{63} + e_{23}t_{13}t_{51}t_{62} + c_{52}e_{23}e_{61}t_{13}\vartheta_1 + \\
&c_{52}e_{23}e_{61}t_{13}\vartheta_2 + c_{52}e_{25}e_{61}t_{13}\vartheta_1 - c_{21}e_{12}e_{56}t_{63}\vartheta_1 + e_{12}e_{23}e_{61}t_{53}\vartheta_1 + e_{12}e_{23}e_{61}t_{53}\vartheta_2 + \\
&e_{12}e_{25}e_{61}t_{53}\vartheta_1 - c_{21}e_{56}t_{13}t_{62}\vartheta_1 - c_{52}e_{61}t_{13}t_{26}\vartheta_1 + e_{12}e_{23}t_{51}t_{63}\vartheta_1 + e_{12}e_{23}t_{51}t_{63}\vartheta_2 + \\
&e_{12}e_{25}t_{51}t_{63}\vartheta_1 - e_{12}e_{61}t_{26}t_{53}\vartheta_1 + e_{23}t_{13}t_{51}t_{62}\vartheta_1 + e_{23}t_{13}t_{51}t_{62}\vartheta_2 + e_{25}t_{13}t_{51}t_{62}\vartheta_1 - \\
&e_{12}t_{26}t_{51}t_{63}\vartheta_1 - t_{13}t_{26}t_{51}t_{62}\vartheta_1), \\
f_{\mathrm{R}}^{(2)}(\vartheta_{\mathrm{s}}) = -(&c_{14}e_{23}t_{51}t_{62} + e_{12}e_{23}e_{61}t_{54} + e_{12}e_{23}t_{51}t_{64} + c_{14}c_{52}e_{23}e_{61} + c_{14}c_{52}e_{23}e_{61}\vartheta_1 + \\
&c_{14}c_{52}e_{23}e_{61}\vartheta_2 + c_{14}c_{52}e_{25}e_{61}\vartheta_1 - e_{12}e_{23}e_{56}e_{61}\vartheta_2 - c_{14}c_{21}e_{56}t_{62}\vartheta_1 - c_{14}c_{52}e_{61}t_{26}\vartheta_1 - \\
&c_{21}e_{12}e_{56}t_{64}\vartheta_1 + e_{12}e_{23}e_{61}t_{54}\vartheta_1 + e_{12}e_{23}e_{61}t_{54}\vartheta_2 + e_{12}e_{25}e_{61}t_{54}\vartheta_1 - e_{12}e_{56}e_{61}t_{24}\vartheta_1 + \\
&c_{14}e_{23}t_{51}t_{62}\vartheta_1 + c_{14}e_{23}t_{51}t_{62}\vartheta_2 + c_{14}e_{25}t_{51}t_{62}\vartheta_1 + e_{12}e_{23}t_{51}t_{64}\vartheta_1 + e_{12}e_{23}t_{51}t_{64}\vartheta_2 + \\
&e_{12}e_{25}t_{51}t_{64}\vartheta_1 - e_{12}e_{61}t_{26}t_{54}\vartheta_1 - c_{14}t_{26}t_{51}t_{62}\vartheta_1 - e_{12}t_{26}t_{51}t_{64}\vartheta_1), \\
f_{\mathrm{R}}^{(3)}(\vartheta_{\mathrm{s}}) = -(&c_{52}e_{23}e_{61}t_{15} + c_{65}e_{12}e_{23}t_{51} + e_{23}t_{15}t_{51}t_{62} - c_{21}c_{65}e_{12}e_{56}\vartheta_1 + \\
&c_{52}e_{23}e_{61}t_{15}\vartheta_1 + c_{65}e_{12}e_{23}t_{51}\vartheta_1 + c_{52}e_{23}e_{61}t_{15}\vartheta_2 + c_{65}e_{12}e_{23}t_{51}\vartheta_2 + \\
&c_{52}e_{25}e_{61}t_{15}\vartheta_1 + c_{65}e_{12}e_{25}t_{51}\vartheta_1 - c_{21}e_{56}t_{15}t_{62}\vartheta_1 - c_{52}e_{61}t_{15}t_{26}\vartheta_1 - \\
&c_{65}e_{12}t_{26}t_{51}\vartheta_1 + e_{23}t_{15}t_{51}t_{62}\vartheta_1 + e_{23}t_{15}t_{51}t_{62}\vartheta_2 + e_{25}t_{15}t_{51}t_{62}\vartheta_1 - \\
&t_{15}t_{26}t_{51}t_{62}\vartheta_1),
\end{aligned}
$$

where

$$
\begin{aligned}
&D_{\mathrm{R}}(\vartheta_{\mathrm{s}}) = c_{52}e_{23}e_{61}t_{13} + c_{52}e_{23}e_{61}t_{15} + c_{65}e_{12}e_{23}t_{51} + e_{12}e_{23}e_{61}t_{53} + e_{12}e_{23}e_{61}t_{54} + \\
&c_{14}e_{23}t_{51}t_{62} + c_{16}e_{23}t_{51}t_{62} + e_{12}e_{23}t_{51}t_{63} + e_{12}e_{23}t_{51}t_{64} + e_{23}t_{13}t_{51}t_{62} + e_{23}t_{15}t_{51}t_{62} + \\
&c_{14}c_{52}e_{23}e_{61} + c_{16}c_{52}e_{23}e_{61} + c_{14}c_{52}e_{23}e_{61}\vartheta_1 + c_{14}c_{52}e_{23}e_{61}\vartheta_2 + c_{14}c_{52}e_{25}e_{61}\vartheta_1 + \\
&c_{16}c_{52}e_{23}e_{61}\vartheta_1 + c_{16}c_{52}e_{23}e_{61}\vartheta_2 + c_{16}c_{52}e_{25}e_{61}\vartheta_1 - c_{21}c_{65}e_{12}e_{56}\vartheta_1 - \\
&e_{12}e_{23}e_{56}e_{61}\vartheta_2 - c_{14}c_{21}e_{56}t_{62}\vartheta_1 - c_{14}c_{52}e_{61}t_{26}\vartheta_1 - c_{16}c_{21}e_{56}t_{62}\vartheta_1 - \\
&c_{16}c_{52}e_{61}t_{26}\vartheta_1 + c_{52}e_{23}e_{61}t_{13}\vartheta_1 + c_{52}e_{23}e_{61}t_{13}\vartheta_2 + c_{52}e_{23}e_{61}t_{15}\vartheta_1 + \\
&c_{52}e_{25}e_{61}t_{13}\vartheta_1 + c_{65}e_{12}e_{23}t_{51}\vartheta_1 - c_{21}e_{12}e_{56}t_{63}\vartheta_1 + c_{52}e_{23}e_{61}t_{15}\vartheta_2 + \\
&c_{65}e_{12}e_{23}t_{51}\vartheta_2 - c_{21}e_{12}e_{56}t_{64}\vartheta_1 + c_{52}e_{25}e_{61}t_{15}\vartheta_1 + c_{65}e_{12}e_{25}t_{51}\vartheta_1 + \\
&e_{12}e_{23}e_{61}t_{53}\vartheta_1 + e_{12}e_{23}e_{61}t_{53}\vartheta_2 + e_{12}e_{23}e_{61}t_{54}\vartheta_1 + e_{12}e_{23}e_{61}t_{54}\vartheta_2 + \\
&e_{12}e_{25}e_{61}t_{53}\vartheta_1 + e_{12}e_{25}e_{61}t_{54}\vartheta_1 - e_{12}e_{56}e_{61}t_{24}\vartheta_1 + c_{14}e_{23}t_{51}t_{62}\vartheta_1 + \\
&c_{14}e_{23}t_{51}t_{62}\vartheta_2 + c_{14}e_{25}t_{51}t_{62}\vartheta_1 + c_{16}e_{23}t_{51}t_{62}\vartheta_1 - c_{21}e_{56}t_{13}t_{62}\vartheta_1 - \\
&c_{52}e_{61}t_{13}t_{26}\vartheta_1 + c_{16}e_{23}t_{51}t_{62}\vartheta_2 + c_{16}e_{25}t_{51}t_{62}\vartheta_1 - c_{21}e_{56}t_{15}t_{62}\vartheta_1 -
\end{aligned}
$$

$$c_{52}e_{61}t_{15}t_{26}\vartheta_1 - c_{65}e_{12}t_{26}t_{51}\vartheta_1 + e_{12}e_{23}t_{51}t_{63}\vartheta_1 + e_{12}e_{23}t_{51}t_{63}\vartheta_2 +$$
$$e_{12}e_{23}t_{51}t_{64}\vartheta_1 + e_{12}e_{23}t_{51}t_{64}\vartheta_2 + e_{12}e_{25}t_{51}t_{63}\vartheta_1 + e_{12}e_{25}t_{51}t_{64}\vartheta_1 -$$
$$e_{12}e_{61}t_{26}t_{53}\vartheta_1 - e_{12}e_{61}t_{26}t_{54}\vartheta_1 - c_{14}t_{26}t_{51}t_{62}\vartheta_1 - c_{16}t_{26}t_{51}t_{62}\vartheta_1 +$$
$$e_{23}t_{13}t_{51}t_{62}\vartheta_1 + e_{23}t_{13}t_{51}t_{62}\vartheta_2 + e_{23}t_{15}t_{51}t_{62}\vartheta_1 + e_{25}t_{13}t_{51}t_{62}\vartheta_1 -$$
$$e_{12}t_{26}t_{51}t_{63}\vartheta_1 + e_{23}t_{15}t_{51}t_{62}\vartheta_2 - e_{12}t_{26}t_{51}t_{64}\vartheta_1 + e_{25}t_{15}t_{51}t_{62}\vartheta_1 -$$
$$t_{13}t_{26}t_{51}t_{62}\vartheta_1 - t_{15}t_{26}t_{51}t_{62}\vartheta_1.$$

We have verified with MathWorks' MATLAB's [Mat22] Symbolic Math Toolbox that these expressions are not equal to each other; that is, $f_{\mathrm{L}}(\vartheta_{\mathrm{s}}) \neq f_{\mathrm{R}}(\vartheta_{\mathrm{s}})$, and therefore f_{Pod} is not continuous on its switching manifold.

§B.4 Parameter values for figures in Chapter I

Figure 1.1 is calculated using the ODEs (6.1), with the initial conditions

$$(X_1, X_2, X_3) = (-0.5551, -0.5551, -0.5551),$$

and the parameter values $c_1 = 0.48$ and $e_1 = 0.4$

Figure 1.4 is calculated using the ODEs (10.2), with the initial conditions

$$(X_1, X_2, X_3, X_4) = \left(0.9973, 4.1875 \times 10^{-6}, 3.6 \times 10^{-2}, 1.085 \times 10^{-11}\right),$$

and the following parameter values:

Table B.4.1: Parameter values for Figure 1.4

ξ_1		ξ_2		ξ_3		ξ_4	
e_{12}	0.8	c_{21}	0.8	e_{31}	0.8	e_{41}	0.9
c_{13}	1.2	e_{23}	0.57	c_{32}	1.2	c_{42}	1.2
c_{14}	1.2	e_{24}	0.9	t_{34}	1	t_{43}	1

§B.5 Parameter values for figures in Chapter III

B.5.1 Figures in §9

Figure 9.1(a) is calculated using (9.4), and Figure 9.2(a) using the corresponding transition matrices, with initial conditions $(x_3, x_4) = (0.9, 0.65)$ and $(x_3, x_4) = (0.4, 0.9)$, and the following parameter values:

Table B.5.1

ξ_1		ξ_2		ξ_3		ξ_4	
e_{12}	0.9	c_{21}	0.6	e_{31}	0.9	e_{41}	0.9
c_{13}	2	e_{23}	1.2	c_{32}	1.2	c_{42}	1.2
c_{14}	1.5	e_{24}	0.8	t_{34}	1	t_{43}	1

Figure 9.1(b) is calculated using (9.4), and Figure 9.2(b) using the corresponding transition matrices, with initial conditions $(x_3, x_4) = (0.875, 0.65)$ and $(x_3, x_4) = (0.45, 0.8)$, and the following parameter values:

Table B.5.2

ξ_1		ξ_2		ξ_3		ξ_4	
e_{12}	0.9	c_{21}	0.6	e_{31}	1.2	e_{41}	0.9
c_{13}	4.5	e_{23}	1.2	c_{32}	1.2	c_{42}	0.9
c_{14}	1.5	e_{24}	0.8	t_{34}	1	t_{43}	1

B.5.2 Figures in §10

Figures 9.4(a) and 9.4(c) are calculated with (9.9), with $c_{14} = 2$ and $c_{42} = 2.3$, and $c_{14} = 1.2$ and $c_{42} = 4.5$, respectively, with initial conditions $\vartheta = -0.16$ and $\vartheta = -0.95$, and $\vartheta = -0.07$ and $\vartheta = -0.95$, respectively, and these common parameter values:

Table B.5.3

ξ_1		ξ_2		ξ_3		ξ_4	
e_{12}	0.8	c_{21}	0.3	e_{31}	0.9	e_{41}	0.8
c_{13}	2.9	e_{23}	1.2	c_{32}	2.9	c_{42}	—
c_{14}	—	e_{24}	0.8	t_{34}	1	t_{43}	3

Figure 9.4(b) is calculated with (9.9), with initial conditions $\vartheta = -0.55$ and $\vartheta = -0.95$, and with the parameter values:

Table B.5.4

ξ_1		ξ_2		ξ_3		ξ_4	
e_{12}	1	c_{21}	1	e_{31}	2	e_{41}	0.8
c_{13}	1.5	e_{23}	1.2	c_{32}	1.5	c_{42}	2.3
c_{14}	2	e_{24}	0.8	t_{34}	1	t_{43}	5

Figure 9.4(d) is calculated with (9.9), with the initial conditions $\vartheta = -0.545$ and $\vartheta = -0.95$, and with the parameter values:

Table B.5.5

ξ_1		ξ_2		ξ_3		ξ_4	
e_{12}	3.6	c_{21}	2.3	e_{31}	9.6	e_{41}	2
c_{13}	10	e_{23}	9	c_{32}	9	c_{42}	20
c_{14}	3	e_{24}	6	t_{34}	4.36	t_{43}	0.1

Figures 10.1(a) and 10.1(b) is calculated with (10.2), with $c_{13} = 0.9$ and $e_{24} = 0.9$, and $c_{13} = 1.1$ and $e_{24} = 1$, respectively, with initial conditions

$$(X_1, X_2, X_3, X_4) = \left(0.995, 2.95 \times 10^{-3}, 2.472 \times 10^{-2}, 1.195 \times 10^{-14}\right)$$

and

$$(X_1, X_2, X_3, X_4) = \left(0.989, 7.22 \times 10^{-3}, 2.536 \times 10^{-2}, 3.424 \times 10^{-7}\right),$$

respectively, and with the following parameter values:

Table B.5.6

ξ_1		ξ_2		ξ_3		ξ_4	
e_{12}	0.8	c_{21}	0.8	e_{31}	0.8	e_{41}	0.9
c_{13}	—	e_{23}	0.57	c_{32}	1	c_{42}	1.4
c_{14}	1	e_{24}	—	t_{34}	1	t_{43}	1

Figure 10.1(c) is calculated with (10.2), with initial conditions

$$(X_1, X_2, X_3, X_4) = \left(10^{-5}, 0.999, 3.72 \times 10^{-44}, 1.452 \times 10^{-48}\right),$$

and the parameter values:

Table B.5.7

ξ_1		ξ_2		ξ_3		ξ_4	
e_{12}	3.6	c_{21}	2.3	e_{31}	9.6	e_{41}	2
c_{13}	10	e_{23}	9	c_{32}	9.96	c_{42}	12
c_{14}	3	e_{24}	6	t_{34}	4.36	t_{43}	5.55

B.5.3 Figures in §11

Figure 11.1(a) is calculated with (11.1), with initial condition $\vartheta = -0.1$, and with the parameter values:

Table B.5.8

ξ_1		ξ_2		ξ_3		ξ_4	
e_{12}	0.8	c_{21}	7.35	t_{31}	7.14	e_{41}	6.48
t_{13}	0.48	e_{23}	1.2	c_{32}	8.24	c_{42}	0.27
c_{14}	4.81	e_{24}	0.8	e_{34}	7.9	c_{43}	6.5

Figure 11.1(b) is calculated with (11.1), with initial condition $\vartheta = -0.965$, and with the parameter values:

Table B.5.9

ξ_1		ξ_2		ξ_3		ξ_4	
e_{12}	8	c_{21}	6.29	t_{31}	4.63	e_{41}	5
t_{13}	2.19	e_{23}	1.2	c_{32}	5.71	c_{42}	3.63
c_{14}	5.43	e_{24}	0.8	e_{34}	9.9	c_{43}	1

Figure 11.1(c) is calculated with (11.1), with the initial conditions $\vartheta = -0.4$, $\vartheta = -0.525$, and $\vartheta = -0.98$, and with the parameter values:

Table B.5.10

ξ_1		ξ_2		ξ_3		ξ_4	
e_{12}	1.22	c_{21}	3.36	t_{31}	0.2	e_{41}	0.67
t_{13}	0.06	e_{23}	1.2	c_{32}	7.13	c_{42}	0.36
c_{14}	4.5	e_{24}	0.8	e_{34}	0.28	c_{43}	7.4

Figure 11.1(d) is calculated with (11.1), with the initial conditions $\vartheta = -0.1$ and -0.9 with the parameter values:

Table B.5.11

ξ_1		ξ_2		ξ_3		ξ_4	
e_{12}	2.28	c_{21}	2.69	t_{31}	7.39	e_{41}	9.73
t_{13}	1.84	e_{23}	1.2	c_{32}	9.32	c_{42}	2.98
c_{14}	8.83	e_{24}	0.8	e_{34}	8.28	c_{43}	7.9

Figure 11.2 is calculated with the following parameter values:

Table B.5.12

ξ_1		ξ_2		ξ_3		ξ_4	
e_{12}	1.1	c_{21}	3	t_{31}	0.4	e_{41}	0.95
t_{13}	0.2	e_{23}	1	c_{32}	2.5	c_{42}	—
c_{14}	3.2	e_{24}	0.8	e_{34}	0.9	c_{43}	—

Figure 11.4(a) is calculated with (11.2), with initial conditions

$$(X_1, X_2, X_3, X_4) = \left(10^{-5}, 0.999, 4.36 \times 10^{-28}, 1.402 \times 10^{-31}\right),$$

and with parameter values:

Table B.5.13

ξ_1		ξ_2		ξ_3		ξ_4	
e_{12}	1.73	c_{21}	0.33	t_{31}	0.59	e_{41}	0.81
t_{13}	0.108	e_{23}	1.2	c_{32}	2	c_{42}	1.43
c_{14}	2	e_{24}	0.8	e_{34}	0.188	c_{43}	2

Figure 11.4(b) is calculated with (11.2), with initial conditions

$$(X_1, X_2, X_3, X_4) = \left(10^{-5}, 0.999, 4.54 \times 10^{-5}, 8.194 \times 10^{-40}\right),$$

and with parameter values:

Table B.5.14

ξ_1		ξ_2		ξ_3		ξ_4	
e_{12}	3.58	c_{21}	0.7	t_{31}	0.4	e_{41}	0.91
t_{13}	0.2	e_{23}	1.2	c_{32}	1.92	c_{42}	1.3
c_{14}	2.95	e_{24}	0.8	e_{34}	1.67	c_{43}	1.96

Figure 11.4(c) is calculated with (11.2), with initial conditions

$$(X_1, X_2, X_3, X_4) = \left(10^{-5}, 0.999, 6.826 \times 10^{-8}, 2.343 \times 10^{-6}\right),$$

and with parameter values:

Table B.5.15

ξ_1		ξ_2		ξ_3		ξ_4	
e_{12}	1.99	c_{21}	0.77	t_{31}	0.02	e_{41}	1.02
t_{13}	0.04	e_{23}	1.5	c_{32}	3.04	c_{42}	1.03
c_{14}	1.41	e_{24}	0.5	e_{34}	0.94	c_{43}	3.45

B.5.4 Figures in §12

All plots in Figure 12.1 are calculated with (12.1) and the following common parameter values:

Table B.5.16

ξ_1		ξ_2		ξ_3		ξ_4	
e_{12}	—	c_{21}	2	e_{31}	1.1	e_{41}	—
c_{13}	—	e_{23}	1.2	c_{32}	—	c_{42}	—
c_{14}	—	e_{24}	0.7	e_{34}	0.9	c_{43}	—

The plot of $\nu_4 < 0, \mu_3 > 0$ in Figure 12.1(a) is calculated with:

Table B.5.17

ξ_1		ξ_2		ξ_3		ξ_4	
e_{12}	6.85	c_{21}	—	e_{31}	—	e_{41}	1.92
c_{13}	2	e_{23}	—	c_{32}	5.37	c_{42}	4.67
c_{14}	7.96	e_{24}	—	e_{34}	—	c_{43}	5.47

The plot of $\nu_4 > 0, \mu_3 < 0$ in Figure 12.1(a) is calculated with:

Table B.5.18

ξ_1		ξ_2		ξ_3		ξ_4	
e_{12}	6.75	c_{21}	—	e_{31}	—	e_{41}	6.06
c_{13}	3.59	e_{23}	—	c_{32}	9.41	c_{42}	9.38
c_{14}	4.2	e_{24}	—	e_{34}	—	c_{43}	9.89

The plot of $\mu_3 > 0, \nu_4 < 0$ in Figure 12.1(b) is calculated with:

Table B.5.19

ξ_1		ξ_2		ξ_3		ξ_4	
e_{12}	1.4	c_{21}	—	e_{31}	—	e_{41}	1.84
c_{13}	2	e_{23}	—	c_{32}	7.65	c_{42}	0.82
c_{14}	12	e_{24}	—	e_{34}	—	c_{43}	5.82

The plot of $\mu_3 > 0, \nu_4 > 0$ in Figure 12.1(b) is calculated with:

Table B.5.20

ξ_1		ξ_2		ξ_3		ξ_4	
e_{12}	1.4	c_{21}	—	e_{31}	—	e_{41}	1.84
c_{13}	2	e_{23}	—	c_{32}	7.65	c_{42}	0.82
c_{14}	5.5	e_{24}	—	e_{34}	—	c_{43}	5.82

The plot of $\mu_3 < 0, \nu_4 < 0$ in Figure 12.1(b) is calculated with:

Table B.5.21

ξ_1		ξ_2		ξ_3		ξ_4	
e_{12}	1.4	c_{21}	—	e_{31}	—	e_{41}	1.84
c_{13}	6.5	e_{23}	—	c_{32}	5	c_{42}	0.82
c_{14}	11	e_{24}	—	e_{34}	—	c_{43}	5.82

The plot of $\mu_3 < 0, \nu_4 > 0$ in Figure 12.1(b) is calculated with:

Table B.5.22

ξ_1		ξ_2		ξ_3		ξ_4	
e_{12}	1.4	c_{21}	—	e_{31}	—	e_{41}	1.84
c_{13}	3.3	e_{23}	—	c_{32}	9	c_{42}	0.82
c_{14}	4.8	e_{24}	—	e_{34}	—	c_{43}	0.52

The plot of $\nu_4 < 0, \mu_3 > 0$ in Figure 12.1(c) is calculated with:

Table B.5.23

ξ_1		ξ_2		ξ_3		ξ_4	
e_{12}	2.64	c_{21}	—	e_{31}	—	e_{41}	3.39
c_{13}	2	e_{23}	—	c_{32}	3.68	c_{42}	1.58
c_{14}	13	e_{24}	—	e_{34}	—	c_{43}	9.98

The plot of $\nu_4 > 0, \mu_3 > 0$ in Figure 12.1(c) is calculated with:

Table B.5.24

ξ_1		ξ_2		ξ_3		ξ_4	
e_{12}	2.64	c_{21}	—	e_{31}	—	e_{41}	3.39
c_{13}	1.76	e_{23}	—	c_{32}	3.68	c_{42}	1.58
c_{14}	6	e_{24}	—	e_{34}	—	c_{43}	9.98

The plot of $\nu_4 > 0, \mu_3 < 0$ in Figure 12.1(c) is calculated with:

Table B.5.25

ξ_1		ξ_2		ξ_3		ξ_4	
e_{12}	2.64	c_{21}	—	e_{31}	—	e_{41}	3.39
c_{13}	5	e_{23}	—	c_{32}	3.68	c_{42}	1.58
c_{14}	5.31	e_{24}	—	e_{34}	—	c_{43}	9.98

The plot of $\nu_4 < 0, \mu_3 > 0$ in Figure 12.1(d) is calculated with:

Table B.5.26

ξ_1		ξ_2		ξ_3		ξ_4	
e_{12}	3.48	c_{21}	—	e_{31}	—	e_{41}	4.01
c_{13}	5.53	e_{23}	—	c_{32}	7.24	c_{42}	8.43
c_{14}	13	e_{24}	—	e_{34}	—	c_{43}	6

The plot of $\nu_4 < 0, \mu_3 < 0$ in Figure 12.1(d) is calculated with:

Table B.5.27

ξ_1		ξ_2		ξ_3		ξ_4	
e_{12}	3.48	c_{21}	—	e_{31}	—	e_{41}	4.01
c_{13}	5.53	e_{23}	—	c_{32}	7.24	c_{42}	8.43
c_{14}	6	e_{24}	—	e_{34}	—	c_{43}	6

The plot of $\nu_4 > 0, \mu_3 < 0$ in Figure 12.1(d) is calculated with:

Table B.5.28

ξ_1		ξ_2		ξ_3		ξ_4	
e_{12}	3.48	c_{21}	—	e_{31}	—	e_{41}	4.01
c_{13}	5.53	e_{23}	—	c_{32}	7.24	c_{42}	8.43
c_{14}	3.22	e_{24}	—	e_{34}	—	c_{43}	6

Figure 12.2 is calculated with the parameter values:

Table B.5.29

ξ_1		ξ_2		ξ_3		ξ_4	
e_{12}	6.07	c_{21}	3	e_{31}	1.1	e_{41}	3.37
c_{13}	—	e_{23}	1.2	c_{32}	6.14	c_{42}	3.15
c_{14}	—	e_{24}	0.7	e_{34}	0.9	c_{43}	8.11

Figure 12.4 is calculated with (12.1), with initial conditions:

$$(X_1, X_2, X_3, X_4) = \left(10^{-5}, 0.999, 1.185 \times 10^{-27}, 4.08 \times 10^{-41}\right)$$

and with parameter values:

Table B.5.30

ξ_1		ξ_2		ξ_3		ξ_4	
e_{12}	5.24	c_{21}	5.52	e_{31}	5.43	e_{41}	6.1
c_{13}	9.41	e_{23}	8.65	c_{32}	6.72	c_{42}	4.65
c_{14}	8.22	e_{24}	6.01	e_{34}	2.78	c_{43}	4.11

§B.6 Parameter values for figures in Chapter V

Figure 17.3(a) is calculated as outlined in §A.2, with parameter values:

Table B.6.1: Parameter values for Figure 17.3(a)

X		Y	
e_{XA}	0.8	e_{YA}	0.9
c_{XB}	1.1	c_{YB}	1.2
c_{XY}	1.2	c_{YX}	0.8

Figure 17.3(b) is calculated as outlined in §A.2, with parameter values:

Table B.6.2: Parameter values for Figure 17.3(b)

X		Y	
c_{XA}	0.4	e_{YA}	0.9
c_{XB}	2.5	c_{YB}	1.1
e_{XY}	0.9	c_{YX}	0.2

Figures 18.2(a) and 18.3(a) are calculated with the completed projected map $f^{(k)}_{\mathrm{KS}}$ and the following parameter values:

Table B.6.3: Parameter values for Figures 18.2(a) and 18.3(a)

A		B		X		Y	
e_{AB}	0.8	c_{BA}	0.8	e_{XA}	0.8	e_{YA}	0.9
c_{AX}	1.2	e_{BX}	1	c_{XB}	1.2	c_{YB}	1.2
c_{AY}	1.2	c_{BY}	0.8	c_{XY}	0.2	c_{YX}	0.1

Figures 18.2(b) and 18.3(b) are calculated with the completed projected map $f_{\Delta}^{(k)}$ and the following parameter values:

Table B.6.4: Parameter values for Figures 18.2(b) and 18.3(b)

A		B		X		Y	
e_{A}	1.2	c_{B}	1.3	c_{XA}	0.8	e_{YA}	0.9
c_{AX}	0.3	e_{BX}	1.2	c_{XB}	2.3	c_{YB}	1
c_{AY}	1.8	e_{BY}	0.9	e_{XY}	0.5	c_{YX}	2.4

§B.7 Parameter values for figures in §19

The common parameter values used to calculate Figures 19.2 and 19.3 are:

Table B.7.1: Parameter values for Figures 19.2 and 19.3

ξ_1		ξ_2		ξ_3		ξ_4		ξ_5		ξ_6	
e_{12}	1	c_{21}	1	t_{31}	0.2	e_{41}	1	t_{51}	0.2	e_{61}	1
t_{13}	0.2	e_{L}	1	c_{32}	1.2	t_{42}	0.2	c_{52}	1.2	t_{62}	0.2
c_{L}	—	t_{24}	0.2	e_{34}	1	c_{43}	1.1	t_{53}	0.2	t_{63}	1
t_{15}	0.2	e_{R}	0.9	t_{35}	0.2	t_{45}	0.57	t_{54}	0.2	t_{64}	0.2
c_{R}	—	t_{26}	0.2	t_{36}	0.2	t_{46}	0.2	e_{56}	1	c_{65}	1.1

Figure 19.2(a) is calculated by integrating (19.1) with the above parameter values and $c_{\mathrm{L}} = 1$ and $c_{\mathrm{R}} = 1$.

Figure 19.2(b) is calculated by integrating (19.1) with the above parameter values and $c_{\mathrm{L}} = 0.1$ and $c_{\mathrm{R}} = 0.9$.

Figure 19.2(c) is calculated by integrating (19.1) with the above parameter values and $c_{\mathrm{L}} = 1.5$ and $c_{\mathrm{R}} = 0.3$.

Figure 19.2(d) is calculated by integrating (19.1) with the above parameter values and $c_{\mathrm{L}} = 1.25$ and $c_{\mathrm{R}} = 0.05$.

Figures 19.2(a) to 19.2(d) are all calculated with the following initial conditions:

$$(x_1, x_2, x_3, x_4, x_5, x_6) = (0.99, 0.01, 0.01, 0.01, 0.01, 0.01).$$

References

[AGR15] Afraimovich V, Gong X, and Rabinovich M (2015). Sequential memory: binding dynamics. *Chaos: An Interdisciplinary Journal of Nonlinear Science*, **25**(10):103118. DOI: https://doi.org/10.1063/1.4932563. Cited on p. 9.

[AMY16] Afraimovich V S, Moses G, and Young T (2016). Two-dimensional heteroclinic attractor in the generalized Lotka–Volterra system. *Nonlinearity*, **29**(5):1645—1667. DOI: https://doi.org/10.1088/0951-7715/29/5/1645. Cited on pp. 9 and 11.

[Agu11] Aguiar M A D (2011). Is there switching for replicator dynamics and bimatrix games? *Physica D: Nonlinear Phenomena*, **240**:1475—1488. DOI: https://doi.org/10.1016/j.physd.2011.06.016. Cited on p. 10.

[AC10] Aguiar M A D and Castro S B S D (2010). Chaotic switching in a two-person game. *Physica D. Nonlinear Phenomena*, **239**(16):1598—1609. DOI: https://doi.org/10.1016/j.physd.2010.04.007. Cited on p. 10.

[ACL04] Aguiar M A D, Castro S B S D, and Labouriau I S (2004). Dynamics near a heteroclinic network. *Nonlinearity*, **18**(1):391. DOI: https://doi.org/10.1088/0951-7715/18/1/019. Cited on pp. 10 and 21.

[ACL06] Aguiar M A D, Castro S B S D, and Labouriau I S (2006). Simple vector fields with complex behavior. *International Journal of Bifurcation and Chaos in Applied Sciences and Engineering*, **16**(2):369—381. DOI: https://doi.org/10.1142/S021812740601485X. Cited on p. 10.

[AD17] Aguiar M A D and Dias A P S (2017). Heteroclinic network dynamics on joining coupled cell networks. *Dynamical Systems*, **32**(1):4—22. DOI: https://doi.org/10.1080/14689367.2016.1197889. Cited on p. 9.

[Arm89a] Armbruster D (1989). More on structurally stable H-orbits. *In* K-T Li, J Marsden, M Golubitsky, and G Iooss (Eds.), *Proceedings of the International Conference on Bifurcation Theory and its Numerical Analysis (Xi'an, 1988)*. Cited on p. 6.

[Arm89b] Armbruster D (1989). Persistent heteroclinic orbits. *In* B Nicolaenko, C Foiaş, and R Temam (Eds.), *The connection between infinite-dimensional and finite-dimensional dynamical systems (Boulder, CO, 1987)*. DOI: https://doi.org/10.1090/conm/099/1034495. Cited on p. 4.

[AC91] Armbruster D and Chossat P (1991). Heteroclinic orbits in a spherically invariant system. *Physica D: Nonlinear Phenomena*, **50**(2):155—176. DOI: https://doi.org/10.1016/0167-2789(91)90173-7. Cited on p. 4.

[ACO01] Armbruster D, Chossat P, and Oprea I (2001). Structurally stable heteroclinic cycles and the dynamo dynamics. *In* P Chossat, D Armbruster, and I Oprea (Eds.), *Dynamo and Dynamics, a Mathematical Challenge*. DOI: https://doi.org/10.1007/978-94-010-0788-7_37. Cited on p. 4.

[AGH88] Armbruster D, Guckenheimer J, and Holmes P (1988). Heteroclinic cycles and modulated travelling waves in systems with O(2) symmetry. *Physica D: Nonlinear Phenomena*, **29**(3):257—282. DOI: https://doi.org/10.1016/0167-2789(88)90032-2. Cited on pp. 4 and 6.

[ACL20] Ashwin P, Castro S B S D, and Lohse A (2020). Almost complete and equable heteroclinic networks. *Journal of Nonlinear Science*, **30**(1):1—22. DOI: https://doi.org/10.1007/s00332-019-09566-z. Cited on p. 35.

[ACN16] Ashwin P, Coombes S, and Nicks R (2016). Mathematical frameworks for oscillatory network dynamics in neuroscience. *Journal of Mathematical Neuroscience*, **6**(1):2. DOI: https://doi.org/10.1186/s13408-015-0033-6. Cited on p. 9.

[AF99] Ashwin P and Field M (1999). Heteroclinic networks in coupled cell systems. *Archive for Rational Mechanics and Analysis*, **148**:107—143. DOI: https://doi.org/10.1007/s002050050158. Cited on p. 9.

[AP13] Ashwin P and Postlethwaite C (2013). On designing heteroclinic networks from graphs. *Physica D: Nonlinear Phenomena*, **265**:26—39. DOI: https://doi.org/10.1016/j.physd.2013.09.006. Cited on pp. 9, 16, 20, 27, 34, 76, 78, and 117.

[AHL88] Aubry N, Holmes P, Lumley J L, and Stone E (1988). The dynamics of coherent structures in the wall region of a turbulent boundary layer. *Journal of Fluid Mechanics*, **192**:115—173. DOI: https://doi.org/10.1017/S0022112088001818. Cited on p. 3.

[AHL89] Aubry N, Holmes P, Lumley J L, and Stone E (1989). Application of dynamical system theory to coherent structures in the wall region. *Physica D: Nonlinear Phenomena*, **37**(1):1—10. DOI: https://doi.org/10.1016/0167-2789(89)90112-7. Cited on p. 3.

[AGS19] Avrutin V, Gardini L, Sushko I, and Tramontana F (2019). *Continuous and Discontinuous Piecewise-smooth One-dimensional Maps: Invariant Sets And Bifurcation Structures*. World Scientific. DOI: https://doi.org/10.1142/8285. Cited on p. 164.

[BSC06] Becker N, Scheel J D, Cross M C, and Ahlers G (2006). Effect of the centrifugal force on domain chaos in Rayleigh–Bénard convection. *Phys. Rev. E*, **73**6:066309. DOI: https://doi.org/10.1103/PhysRevE.73.066309. Cited on p. 3.

[BHL91] Berkooz G, Holmes P, and Lumley J L (1991). Intermittent dynamics in simple models of the turbulent wall layer. *Journal of Fluid Mechanics*, **230**:75—95. DOI: https://doi.org/10.1017/S002211209100071X. Cited on p. 3.

[BBC08] di Bernardo M, Budd C J, Champneys A R, and Kowalczyk P (2008). *Piecewise-smooth Dynamical Systems: Theory and Applications*. Springer London. DOI: https://doi.org/10.1007/978-1-84628-708-4. Cited on pp. 32 and 164.

[Bra94] Brannath W (1994). Heteroclinic networks on the tetrahedron. *Nonlinearity*, **7**(5):1367—1384. DOI: https://doi.org/10.1088/0951-7715/7/5/006. Cited on pp. 7, 8, 9, 13, 20, 33, 161, and 162.

[BH80] Busse F H and Heikes K E (1980). Convection in a rotating layer: a simple case of turbulence. *Science*, **208**(4440):173—175. DOI: https://doi.org/10.1126/science.208.4440.173. Cited on p. 3.

[BC79] Busse F H and Clever R M (1979). Nonstationary convection in a rotating system. *In* U Müller, K G Roesner, and B Schmidt (Eds.), *Recent Developments in Theoretical and Experimental Fluid Mechanics: Compressible and Incompressible Flows*. DOI: https://doi.org/10.1007/978-3-642-67220-0_39. Cited on p. 3.

[CH91] Campbell S A and Holmes P (1991). Bifurcation from O(2) symmetric heteroclinic cycles with three interacting modes. *Nonlinearity*, **4**(3):697. DOI: https://doi.org/10.1088/0951-7715/4/3/005. Cited on pp. 4 and 6.

[CFG22] Castro S B S D, Ferreira A, Garrido da Silva L, and Labouriau I S (2022). Stability of cycles in a game of Rock–Scissors–Paper–Lizard–Spock. *SIAM Journal on Applied Dynamical Systems*, **21**(4):2393—2431. DOI: https://doi.org/10.1137/21M1435215. Cited on p. 11.

[CFL24] Castro S B S D, Ferreira A M J, and Labouriau I S (2024). Stability of cycles and survival in a jungle game with four species. *Dynamical Systems: An International Journal*, **39**:1—19. DOI: https://doi.org/10.1080/14689367.2024.2307515. Cited on pp. 35, 54, and 68.

[CG23] Castro S B S D and Garrido da Silva L (2023). Finite switching near heteroclinic networks. *Nonlinearity*, **36**(12):6239. DOI: https://doi.org/10.1088/1361-6544/ad03cf. Cited on pp. 10 and 21.

[CLP10] Castro S B S D, Labouriau I S, and Podvigina O (2010). A heteroclinic network in mode interaction with symmetry. *Dynamical Systems*, **25**(3):359—396. DOI: https://doi.org/10.1080/14689367.2010.506183. Cited on p. 9.

[CL14] Castro S B S D and Lohse A (2014). Stability in simple heteroclinic networks in $\mathbb{R}^4$. *Dynamical Systems*, **29**(4):451—481. DOI: https://doi.org/10.1080/14689367.2014.940853. Cited on p. 9.

[CL16a] Castro S B S D and Lohse A (2016). Construction of heteroclinic networks in $\mathbb{R}^4$. *Nonlinearity*, **29**(12):3677—3695. DOI: https://doi.org/10.1088/0951-7715/29/12/3677. Cited on pp. 9 and 35.

[CL16b] Castro S B S D and Lohse A (2016). Switching in heteroclinic networks. *SIAM Journal on Applied Dynamical Systems*, **15**(2):1085—1103. DOI: https://doi.org/10.1137/15M1042176. Cited on pp. 9, 21, 81, 144, 163, and 164.

[CA91] Chossat P and Armbruster D (1991). Structurally stable heteroclinic cycles in a system with O(3) symmetry. *In* M Roberts and I Stewart (Eds.), *Singularity Theory and its Applications*. DOI: https://doi.org/10.1007/BFb0085422. Cited on p. 4.

[CG96] Chossat P and Guyard F (1996). Heteroclinic cycles in bifurcation problems with O(3) symmetry and the spherical Bénard problem. *Journal of Nonlinear Science*, **6**(3):201—238. DOI: https://doi.org/10.1007/s003329900009. Cited on p. 4.

[CKM97] Chossat P, Krupa M, Melbourne I, and Scheel A (1997). Transverse bifurcations of homoclinic cycles. *Physica D: Nonlinear Phenomena*, **29**(6):85—100. DOI: https://doi.org/10.1016/S0167-2789(96)00186-8. Cited on pp. 4, 6, and 137.

[CLP18] Chossat P, Lohse A, and Podvigina O (2018). Pseudo-simple heteroclinic cycles in R4. *Physica D: Nonlinear Phenomena*, **372**:1—21. DOI: https://doi.org/10.1016/j.physd.2018.01.008. Cited on p. 4.

[CPC79] Coste J, Peyraud J, and Coullet P (1979). Asymptotic behaviors in the dynamics of competing species. *SIAM Journal on Applied Mathematics*, **36**(3):516—543. DOI: https://doi.org/10.1137/0136039. Cited on p. 2.

[Daw01] Dawes J H P (2001). A Hopf/steady-state mode interaction in rotating convection: bursts and heteroclinic cycles in a square periodic domain. *Physica D: Nonlinear Phenomena*, **149**(3):197—209. DOI: https://doi.org/10.1016/S0167-2789(00)00201-3. Cited on p. 3.

[DH09] Driesse R and Homburg A J (2009). Essentially asymptotically stable homoclinic networks. *Dynamical Systems*, **24**(4):459—471. DOI: https://doi.org/10.1080/14689360903039664. Cited on p. 9.

[DMS05] Dullin H R, Meiss J D, and Sterling D G (2005). Symbolic Codes for Rotational Orbits. *SIAM Journal on Applied Dynamical Systems*, **4**(3):515—562. DOI: https://doi.org/10.1137/040612877. Cited on p. 136.

[Eas76] Easton R W (1976). Some Qualitative Aspects of the Three-Body Flow. *In* L Cesari, J K Hale, and J P LaSalle (Eds.), *Dynamical Systems: An International Symposium, Volume 2*. DOI: https://doi.org/10.1016/B978-0-12-164902-9.50006-X. Cited on p. 2.

[Fie80] Field M J (1980). Equivariant dynamical systems. *Transactions of the American Mathematical Society*, **259**(1):185—205. DOI: https://doi.org/10.2307/1998153. Cited on p. 4.

[Fie96] Field M (1996). *Lectures on Bifurcations, Dynamics and Symmetry*. Addison Wesley Longman. DOI: https://doi.org/10.1201/9780429332692. Cited on pp. 24, 36, 54, 65, 73, 97, and 142.

[Fie15] Field M J (2015). Heteroclinic networks in homogeneous and heterogeneous identical cell systems. *Journal of Nonlinear Science*, **25**(3):779—813. DOI: https://doi.org/10.1007/s00332-015-9241-1. Cited on p. 9.

[FR92] Field M J and Richardson R W (1992). Symmetry breaking and branching patterns in equivariant bifurcation theory. II. *Archive for Rational Mechanics and Analysis*, **120**(2):147—190. DOI: https://doi.org/10.1007/BF00418498. Cited on pp. 8 and 11.

[FS91] Field M and Swift J W (1991). Stationary bifurcation to limit cycles and heteroclinic cycles. *Nonlinearity*, **4**(4):1001—1043. DOI: https://doi.org/10.1088/0951-7715/4/4/001. Cited on p. 6.

[GC19] Garrido da Silva L and Castro S B S D (2019). Stability of quasi-simple heteroclinic cycles. *Dynamical Systems*, **34**(1):14—39. DOI: https://doi.org/10.1080/14689367.2018.1445701. Cited on pp. 4, 6, 27, 28, and 76.

[Gil75] Gilpin M E (1975). Limit cycles in competition communities. *The American Naturalist*, **109**(965):51—60. DOI: https://doi.org/10.1086/282973. Cited on p. 2.

[Gle94] Glendinning P (1994). *Stability, Instability and Chaos: An Introduction to the Theory of Nonlinear Differential Equations*. Cambridge University Press. DOI: https://doi.org/10.1017/CBO9780511626296. Cited on p. 22.

[GAK17] Granados A, Alsedà L, and Krupa M (2017). The period adding and incrementing bifurcations: from rotation theory to applications. *SIAM Review*, **59**(2):225—292. DOI: https://doi.org/10.1137/140996598. Cited on p. 136.

[GP23] Groothuizen Dijkema D C and Postlethwaite C M (2023). Travelling waves and heteroclinic networks in models of spatially-extended cyclic competition. *Nonlinearity*, **36**(12):6546—6588. DOI: https://doi.org/10.1088/1361-6544/ad0212. Cited on p. 9.

[GKP24] Groothuizen Dijkema D C, Kirk V, and Postlethwaite C M (2024). Analysis of dynamics near heteroclinic networks in $\mathbb{R}^4$ with a projected map. *Preprint*, arXiv:2410.21486 [math.DS]. DOI: https://doi.org/10.48550/arXiv.2410.21486. Cited on pp. 33 and 75.

[GPR25] Groothuizen Dijkema D C, Postlethwaite C M, and Rucklidge A M (2025). Continuity of projected maps of heteroclinic networks in $\mathbb{R}^4$. *In preparation.* Cited on p. 89.

[Gro25a] Groothuizen Dijkema D C (2025). https://dcgroothuizendijkema.github.io/media/gh_cyc_animation.mp4. Cited on p. 3.

[Gro25b] Groothuizen Dijkema D C (2025). https://dcgroothuizendijkema.github.io/media/A_to_chaos_stable_regions.mp4. Cited on p. 156.

[Gro78] Grossberg S (1978). Decisions, patterns, and oscillations in nonlinear competitive systems with applications to Volterra–Lotka systems. *Journal of Theoretical Biology*, **73**(1):101—130. DOI: https://doi.org/10.1016/0022-5193(78)90182-0. Cited on p. 2.

[GH83] Guckenheimer J and Holmes P (1983). *Nonlinear Oscillations, Dynamical Systems, and Bifurcations of Vector Fields*. Springer New York. DOI: https://doi.org/10.1007/978-1-4612-1140-2. Cited on p. 7.

[GH88] Guckenheimer J and Holmes P (1988). Structurally stable heteroclinic cycles. *Mathematical Proceedings of the Cambridge Philosophical Society*, **103**(1):189—192. DOI: https://doi.org/10.1017/S0305004100064732. Cited on pp. 3, 4, 6, 8, 22, and 25.

[HNW08] Hairer E, Nørsett S, and Wanner G (2008). *Solving Ordinary Differential Equations I: Nonstiff Problems*. Springer Berlin Heidelberg. DOI: https://doi.org/10.1007/978-3-540-78862-1. Cited on p. 168.

[HOP21] Hasan C R, Osinga H M, Postlethwaite C M, and Rucklidge A M (2021). Numerical continuation of spiral waves in heteroclinic networks of cyclic dominance. *IMA Journal of Applied Mathematics*, **86**:1141—1163. DOI: https://doi.org/10.1093/imamat/hxab027. Cited on p. 9.

[HB80] Heikes K E and Busse F H (1980). Weakly nonlinear turbulence in a rotating convection layer. *Annals of the New York Academy of Sciences*, **357**(1):28—36. DOI: https://doi.org/10.1111/j.1749-6632.1980.tb29672.x. Cited on p. 3.

[HU06] Heinzle J M and Uggla C (2006). Dynamics of the spatially homogeneous Bianchi type I Einstein–Vlasov equations. *Classical and Quantum Gravity*, **23**(10):3463. DOI: https://doi.org/10.1088/0264-9381/23/10/016. Cited on p. 9.

[Hof87] Hofbauer J (1987). Heteroclinic cycles on the simplex. *In* M Farkas, V Kertesz, and G Stepan (Eds.), *Proceedings of the International Conference on Nonlinear Oscillations*. Cited on p. 6.

[Hof94] Hofbauer J (1994). Heteroclinic cycles in ecological differential equations. *In* P Brunovský and M Medved' (Eds.), *Equadiff 8, Czech - Slovak Conference on Differential Equations and Their Applications. Bratislava, August 24-28, 1993*. Cited on pp. 22 and 24.

[HK10] Homburg A J and Knobloch J (2010). Switching homoclinic networks. *Dynamical Systems*, **25**(3):351—358. DOI: https://doi.org/10.1080/14689361003769770. Cited on p. 10.

[HPA98] Hu Y, Pesch W, Ahlers G, and Ecke R E (1998). Convection under rotation for Prandtl numbers near 1: Küppers–Lortz instability. *Phys. Rev. E*, **58**((5)):5821—5833. DOI: https://doi.org/10.1103/PhysRevE.58.5821. Cited on p. 3.

[IR15] Ibáñez S and Rodrigues A (2015). On the dynamics near a homoclinic network to a bifocus: switching and horseshoes. *International Journal of Bifurcation and Chaos*, **25**(11):1530030. DOI: https://doi.org/10.1142/S021812741530030X. Cited on p. 10.

[KLP10] Kirk V, Lane E, Postlethwaite C M, Rucklidge A M, and Silber M (2010). A mechanism for switching near a heteroclinic network. *Dynamical Systems*, **25**(3):323—349. DOI: https://doi.org/10.1080/14689361003779134. Cited on pp. 95 and 99.

[KPR12] Kirk V, Postlethwaite C, and Rucklidge A M (2012). Resonance bifurcations of robust heteroclinic networks. *SIAM Journal on Applied Dynamical Systems*, **11**(4):1360—1401. DOI: https://doi.org/10.1137/120864684. Cited on pp. 9, 95, 99, and 102.

[KS94] Kirk V and Silber M (1994). A competition between heteroclinic cycles. *Nonlinearity*, **7**(6):1605—1621. DOI: https://doi.org/10.1088/0951-7715/7/6/005. Cited on pp. xiii, 7, 8, 9, 21, 22, 33, 34, 35, 36, 37, 39, 48, and 117.

[Kir89] Kirlinger G (1989). Two predators feeding on two prey species: A result on permanence. *Mathematical Biosciences*, **96**(1):1—32. DOI: https://doi.org/10.1016/0025-5564(89)90080-1. Cited on p. 2.

[KS93] Knobloch E and Silber M (1993). Oscillatory convection in a rotating layer. *Physica D. Nonlinear Phenomena*, **63**(1-2):213—232. DOI: https://doi.org/10.1016/0167-2789(93)90156-U. Cited on p. 3.

[Kru97] Krupa M (1997). Robust heteroclinic cycles. *Journal of Nonlinear Science*, **7**(2):129—176. DOI: https://doi.org/10.1007/BF02677976. Cited on pp. 24 and 36.

[KM95a] Krupa M and Melbourne I (1995). Asymptotic stability of heteroclinic cycles in systems with symmetry. *Ergodic Theory and Dynamical Systems*, **15**(1):121—147. DOI: https://doi.org/10.1017/S0143385700008270. Cited on p. 22.

[KM95b] Krupa M and Melbourne I (1995). Non-asymptotically stable attractors in $O(2)$ mode interaction. *In* W F Langford and W Nagata (Eds.), *Normal Forms and Homoclinic Chaos*. DOI: https://doi.org/10.1090/fic/004/11. Cited on pp. 4 and 20.

[KM04] Krupa M and Melbourne I (2004). Asymptotic stability of heteroclinic cycles in systems with symmetry. II. *Proceedings of the Royal Society of Edinburgh: Section A Mathematics*, **134**(6):1177—1197. DOI: https://doi.org/10.1017/S0308210500003693. Cited on pp. 4, 6, 8, 17, 18, 34, 52, 118, and 137.

[KL69] Küppers G and Lortz D (1969). Transition from laminar convection to thermal turbulence in a rotating fluid layer. *Journal of Fluid Mechanics*, **35**(3):609—620. DOI: https://doi.org/10.1017/S0022112069001327. Cited on p. 3.

[LR23] Labouriau I S and Rodrigues A A P (2023). Periodic forcing of a heteroclinic network. *Journal of Dynamics and Differential Equations*, **35**(4):2951—2969. DOI: https://doi.org/10.1007/s10884-021-10054-w. Cited on p. 9.

[LU24] Lappicy P and Uggla C (2024). Oscillatory spacelike singularities: The Bianchi type $\mathrm{VI}_{-1/9}$ vacuum models. *Preprint,* arXiv:2410.10375 [gr-qc]. DOI: https://doi.org/10.48550/arXiv.2410.10375. Cited on p. 9.

[Lau01] Lauterbach R (2001). Heteroclinic cycles and fluid motions in rotating spheres. *In* P Chossat, D Armbruster, and I Oprea (Eds.), *Dynamo and Dynamics, a Mathematical Challenge*. DOI: https://doi.org/10.1007/978-94-010-0788-7_41. Cited on p. 3.

[LRT13] Liebscher S, Rendall A D, and Tchapnda S B (2013). Oscillatory singularities in Bianchi models with magnetic fields. *Annales Henri Poincaré. A Journal of Theoretical and Mathematical Physics*, **14**(5):1043—1075. DOI: https://doi.org/10.1007/s00023-012-0207-7. Cited on p. 9.

[Loh15] Lohse A (2015). Stability of heteroclinic cycles in transverse bifurcations. *Physica D: Nonlinear Phenomena*, **310**:95—103. DOI: https://doi.org/10.1016/j.physd.2015.08.005. Cited on pp. 6 and 20.

[Loz78] Lozi R (1978). Un attracteur étrange (?) du type attracteur de Hénon. *Journal de Physique Colloques*, **39**(C5):5—10. DOI: https://doi.org/10.1051/jphyscol:1978505. Cited on p. 157.

[Mat22] MathWorks Inc (2022). *MATLAB R2025a*. Natick, Massachusetts, United States: The MathWorks Inc. https://www.mathworks.com. Cited on p. 181.

[ML75] May R M and Leonard W J (1975). Nonlinear aspects of competition between three species. *SIAM Journal on Applied Mathematics*, **29**(2):243—253. DOI: https://doi.org/10.1137/0129022. Cited on pp. 2, 3, 4, 6, 8, 22, and 25.

[Mel91] Melbourne I (1991). An example of a nonasymptotically stable attractor. *Nonlinearity*, **4**(3):835—844. DOI: https://doi.org/10.1088/0951-7715/4/3/010. Cited on pp. 5, 20, and 22.

[MCG89] Melbourne I, Chossat P, and Golubitsky M (1989). Heteroclinic cycles involving periodic solutions in mode interactions with $\mathrm{O}(2)$ symmetry. *Proceedings of the Royal Society of Edinburgh: Section A Mathematics*, **113**(3-4):315—345. DOI: https://doi.org/10.1017/S0308210500024173. Cited on p. 4.

[MPR01] Melbourne I, Proctor M, and Rucklidge A (2001). A heteroclinic model of geodynamo reversals and excursions. *In* P Chossat, D Armbruster, and I Oprea (Eds.), *Dynamo and Dynamics, a Mathematical Challenge*. DOI: https://doi.org/10.1007/978-94-010-0788-7_43. Cited on p. 4.

[NMQ05] Nore C, Moisy F, and Quartie L (2005). Experimental observation of near-heteroclinic cycles in the von Kármán swirling flow. *Physics of Fluids*, **17**(6):064103. DOI: https://doi.org/10.1063/1.1926827. Cited on p. 4.

[PR23] Peixe T and Rodrigues A A (2023). Stability of heteroclinic cycles: a new approach based on a replicator equation. *Journal of Nonlinear Science*, **33**(6):99. DOI: https://doi.org/10.1007/s00332-023-09953-7. Cited on pp. 9 and 145.

[Pod12] Podvigina O (2012). Stability and bifurcations of heteroclinic cycles of type Z. *Nonlinearity*, **25**(6):1887—1917. DOI: https://doi.org/10.1088/0951-7715/25/6/1887. Cited on pp. 4, 5, 6, 7, 8, 19, 27, 28, 29, 31, 33, 36, 64, 76, 77, 78, and 130.

[Pod13] Podvigina O (2013). Classification and stability of simple homoclinic cycles in $\mathbb{R}^5$. *Nonlinearity*, **26**(5):1501. DOI: https://doi.org/10.1088/0951-7715/26/5/1501. Cited on p. 4.

[Pod23] Podvigina O (2023). Behaviour of trajectories near a two-cycle heteroclinic network. *Dynamical Systems*, **38**(4):576—596. DOI: https://doi.org/10.1080/14689367.2023.2225463. Cited on pp. 9, 11, 13, 21, 117, 118, 119, 120, 122, and 132.

[PA07] Podvigina O and Ashwin P (2007). The 1 : 2 mode interaction and heteroclinic networks in Boussinesq convection. *Physica D: Nonlinear Phenomena*, **234**(1):23—48. DOI: https://doi.org/10.1016/j.physd.2007.06.024. Cited on p. 9.

[PA11] Podvigina O and Ashwin P (2011). On local attraction properties and a stability index for heteroclinic connections. *Nonlinearity*, **24**(3):887—929. DOI: https://doi.org/10.1088/0951-7715/24/3/009. Cited on pp. 6 and 20.

[PCL19] Podvigina O, Castro S B S D, and Labouriau I S (2019). Stability of a heteroclinic network and its cycles: a case study from Boussinesq convection. *Dynamical Systems*, **34**(1):157—193. DOI: https://doi.org/10.1080/14689367.2018.1486807. Cited on p. 9.

[PCL20] Podvigina O, Castro S B S D, and Labouriau I S (2020). Asymptotic stability of robust heteroclinic networks. *Nonlinearity*, **33**(4):1757—1788. DOI: https://doi.org/10.1088/1361-6544/ab6817. Cited on pp. 9, 11, 18, and 35.

[PC15] Podvigina O and Chossat P (2015). Simple heteroclinic cycles in $\mathbb{R}^4$. *Nonlinearity*, **28**(4):901. DOI: https://doi.org/10.1088/0951-7715/28/4/901. Cited on p. 4.

[PC17] Podvigina O and Chossat P (2017). Asymptotic stability of pseudo-simple heteroclinic cycles in $\mathbb{R}^4$. *Journal of Nonlinear Science*, **27**(1):343—375. DOI: https://doi.org/10.1007/s00332-016-9335-4. Cited on p. 4.

[PL19] Podvigina O and Lohse A (2019). Simple heteroclinic networks in $\mathbb{R}^4$. *Nonlinearity*, **32**(9):3269—3293. DOI: https://doi.org/10.1088/1361-6544/ab1818. Cited on pp. 9 and 35.

[PK01] Porter J and Knobloch E (2001). New type of complex dynamics in the 1 : 2 spatial resonance. *Physica D: Nonlinear Phenomena*, **159**(3):125—154. DOI: https://doi.org/10.1016/S0167-2789(01)00340-2. Cited on p. 4.

[Pos10] Postlethwaite C M (2010). A new mechanism for stability loss from a heteroclinic cycle. *Dynamical Systems*, **25**(3):305—322. DOI: https://doi.org/10.1080/14689367.2010.495708. Cited on pp. 7 and 41.

[PD05] Postlethwaite C M and Dawes J H P (2005). Regular and irregular cycling near a heteroclinic network. *Nonlinearity*, **18**(4):1477—1509. DOI: https://doi.org/10.1088/0951-7715/18/4/004. Cited on pp. 9, 11, 21, and 54.

[PD06] Postlethwaite C M and Dawes J H P (2006). A codimension-two resonant bifurcation from a heteroclinic cycle with complex eigenvalues. *Dynamical Systems*, **21**(3):313—336. DOI: https://doi.org/10.1080/14689360600552928. Cited on p. 6.

[PD10] Postlethwaite C M and Dawes J H P (2010). Resonance bifurcations from robust homoclinic cycles. *Nonlinearity*, **23**(3):621—642. DOI: https://doi.org/10.1088/0951-7715/23/3/011. Cited on p. 6.

[PR22] Postlethwaite C M and Rucklidge A M (2022). Stability of cycling behaviour near a heteroclinic network model of Rock–Paper–Scissors–Lizard–Spock. *Nonlinearity*, **35**(4):1702—1733. DOI: https://doi.org/10.1088/1361-6544/ac3560. Cited on pp. 11, 14, 20, 21, 22, 31, 117, 122, 125, 136, 137, 138, 139, 140, 141, 142, 143, 144, 155, 156, and 157.

[Rei84] dos Reis G L (1984). Structural stability of equivariant vector fields on two-manifolds. *Transactions of the American Mathematical Society*, **283**(2):633—643. DOI: https://doi.org/10.2307/1999151. Cited on p. 4.

[Rod16] Rodrigues A A P (2016). Is there switching without suspended horseshoes? *Boletim da Sociedade Portuguesa de Matemática*, **74**:61—79. URL: https://revistas.rcaap.pt/boletimspm/article/view/21590. Cited on p. 10.

[RC23] Rodrigues A A P and Castro L (2023). Abundance of infinite switching. *SIAM Journal on Applied Dynamical Systems*, **22**(3):2570—2600. DOI: https://doi.org/10.1137/22M151371X. Cited on p. 10.

[RL14] Rodrigues A A P and Labouriau I S (2014). Spiralling dynamics near heteroclinic networks. *Physica D: Nonlinear Phenomena*, **268**:34—49. DOI: https://doi.org/10.1016/j.physd.2013.10.012. Cited on p. 9.

[RLA11] Rodrigues A A P, Labouriau I S, and Aguiar M A D (2011). Chaotic double cycling. *Dynamical Systems*, **26**:199—233. DOI: https://doi.org/10.1080/14689367.2011.557179. Cited on p. 10.

[SC92] Scheel A and Chossat P (1992). Bifurcation d'orbites périodiques à partir d'un cycle homocline symétrique. *Comptes Rendus de l'Académie des Sciences. Série I. Mathématique*, **314**(1):49—54. URL: https://gallica.bnf.fr/ark:/12148/bpt6k58688425/f53.item. Cited on pp. 6 and 88.

[SSW79] Schuster P, Sigmund K, and Wolff R (1979). On ω-limits for competition between three species. *SIAM Journal on Applied Mathematics*, **37**(1):49—54. DOI: https://doi.org/10.1137/0137004. Cited on p. 2.

[SR94] Sikder A and Roy A B (1994). Persistence of a generalized Gause-type two prey-two predator pair linked by competition. *Mathematical Biosciences*, **122**(1):1—23. DOI: https://doi.org/10.1016/0025-5564(94)90080-9. Cited on p. 2.

[Sim10] Simpson D J W (2010). *Bifurcations in Piecewise-smooth Continuous Systems*. World Scientific. DOI: https://doi.org/10.1142/7612. Cited on p. 164.

[Sim16] Simpson D J W (2016). Border-collision bifurcations in $\mathbb{R}^N$. *SIAM Review*, **58**(2):177—226. DOI: https://doi.org/10.1137/15M1006982. Cited on pp. 32, 135, 141, and 155.

[Sim17] Simpson D J W (2017). The structure of mode-locking regions of piecewise-linear continuous maps: I. Nearby mode-locking regions and shrinking points. *Nonlinearity*, **30**(1):382—444. DOI: https://doi.org/10.1088/1361-6544/aa4f49. Cited on pp. 141 and 164.

[Sim20] Simpson D J W (2020). Unfolding codimension-two subsumed homoclinic connections in two-dimensional piecewise-linear maps. *International Journal of Bifurcation and Chaos in Applied Sciences and Engineering*, **30**(3):2030006. DOI: https://doi.org/10.1142/S0218127420300062. Cited on p. 135.

[SG24] Simpson D J W and Glendinning P A (2024). Inclusion of higher-order terms in the border-collision normal form: Persistence of chaos and applications to power converters. *Physica D: Nonlinear Phenomena*, **462**:134131. DOI: https://doi.org/10.1016/j.physd.2024.134131. Cited on p. 157.

[SM09] Simpson D J W and Meiss J D (2009). Shrinking point bifurcations of resonance tongues for piecewise-smooth, continuous maps. *Nonlinearity*, **22**(5):1123—1144. DOI: https://doi.org/10.1088/0951-7715/22/5/009. Cited on p. 139.

[SMH05] Smith T R, Moehlis J, and Holmes P (2005). Heteroclinic cycles and periodic orbits for the $\mathrm{O}(2)$-equivariant $0:1:2$ mode interaction. *Physica D: Nonlinear Phenomena*, **211**(3):347—376. DOI: https://doi.org/10.1016/j.physd.2005.09.002. Cited on p. 4.

[Sot02a] Sottocornola N (2002). Complete classification of homoclinic cycles in $\mathbb{R}^4$ in the case of a symmetry group $G \subset \mathrm{SO}(4)$. *Comptes Rendus. Mathématique*, **334**(10):859—864. DOI: https://doi.org/10.1016/S1631-073X(02)02371-3. Cited on p. 4.

[Sot02b] Sottocornola N (2002). Robust homoclinic cycles in $\mathbb{R}^4$. *Nonlinearity*, **16**(1):1. DOI: https://doi.org/10.1088/0951-7715/16/1/301. Cited on p. 4.

[Sot05] Sottocornola N (2005). Simple homoclinic cycles in low-dimensional spaces. *Journal of Differential Equations*, **210**(1):135—154. DOI: https://doi.org/10.1016/j.jde.2004.10.023. Cited on p. 4.

[Sow85] Soward A M (1985). Bifurcation and stability of finite amplitude convection in a rotating layer. *Physica D: Nonlinear Phenomena*, **14**(2):227—241. DOI: https://doi.org/10.1016/0167-2789(85)90181-2. Cited on p. 3.

[SH89] Stone E and Holmes P (1989). Noise induced intermittency in a model of a turbulent boundary layer. *Physica D: Nonlinear Phenomena*, **37**(1):20—32. DOI: https://doi.org/10.1016/0167-2789(89)90114-0. Cited on p. 3.

[SH91] Stone E and Holmes P (1991). Unstable fixed points, heteroclinic cycles and exponential tails in turbulence production. *Physics Letters A*, **155**(1):29—42. DOI: https://doi.org/10.1016/0375-9601(91)90503-Z. Cited on p. 3.

[Swi84] Swift J W (1984). Convection in a rotating fluid layer. *In* J E Marsden (Ed.), *Fluids and Plasmas: Geometry and Dynamics*. Cited on p. 3.

[SN23] Szybka S J and Naqvi S U (2023). Chaos and Einstein–Rosen gravitational waves. *Physical Review D*, **108**(8):L081501. DOI: https://doi.org/10.1103/PhysRevD.108.L081501. Cited on p. 9.

[TMG00] Toral R, Miguel M S, and Gallego R (2000). Period stabilization in the Busse–Heikes model of the Küppers–Lortz instability. *Physica A: Statistical Mechanics and its Applications*, **280**(3):315—336. DOI: https://doi.org/10.1016/S0378-4371(00)00076-5. Cited on p. 3.

[Ura64] Ura T (1964). On the flow outside a closed invariant set: stability, relative stability and saddle sets. *Contributions to Differential Equations*, **3**:249—294. Cited on p. 19.

[VGO20] Virtanen P, Gommers R, Oliphant T E, Haberland M, Reddy T, Cournapeau D, Burovski E, Peterson P, Weckesser W, Bright J, *et al.* (2020). SciPy 1.0: Fundamental Algorithms for Scientific Computing in Python. *Nature Methods*, **17**:261—272. DOI: https://doi.org/10.1038/s41592-019-0686-2. Cited on p. 168.

[VVM20] Voit M, Veneziale S, and Meyer-Ortmanns H (2020). Coupled heteroclinic networks in disguise. *Chaos: An Interdisciplinary Journal of Nonlinear Science*, **30**(8):083113. DOI: https://doi.org/10.1063/5.0006720. Cited on p. 9.

[YZS24] Yang L, Zhang H, and Sun Z (2024). Hippocampus encoding memory engrams as stable heteroclinic network. *Chaos: An Interdisciplinary Journal of Nonlinear Science*, **34**(12):123118. DOI: https://doi.org/10.1063/5.0223045. Cited on p. 9.

[YH87] Yang W-M and Hao B-L (1987). How the Arnold tongues become sausages in a piecewise linear circle map. *Communications in Theoretical Physics*, **8**(1):1. DOI: https://doi.org/10.1088/0253-6102/8/1/1. Cited on pp. 135, 141, and 164.

[ZM03] Zhusubaliyev Z and Mosekilde E (2003). *Bifurcations and Chaos in Piecewise-smooth Dynamical Systems*. World Scientific. DOI: https://doi.org/10.1142/5313. Cited on p. 164.